Microstructural Investigation of Tablet Compaction and Tablet Pharmacological Properties

by

Kangyi Mao

B.E. Chemical Engineering
Tsinghua University, 2003

M.S. Chemical Engineering Practice
Massachusetts Institute of Technology, 2006

SUBMITTED TO THE DEPARTMENT OF CHEMICAL ENGINEERING
IN PARTIAL FULFILLMENT OF THE REQUIREMENTS FOR THE DEGREE OF

DOCTOR IN PHYLOSOPHY IN CHEMICAL ENGINEERING
AT THE
MASSACHUSETTS INSTITUTE OF TECHNOLOGY

JULY 2010
[September 2010]

Author: .....
Kangyi Mao
Department of Chemical Engineering
July, 2010

Certified by: .....
Charles L. Cooney
Professor of Chemical and Biochemical Engineering
Thesis supervisor

Accepted by: .....
William Deen
Chairman, Committee for Graduate Students

Microstructural Investigation of Tablet Compaction and Tablet Pharmacological Properties

by

Kangyi Mao

Submitted to the Department of Chemical Engineering
on July 29th, 2010 in Partial Fulfillment of the
Requirements for the Degree of Doctor of Philosophy in
Chemical Engineering

ABSTRACT

In current tablet manufacturing processes, there is a knowledge gap concerning material transformation and the subsequent impact on tablet properties; this gap presents a barrier to rational formulation / process design. In this study, it was hypothesized that the understanding of tablet microstructure is pivotal in bridging our knowledge about the materials, the manufacturing process, and the tablet properties.

A series of X-ray micro computed tomography (microCT) characterization methods were developed to untangle material interactions during tablet manufacturing process, leading to an interpretation of tablet compaction mechanisms through 3-D representation of microstructural features. Numerical simulation of liquid intrusion based on microCT data was utilized in calculating tablet microstructure permeability, introducing a novel parameter for characterization of tablet dissolution properties.

A tablet holder was designed and used in combination with paddle dissolution test to investigate tablet dissolution process, enabling the classification of dissolution mechanisms and identification of correspondent formulation design strategies. When incorporated with permeability results, a quantitative dissolution model capable of separating the contributions from disintegration and surface dissolution was derived. The dissection of the dissolution process provides a scientific framework supporting the Quality by Design paradigm for product and process development. .

This work provides a strategy for building an integrated formulation design and characterization system incorporating microstructural analysis. It opens up an approach in which microstructure becomes a critical target for design and optimization.

Thesis Supervisor: Charles L. Cooney
Title: Professor of Chemical and Biochemical Engineering

Acknowledgement

My time at MIT has been the longest and most dramatic journey in my life. In these years, I evolved from a single young man to a husband and father; I explored the endless opportunities MIT provided with me, stumbled, and stood up against the odds; I met numerous splendid people along the way, learned from them, and strived to become one of them. Without the help and inspiration from these people, I could not have completed what is documented in this thesis.

Professor Charles L. Cooney, my thesis advisor, has been an extraordinary guide on this journey of mine. His clear vision of the big picture keeps me on the right track; his rigorous requirement on scientific writing trains the precision of my mind; his deep knowledge about the pharmaceutical industry gives me unique insights in linking scientific exploration with real world applications. I would also like to show my appreciation for Professor Bernhardt L. Trout and Professor T. Alan Hatton, my thesis committee members. They have always been supporting my study with clear-cut critiques and generous guidance.

Dr. Shawn Zhang and Dr. Mike Marsh from Visualization Sciences Group have provided critical technical support in microstructure image analysis. Dr Doug Wei from Zeiss U.S.A. helped carry out the preliminary experiments with FIB-SEM. Professor Whitey Hagadorn from Amherst College generously offered free usage of microCT instrument as well as technical advice.

My UROP students Kellie Courtney and Kavita Chandra have contributed a lot of their time in dissolution studies of the thesis. They are both competent and candid researchers with a brilliant future. My colleagues in the Cooney lab have been great sources of intellectual inspiration as well as friendship. I can't image there is a better lab to work in. Special acknowledge goes to Erin Bell (and her fish Neil), who as the safety officer, has kept the whole lab clean like home!

I would like to acknowledge the generous financial and technical support from the Novartis-MIT Center for Continuous Manufacturing. I learned a lot about scientific and industrial practices from my interaction with the downstream and redline teams.

Finally, I would like to dedicate this thesis to my wife Jie and my daughter Joanna, for all the support and understanding they have given me, and all the fun they had at home without me.

TABLE OF CONTENTS

TABLE OF FIGURES

TABLE OF TABLES

Chapter 1 Introduction

On a retail package of pharmaceutical tablets, one can often find a long list of inactive ingredients, including fillers/binders, disintegrants, lubricants, glidants, coating materials, etc. These materials, called excipients, facilitate the manufacturing process and provide the tablets with adequate properties. The selection of excipients and subsequent processing designs has been studied extensively in the pharmaceutical industry for the last several decades. Currently, major excipients are picked to match the active pharmaceutical ingredient (API) based on their physicochemical properties, with the overall formulation and manufacturing process improved via statistical design of experiments (DOE). In order to achieve rational formulation development, we hypothesize that an in-depth understanding about the tablet itself, especially the microstructure, is required to bridge our knowledge about the other components of pharmaceutical manufacturing (Figure 1-1).

Figure 1-1 Relationship among different components in formulation development.

Tablet microstructure refers to the arrangement of materials within a tablet as a direct result of material interactions through the manufacturing process. It includes not only the arrangement of materials and void space, but also the distribution of different materials. Due to limitations in technological and analytical capability, no detailed 3-D characterization of tablet microstructure has been described in literature to date.

In this study, tablet microstructure analysis via micro-computed tomography (microCT) is coupled with analysis of dissolution mechanism using a built for purpose tablet holder, leading to comprehensive insights of the material interactions during the manufacturing process, the

resulting microstructure, and the impact on pharmacological properties like dissolution. The analytical toolbox compiled and evaluated in this work facilitates rational microstructure design, providing scientific rationale in the selection of ingredients and manufacturing process.

1.1 Motivation

In order to be administered successfully, medication needs to be in a certain physical format, or a dosage form. A dosage form can be liquid, aerosol or gas, but more often solid. Tablet is the most popular solid dosage form due to its stability, transportability, and ease of manufacturing. It is the single largest dosage form of final drug products, accounting for 48% of all the drugs available in U.S.A according to drugs@FDA database as of 03/2009. A huge number of publications on tablet exist today in the pharmaceutical literature. One category of publications deals with the design and performance of specific formulations, another focuses on the elucidation of general processing behaviors and their implications for pharmacological properties, with a specific emphasis on commonly used ingredients.

To obtain satisfactory tablet production, consistency in a few analytical test categories needs to be achieved (Table 1-1). In physical properties, content uniformity in terms of API loading per tablet, API distribution within the tablet, and crystalline form stability are important quality attributes to control; in chemical properties, the formulation or manufacturing process should lead to a tablet that can endure stability testing at elevated temperature/moisture conditions, with no API degradation or API-excipient reactions; in mechanical properties, the hardness and friability determines a tablet's ability to survive handling and transportation; in pharmacological properties, dissolution test (and sometimes disintegration test), often acting as *in vitro* surrogate test for bioavailability, need to yield consistent and satisfactory dissolution behaviors conforming to the desired *in vivo* pharmacokinetics (PK) and pharmacodynamics (PD) profiles. We believe that a wide range of the properties are directly impacted by tablet microstructure, e.g., content

uniformity, hardness, friability, and dissolution/disintegration. Therefore, a quantitative understanding of tablet microstructure could lead to new insights into the tablet properties.

Table 1-1 In vitro analytical tests for quality assessment of pharmaceutical tablets.

In Vitro Quality Matrix for Tablets	
Properties	**Analytical Tests**
Physical	Uniformity, Stability
Chemical	Stability
Mechanical	Hardness, Friability
Pharmacological	Dissolution, Disintegration

The key hurdle in understanding tablet microstructure stems from the limitations of technologies and methodologies currently applied in formulation development. Microscopic methods provide high resolution but can not go beyond the surface layer of the materials; some also require surface treatment which might mask structural characteristics. Spectroscopic methods have the penetration power to resolve 3-D structure of the formulation dosages, but do not provide enough resolution until the emergence of microCT. Other physical methods, especially mercury porosimetry, have been adapted to probe into tablet microstructure. However, as will be demonstrated in this study, mercury porosimetry is intrinsically limited by the problematic assumptions it made in theory. The collaborative lack of quantitative 3-D characterization of tablet microstructure prohibits clear understanding of the interactions among materials during manufacturing process, which further prohibits a rational formulation design leading to predictable tablet properties.

On the other hand, the current analytical methods for characterizing tablet properties often do not facilitate mechanistic investigation of the testing process. Paddle dissolution test, a critical

analytical test for *in vitro* bioavailability evaluation and many other purposes, allows a tablet to dissolve freely in a complex hydrodynamics condition. The uncontrolled hydrodynamics and tablet morphology makes it difficult to identify the key drivers to dissolution process, deterring rational formulation designs specifically promoting these key drivers.

The lack of mechanistic knowledge for tablet microstructure and tablet properties creates a knowledge gap within pharmaceutical manufacturing process, preventing a thorough understanding and rational design of the system.

1.2 Strategy and Specific Aims

In this Ph.D. study, a systematic approach was adopted in designing and testing a toolbox to bridge a knowledge gap concerning material transformation in manufacturing process and the subsequent impact on tablet properties. The goals of the study are to develop a tomography imaging method for quantitative description and 3-D visualization of tablet microstructure, to develop a novel tablet holder to be used in combination with paddle dissolution test for dissolution mechanism investigation, and to develop a quantitative analysis tool for understanding the relationship between microstructure and dissolution process (Figure 1-2).

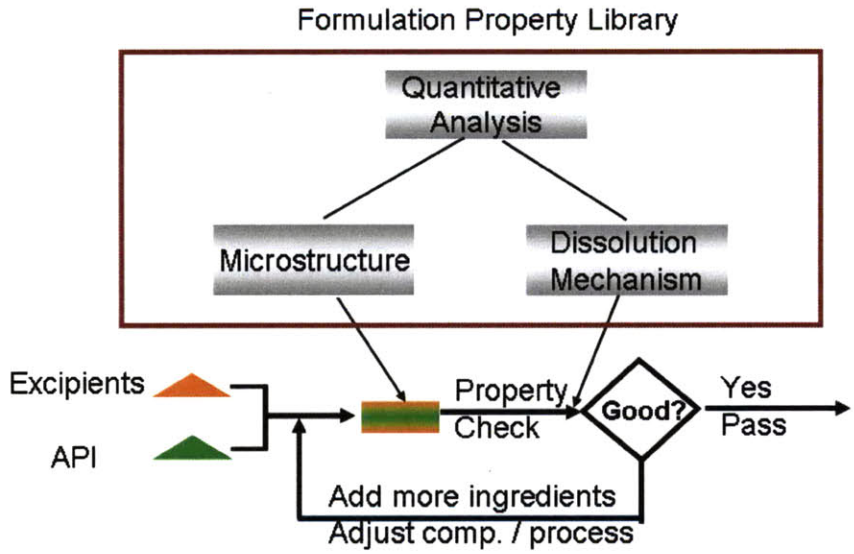

Figure 1-2 Illustration of traditional route for formulation development and the incorporation of new tools.

This toolkit would be applied to both a caffeine-lactose direct compressed tablet formulation as well as a roller compacted tablet formulation that is developed in this study for Novartis compound-A. The case studies should pave the way for the establishment of a novel tablet characterization system, providing scientific guidance in both development and manufacturing settings. The specific aims of the study are listed as follows:

Specific Aims #1: Develop a microCT imaging method with 3-D analysis toolkit for visualization and quantitative characterization of tablet microstructure.

First, a proper microCT scanning configuration for pharmaceutical tablets would be tested and established; a digital post-processing workflow would then be developed to prepare the raw data for further quantitative analysis; lastly, sophisticated algorithms will be prepared to regenerate tablet pore space with structural modules, illustrating the arrangement patterns of the microstructure and providing guidance for quantitative analysis.

Specific Aims #2: Develop a novel tablet holder for dissecting dissolution mechanism.

A novel tablet holder would be developed and used in combination with standard paddle dissolution test for understanding the dissolution mechanisms of pharmaceutical tablets. Correspondent physical/mathematical models would be used to establish dissolution mechanisms and interpret the dissolution results. Comparison between the paddle test and the holder test would be used to evaluate the contribution of tablet disintegration to overall dissolution speed.

Specific Aims #3: Develop a roller compaction formulation for Novartis compound-A that is amenable for continuous manufacturing using QbD methodology.

A compound-A tablet formulation would be developed based on the understanding of material properties rather than the empirical evidences for ingredient selection. The formulation is targeted to minimize the number of ingredients and manufacturing steps, facilitating continuous manufacturing while maintaining superior tablet properties.

Specific Aims #4: Understand the relationship between microstructure and compaction / dissolution mechanism of compound-A/caffeine-lactose tablets with microCT/holder toolbox.

The microCT/holder toolbox will be tested on the tablet formulations developed in this study. Microstructure models derived from microCT scans would be used in 3-D computerized simulation of liquid intrusion, generating reliable permeability information. A quantitative interpretation of dissolution behaviors based on dissolution mechanism and tablet microstructure would be established, providing valuable insight in microstructure design for fine-tuning tablet properties.

1.3 Background

This section gives an overview of tablet compaction, pharmacological properties and tablet microstructure, providing the basic knowledge important for understanding the discussions in the following chapters.

1.3.1 Tablet Compaction in Pharmaceutical Manufacturing

The major forming method for pharmaceutical tablets is compaction, realized via a pressurizing process for powder mixtures conducted on a tablet press. As simple as it looks, tablet compaction remains a process that is based more on empirical knowledge than on scientific theory (1). The use of basic physicochemical data in formulation work for prediction of tabletting properties, for example compressibility (ability to reduce in volume) and compactibility (ability to form compacts), is relatively limited due to insufficient understanding of the underlying physical interactions of the materials in use (1).

1.3.1.1 Secondary Pharmaceutical Manufacturing

There are two phases of pharmaceutical manufacturing. Primary pharmaceutical manufacturing refers to the process during which active pharmaceutical ingredient (API) is produced, while secondary pharmaceutical manufacturing refers to the process that API is mixed with excipients and produced into a final dosage form, e.g. a tablet. As tablet compaction is a critical step for shaping the pharmacological properties, a series of other unit operations ahead of it are used to prepare the materials for the tabletting process.

In order to achieve good performance for the quality matrix listed in Table 1-1, multiple routes of secondary pharmaceutical manufacturing have been devised; the most popular three routes are direct compression, dry granulation, and wet granulation (Figure 1-3).

Direct compression is the most desired manufacturing route, in which dry API powder is blended with appropriate excipients and fed directly to the tablet press. It is theoretically straightforward, easy to control, and bears low cost. However, it also imposes high requirement on material consistency and on the proper interaction between the API and excipients in blending and compaction. No segregation should happen in the blending process, which could lead to heterogeneous mixtures. The powders should be free flowing and of sufficient density, ensuring consistent feeding to the press to obtain adequate tablet weight. The excipients should yield proper binding to the API and form tablets with good mechanical and physical strengths. Direct compression is a top choice upon satisfaction of the criteria listed above, but often requires longer development time due to insufficient understanding of material interactions. It also bears a much higher risk in scale up, as there is less room for adjustment of particle size or moisture level when compared with the other two routes. This prolonged development time coupled with higher potential variation in scale-up / production dramatically reduces the utilization of direct compression.

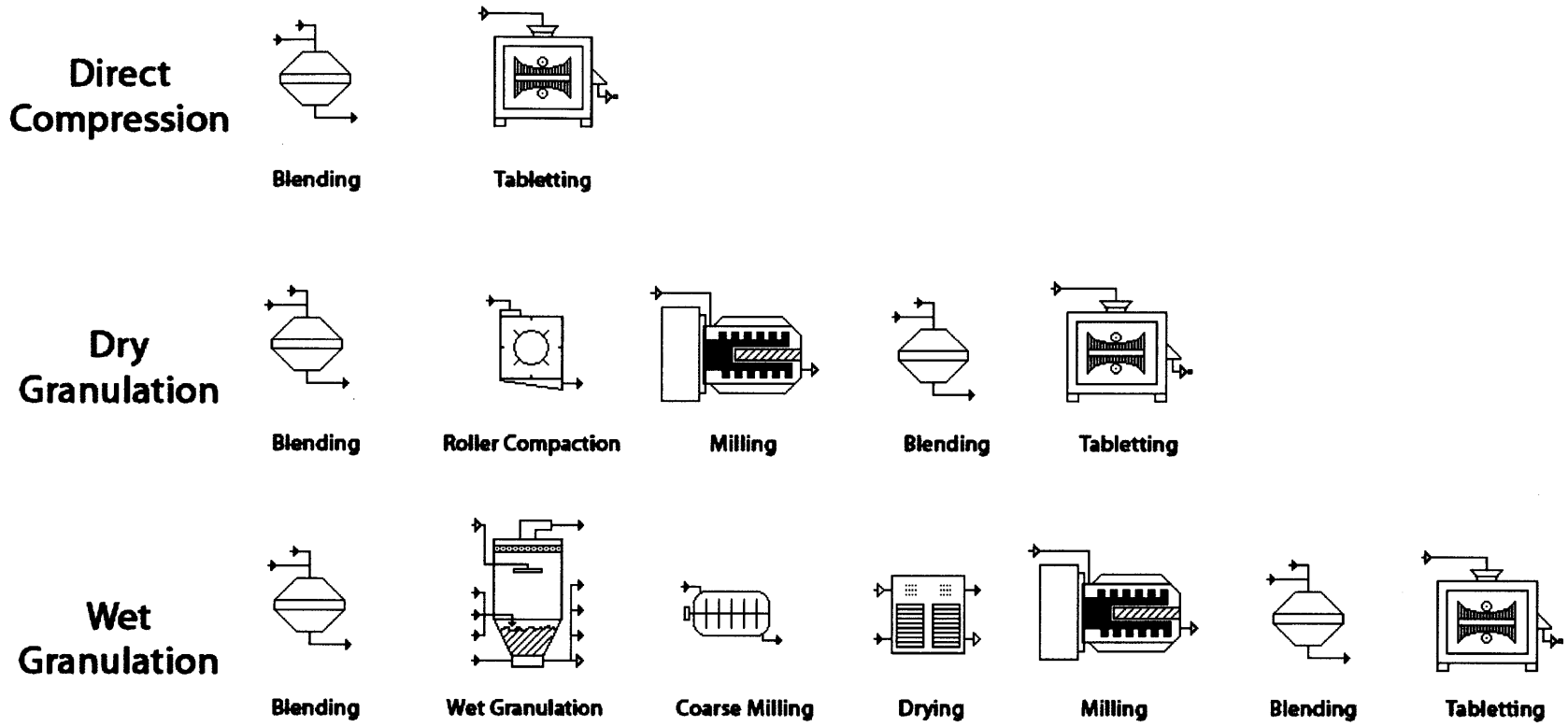

Figure 1-3 Illustration of common routes for secondary pharmaceutical manufacturing

Notes: The blending step right before tabletting in dry/wet granulation might be dispensable;

In this illustration, the starting materials are assumed to be dry API and excipient powders;

The coating and packaging steps after tabletting are omitted in this illustration for simplicity reasons.

More commonly seen in new drug applications (NDA) is wet granulation, which is relatively established but requires additional manufacturing steps. The powder blend is thoroughly mixed with a liquid binder/adhesive in a high shear mixer, e.g. aqueous preparation of cellulose derivatives, and passed through coarse screens. The materials are then dried and subjected to further milling, resulting in granules of desired size for tabletting (typically a few hundred microns). After a final blending step, the powder is fed to the tablet press. The wet granulation procedure is considerably more complicated than direct compression, with seven unit operations vs. ideally two for the latter. The operational cost is higher and due to the additional steps, there is a need for additional process control. However, because wet granulation better accommodates material variability, it is a more universal process.

Sitting right between direct compression and wet granulation is dry granulation (roller compaction), where the powder blend goes through light compression under relatively low pressure to enhance cohesiveness and density. The compressed material, often called ribbon, is then passed through a mill to generate granules, which are typically further blended with lubricants/free-flowing agents/excipients before tabletting. Dry granulation does not introduce a liquid phase into the process, and thus spares the need for wet milling and drying. This is especially important for an API that is sensitive to water or heat. But the number of unit operations is still more than twice that for direct compression. Plus, dry granulation is more prone to produce fine powders before tabletting, potentially reducing the yield and generating uncertainties in tabletting behaviors. Powder flowability prior to dry granulation should also be excellent.

It is obvious that direct compression is the most desirable route for secondary pharmaceutical manufacturing. In reality, the semi-empirical nature of the current formulation development practice and the insufficient understanding of material interactions make direct compression a time-consuming target to reach. For candidates that are being prepared for New Drug Application (NDA), time-to-market is critical to maximize patent-protected sales period. As a result, a majority of NDA drugs end up with wet granulation. The cost of goods sold (COGS) for brand name drugs has been

around 25% of revenues, while that for generic drugs is around 50% (2). According to Ruey-Ching (Richard) Hwang, a senior director of pharmaceutical sciences at Pfizer Global Research and Development (Kalamazoo, MI), "more than 50% of the generic formulations I've worked on use direct compression. About 30%-40% wind up using wet granulation and 10% or less use roller compaction."(3) With an adequate knowledge about material interaction and the subsequent impact on tablet microstructure / properties, there is a much better chance (and confidence) to promote direct compression for NDA drugs.

1.3.1.2 Mechanism of Tablet Compaction

The process of tablet compaction involves a few basic steps (Figure 1-4). The powder is first filled into the die with excessive portion removed, after which the upper punch of the press travels down in coordination with lower punch to compress the powder into a tablet, and then the lower punch travels up to eject the tablet.

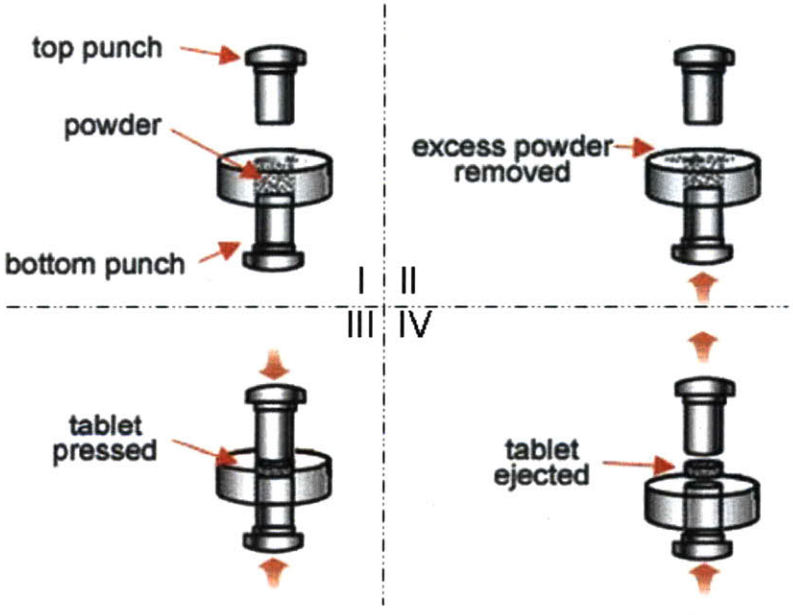

Figure 1-4 The basic steps of tablet compaction. Adapted from ABPI resources for schools.

The powder goes through two stages in this process. First, the particles rearrange themselves and are subjected to (reversible) elastic deformation, after which they undergo (irreversible) plastic deformation and/or fragmentation and develop strong inter-particle

solid bonding. In manufacturing processes, in order to allow displacement of air and the material to relax and form greater solid bonds, there may be a pre-compaction step that is performed at lower pressure than the main compaction. The terminology compaction and compression are often used interchangeably in the industry, causing unnecessary confusions. In this study we define that compression is the reduction in volume of a powder bed due to the application of a pressure, while compaction is the transformation of a powder into a coherent specimen of defined shape by powder compression.

Multiple factors could influence the quality of tablet production. Moisture-powder interaction is a major factor in formulation, processing, and performance of solid dosage forms (4). Appropriate control of material moisture level and relative humidity (RH) of manufacturing facility could be critical in achieving desired and consistent final product quality. Particle size/shape distribution could potentially affect both the particle rearrangement and elastic/plastic consolidation of the powders. Typically, at the same compaction pressure, tablet hardness increases with decreasing particle size due to larger numbers of contact points(5), although the flowability of the powder could decrease simultaneously. Other important properties of the API and excipients include crystallinity(6), polymorphism(7, 8) / amorphism(9), salt form(10). On the process side, the manufacturing steps prior to tablet compaction have direct impact on material properties and interactions, as discussed above. The speed of compaction can have significant impact on tablet properties, as materials response differently when subjected to the same pressure at various speeds, which often presents a big challenge for scale-up and technology transfer when tabletting speed increases significantly (11). The force of the main compaction, the existence of pre-compaction, and their relative magnitude might impact the mechanical strength and defect rates of the tablets (12).

Tablet manufacturing is a multi-step process that involves a lot of different factors. Through deciphering tablet microstructure, this study aims to rationalize the development process.

1.3.2 Tablet Properties and Analytical Methods

Due to the desired efficacy and potential toxicity of the pharmaceutical tablets, the tablet properties as listed in Table 1-1 are measured with correspondent analytical methods to ensure quality compliance. In this section we discuss the physical/chemical, mechanical, and pharmacological properties of the tablets, as well as the associated analytical methods.

1.3.2.1 Physical/Chemical Properties

The shape and size of a tablet is mainly determined by the shape of the tooling, operational setups, and material loading. Thickness plays an important role for the mechanical stability of the tablets during transport and packaging (especially when tablets are blistered). For the same level of die filling, tablet thickness is determined by the compressive load and material elasticity. Tablet thickness is typically measured with a micrometer and is controlled within 5% deviation from a standard value. The tablet should look generally appealing and free of defects, with coating applied to enhance surface texture if necessary.

Content uniformity or weight variation is used to determine dosing consistency. Content uniformity test is required by US Pharmacopeia (USP) for most tablets that have less than 50mg or 50% of API by weight[1]. Ten units of tablets are assayed for accurate API content, all of which should stay within +/- 15% from the standard value, with a standard deviation of less than 6%. Should either criterion not be met, additional testing would be needed and the batch might fail. For tablets that content uniformity test is not required, weight variation test might be adopted instead. Weight is controlled via die filling volume. To have consistent tablet weight, the powder should have uniform density as well as good flowability.

Physical and chemical stability are usually tested under temperature and moisture levels specified by pharmacopeias. Long term stability test is typically done at 25 °C and 60%

[1] USP 29 – NF 24, General Chapters <905>, Uniformity of Dosage Units.

RH for up to three years. An accelerated condition of 40°C and 75% RH allows examination of stability in a much shorter time frame (max 6 months). Physical stability mainly refers to the capability of maintaining hardness and dimensions as well as original crystalline forms, with the latter typically assessed by X-ray powder diffraction (XRPD). Chemical stability examines the self-degradation of API or its reaction with other ingredients in the formulation, which is typically assessed with high performance liquid chromatography (HPLC).

1.3.2.2 Mechanical Properties

The mechanical strength of a tablet indicates the degree of bonding among the materials after the manufacturing process. The bonding should neither be so strong that disintegration/dissolution of tablet is impeded, nor so weak that the tablet can not endure normal handling, packaging, or transportation. There are mainly two types of USP compendial tests for mechanical strength. Tablet hardness/tensile strength test focuses on the strength while friability test focuses on the weakness.

The hardness test measures the breaking force, the force required to cause tablet to fail in a specific plane. The tablets are generally placed between two plates, one of which moves and applies sufficient force to the tablet to cause fracture. For round tablets, diametral loading is adopted. The case of point-loading of a homogeneous disk at diametrically opposite points can be solved analytically using continuum mechanics equations, which indicates that tension is induced in the direction perpendicular to loading(13). In reality, three modes of failure have been observed (Figure 1-5). Tensile failure is characterized by a clean split into halves along the loaded diameter (parallel to the direction of loading) or by a triple cleft failure. Shear failure is characterized by crushing at the contacts and the progression of failure zones until the tablet collapses. It has been shown that to obtain reproducible results for the strength of tablets prepared at a given compression force, the tablet must break in such a manner that the tensile stress is the major stress(14). As a result, hardness is not exactly a good description of the test, while breaking force is really measuring the tensile strength.

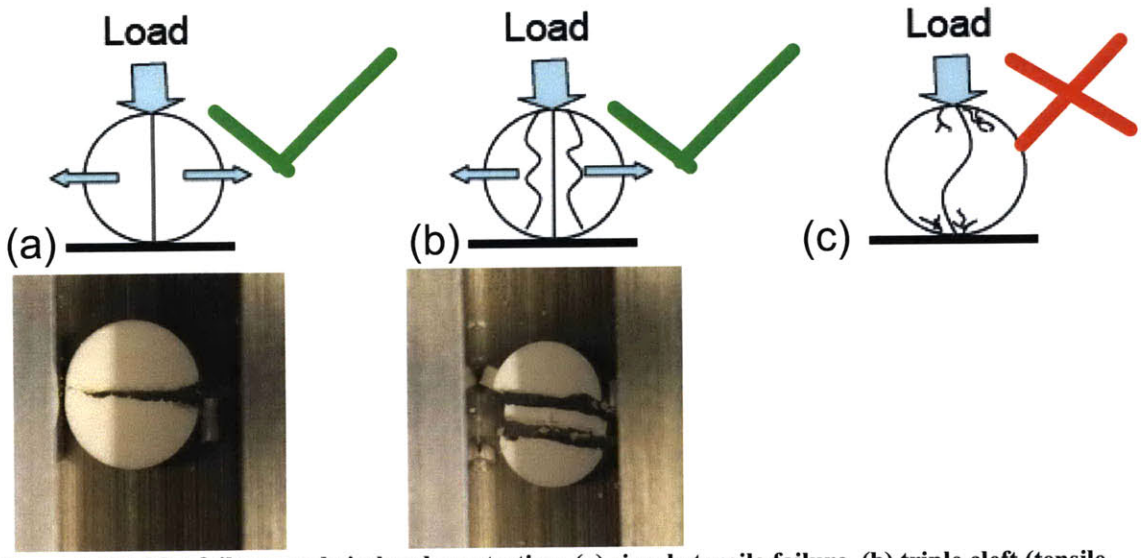

Figure 1-5 Tablet failure mode in hardness testing. (a) simple tensile failure, (b) triple cleft (tensile failure) (c) shear-induced failure (illustration was adapted from Davies and Newton, Pharmaceutical Powder Compaction Technology, 1996, pg 165).

Tensile strength is a more accurate measurement of mechanical strength as it also takes into account the geometry of the tablet. Based on elastic theory and a few assumptions, the tensile strength of cylindrical tablets has been derived as follows(15):

$$\sigma = \frac{2F}{\pi DH} \tag{1.1}$$

Where F is the breaking force/hardness, D is the diameter and H is the tablet thickness.

In daily practice of pharmaceutical formulation development, hardness in unit of N is often adopted. Oral round tablets normally have a hardness value of 40-100N, some chewable or hypodermic tablets could have hardness less than 30N, while some extended release tablets or larger ovaloid tablets could carry hardness values of 100-200N (16).

A friability test is complementary to the hardness test, evaluating the ability of tablets to withhold abrasions resulting from coating, packaging, shipping, and handling. A number of tablets adding up to 6.5g (or 10 tablets if single weight more than 650mg) are placed in a Roche friabilator, which rotates and subjects the tablets to repeated rolling and falling shocks from 6 inch height (Figure 1-6). After 100 rotations (or 500 if the tablets will later be coated), the weight loss of the tablets is recorded and should not exceed 1%. If a tablet cracks, the test automatically fails.

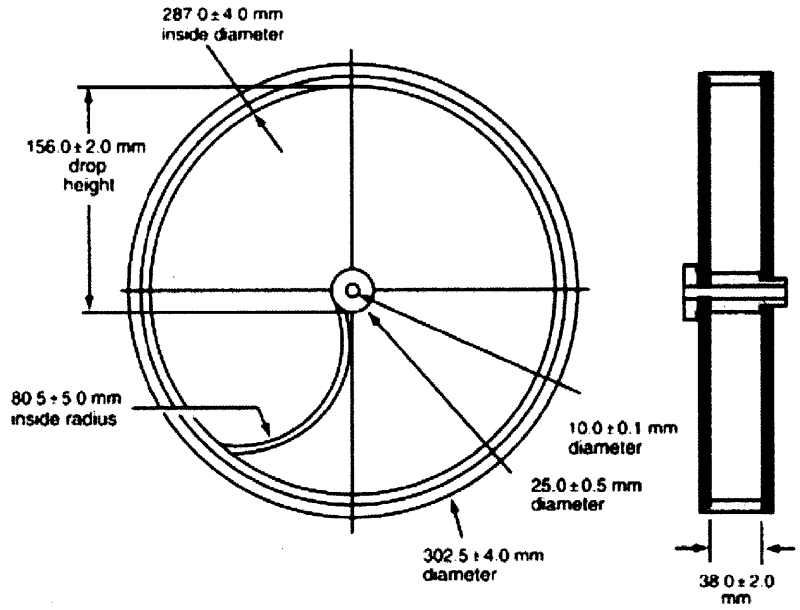

Figure 1-6 USP Standard tablet friability apparatus. Adopted from USP 31 Chapter <1216>

1.3.2.3 Pharmacological Properties

Pharmacology refers to the study of interactions between a living organism and chemicals, and the consequently altered biological functions. It mainly includes pharmacokinetics (PK) and pharmacodynamics (PD). PK refers to the impact of body on the drug, e.g., the plasma drug concentration vs. time, while PD refers to the impact of drug on the body, e.g., efficacy and toxicity profile. Both PK and PD are *in vivo* studies. In order to develop an *in vitro* tool to mirror the *in vivo* activities, the pharmaceutical industry started with disintegration test and settled with dissolution test. It is worth clarifying that disintegration test and dissolution test are different from the disintegration and dissolution of tablets. The former are tests and the latter are processes.

As early as 1950, disintegration test was adopted in US Pharmacopeia 14 as an *in vitro* method for assessing bioavailability. It combines mechanical shear force and hydrodynamics penetration to expedite the disintegration of the tablet and record the time it takes to complete. The disintegration apparatus consists of a basket rack holding six plastic tubes open at the top and bottom. The bottom is covered with a 10 mesh screen. The tubes are immersed in a suitable liquid (often water) at 37°C and moves up and down

at 30 RPM. One tablet is placed into each tube and the time for the tablet to disintegrate and fall through the screen is taken as the disintegration time. Disintegration time does not necessarily indicate complete dissolution of the tablet, neither does it have good correlation with *in vivo* PK. It was found out that gastric movement creates a much milder mechanical stress than the disintegration test(17). Disintegration test is currently used in quality control for batch-to-batch variation, but is not used to provide too much additional information about tablet properties.

The shortfalls of disintegration test were soon realized by the industry. Dissolution test, in which the concentration of dissolved active ingredient in a preset agitation regime is tracked against time, emerged as a closer resemblance of the *in vivo* activities. In 1957, Nelson demonstrated that the blood level of orally administered theophylline salts was directly related with their in vitro dissolution rates (18). In 1960s and 70s, studies started to emerge demonstrating the impact of dissolution rate on bioavailability (19-21). A study of digoxin bioavailability demonstrated that different formulations of digoxin yielded up to sevenfold of difference in serum digoxin level (22). After years of experiments with different setups, a rotating basket dissolution test was first adopted as a standard test method (USP #1) by USP 18 in 1970. As early as 1976, USP essentially requires most of tablets and capsules to have dissolution requirement. In another two years, a rotating paddle dissolution test was adopted as USP #2 test by USP and soon gained popularity partially due to its simple design. There are 7 compendial dissolution tests currently in USP, but the basket test and paddle test remain the dominant tests used by the industry.

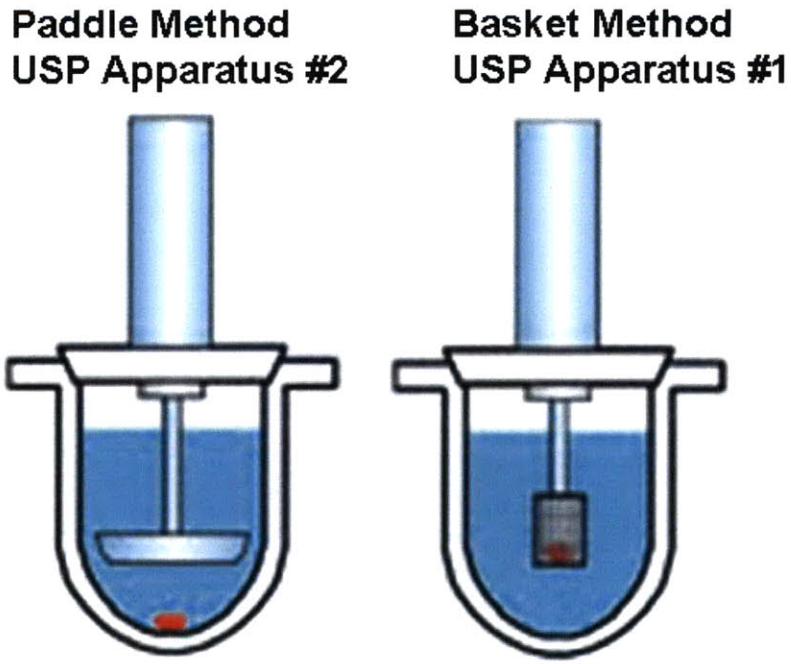

Figure 1-7 Illustration of paddle and basket dissolution setup. Adapted from Jascofrance, Inc.

An illustration of the basket and paddle dissolution apparatus is shown in Figure 1-7. Both tests are utilizing the same dissolution vessels, typically with a 1L volume. The vessels are immersed in a water bath or bathless heating jacket, with a typical temperature of 37-37.5 °C. The difference is in the mechanism of agitation. Basket method utilizes a rotating basket, with tablet placed inside. The basket is made from stainless steels and has an inner diameter/height of 20mm/27mm. The basket is positioned so that the bottom is 25mm away from the vessel bottom. The side wall and bottom wall are screens with welded seam of specified diameter and openings. The tablet goes through dissolution when in contact with the medium agitated by the rotating basket. Basket dissolution has a series of drawbacks, where the complexity of hydrodynamics inside the basket is to be blamed. There is a high shear region near the side wall, ejecting disintegrated tablet fragments out of the mesh, while at the bottom region of the basket the agitation is relatively mild, where the fragments are often deposited until dissolved (23, 24). Simulation of basket hydrodynamics with Computational Fluid Dynamics (CFD) suggests that when a tablet lays flat at the bottom of the basket, free convection contributes significantly to the dissolution process (24) (Figure 1-8). Unfortunately, the

position of the tablet inside of the basket is not consistent. It was often observed that a tablet could flow atop the basket, lean against the side wall, or lay flat on the bottom. The very complex nature of the hydrodynamics in this small basket makes it difficult to understand how dissolution is impacted by the surrounding flow patterns.

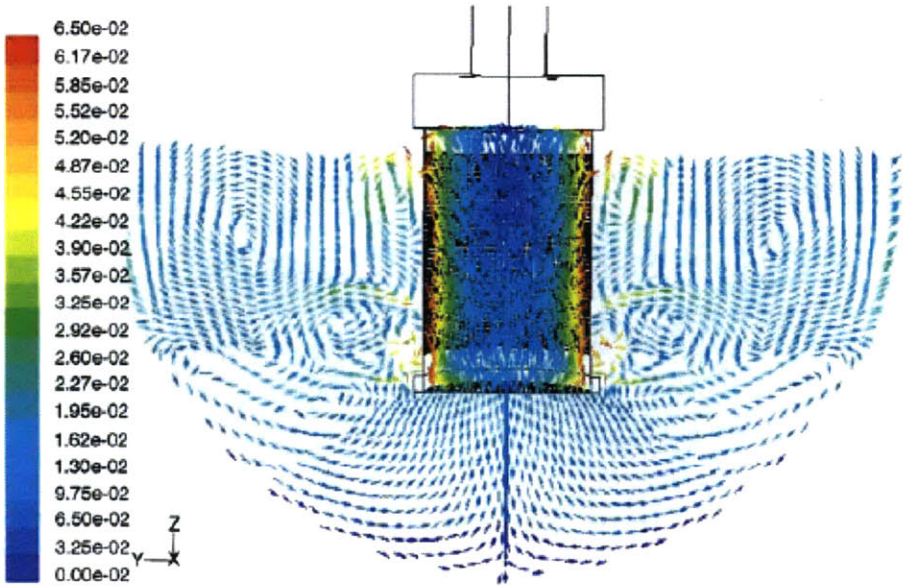

Figure 1-8 CFD simulation of hydrodynamics in USP basket dissolution. Adapted from D' Arcy, et al., 2006

The paddle dissolution method utilizes agitation of a center-shafted paddle to drive medium flow. The tablet typically sits in the hemispherical bottom region of the vessel, but could be floating if density is low. The paddle has an upper width of 75mm and a lower width of 42mm, with a height of 19mm. The paddle is positioned so that the lower edge is 25mm away from the vessel bottom. Paddle dissolution is currently the most widely used method, due to its simplicity of design and the ambient amount of data on In-Vitro-In-Vivo Correlation (IVIVC). The hydrodynamics situation of paddle dissolution is also relatively complex. From CFD simulation (25) and experimental results, it is observed that right under the paddle there is a region with highly unpredictable swirling flows (Figure 1-9). This region, nicknamed the "dead zone", is often the region that tablet sits in during most of the dissolution period. The flow speed at 1cm away from the bottom center could be three times as high as that at the bottom center, so the positioning of the tablet could potentially have a big impact on the dissolution results (26). Tablet

could also collapse into a pile of debris, further complicating the understanding of the dissolution mechanism and impede IVIVC studies.

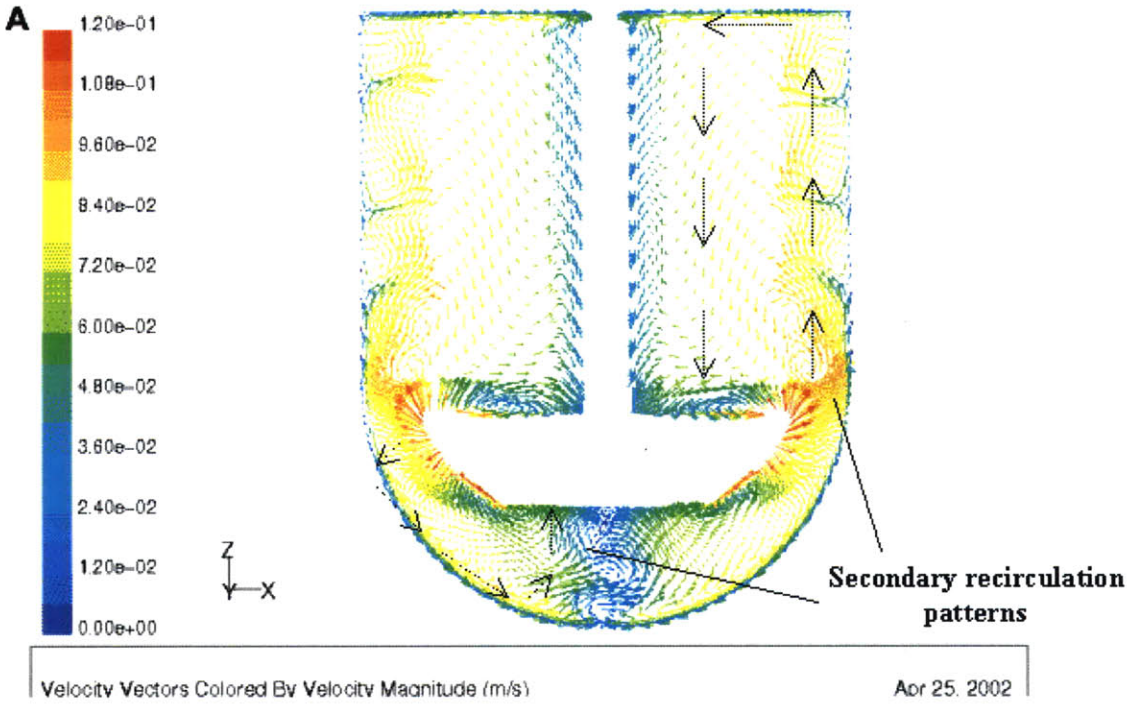

Figure 1-9 CFD simulation of hydrodynamics in USP paddle dissolution test, 50 RPM, adapted from McCarthy, et al., 2003

In spite of the difficulty in hydrodynamics investigation and thus mechanistic understanding, dissolution has been widely adopted by the pharmaceutical industry in multiple functionalities (Figure 1-10). It is being used extensively in formulation development as an *in vitro* bioavailability test, establishing IVIVC. Dissolution is a routine quality assurance test in examining batch-to-batch reproducibility and influences the decision of product release. Failed dissolution tests resulted in 14 product recalls in 1999, which is 18% of non-manufacturing recalls for oral solid dosages of the year (27). The numbers climbed to 20 and 24% for the year of 2000 (28). More recently, dissolution is used in approval of scale-up / post-approval changes (SUPAC) (29, 30), which allows the pharmaceutical companies to optimize the manufacturing procedures after the approval of the initial manufacturing setup. The most notable recent development lies in the central role of dissolution test in determining biowaiver eligibility of certain immediate-release dosage forms (31). Since in vivo bioavailability and

bioequivalence study is costly to conduct, this development represents a powerful cost-saving functionality provided by the dissolution test.

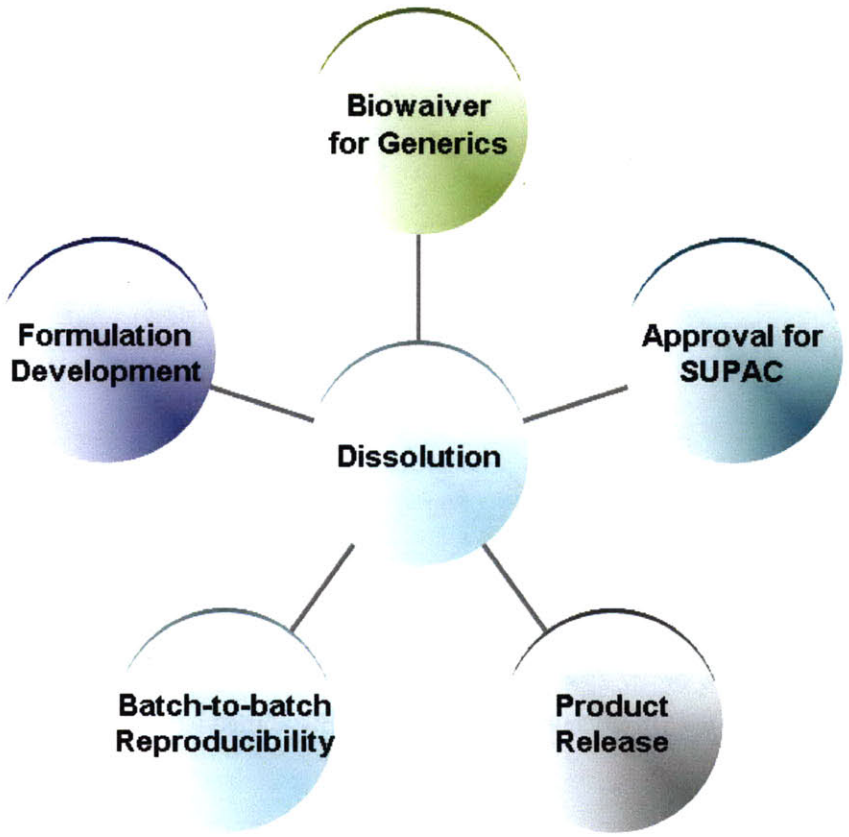

Figure 1-10 The central position of dissolution test in pharmaceutical industry functionalities.

1.3.3 Tablet Microstructure

Pharmaceutical tablets are typically produced from powders of active ingredients and excipients via the process of compaction. The internal microstructure of tablets often takes a porous configuration that depends on the nature of the raw materials and the compaction process itself. Such a microstructure has a direct impact on the quality of the pharmaceutical tablets. Tablet bulk porosity was demonstrated to have an exponential relationship with tablet tensile strength (32), while increasing pore size within a tablet has a negative impact on tensile strength (33). Porosity can also directly impact dissolution. When diffusion through the outer layer is the rate limiting step of the process, high porosity leads to fast dissolution in both pharmaceutical granules (34) and tablets (35) due to a larger surface area. Quantitative characterization of the microstructure will help

understand tablet properties and thus facilitate rational formulation design based on material properties and processing conditions.

In pharmaceutical science, common experimental techniques to study porosity are helium pycnometry, gas adsorption and mercury porosimetry. Helium pycnometry is used to measure the "true density" of the powders, based on which a theoretical bulk porosity of the tablet can be calculated (36). Gas adsorption has been adopted to measure tablet internal surface area (37). Mercury porosimetry is the only method capable of measuring a pore size distribution of the tablet and has been widely utilized in the pharmaceutical industry for this purpose (38). It involves the intrusion of mercury at high pressure into a material. The pore size can be determined based on the external pressure needed to force the liquid into a pore against the opposing force of the liquid's surface tension (Figure 1-11). However, it was indicated that in pharmaceutical granules, the pore diameter it measures is the diameter of the necks connecting the pores, and it can not reach the pores that are isolated from external connections (39). It records the total volume of pores at a certain indicated diameter but does not contain individual pore information. It also does not contain any location-dependant information, while it is known that uni-axially compacted tablets have anisotropic density and porosity distribution (40, 41). Furthermore, it is destructive and environmentally hazardous.

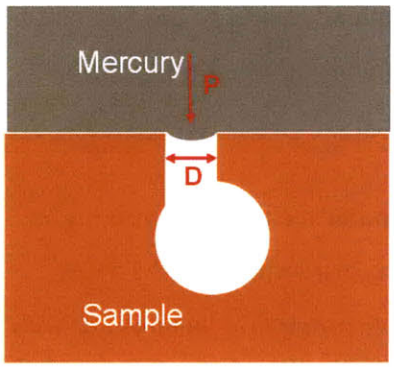

Based on a capillary law for non-wetting liquid, the Washburn Equation:

$$D = -4 \gamma \cos(\theta) / P$$

Where:

- γ **: surface tension of pure mercury (480 dyne/cm)**
- θ **: contact angle between mercury and the solid**
- **P: mercury penetration equilibrated pressure**
- **D: pore diameter**

Figure 1-11 Illustration and theory of mercury porosimetry.

The current standard methods fail to provide adequate and accurate information of tablet microstructure. With the recent advancement in microscopic and tomographic sciences, new approaches have become available to characterize tablet microstructure. Donoso et

al. used near-infrared (NIR) diffuse reflectance spectroscopy to predict porosity of theophylline tablets and obtained generally good agreement with results from helium pycnometry (42). Similar tests were conducted on Metoprololtartrate tablets not only with NIR but also with Raman spectroscopy (43). These studies indicate an opportunity for on-line porosity monitoring, but no detailed porosity profile information is obtained. Wu et al. analyzed scanning electronic microscopic (SEM) images of different mechanically-cut sections of sodium chloride tablets with a binarization method and showed an increase in porosity toward the bottom of a tablet and a preferred orientation of the pores in the direction of compaction (40). In a follow-up study, they further adopted a digital processing method called a morphological sieve (44). A porosity profile was obtained after filtration of floating grains and small pores in SEM images. The degree of filtration is determined so that bulk porosity is in good agreement with data obtained from traditional methods. As a result, this method does not provide an independent characterization of porosity profile.

Micro computed tomography (microCT) is a promising technology that has emerged in the last decade with potentially sufficient resolution power to probe tablet microstructure. In Chapter 4 & 6, we will discuss novel methods in applying microCT toward tablet microstructure study, revealing microstructure information that has never been accessible in the past. The new information is critical in aiding our understanding of the formation and impact of microstructure, bringing us one step closer toward rational formulation design.

The development of microCT technology also leads to a similar technology with higher resolution, the nanoCT. MicroCT currently has a maximum resolution of 1 – 10 μm / pixel, while nanoCT can reach 50 – 150 nm / pixel. Another promising technology with a maximum resolution of 5 – 20 nm / pixel is focused ion beam scanning electron microscopy (FIB-SEM). It transforms the traditional SEM from 2-D into 3-D by utilizing an ion beam to cut off sample slides between SEM scans. A preliminary study using FIB-SEM is described in Chapter 7, demonstrating its potential as well as problems.

1.4 Chapter Bibliography

1. G. Alderbornand C. Nystrom. Pharmaceutical Powder Compaction Technology, Marcel Dekker, Inc, 1996.
2. G.J. Prabir Basu, Saket Rai, Pradeep Suresh and John Vernon. Analysis of Manufacturing Costs in Pharmaceutical Companies Journal of Pharmaceutical Innovation. 3:30-40 (2008).
3. D. McCormick. Evolutions in Direct Compression. Pharmaceutical Technology. 29:52-63 (2005).
4. G. Schepky. Preformulation - the Role of Moisture in Solid Dosage Forms. Drug Development and Industrial Pharmacy. 15:1715-1741 (1989).
5. C.Q. Sunand D.J.W. Grant. Effects of initial particle size on the tableting properties of L-lysine monohydrochloride dihydrate powder. International Journal of Pharmaceutics. 215:221-228 (2001).
6. N.E.F. J. Jaffe. Compression of crystalline substances. J Amer Pharm Ass Sci Ed. 48:9 (1959).
7. Y.S. Feng, D.J.W. Grant, and C.C. Sun. Influence of crystal structure on the tableting properties of n-alkyl 4-hydroxybenzoate esters (Parabens). Journal of Pharmaceutical Sciences. 96:3324-3333 (2007).
8. C.Q. Sunand D.J.W. Grant. Influence of crystal structure on the tableting properties of sulfamerazine polymorphs. Pharmaceutical Research. 18:274-280 (2001).
9. T. Sebhatu, A.A. Elamin, and C. Ahlneck. Effect of Moisture Sorption on Tabletting Characteristics of Spray-Dried (15-Percent Amorphous) Lactose. Pharmaceutical Research. 11:1233-1238 (1994).
10. C.Q. Sunand D.J.W. Grant. Compaction properties of L-lysine salts. Pharmaceutical Research. 18:281-286 (2001).
11. C.K. Tye, C.C. Sun, and G.E. Amidon. Evaluation of the effects of tableting speed on the relationships between compaction pressure, tablet tensile strength, and tablet solid fraction. Journal of Pharmaceutical Sciences. 94:465-472 (2005).
12. C.E. Rueggerand M. Celik. The influence of varying precompaction and main compaction profile parameters on the mechanical strength of compacts. Pharmaceutical Development and Technology. 5:495-505 (2000).
13. J.P.D. Hartog. Advanced Strength of Materials, McGraw-Hill, New York, 1952.
14. J.T. Felland J.M. Newton. Determination of Tablet Strength by Diametral-Compression Test. Journal of Pharmaceutical Sciences. 59:688-& (1970).
15. S. Tomoshenko. Theory of Elasticity, McGraw-Hill, New York, 1934.
16. E. Rudnicand J.B. Schwartz. Remington's Pharmaceutical Sciences, A. R. Mack Publishing Company, Easton, Pennsylvania, 1990, pp. 1633-1665.
17. A. Guyot-Herman. Tablet disintegration and disintegrating agents. STP Pharma Sci. 2:445-462 (1992).
18. E. Nelson. Solution rate of theophylline salts and effects from oral administration. J Am Pharm Assoc. 46:607-614 (1957).
19. G. Levy. Effect of dosage form properties on therapeutic efficacy of tolbutamide tablets. Can Med Assoc J. 90:978-979 (1964).
20. A.B. Varley. The generic inequivalence of drugs. Journal of American Medical Association. 206:1745-1748 (1968).

21. C. MacLeod, Rabin, H., Ruedy, J., Caron, M., Zarowny, D., Davies, R.,. Comparative bioavailability of three brands of ampicillin. Can Med Assoc J. 107:203-209 (1972).
22. J. Lindenbaum, Mellow, M.H., Blackstone, M.O., Butler Jr., V.P.,. Variation in biologic availability of digoxin from four preparations. N Engl J Med. 285:1344-1347 (1971).
23. M. Morihara, N. Aoyagi, N. Kaniwa, N. Katori, and S. Kojim. Hydrodynamic flows around tablets in different pharmacopeial dissolution tests. Drug Development and Industrial Pharmacy. 28:655-662 (2002).
24. D.M. D'Arcy, O.I. Corrigan, and A.M. Healy. Evaluation of hydrodynamics in the basket dissolution apparatus using computational fluid dynamics - Dissolution rate implications. European Journal of Pharmaceutical Sciences. 27:259-267 (2006).
25. L.G. McCarthy, C. Kosiol, A.M. Healy, G. Bradley, J.C. Sexton, and O.I. Corrigan. Simulating the hydrodynamic conditions in the United States Pharmacopeia paddle dissolution apparatus. AAPS PharmSciTech. 4:E22 (2003).
26. D.M. D'Arcy, O.I. Corrigan, and A.M. Healy. Hydrodynamic simulation (computational fluid dynamics) of asymmetrically positioned tablets in the paddle dissolution apparatus: impact on dissolution rate and variability. Journal of Pharmacy and Pharmacology. 57:1243-1250 (2005).
27. The Gold Sheet, *FDC Reports*, 34 (2), 2000, pp. 1-15.
28. The Gold Sheet, *FDC Reports*, 35 (3), 2001, pp. 1-19.
29. FDA. Guidance for Industry: SUPAC IR, 1995.
30. FDA. Guidance for Industry: SUPAC MR, 1997.
31. FDA. Guidance for Industry: Waiver of In Vivo Bioavailability and Bioequivalence Studies for Immediate-Release Solid Oral Dosage Forms Based on a Biopharmaceutics Classification System, 2000.
32. E. Ryshkewitch. Compresssion strength of porous sintered alumina and zirconia. Journal of American Ceramics Society. 36:65-68 (1953).
33. A.M. Juppo. Relationship between breaking force and pore structure of lactose, glucose and mannitol tablets. International Journal of Pharmaceutics. 127:95-102 (1996).
34. M.A. Ansariand F. Stepanek. The effect of granule microstructure on dissolution rate. Powder Technology. 181:104-114 (2008).
35. M. Delalondeand T. Ruiz. Dissolution of pharmaceutical tablets: The influence of penetration and drainage of interstitial fluids. Chem Eng Process. 47:370-376 (2008).
36. C.Q. Sun. A novel method for deriving true density of pharmaceutical solids including hydrates and water-containing powders. Journal of Pharmaceutical Sciences. 93:646-653 (2004).
37. C. Gustafsson, H. Lennholm, T. Iversen, and C. Nystrom. Evaluation of surface and bulk characteristics of cellulose I powders in relation to compaction behavior and tablet properties. Drug Development and Industrial Pharmacy. 29:1095-1107 (2003).
38. A.M. Juppo. Porosity parameters of lactose, glucose and mannitol tablets obtained by mercury porosimetry. International Journal of Pharmaceutics. 129:1-12 (1996).

39. L. Farber, G. Tardos, and J.N. Michaels. Use of X-ray tomography to study the porosity and morphology of granules. Powder Technology. 132:57-63 (2003).
40. Y.S. Wu, H.W. Frijlink, L.J. van Vliet, I. Stokroos, and K.V.V. Maarschalk. Location-dependent analysis of porosity and pore direction in tablets. Pharmaceutical Research. 22:1399-1405 (2005).
41. A. Djemaiand I.C. Sinka. NMR imaging of density distributions in tablets. International Journal of Pharmaceutics. 319:55-62 (2006).
42. M. Donoso, D.O. Kildsig, and E.S. Ghaly. Prediction of tablet hardness and porosity using near-infrared diffuse reflectance spectroscopy as a nondestructive method. Pharmaceutical Development and Technology. 8:357-366 (2003).
43. R.B. Shah, M.A. Tawakkul, and M.A. Khan. Process analytical technology: Chemometric analysis of Raman and near infra-red spectroscopic data for predicting physical properties of extended release matrix tablets. Journal of Pharmaceutical Sciences. 96:1356-1365 (2007).
44. Y.S. Wu, L.J. van Vliet, H.W. Frijlink, and K.V. Maarschalk. Pore size distribution in tablets measured with a morphological sieve. International Journal of Pharmaceutics. 342:176-183 (2007).

Chapter 2 Characterization of Caffeine-Lactose Tablet Compaction and Tablet Properties

Lactose has been used as a common excipient in the pharmaceutical industry for more than 50 years (1), while caffeine is often a model drug for development and characterization of formulations (2, 3). In previous Ph.D. theses of the Cooney lab, the micro and macro properties of the materials and case studies in pharmaceutical manufacturing were thoroughly investigated. Inter-particle forces were characterized with atomic force microscopy measurements (4, 5). Performance of spray-dried lactose and caffeine in various continuous blending scenarios was investigated experimentally (4, 6) and modeled with discrete element method (DEM) simulation (4, 7). Physical and mechanical properties of the powder granules as well as tablets were evaluated (8). In this chapter, we describe the manufacturing and characterization of caffeine-lactose directly compressed tablets, which are used as a model system to explore the relationship between tablet microstructure and properties.

2.1 Manufacturing of Caffeine-Lactose Tablets

2.1.1 Powder properties of spray-dried lactose and caffeine

Since its introduction in 1960s, spray dried lactose has demonstrated superior performance in pharmaceutical solid dosage formation, especially in direct compression (1, 9). Spray-dried lactose is manufactured by spray-drying a suspension of α-lactose monohydrate crystals in a saturated aqueous solution of lactose. The final composition for the DCL11 and DCL14 materials (now called SuperTab SD11 and SD14, DMV International) used in this study is 85% α-lactose monohydrate with 15% amorphous lactose, the dried portion of the sprayed lactose solution. The primary material α-lactose monohydrate undergoes fragmentation during compaction process, supplemented with a strong binding capability of the amorphous lactose. The only difference between DCL11 and DCL14 is that DCL14 has slightly smaller primary particle size. The granules are spherical in shape and are generally uniform in size, resulting in superior flowability (Figure 2-1).

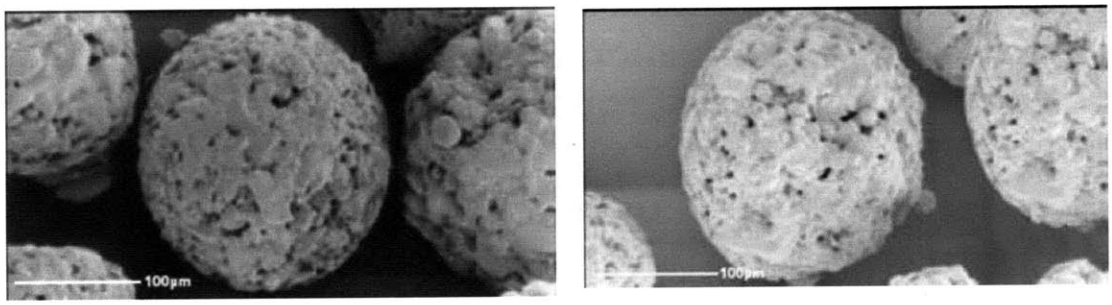

Figure 2-1 Environmental scanning electron microscopic images of DCL11 (left) and DCL14 (right). (DMV International, 2005)

Anhydrous Caffeine (1,3,7-trimethyl Xanthine) is a central nervous system stimulant. The material used in this study is USP grade caffeine powder (Sigma Inc., St. Louis, MO.) It has an irregular particle shape with an average particle size of 196 µm and a standard deviation of about 100 µm. Caffeine is not a free flowing powder and usually agglomerates in the presence of atmospheric moisture. Therefore, proper moisture barrier is critical to maintain original particle size of caffeine powders.

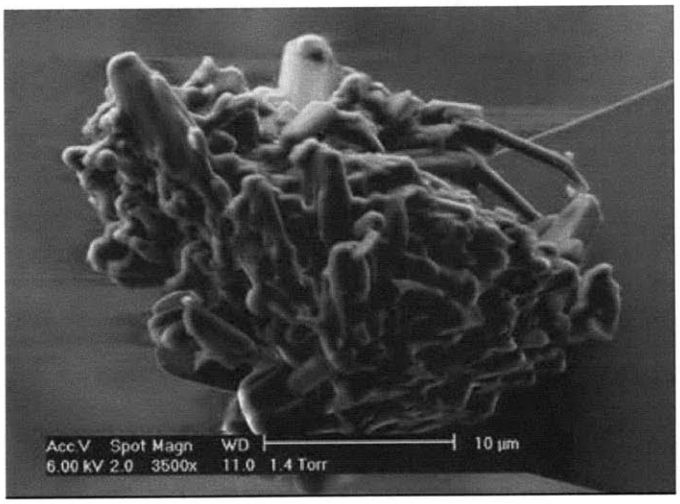

Figure 2-2 ESEM image of caffeine particle. S. Ngai 2005

A third material used in the formulation is magnesium stearate, a commonly used lubricant in pharmaceutical solid dosage forms. In tabletting, lubricant is used for two purposes: one is to enhance the flowability of the powder itself, two is to reduce the friction between the powder and the tooling. Magnesium stearate forms thin layers with very low friction on the surface of the particles in the final mixture, facilitating the relative flowing of the powder.

2.1.2 Manufacturing setup and formulations

Material Preparation

In order to ensure adequate flowability, lactose and caffeine powders were sieved with a standard sieve tester SS-15 (Gilson Company Inc., Ohio) for 5 minutes. Particles in the range of 106-212 μm were collected and equilibrated at 25°C and 20% relative humidity (RH) for 2 days. The powders were then blended at 10 rpm for 15 minutes with a 42ml V-shaped blender at the following composition: 10% Caffeine, 0.5% Magnesium Stearate, and the rest 89.5% in DCL11, DCL14, or half/half. The mixture was stored in air-tight jars before compaction.

Tablet Compaction

Tablet compaction in this study is done with a Korsch EK-0 single station tablet press (Korsch AG, Berlin, Germany) (Figure 2-3). The press is not instrumented, meaning no force data is collected.

- Maximum compression force: 30kN
- Single punch eccentric press
- Maximum speed: 3600 tablets/hr
- Known: fill depth
- Unknown: compression force
  dwell time
- Measurable: weight
  thickness

Figure 2-3 Photo and parameters of Korsch EK-0 tablet press.

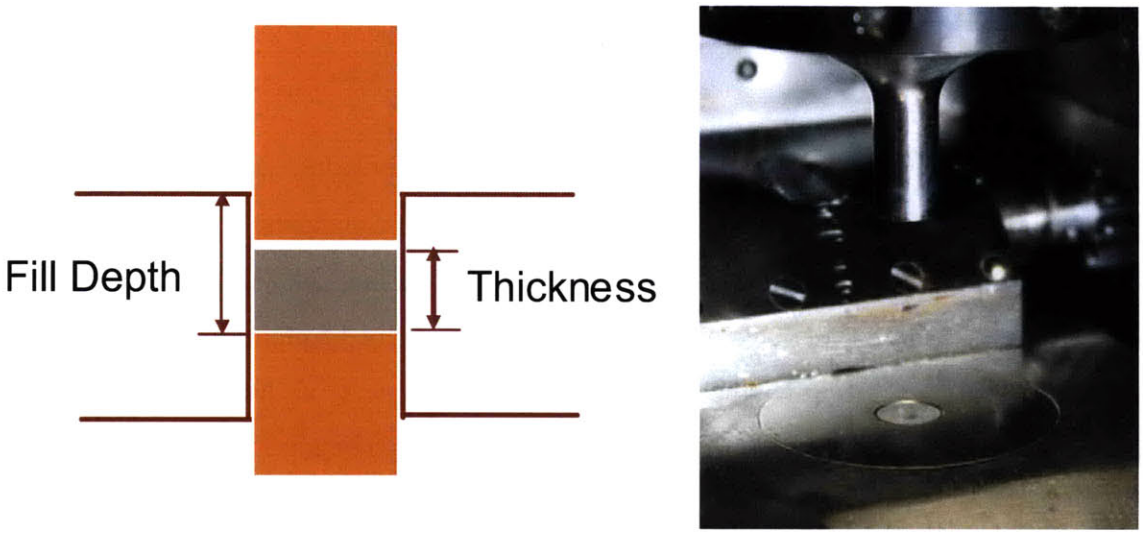

Figure 2-4 Illustration of the tablet compaction station.

In order to obtain a relatively consistent way to manufacture the tablets, three parameters are tracked for the tablet products: weight, thickness, and hardness. Tablet weight is controlled via adjustment of the powder fill depth in the die (Figure 2-4). Tablet thickness is controlled via the insertion depth of the upper punch, while the lower punch remain fixed during compaction. The hardness of the tablet is a direct result of the compaction process and is discussed in detail later. The diameter of the tablet is fixed at 9mm and tabletting speed is fixed at 20 tablets per minute. The weight of the tablet is controlled at 200mg +- 10mg, for which an initial fill depth of 4.8mm is required. Final tablet thickness range from 2.3mm to 3.2mm, representing the hardest and softest tablet that could be produced by the press for the conditions specified.

After compaction, tablets are either placed in glass jars sealed with parafilm^{TM} or in closed containers above over-saturated magnesium nitrite solution, where a relative humidity of 55% is maintained under ambient temperature.

2.2 Tablet Mechanical Strength

The mechanical strength of a tablet is evaluated with a diametrical compression test, which records the minimum force necessary for tablet tensile failure. (For more background information about the test, please refer to section 1.3.2.) The recorded force

is regarded as the "hardness" of the tablet. Tablet hardness is mainly a result of material interaction during the compaction process. In a head-to-head comparison of α-lactose monohydrate, anhydrous α-lactose, roller-dried β lactose and crystalline β lactose, it was revealed that tablet strength is simply a function of tablet internal surface area and does not depend on the crystalline form (10). This suggests that the same binding mechanism applies to all forms of crystalline lactose. For amorphous lactose this is a different story. Increasing amount of amorphous lactose in spray-dried lactose was found to enhance tablet strength without generating a larger internal surface area (11). Moisture could also change the mechanical strength of lactose-dominant tablets. Sebhatu et al. investigated the impact of storage at 55% RH environment pre- and post- compaction for lactose tablet strength (12). It was shown that exposure to high RH for the tablets resulted in higher tablet strength due to crystallization of the amorphous lactose. The amorphous lactose selectively absorbs moisture, reducing glass transition temperature below the operation temperature and facilitating crystallization toward α-lactose. Once the crystallization is completed, most of the absorbed moisture would be released again.

In this study, we first examined the impact of moisture on tablets of different hardness and lactose composition. The formulations tested were 10% Caffeine, 0.5% Magnesium Stearate, and the rest 89.5% in DCL11, DCL14, or half/half. The tablets made had initial powder fill depth of 4.8mm and final tablet thickness of 3.2 mm (soft) or 2.4 mm (hard). The tablets were subjected to 55% RH after compaction. Tablet strength is tracked at various time points until 2 weeks after compaction (Figure 2-5 and Figure 2-6). In general, higher composition of DCL14 leads to slightly higher tablet strength. The smaller size of primary particles in DCL14 could lead to higher surface area for binding, which in turn results in stronger tablets. For tightly compacted caffeine-lactose tablets, all the formulations registered a 15%-20% strength decrease within the first two minutes after compaction. This is due to the elasticity of the materials, which caused the tablet to increase in volume immediately following ejection and breaking some of the bonds established during tabletting (13). No significant change in hardness is observed afterwards, indicating that the low porosity of tightly compacted tablets permits a low level of moisture penetration, reducing the potential impact by moisture.

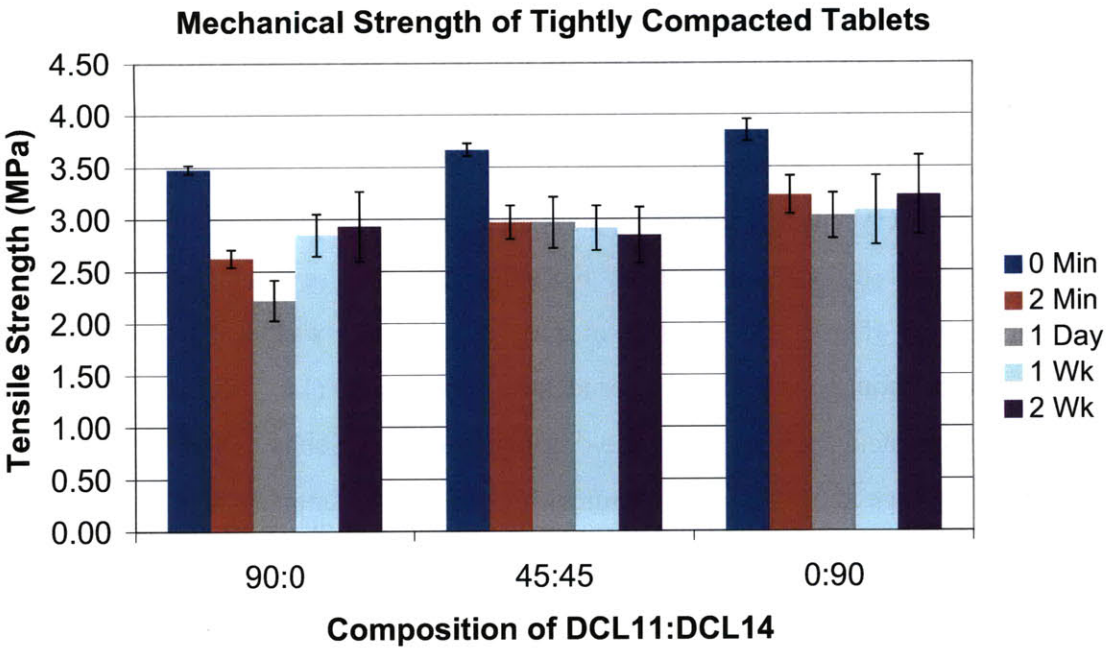

Figure 2-5 Mechanical strength of tightly compacted caffeine-lactose tablets.

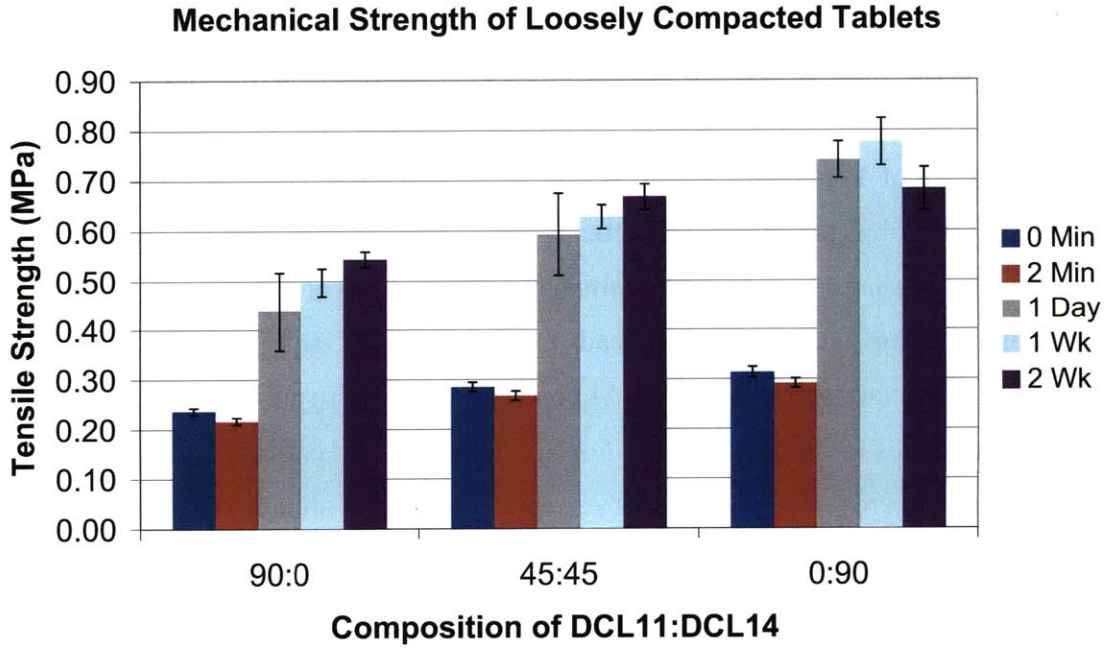

Figure 2-6 Mechanical strength of loosely compacted caffeine-lactose tablets.

The scenario of mechanical strength for loosely compacted tablets is different from that for tightly compacted tablets. The initial strength drop is much smaller when compared with that for tightly compacted tablets, as much less extensive deformation happens in a loose compaction. The impact of high moisture, however, is significant. One day after storage in 55% RH, the tensile strength doubles and remains at the same level throughout the two weeks of testing period. The much more porous tablet structure allows the invasion of moisture into the tablet and probably facilitates crystallization and the establishment of much stronger solid bonds (12).

In a next step, caffeine-DCL11 tablets subjected to various degrees of compaction were further examined for patterns in tensile strength. This time direct readings of crushing force are used instead of the tensile strength. The two are presenting the same mechanical property from slightly different perspectives. Crushing force (or hardness) describes the absolute strength of the tablet, while tensile strength describes the relative strength of the tablet when dimension is taken into consideration. Description of hardness is more common in daily practice of the pharmaceutical industry.

In this new test, tablets were compacted from an original loading powder of 200mg (~4.8mm fill depth) to a range of final tablet thickness from 2.3 to 3.2mm. Hardness at Day 0 (D0) was measured 2 min after compaction. For tablets of all strengths, hardness value does not change significantly across a 4-week storage period within sealed moisture-barrier bags made with alternative layers of aluminum and polyethylene glycol (PEG) (Figure 2-7). When stored in 55% RH, the tablets demonstrated higher hardness after 1 day and maintained the levels thereafter (Figure 2-8). It is also observed that the strength of the tablets in 55% RH had much higher variation when compared with those in moisture bags. It is likely that the penetration of moisture depends on the local microstructure. The lower porosity in hard tablets leads to less accessible internal space and thus a more case-specific impact of moisture. A higher porosity in soft tablets allowed extensive penetration of moisture, leading to much higher impact on tablet strength. The relative strength gain from sealed condition to 54% RH for 3.2mm tablet is 300%, compared with 20% for 2.3mm tablets (Figure 2-9).

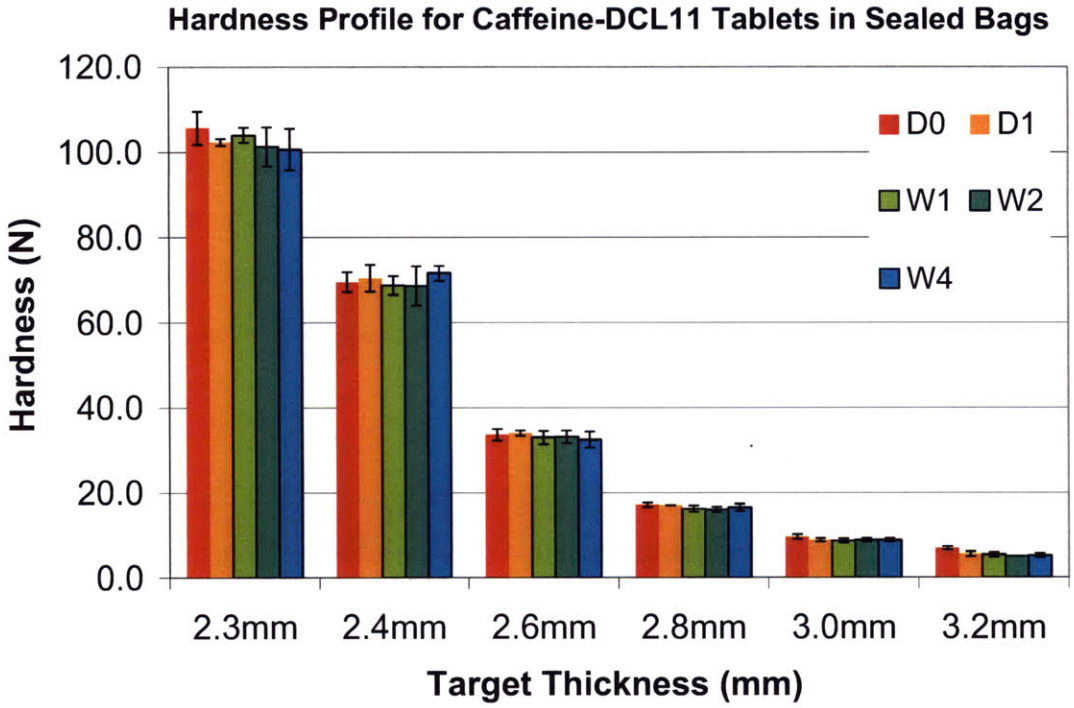

Figure 2-7 Hardness profile for caffeine-DCL11 tablets of different strengths in sealed bags.

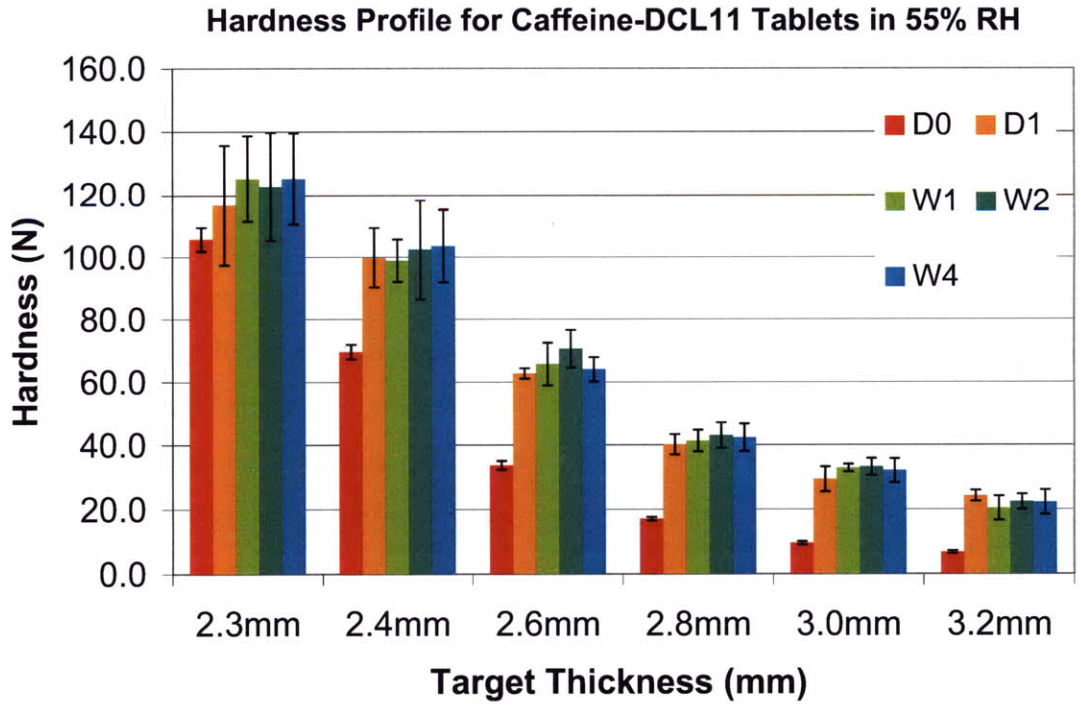

Figure 2-8 Hardness profile for caffeine-DCl11 tablets of different strengths in 55% RH

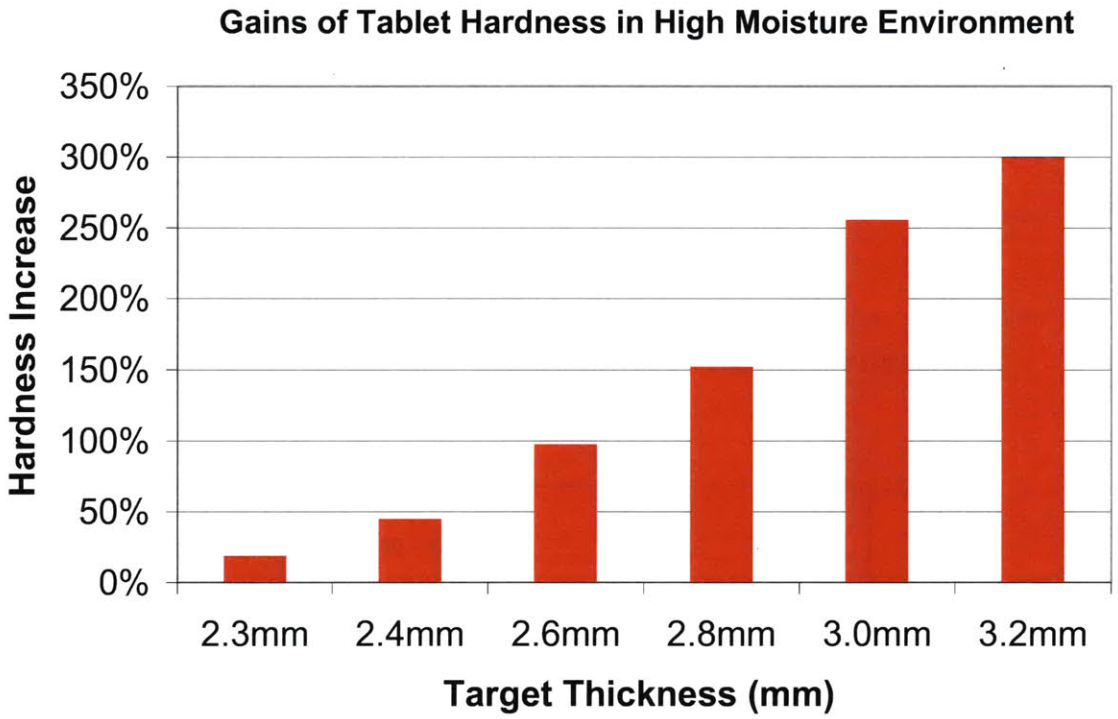

Figure 2-9 Hardness gain for caffeine-DCL11 tablets in 55% RH compared with sealed condition.

2.3 Tablet Dissolution Profiles

As discussed in section 1.3.2.3, dissolution test holds a key position in the analytical tests for pharmaceutical tablets. Dissolution speed was found to have a direct relationship with tablet porosity, but detailed correlation between porosity profile and dissolution speed was not established (14). In another study, it was proposed that the porosity of the tablet could switch the dissolution mechanism between surface dissolution and penetration-induced disintegration (15). The dissolution of lactose has been extensively studied. It was found out that α-lactose goes through a mutarotation reaction and converts to β-lactose (16) (Figure 2-10). The initial solubility of several different formats of lactose powder was measured by Kamp et al. (17). α-lactose was shown to have a much lower solubility than β-lactose (Figure 2-11). Specifically, α-lactose monohydrate has the lowest solubility. The final solubility would be the same due to mutarotation reaction in favor of the β-lactose with higher solubility.

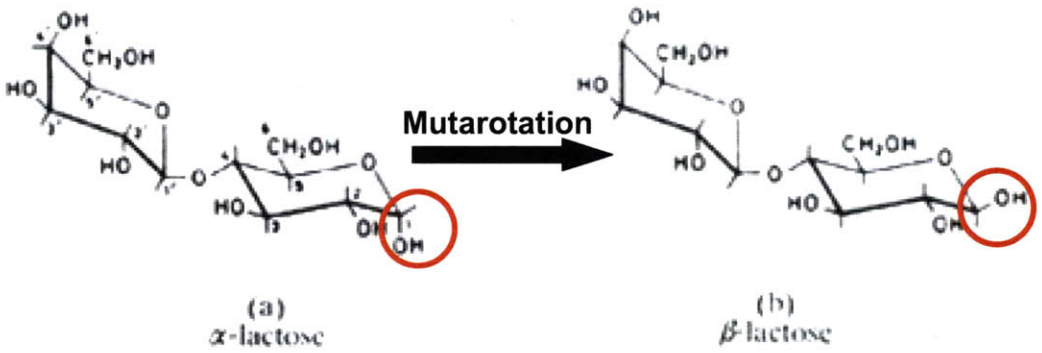

Figure 2-10 Mutarotation reaction of lactose. Modified from lactose.com.

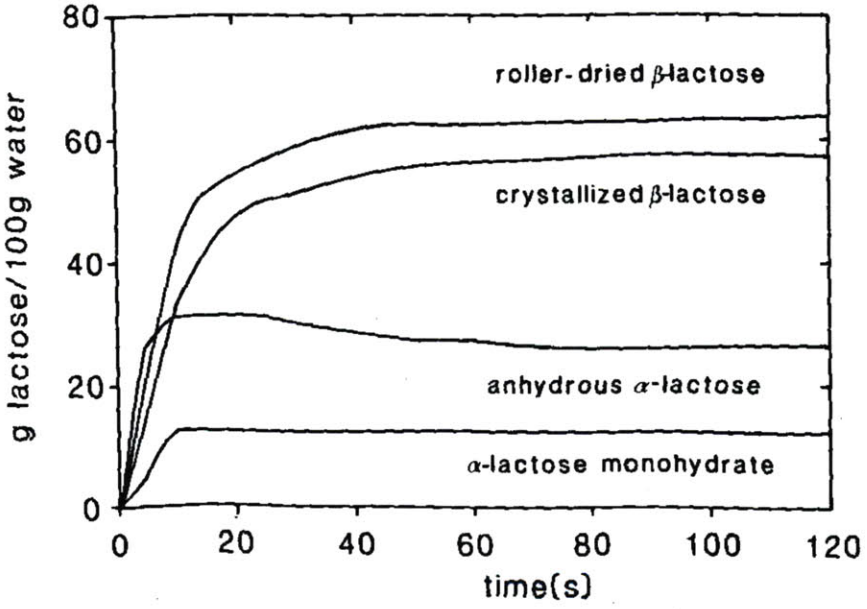

Figure 2-11 Initial solubility profile of different crystalline lactose powders in 37 °C water. Kamp et al. 1986.

In disintegration testing, tablets made of α-lactose monohydrate had very short disintegration time, while tablets made of amorphous α-lactose dissolved gradually instead of disintegration. The lack of disintegration was attributed to both a small pore size and the precipitation of α-lactose monohydrate in pore space due to lower initial solubility (17).

In the current study, dissolution testing was conducted with a Varian VK7010 dissolution apparatus (Varian Inc, Palo Alto, CA) coupled with a C-Technologies IO® fiber-optic

system (C-Technologies, Bridgewater, NJ), which directly transmits the light signal acquired in the dissolution medium to a Varian Cary50 spectrophotometer (Varian Inc, Palo Alto, CA). The specific UV absorbance of the API is compared with a calibration curve, based on which the concentration of API in the dissolution medium is calculated. During the calibration stage, no signal interference from lactose or magnesium stearate was observed at the 273nm characteristic wavelength adopted for caffeine measurement. The whole caffeine concentration range during dissolution fell into the linear response zone of the 10mm fiber-optic heads used for signal collection. Paddle dissolution test was adopted with 50 RPM agitation and 900ml water dissolution medium at 37°C.

During agitation, the air dissolved in the dissolution medium might form bubbles on the surface of tablets, altering the dissolution behavior. A degassing procedure was performed on dissolution medium immediately before testing. The steps are as follows: Heat the medium up to 41°C with gentle agitation, then filter the medium through 0.47um filtration system under vacuum with strong agitation. Keep the vacuum and agitation on for 5 min, with proper heating to keep medium temperature at 37 °C. Using a funnel, carefully pour 900ml medium along the wall of the vessel without generating a lot of bubbles. Wait 15 minutes for temperature equilibration before conducting experiments.

Paddle dissolution profiles were collected for caffeine-DCL11 tablets of various strengths at different time points up to 2 weeks post compaction. The tablets were stored in closed glass jars in ambient condition and sealed with parafilm™. At one day after compaction, most of the dissolution profiles were well separated from each other, with the exception of the two softest tablets (Figure 2-12). The situation changed dramatically by one week of storage, when all the dissolution profiles converge toward a narrow region (Figure 2-13). It is also clear that the dissolution speed for all the tablets slowed down. By two weeks of storage, all the dissolution profiles, except that for the softest tablet, continue to slow down and converge (Figure 2-14). The dissolution profiles seemed to approach a set of limit profile as storage time goes longer (Figure 2-15). As will become clear in chapter 5, the limit profile represents pure surface dissolution whose rate is controlled by convective diffusion.

The next step is to identify the physical/chemical changes that affected the dissolution profiles of the tablets. Caffeine is not considered a factor here, because (a) lactose forms the dominant structure and is thus mainly responsible for the dissolution or disintegration of the tablet matrix, (b) after release from tablet, caffeine dissolution should not be a rate limiting factor, as final concentration of caffeine in dissolution medium is less than 0.1% of its saturated concentration. The solubility of caffeine in water at 37°C is 37 g/L (18), the volume of the dissolution medium is 0.9L, while the total amount of caffeine present in a tablet is 0.02 g. For lactose, a possible interaction with moisture is considered, as parafilm™ was found to be a poor moisture barrier (internal communication with Novartis expert) and the set of experiments was conducted in hot and humid summer time.

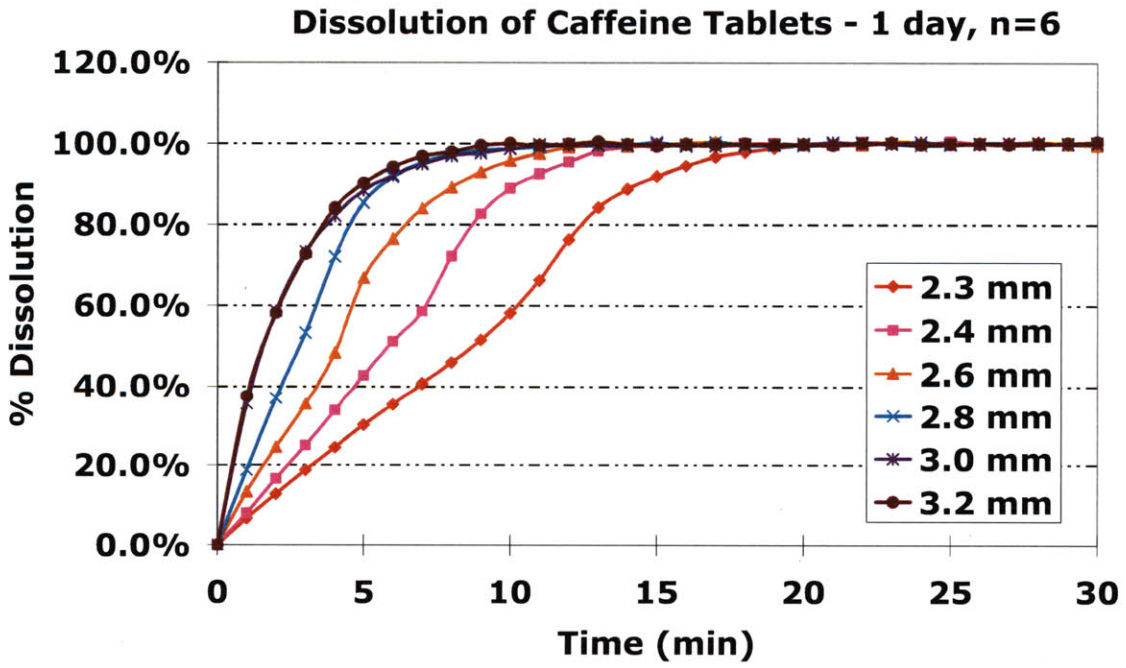

Figure 2-12 Dissolution profiles of caffeine-DCL11 tablets at 1 day after compaction.

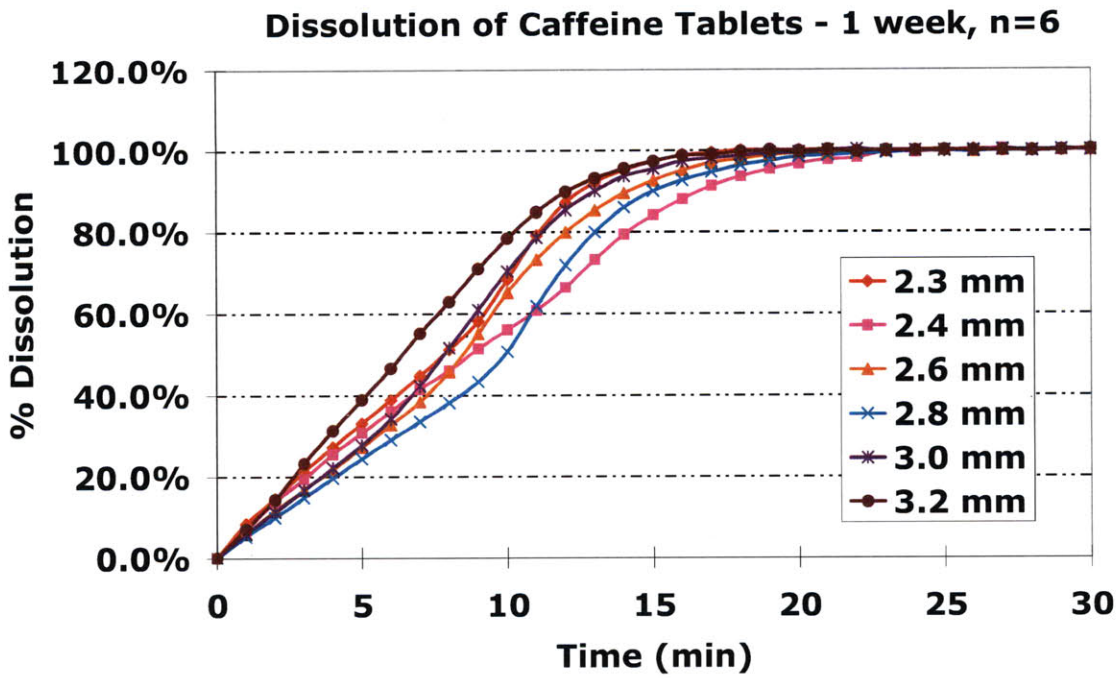

Figure 2-13 Dissolution profiles of caffeine-DCL11 tablets at 1 week after compaction.

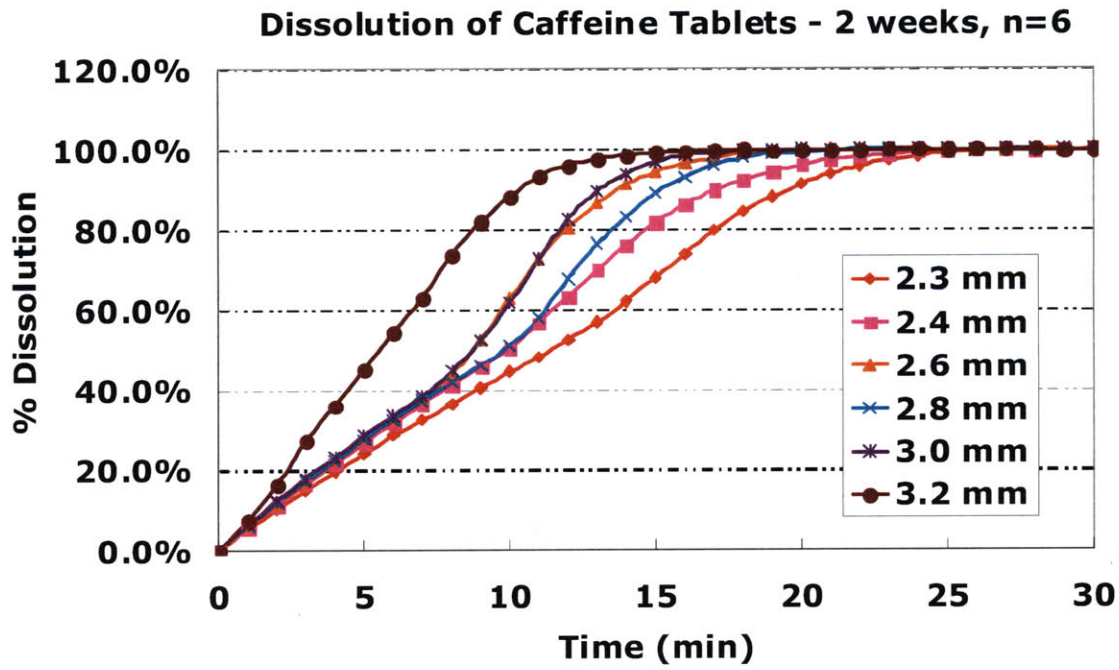

Figure 2-14 Dissolution profiles of caffeine-DCL11 tablets at 2 weeks after compaction.

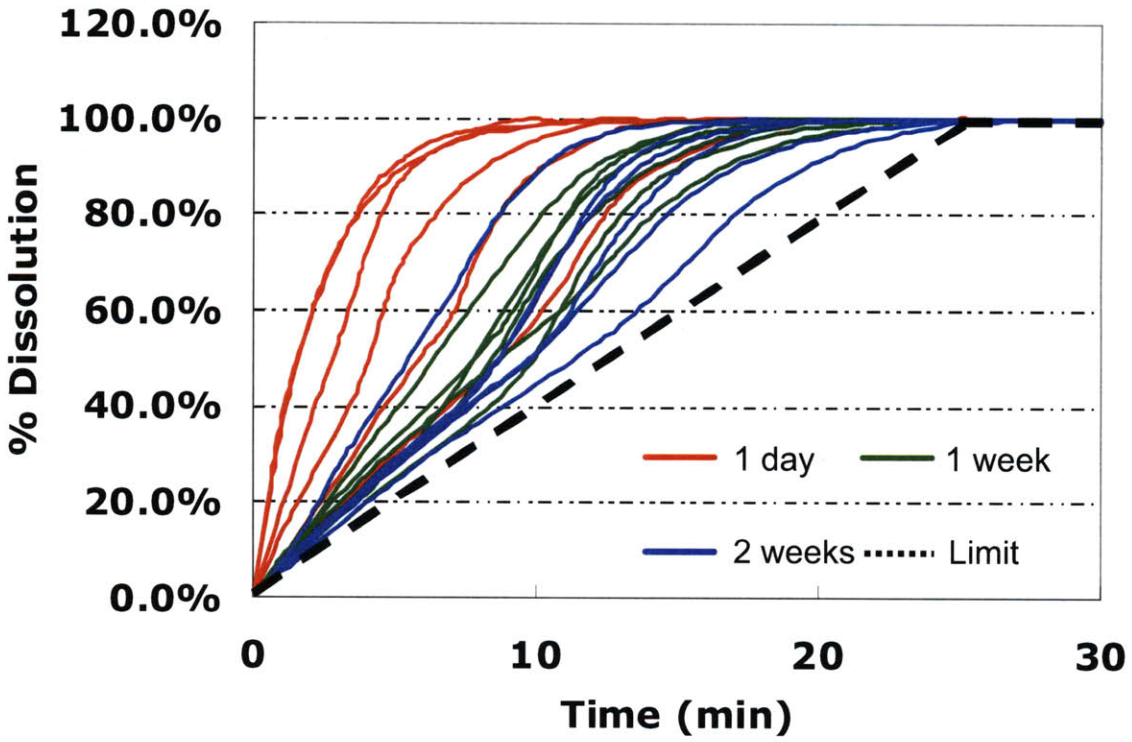

Figure 2-15 Summary of caffeine-DCL11 tablet dissolution profiles within 2 weeks after compaction

In order to verify the impact of moisture, the above experiments were repeated with two sets of storage conditions: in sealed moisture barrier bags and in 55% RH humidity chamber at ambient temperature. Dissolution tests were run at 1day, 1 week, 2 weeks, and 4 weeks after compaction. The time required for the completion of 60% dissolution T60 is calculated from the dissolution profiles. In sealed condition, no obvious shift in 60% dissolution time is observed (Figure 2-16). This is in agreement with our assumption that moisture caused the shift of dissolution profiles. In 54% RH condition, except for the hardest tablets, all other tablets experienced moderate slow-down of dissolution speed from 1 day to 1 week post compaction (Figure 2-17). After 1 week, dissolution time remain at the same level. A further examination of T60 was done by combining all the sealed tablet data and comparing that with the 54% RH tablet data after 1 day (Figure 2-18). Higher environmental moisture level leads to apparent slow-down for caffeine-DCL11 tablets with medium to low strength. This may be due to the conversion of amorphous lactose toward α-lactose monohydrate, with the latter having a

lower solubility. The conversion also seemed to lead to a structure that is less susceptible to disintegration, potentially due to the formation of moisture-mediated interparticle-bonding when a higher molecular mobility is incurred (19).

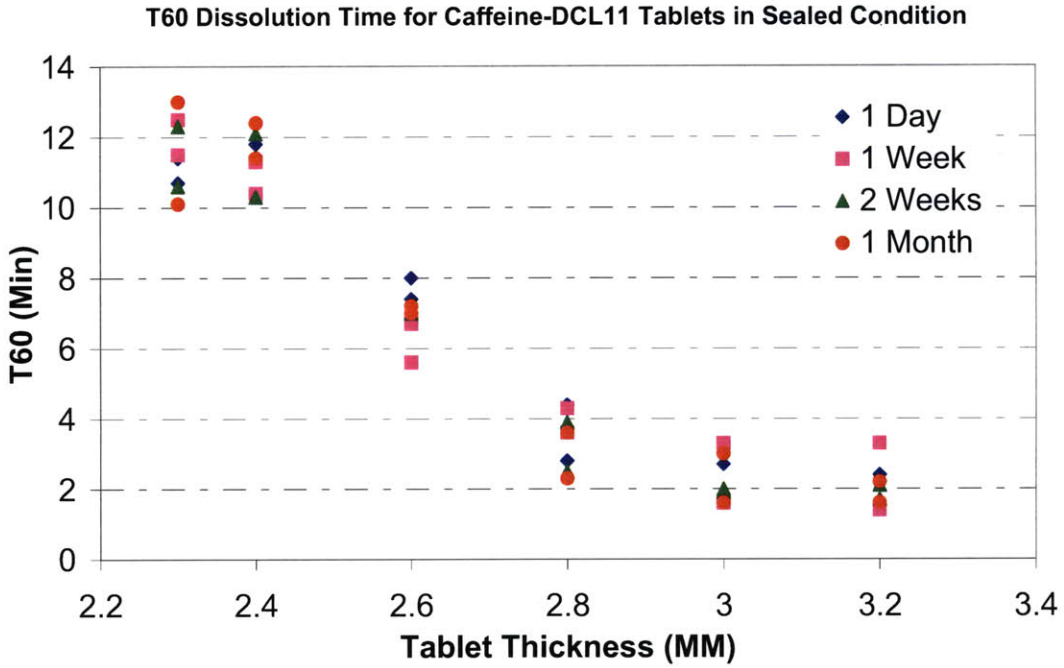

Figure 2-16 60% dissolution time for caffeine-DCL11 tablets in sealed condtion.

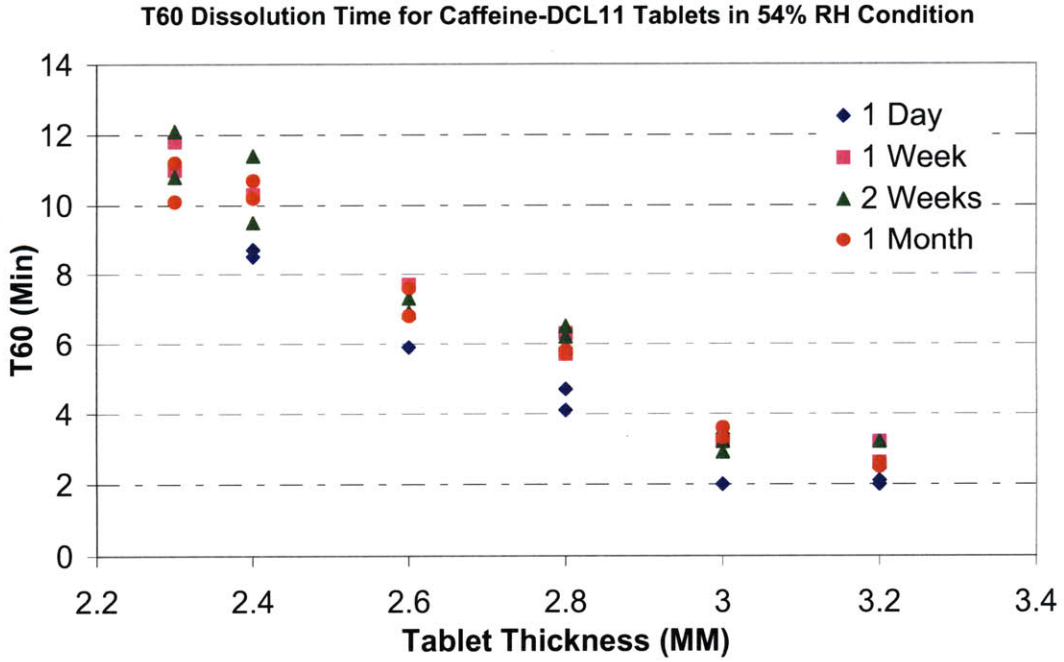

Figure 2-17 60% dissolution time for caffeine-DCL11 tablets stored in 54% RH.

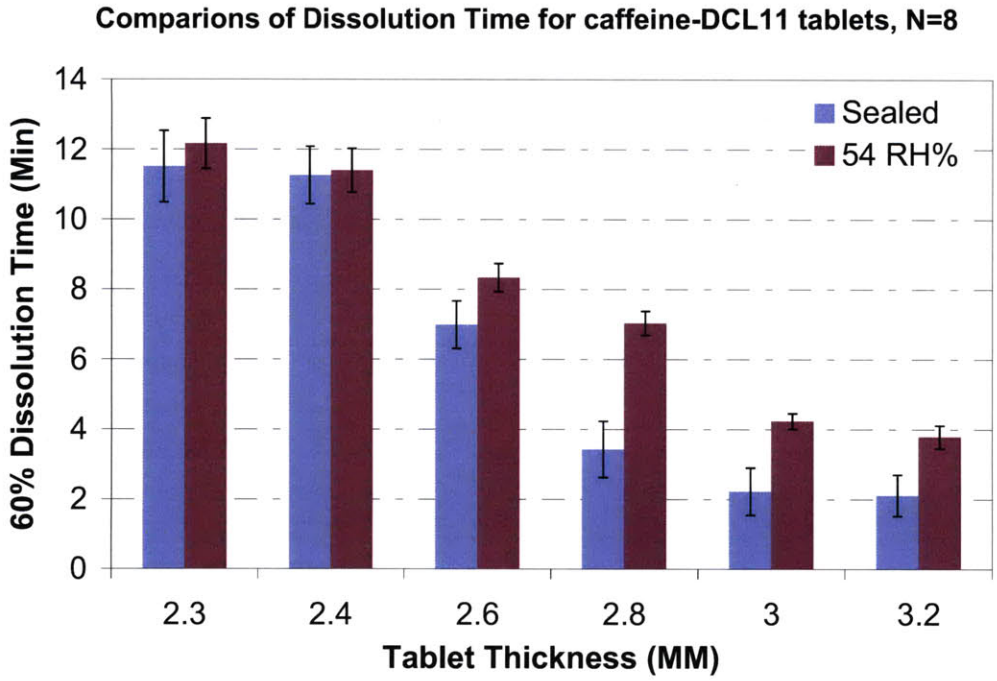

Figure 2-18 Comparison of dissolution time for caffeine-DCL11 tablets in sealed bags and 54% RH.

2.4 Summary

In this chapter we have discussed the manufacturing and testing of caffeine-lactose directly compressed tablets, which are to be used in subsequent studies of microstructure and dissolution mechanism. The impact of composition, compaction degree, and storage moisture level was investigated in terms of tablet mechanical strength and dissolution profiles.

It is demonstrated that tablet hardness drops within the first two minutes post compaction, which we believe is due to tablet elastic expansion and the breakage of inter-particle bonds. The drop is most obvious with the harder tablets, which were subjected to a higher compaction force and thus incurred a higher degree of elastic recovery. Exposure to high level moisture led to an increase in tablet hardness, especially that for the tablets with medium to low strength to start with. A much higher porosity in soft tablets would be expected to allow extensive penetration of moisture, leading to much higher impact on tablet strength. The higher tablet strength under moisture exposure is probably a

combined result of crystallization of amorphous lactose and the establishment of moisture-mediated solid bonds. Usage of DCL14 leads to a slightly higher tablet strength than that of DCL11, with the former having a smaller primary particle size and thus generating a higher surface area for inter-particle bond formation.

A detailed dissolution study was conducted for caffeine-DCL11 tablets. Tablets of various compaction degrees demonstrated distinctive dissolution profiles. Paddle dissolution of harder tablets takes longer to complete than that for softer tablets. However, moisture exposure could lead to conversion of amorphous lactose toward α-lactose monohydrate with lower solubility. The establishment of moisture-mediated solid bonds also seems to deter the disintegration of the caffeine-DCL11 tablets. Combined effect of the two leads to slower dissolution for tablets exposed to high moisture, especially for softer tablets with a much more porous structure to allow effective moisture penetration. The general convergence toward a common dissolution profile limit represents a pure surface dissolution scenario with no disintegration taking place, which we will discuss in detail in Chapter 5.

2.5 Chapter Bibliography

1. W.C. Gunseland L. Lachman. Comparative Evaluation of Tablet Formulations Prepared from Conventionally-Processed and Spray-Dried Lactose. Journal of Pharmaceutical Sciences. 52:178-& (1963).
2. D. Brachteland E. Richter. Absolute Bioavailability of Caffeine from a Tablet Formulation. Journal of Hepatology. 16:385-385 (1992).
3. D. Tan, B. Zhao, S. Moochhala, and Y.Y. Yang. Sustained-release of caffeine from a polymeric tablet matrix: An in vitro and pharmacokinetic study. Materials Science and Engineering B-Solid State Materials for Advanced Technology. 132:143-146 (2006).
4. S.S. Ngai. Multi-Scale Analysis and Simulation of Powder Blending in Pharmaceutical Manufacturing, *Chemical Engineering*, Vol. Ph.D., MIT, Cambridge, MA, 2005.
5. Y. Pu. Theoretical and Experimental Investigation of Particle Interactions in Pharmaceutical Powder Blending, *Chemical Engineering*, Vol. Ph.D., MIT, Cambridge, MA, 2007.
6. L. Pernenkil. Continuous Blending of Dry Pharmaceutical Powders, *Chemical Engineering*, Vol. Ph.D., MIT, Cambridge, MA, 2006.
7. M.J. Abel. Process Systems Engineering of Continuous Pharmaceutical Manufacturing, *Chemical Engineering*, Vol. Ph.D., MIT, Cambridge, MA, 2009.
8. M. Pore. Pharmaceutical Tablet Compaction: Product and Process Design, *Chemical Engineering*, Vol. Ph.D., MIT, Cambridge, MA, 2007.
9. G. Bolhuis, K. Kussendrager, and J. Langridge. New Developments in Spray-Dried Lactose. Pharmaceutical Technology Supplimental Issue EXCIPIENTS & SOLID DOSAGE FORMS:26-31 (2004).
10. A.H. Deboer, H. Vromans, C.F. Lerk, G.K. Bolhuis, K.D. Kussendrager, and H. Bosch. Studies on Tableting Properties of Lactose .3. The Consolidation Behavior of Sieve Fractions of Crystalline Alpha-Lactose Monohydrate. Pharmaceutisch Weekblad-Scientific Edition. 8:145-150 (1986).
11. H. Vromans, G.K. Bolhuis, C.F. Lerk, K.D. Kussendrager, and H. Bosch. Studies on Tableting Properties of Lactose .6. Consolidation and Compaction of Spray-Dried Amorphous Lactose. Acta Pharmaceutica Suecica. 23:231-240 (1986).
12. T. Sebhatu, A.A. Elamin, and C. Ahlneck. Effect of Moisture Sorption on Tabletting Characteristics of Spray-Dried (15-Percent Amorphous) Lactose. Pharmaceutical Research. 11:1233-1238 (1994).
13. A. Adolfssonand C. Nystrom. Tablet strength, porosity, elasticity and solid state structure of tablets compressed at high loads. International Journal of Pharmaceutics. 132:95-106 (1996).
14. M. Riippi, J. Yliruusi, T. Niskanen, and J. Kiesvaara. Dependence between dissolution rate and porosity of compressed erythromycin acistrate tablets. European Journal of Pharmaceutics and Biopharmaceutics. 46:169-175 (1998).
15. M. Delalondeand T. Ruiz. Dissolution of pharmaceutical tablets: The influence of penetration and drainage of interstitial fluids. Chemical Engineering and Processing. 47:370-376 (2008).

16. G. Haaseand Nickerso.Ta. Kinetic Reactions of Alpha and Beta Lactose .I. Mutarotation. Journal of Dairy Science. 49:127-& (1966).
17. H.V. Vankamp, G.K. Bolhuis, K.D. Kussendrager, and C.F. Lerk. Studies on Tableting Properties of Lactose .4. Dissolution and Disintegration Properties of Different Types of Crystalline Lactose. International Journal of Pharmaceutics. 28:229-238 (1986).
18. S. sumathiand A.R. Ray. Role of Modulating Factors on Release of Caffeine from Tamarind Seed Polysaccharide Tablets. Trends Biomater Artif Organs. 17:41-46 (2003).
19. G. Alderbornand C. Nystrom. Pharmaceutical Powder Compaction Technology, 1995.

Chapter 3 Rational Formulation Development of Compound-A Tablets

In pharmaceutical manufacturing, formulation development largely determines the complexity of material composition and manufacturing process. The knowledge derived from the development process is also directly utilized in manufacturing control. However, as introduced in Chapter 1, the current formulation development process is often a combination of empirical property matching and design of experiments. The development of formulations with high drug load is particularly difficult, as the properties of the API might become equally important or even dominant when compared with those of the excipients. For such a formulation, it is also critical to minimize the addition of excipients so that tablet size remains manageable.

In this chapter we describe the development of a high-loading compound-A tablet formulation, focusing on the material properties and the impact of manufacturing process on these properties. Compared to rather "tradional" formulations, the new MIT composition features fewer manufacturing steps and ingredients, is continuous-manufacturing friendly, and exhibits comparable or better dissolution properties.

3.1 Compound-A Formulation by Direct Compression

Compound-A powder has very low bulk density and poor flowability. The desired dose would usually require a final tablet weight of > 600 mg leading to unfavourable size of the tablet. In order to develop a simple formulation and manufacturing process while achieving high drug load and excellent tablet quality, formulation development was carried out utilizing our understanding of material properties and interactions.

Based on our discussion in section 1.3.1.1, it is apparent that direct compression would be the best choice if feasible, requiring minimal manufacturing steps and materials. However, we also understand that direct compression has stringent criteria in material

property, e.g., flowability and density, and thus presents a big challenge with the active ingredient under formulation development in this study.

6.2.1 Direct compression with reference formulations

The trial was started with a couple of reference formulations (Table 3-1) (The details of the formulations are masked for confidentiality reasons). A 50% active drug - 50% excipient combination was sought after as a first step. The powder mixture was blended in a V-shaped blender for 15 minutes at 10 RPM and then compacted with a Korsch EK-0 single station tablet press. The powder fill depth was 6mm. Final tablet was around 100mg in weight, 9mm in diameter, and 1.5mm in thickness, implying a very high 4:1 compression ratio.

Due to the low density of compound-A powder, its volume is more than twice that for the rest of the formulation at a 50% drug load (Figure 3-1). The volumetric ratio indicates that the compound-A properties would probably become dominant in the formulations.

Table 3-1 Initial selection of direct compression formulations.

Excipient Formulation 1 (F1)

- -Filler/Binder 1
- -Filler/Binder 2
- -Superdisintegrant 1
- -Free-flowing Glidant
- -Lubricant

Excipient Formulation 2 (F2)

- -Filler/Binder 2
- -Filler/Binder 3
- -Superdisintegrant 2
- -Free-flowing Glidant
- -Lubricant

Figure 3-1 Volumetric dominance of compound-A (left) in a 50% formulation.

During the manufacturing process, the following observations were made:

- The final blends are still of relatively poor flowability. At a 50g material load in the feeding hopper, the die can not be fully filled at first try. Hopper needs to be manually moved back and forth 3-5 times to achieve good fill, which indicated the non- processability of the mixture at bigger scale with a high- speed tabletting machine. Only ~100 tablets could be made manually per batch.

- Re-lubrication of the upper punch and lower punch with magnesium stearate (Mg St) was necessary for every 15 tablets manufactured, otherwise the tablets become sticky to the lower punch and chipping happens when ejection takes place.

- F1 and F2 formulations share the problems stated above, but filler/binder 3 in F2 seems to accumulate electrostatic charge easily, resulting in further stickiness.

- In the formulation of 50% F1 with double amount of lubricant, there is no need to re-lubricate punches. Die fill is slightly more consistent but still not satisfactory.

Tablet hardness and thickness are measured at 2 minutes post-compaction (Day 0, 10 tablets) and then 1 day post-compaction (Day 1, 5 tablets). Weight is measured at the time of hardness test. The data are presented in Figure 3-2 and Figure 3-3. A dramatic range of weight was recorded on the samples, demonstrating a significant die-fill problem. A clear linear correlation between hardness/thickness and weight was observed. The correlation of thickness with weight indicates considerable elasticity of the material, as elastic recovery is proportional to material mass. The hardness data demonstrates that it is possible to achieve a 70-80N strength satisfactory for 9mm tablets. The correlation between hardness and tablet weight reflects a higher compaction force incurred by tablets that started with more materials, as the upper punch travels the same distance regardless of initial fill difference.

With two major excipients, one super disintegrant, and two flowing aids in F1/F2 formulations, it is difficult to determine a best process to optimize the mixture flowability. We decided that starting from scratch with basic understandings of material properties represents a rational approach to formulation development.

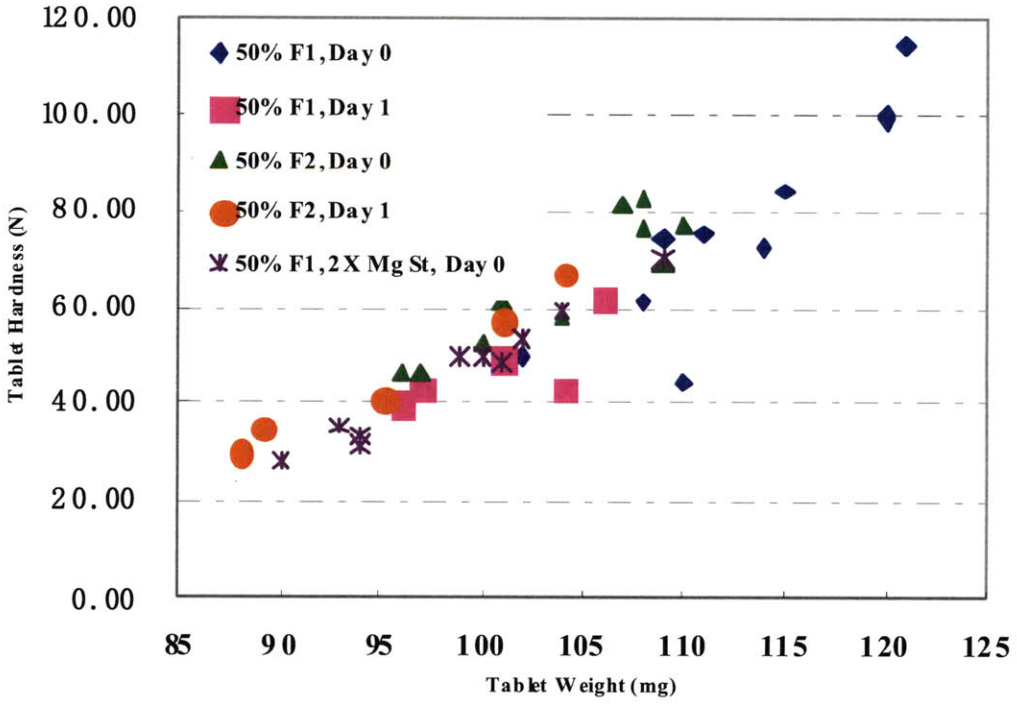

Figure 3-2 Hardness and weight data of F1/F2 Compound-A tablets, N=1.

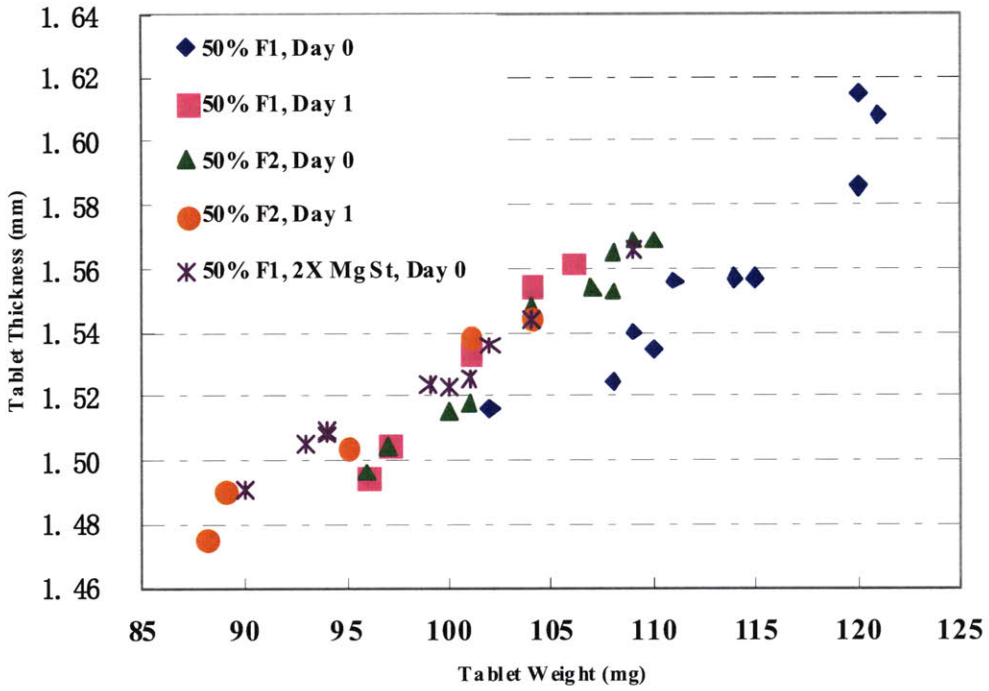

Figure 3-3 Thickness and weight data of F1/F2 Compound-A tablets, N=1.

3.1.2 Direct compression with lactose-based formulation

In a previous study in the lab, Domike investigated the interparticle friction coefficient of common pharmaceutical materials via atomic force microscopy (AFM) study (1). It was found out that lactose particles lose asperity quickly upon abrasion against each other. The lactose particles exhibit a friction level close to that of glass beads, much lower than that of MCC.

Table 3-2 Interparticle friction coefficient of lactose and MCC by AFM. Adapted from Domike 2003.

Material	Spray-dried Lactose DCL14	Micro Crystalline Cellulose PH102	Glass Beads
Interparticle Friction Coefficient	0.26	0.44	0.224

Based on the microscopic friction level, an important indicator of powder flowability, spray dried lactose DCL14 was chosen as the primary excipient. We further picked magnesium stearate, the most widely used lubricant in the pharmaceutical industry, and

Aerosil 200®, an excellent free flowing agent of amorphous fumed silica, to enhance the flowability of the powder mixture. The formulations in Table 3-3 were tested following the manufacturing procedure described above.

Table 3-3 Direct compression formulations of compound-A tablets (wt%)

Formulation	Compound-A	DCL14	Mg St	Aerosil
D30	30	67.5	2	0.5
D40	40	56.5	3	0.5
D50	50	45	4	1

In spite of a very high lubricant loading, the D50 powder was not flowing well in the tablet press and was not further pursued. The hardness/weight data of D30 at target hardness levels of 60N/90N and D40 at target hardness level of 60N is shown in Figure 3-4. When compared with F1/F2 formulations, the weight variation in D30/D40 has seen improvement but is still not satisfactory. Tablet hardness for both D30/D40 at 60N is not very sensitive to weight variation, demonstrating a similar slope. However, strength of D30 tablets at 90N exhibits significant reliance on weight. A 5% weight increase could double the tablet hardness.

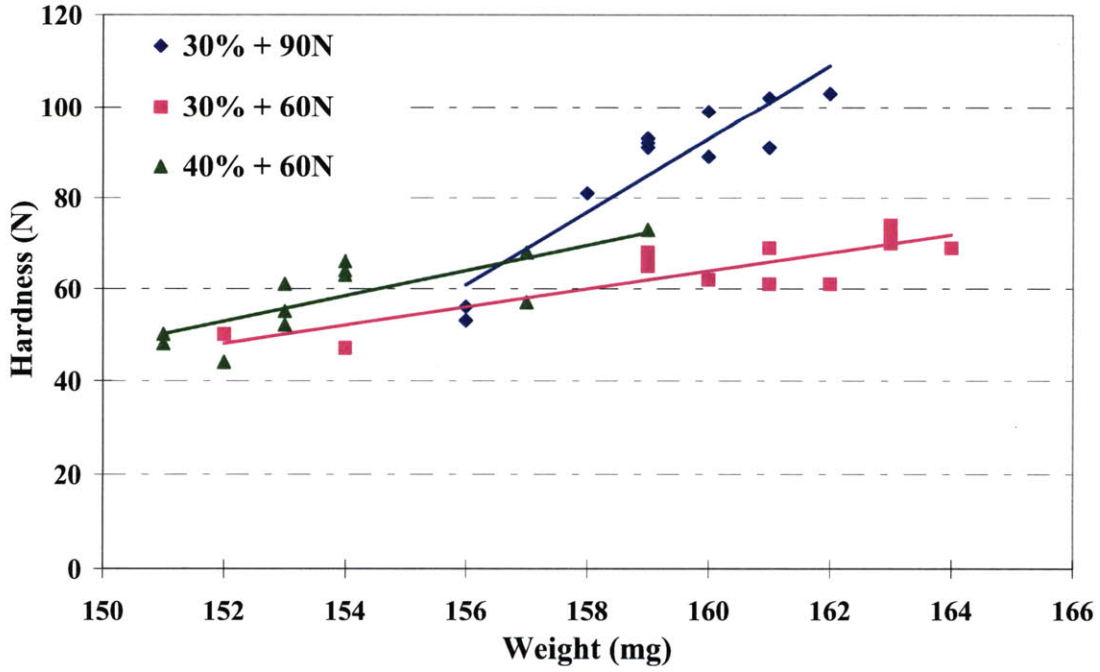

Figure 3-4 Hardness/weight data of Compound-A tablets made from direct compression, N=1.

Table 3-4 Summary of direct compression trials for compound-A tablets. (Average + - Stdev)

Formulation	Weight (mg)	Thickness (mm)	Hardness (N)
F1/F2	100 + - 6	1.50 + - 0.03	55 + - 15
D30	160 + - 3	2.23/2.12+ -0.02	65/95 + - 8
D40	154 + - 2.5	2.22 + - 0.01	58 + - 9
D50	Not flowing		

The results of direct compression trials are summarized in Table 3-4. From the trials, it becomes clear that a drastically simplified formulation is capable of producing tablets with sufficient strength. However, inconsistent die fill is a major issue due to the poor flowability of the dominant compound-A powder in the mixture. Multiple factors contribute to the poor flowability, e.g., the needle shaped crystals have a very high surface to volume ratio, magnifying the impact of intermolecular forces and increasing cohesion/adhesion activities. However, low density is also a primary concern because of the following reasons: (1). A low density alleviates the interaction between compound-A and lactose, reducing the binding power of the latter; (2). A low density renders the necessity of deep die fill to reach target weight, making it more difficult to achieve consistent loading especially under high-speed manufacturing scenario; (3). A low density of compound-A is not beneficial for the smoothing of lactose particle surfaces, which requires certain level of abrasion to happen. In order to address the low density problem while maintaining the advantage of the current formulation, a modified manufacturing process utilizing roller compaction is tested.

3.2 Compound-A Formulation by Roller Compaction

Roller compaction seems to be a perfect solution for the low density issue incurred in the direct compression trials. It could dramatically increase the powder density and improve flowability. Although spray-dried lactose is not a most common excipient used in roller compaction and exhibits a tendency for fragmentation, the roller compaction trial was

deemed worthwhile due to the high drug loading of the formulation. The dominant compound-A powder is a material that is prone to plastic densification and could thus potentially act as a cushion for the lactose particles.

A typical roller compaction process is described in section 1.3.1.1. Depending on the specific roller compaction formulation tested, there might be a final blending step with addition of extra lubricants/excipients before the tabletting. The granulates obtained from compacting the original mixture fed to the roller compactor is called the "internal phase", while the additional material added at the final blending step is called the "external phase". External phase could be comprised of lubricants and other excipients, which are often necessary to enhance the flowability of the final blend. However, it reduces drug loading and adds an extra manufacturing step. For continuous pharmaceutical manufacturing where ingredients are added at a constant rate, external phase could also present a feeding accuracy problem if it only comprises of lubricants in small amount.

3.2.1 Roller compaction simulated with pre-compaction

In order to evaluate the effectiveness of density reduction on flowability improvement, a two-step compaction process is designed to simulate the roller compaction process.

- First Blending: 40% compound-A + 56% DCL14 Lactose + 1.5% Mg St + 0.5% Aerosil, V-shaped blender, 50g batch, 20 RPM for 10 min
- Pre-compaction to simulate roller compaction: material compacted into large, soft tablets with an average strength of 3N
- Milling: 1mm mesh, 3000 RPM
- Final Blending: Milled powder + 1.5% Mg St + 0.5% Aerosil 200, V-shaped blender, 20 RPM for 5 min
- Tabletting: target weight 150mg, strength 60N, diameter 9mm
- Final composition: 40% compound-A + 56% DCL14 + 3% Mg St + 1% Aerosil

Blending was done in a 100ml V-shaped blender made in house. Milling was done with a hammer mill (GlenMills, Inc., Glifton, NJ). Pre-compaction and tabletting was conducted with a Korsch EK-0 single punch eccentric tablet press (Korsch AG, Berlin, Germany).

With the simulated roller compaction process, powder flow problem was totally eliminated. Tablets produced were consistent in shape, appearance, weight, thickness, as well as mechanical strength (Table 3-5).

Table 3-5 Simulated roller compaction produces satisfactory tablets.

Sample (n=12)	Weight (mg)	Thickness (mm)	Hardness (N)
Average	155	2.243	63
StandardDev	0.7%	0.5%	9.1%

Dissolution profile of the produced tablets was tested using 0.01N HCl solution. The tablet dissolution was very rapid, with 95% dissolution completed by 8 minutes. As an instant-release formulation, the performance is at least twice faster than a reference formulation, which already contain super disintegrant to expedite dissolution process. The fast dissolution of the tablets can most probably be attributed to the superb dissolution behavior of spray-dried lactose.

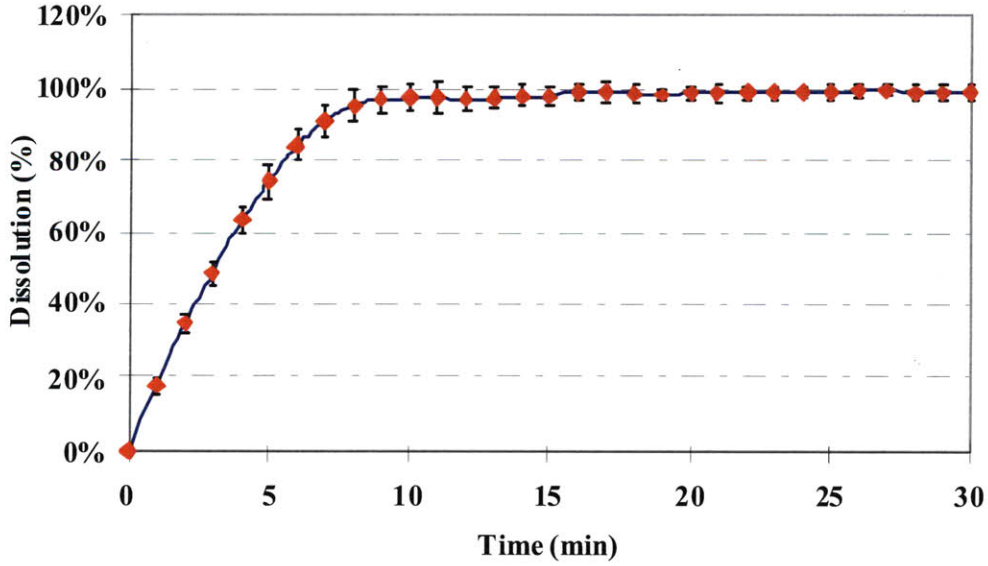

Figure 3-5 Dissolution profile of 40% compound-A tablets via simulated roller compaction.

3.2.2 Roller compaction with bench-top compactor

After the successful proof-of-concept tests with simulated roller compaction, we then moved on to a roller compactor for formulation development. The performance of a series of lactose-based formulations (M50/M60/M70) was compared with that for two reference formulations, N68 and N50. Only N68 has an external phase, which is eliminated in all the other formulations to facilitate continuous manufacturing. The formulations are presented in Table 3-6. Roller compaction trials were carried out with a TFC-Micro roller compactor (Vector Corp, Marion, IA). The operational condition of roller compaction is presented in Table 3-7.

Table 3-6 Compound-A formulations for roller compaction.

MIT (M50/M60/M70)	**wt%**
Compound-A	50/60/70
Spray-dried Lactose DCL14 (DMV)	45/35/25
Colloidale silicon anhydrous (Aerosil 200)	1
Magnesium stearate (Faci)	4

N68 - Internal Phase	**wt%**
Compound-A	N/A
Filler/Binder-1	N/A
Filler/Binder-2	N/A
Superdisintegrant	N/A
Free-flowing Glidant	N/A
Lubricant	N/A
N68 - External Phase	**wt%**
Free-flowing Glidant	N/A
Lubricant	N/A

N50	**wt%**
Compound-A	N/A
Filler/Binder-1	N/A
Filler/Binder-2	N/A
Superdisintegrant	N/A
Free-flowing Glidant	N/A
Lubricant	N/A

Table 3-7 Operational conditions for roller compaction.

TFC-LAB Micro Roller Compactor	Setting
Roll Speed	2 RPM
Roll Current	0.25-0.3 A
Feeding Screw Speed	6.8 RPM
Feeding Screw Current	0.075 A
Roll Pressure	600 PSI

In the process of roller compaction, N68 and N50 exhibited excellent flowing properties, with adequate ribbons produced. However, after milling and blending with external phase, the final powder mixture of N68 had poor flowability and was not capable of adequate die-fill in the tabletting process. M50/M60/M70 had static charge build-up in the roller compaction process, increasing with drug load, but all the formulations were capable of producing ribbons with adequate shape and strength. There was also an tendency of material sticking to feeding hopper wall. Considering the simple single screw feeding mechanism adopted in the bench-top roller compactor used, this might not be a major concern for commercial scale instrument, where multiple screw feeding with vacuum aid is the standard.

Without an external phase, all the M-series formulation exhibited superb tabletting behavior. Die fill was very consistent and the tablets produced were of excellent quality. The data of the tablets is presented in Table 3-8. Twelve samples were measured at the beginning of the automatic tabletting process (20 tablets/minute) and after 100 tablets were produced. (For N50 tablets, data was also collected at 200 tablets.) M50/M60/M70 all produced consistent and high quality tablets, with an average hardness level of 100N, a satisfactory strength for commercial tablets of 9mm diameter. There is a slight upward shift of weight (<2%) as tabletting progresses. This is due to the small size of the batch and the potential segregation of smaller particles to the bottom of the hopper. In the case of M70, a final mild blending of 5 min at 10 RPM was capable of eliminating the density difference. In commercial scale high speed tabletting with force feeding of the dies, this density variation might not be present due to the large batch size.

N50 had very consistent tabletting behavior, matching the performance of the M-series formulations. N68, however, was not capable of automatic tabletting even with fresh addition of lubricant, manual agitation of feeding hopper, or additional blending before tabletting. Manual tabletting was conducted to produce some tablets for further comparison tests.

Table 3-8 Compound-A tablet data of roller compaction formulations.

M50	n=12	Weight (mg)	Hardness (N)	Thickness (mm)
0 tablet	Average	225	96	3.157
	Stdev	0.7%	4.6%	0.2%
100 tablets	Average	229	95	3.200
	Stdev	1.2%	7.2%	0.2%

M60	n=12	Weight (mg)	Hardness (N)	Thickness (mm)
0 tablet	Average	231	99	3.201
	Stdev	1.1%	5.7%	0.4%
100 tablets	Average	235	101	3.241
	Stdev	0.9%	7.1%	0.3%

M70	N=12	Weight (mg)	Hardness (N)	Thickness (mm)
0 tablet	Average	224	101	3.215
	Stdev	0.7%	3.9%	0.3%
100 tablets	Average	225	103	3.210
	Stdev	0.9%	9.6%	0.3%

N50	n=12	Weight (mg)	Hardness (N)	Thickness (mm)
0 tablet	Average	230	100	3.106
	Stdev	0.7%	4.7%	0.2%
100 tablets	Average	233	103	3.145
	Stdev	0.8%	5.8%	0.3%
200 tablets	Average	239	99	3.226
	Stdev	0.6%	4.7%	0.2%

When compared with N series formulation, M series requires fewer ingredients and is capable of tabletting at a higher drug load. Additional characterization tests were carried out to further test its robustness. A prolonged tabletting run of M50 was conducted to probe the lower limit of materials required in the hopper for normal tabletting. It was demonstrated that tabletting was very consistent even when there were only 40g materials left in the hopper (after 200 tablets made) (Table 3-9). When the amount of powder drops to 18g, the tablets produced were no longer consistent in weight and hardness as it is shown in the results of the 300 tablets with increased standard deviations for all parameters tested.

Table 3-9 Prolonged tabletting test of M50 formulation.

M50	n=12	Weight (mg)	Hardness (N)	Thickness (mm)
0 tablet	Average	229	100	3.157
	Stdev	0.5%	8.0%	0.2%
100 tablets	Average	231	97	3.180
	Stdev	0.5%	10.5%	0.2%
200 tablets	Average	232	99	3.182
	Stdev	0.4%	9.2%	0.1%
300 tablets	Average	212	53	3.108
	Stdev	2.2%	15.2%	0.5%

The impact of tabletting speed was also evaluated on the M50 formulation (Table 3-10). The speeds tested were 10 / 20 / 40 strokes per minute. The tabletting process went fine at all the three speeds. However, the standard deviation of hardness increased with tabletting speed. There is also a tendency of higher tablet weight at higher tabletting speed. This is due to the feeding mechanism of the tablet press used, in which a hopper moves over onto the die hole and fills it under gravity. A faster tabletting speed corresponds to a more forceful stop of the hopper over the die, creating a higher pressure within the hopper. As a result, slightly more materials might be pushed into the die. As the punch movement pattern and feeding mechanism of eccentric single station tablet press are different from those of commercial scale multi-station tablet press, the actual impact of tabletting speed needs to be evaluated in a larger scale production setup.

Table 3-10 Tabletting speed test for M50 formulation.

M50	n=12	Weight (mg)	Hardness (N)	Thickness (mm)
10 RPM	Average	229	97	3.165
	Stdev	1.0%	7.2%	0.2%
20 RPM	Average	231	97	3.180
	Stdev	0.5%	10.3%	0.2%
40 RPM	Average	236	107	3.211
	Stdev	1.4%	15.9%	0.6%

Next, the capability of M-series formulation in generating commercial scale products was tested. M60 formulation was adopted to produce a tablet with a diameter of 11mm and a drug load of 300mg (Table 3-11). The tabletting process was very smooth and consistent, with no additional lubrication of the instrumentation necessary. A steady state operation was reached within 2 minutes. The hardness of the tablets was comparable to that of benchmark formulations, and the thickness was within an acceptable range.

Table 3-11 Tabletting production of commercial scale tablets for M60 formulation.

M60	n=12	Weight (mg)	Hardness (N)	Thickness (mm)
0 tablet	Average	496	167	4.559
	Stdev	0.6%	12.9%	0.2%
50 tablets	Average	489	152	4.543
	Stdev	0.6%	7.9%	0.2%
100 tablets	Average	490	154	4.548
	Stdev	0.6%	6.2%	0.2%

The dissolution profile of the M60 11mm tablets indicates a comparable or better dissolution speed than benchmark formulations, with 90% dissolution completed in 20 minutes (Figure 3-6). Dissolution setup was as described in section 3.2.1. The variation observed beyond 80% dissolution is due to sample absorbance signal exceeding the linear transmission range of the fiber-optic probes.

The dissolution profiles of M50 / M60 / M70 / N50 / N68 tablets with a total weight of 200mg and a diameter of 9mm were also examined. M50 / M60 / M70 had very consistent dissolution profiles, with 90% dissolution by 11.5 – 13 minutes (Figure 3-7, Figure 3-8, and Figure 3-9). N50 / N68 dissolution profiles exhibited much higher variation (Figure 3-10 and Figure 3-11), caused by a large amount of white debris released interfering with fiber-optic signals. They also underwent slower dissolution, with 90% dissolution finished by 14 minutes and 16 minutes, respectively.

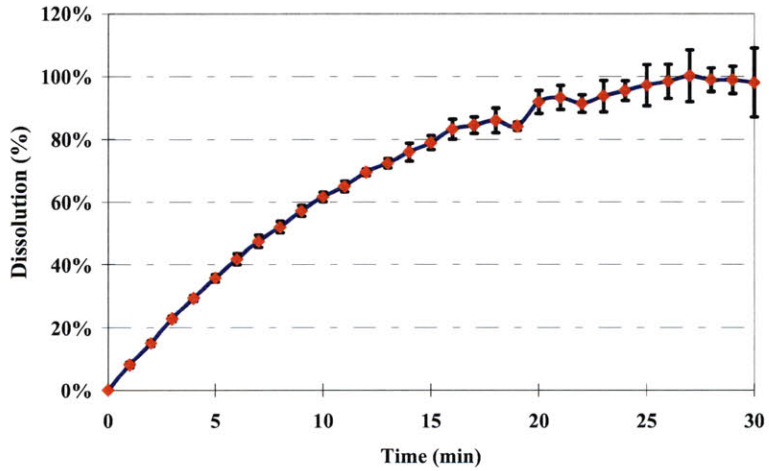

Figure 3-6 Dissolution profile of M60 tablets with 300mg drug loading. N=6.

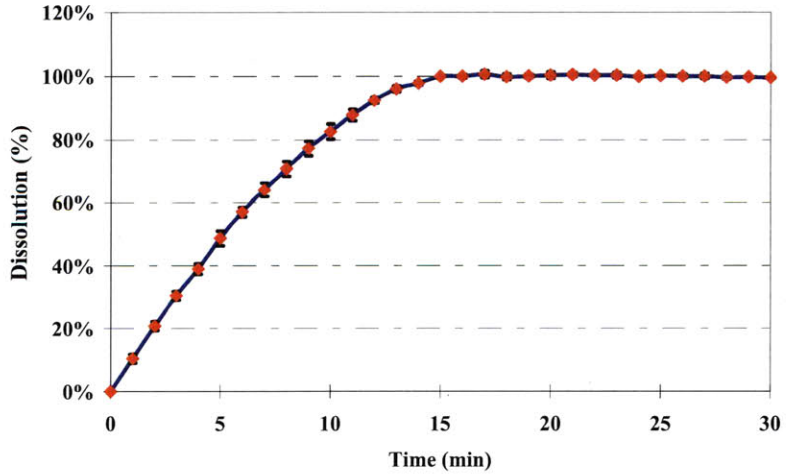

Figure 3-7 Dissolution profile of M50 tablets, N=6.

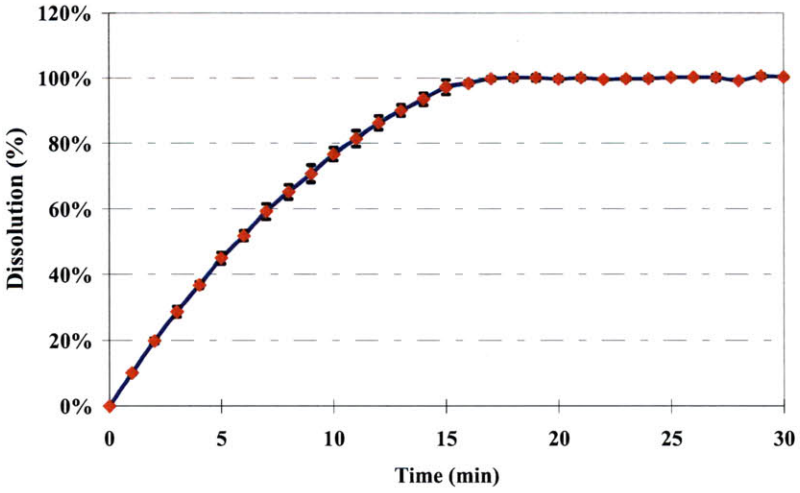

Figure 3-8 Dissolution profile of M60 tablets, N=6.

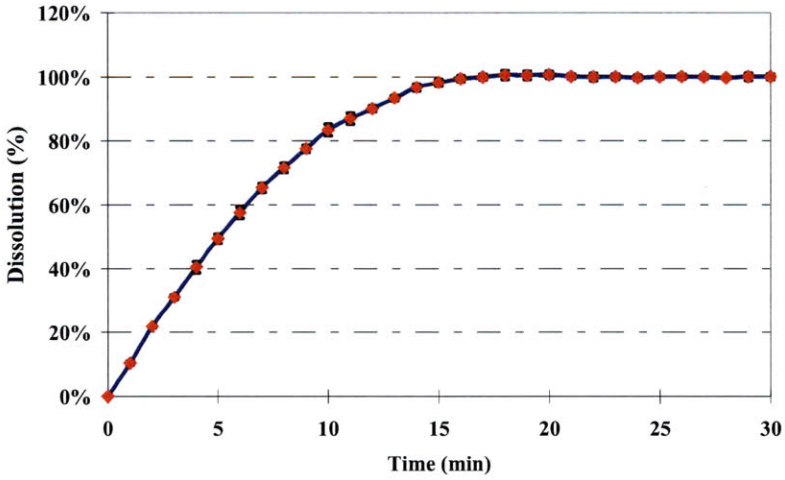

Figure 3-9 Dissolution profile of M70 tablets, N=6.

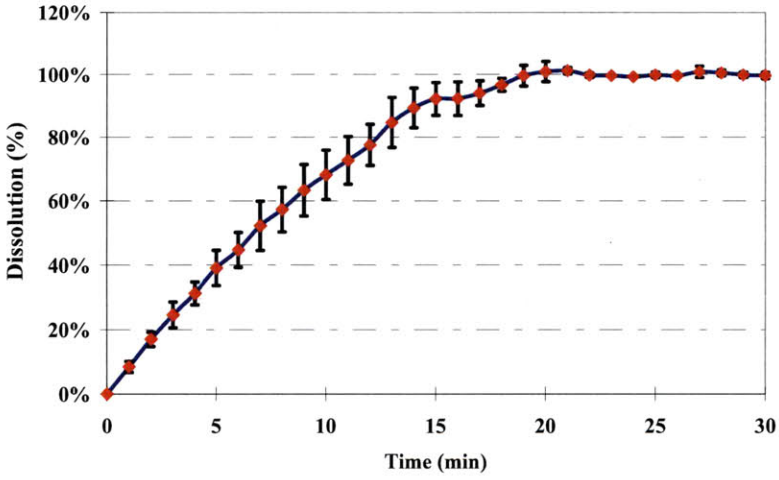

Figure 3-10 Dissolution profile of N50 tablets, N=3.

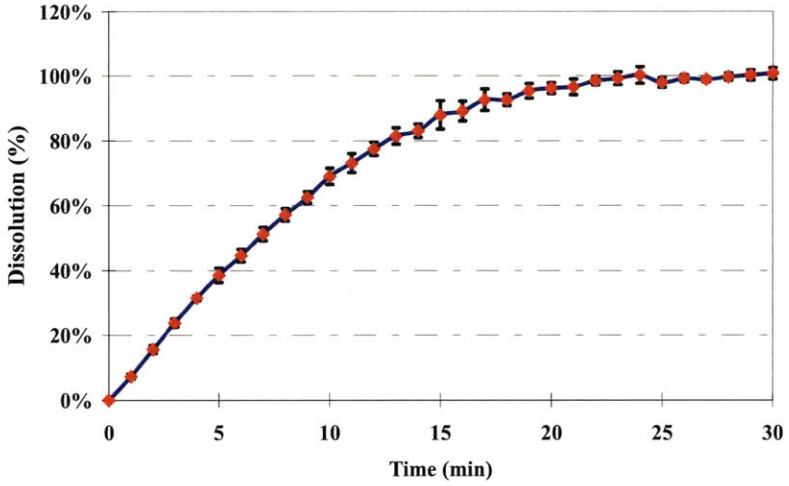

Figure 3-11 Dissolution profile of N68 tablets, N=4.

3.3 Characterization of M-Series Formulations

In order to evaluate the benefit of roller compaction, the flowability and particle size distribution of M50 and M70 powders were characterized.

3.3.1 Flowability of M50/M70 Powders

Flowability refers to the capability of a material, e.g. a powder, to move in a certain geometrical environment under certain driving forces, e.g. gravity. Flowability is a key property for pharmaceutical powders. A good flowability is essential to the consistency of a manufacturing process and its final products. In the tabletting step, improper flowability could lead to variations in die fill or powder segregation, which in turn leads to inconsistent tablet weight, content uniformity, and mechanical strength.

Two techniques as specified in U.S. Pharmacopeia, angle of repose and compressibility index, were used to evaluate the flowability of M50/M70 powder mixtures before and after roller compaction. Angle of repose is related with multiple aspects of powder flow properties like inter-particulate friction and powder density. Experiments were set up according to USP 32 Chapter 1174, where a powder feeder is placed at 4 cm above a flat round plate with a 2 cm diameter (Figure 3-12). Powder is tapped slowly through the

funnel and fell onto the plate. A maximum angle formed is recorded and measured with ImageJ® software developed by National Institute of Health (NIH).

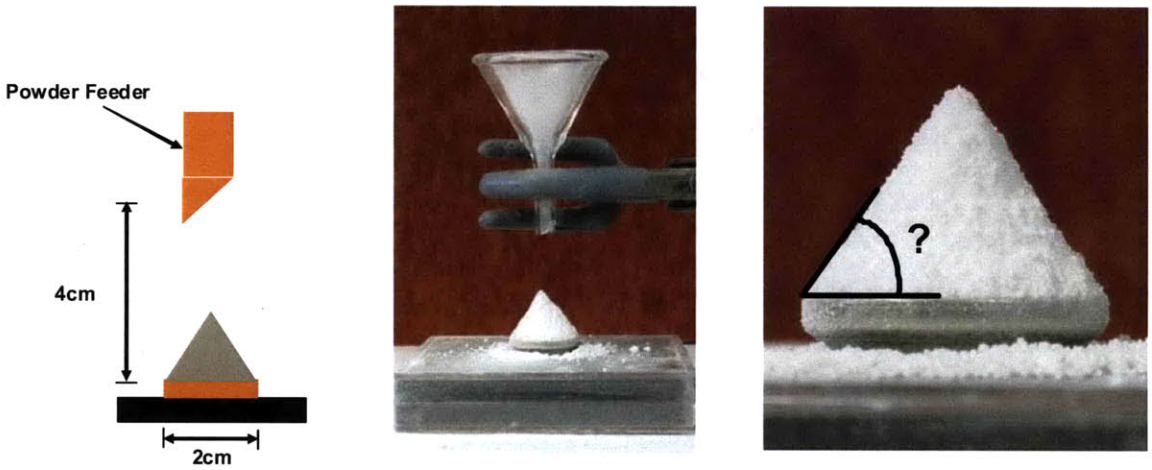

Figure 3-12 Illustration of angle of repose test.

Compressibility index uses a simple formulation to quantify complex powder interactions. It is defined as a function of tapped density and bulk density:

$$Compressibility\ Index = 100 \times \left[\frac{\rho_{tapped} - \rho_{bulk}}{\rho_{tapped}} \right]$$

The scales of flowability test results and correspondent flow properties are presented in Figure 3-13. The smaller the angle of repose or compressibility index, the better flow property a powder has. It is worth mentioning that for both methods, especially angle of repose, the final result is dependent upon the actual measurement setup. Therefore, data should be interpreted with caution.

Table 1. Flow Properties and Corresponding Angles of Repose*

Flow Property	Angle of Repose (degrees)
Excellent	25–30
Good	31–35
Fair—aid not needed	36–40
Passable—may hang up	41–45
Poor—must agitate, vibrate	46–55
Very poor	56–65
Very, very poor	>66

Table 2. Scale of Flowability*

Compressibility Index (%)	Flow Character
≤10	Excellent
11–15	Good
16–20	Fair
21–25	Passable
26–31	Poor
32–37	Very poor
>38	Very, very poor

Figure 3-13 Scales for characterization of flowability. Source: USP 32, Chapter 1174

Table 3-12 Flowability test results for M50 / M70 formulations. N=3.

	Powder Status	Angle of Repose (degree)	Bulk Density (g/ml)	Tapped Density (g/ml)	Compressibility Index
M50	Before RC	56.3 + - 1.4	0.30	0.39	23
	After RC	42.8 + - 0.3	0.42	0.46	9
M70	Before RC	58.7 + - 1.5	0.26	0.33	21
	After RC	43.4 + - 0.8	0.38	0.41	7

The testing results for M50 / M70 powder mixtures before and after roller compaction are summarized in Table 3-12. According to both methods, flowability is improved in M50 / M70 formulations after roller compaction. For angle of repose test, it is indicated that flowability advanced one level from "poor" to "passable", while for compressibility index, flowability advanced three levels from "passable" to "excellent". According to the observations made in tabletting experiments, compressibility index was more accurately reflecting the actual dramatic improvement in powder flowability.

3.3.2 Particle Size Distribution of M50/M70 Powders

In addition to compressibility index and angle of repose, particle size distribution of the powders was examined for changes after roller compaction. A coarser particle size in general leads to better flowability, as less surface area is available for inter-particle adhesion / cohesion interactions. The particle size distributions of the M50 / M70 powders were measured with a technique called focused beam reflectance measurement (FBRM).

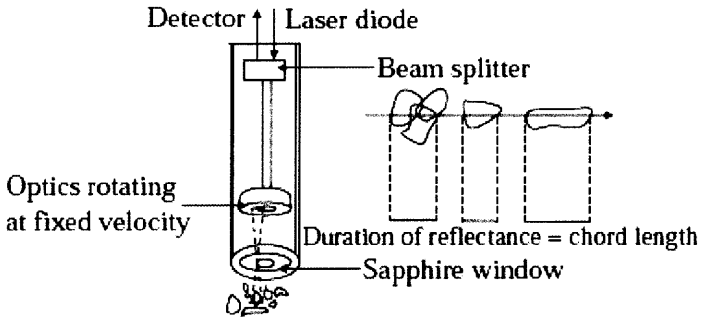

Figure 3-14 Mechanism of FBRM. Adopted from Kougoulos et al., 2004.

In a FBRM experiment, a measurement tube is inserted into a liquid carrying the non-dissolving particles to be analyzed. A beam of laser light is rotated at a constant speed and focused on the outside of a sapphire glass window, where it is back scattered by the particles on or near the window (Figure 3-14) (2). The duration of the back scattered light signal is then measured by a detector at the end of the tube, based on which a particle cord length can be calculated. For sample preparation of the current study, 1 g of M50 / M70 powder mixture was dispersed in 20ml of Acetonitrile liquid. Measurement was done under gentle agitation.

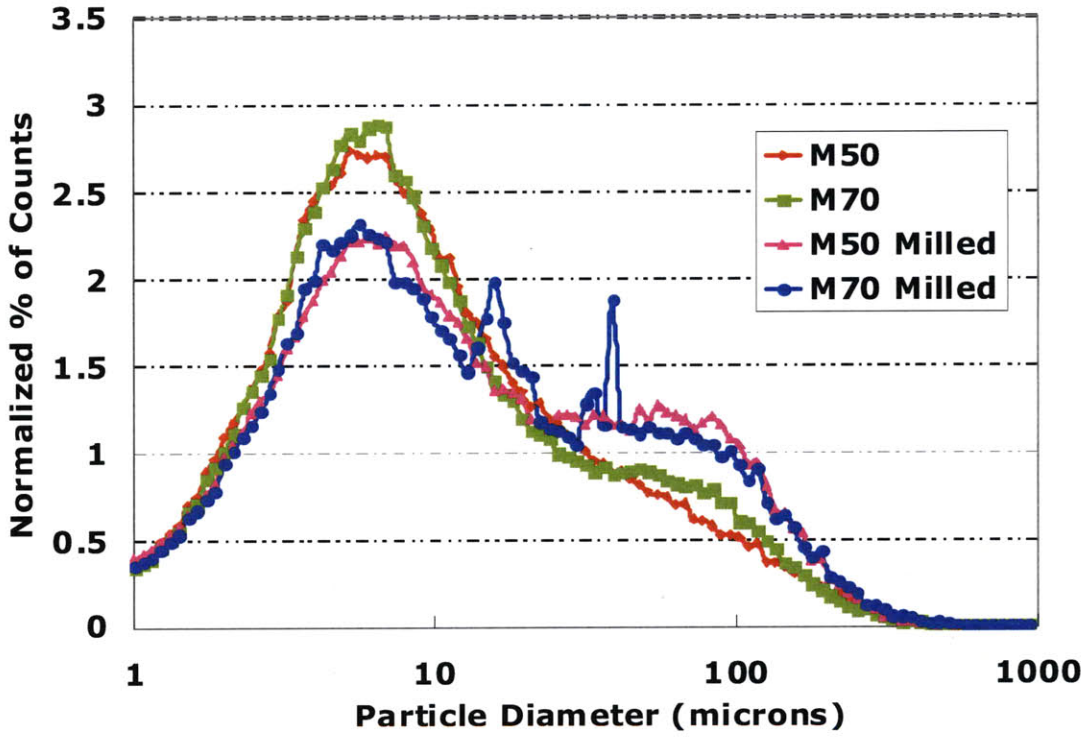

Figure 3-15 Particle size distribution measurement of M50 / M70 formulations.

FBRM data indicates that before roller compaction, a majority of the particles for both formulations have a particle diameter (or cord length as measured) between 5 μm and 15 μm (Figure 3-15). After roller compaction, the % count in this range shrank by 20%, while the particles in the range of 25 μm to 250 μm increased significantly. The abrupt peaks in M70 Milled data are artifacts resulted from powder sticking to the sapphire window. The roller compaction process in general lifted the particle size of the powders, which in turn contributed to a better flowability.

3.4 Stability Testing of M-Series Formulations

For pharmaceutical dosage forms, physical and chemical stability are critical to maintaining adequate shelf-life in various potential storage environments. The outcome of stability tests not only depends on the dosage form itself, but also the way it is packaged. As descbribed in section 1.3.2.1, we adopted an accelerated stability testing condition in order to obtain a proper evaluation of both physical and chemical stabilities within a short period of time. M70 tablets of 100N strength are placed inside plastic bottles induction sealed with aluminum foil. The bottles are then stored inside humidity chambers at 40°C and 75% RH for 1.5 months. After the storage period, tablet samples are analyzed and compared with standards that have been stored in moisture-barrier bags at room temperature.

3.4.1 Physical Stability

Physical stability was assessed with x-ray powder diffraction technique (XRPD), which obtains information about crystalline structures and their relative abundance by analyzing the x-ray diffraction pattern of a powder sample (3). The XRPD data for M70 samples are presented in Figure 3-16. The position, shape, and size of the diffraction peaks for M70 tablets under two storage conditions match each other very well, indicating identical crystalline compositions. No visual evidence, e.g., the change of tablet shape or color, was observed to suggest any physical deterioration of tablets under accelerated stability testing condition.

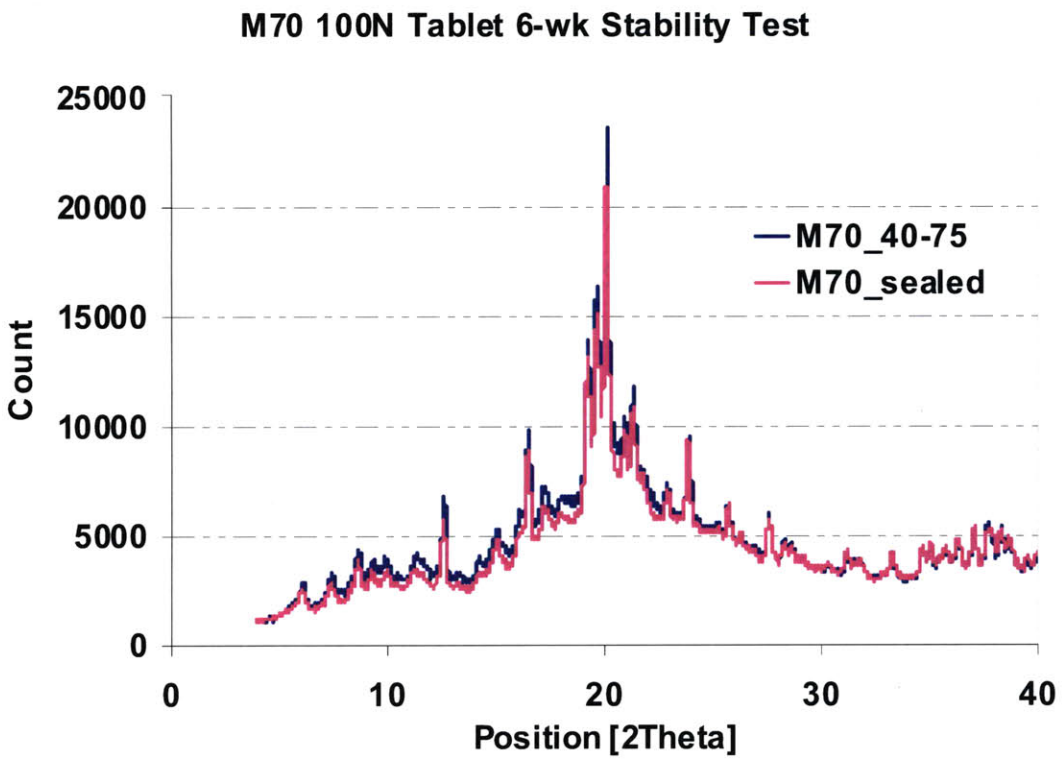

Figure 3-16 XRPD data of M70 tablets under different storage conditions.

3.4.2 Chemical Stability

The chemical stability of the tablets was evaluated via high performance liquid chromatography (HPLC), a technique that separates and identifies compounds based on their interaction duration / strength with the stationary phase of a column (4). The HPLC data for M70 samples are presented in Figure 3-17. Three samples were tested for M70 tablets from each condition. All the sample files overlay with each other very well. No additional peaks or shift of peak positions were detected with samples in accelerated stability testing condition, indicating the absence of product degradation.

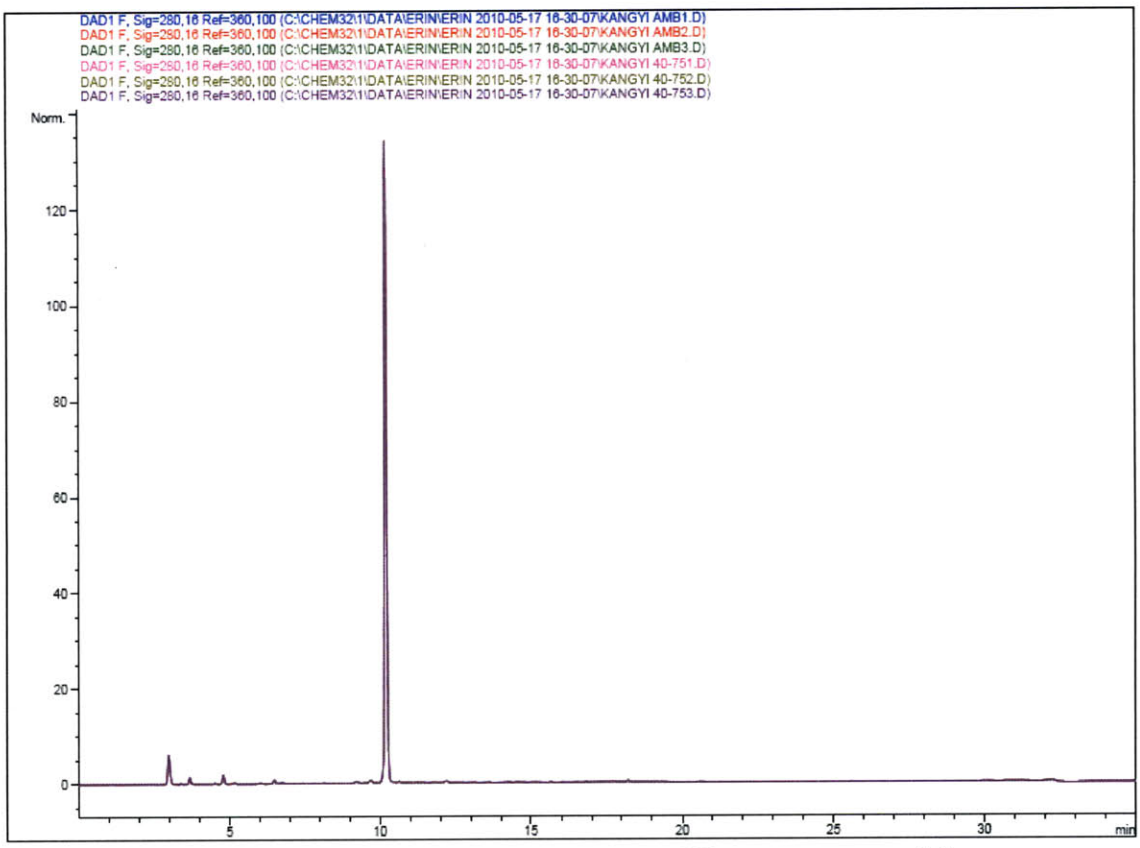

Figure 3-17 HPLC data for M70 tablets under different storage conditions.

3.5 Summary

In this chapter we described the development of an M-series compound-A tablet formulation based on roller compaction. The development started with fundamental understanding of material flowability and was adjusted according to specific problems discovered through the process. The data indicates that it is possible to develop a well processable formulation with a considerable high drug load of 60% of compound A despite its unfavourable physical properties. When compared with a benchmark formulation, the M-series formulation features fewer manufacturing steps and ingredients, is continuous-manufacturing friendly, and exhibits comparable or better dissolution properties. However, further trials on commercial scale production are required to confirm its viability in manufacturing settings.

Characterization of M-series powder reveals the positive impact of roller compaction on powder flowability, evidenced by the smaller angle of repose, lower compressibility index, and larger particle size after roller compaction.

Accelerated stability test of 1.5-month storage at 40°C and 75% RH did not result in any detectable changes in crystalline forms or chemical composition of M70 tablets, indicating an acceptable stability of the formulation.

The M-series compound-A formulation represents an effort moving toward rational formulation development, in which fundamental understandings of material properties are utilized to guide the selection of ingredients and optimization of manufacturing processes. Such a design process can lead to leaner formulation and manufacturing process, as well as a much better understanding and control of them.

1. R.D. Domike. Pharmaceutical Powders in Experiment and Simulation: Towards A Fundamental Understanding, *Chemical Engineering*, Vol. Ph.D. in Chemical Engineering, MIT, Cambridge, MA, 2003.
2. E. Kougoulos, A.G. Jones, K.H. Jennings, and M.W. Wood-Kaczmar. Use of focused beam reflectance measurement (FBRM) and process video imaging (PVI) in a modified mixed suspension mixed product removal (MSMPR) cooling crystallizer. Journal of Crystal Growth. 273:529-534 (2005).
3. R. Jenkinsand R. Snyder. Introduction to X-Ray Powder Diffractometry, Wiley-Interscience, 1996.
4. Y. Kazakevichand R. loBrutto. HPLC for Pharmaceutical Scientists Wiley-Interscience, 2007.

Chapter 4 MicroCT Imaging and Analysis of Tablet Microstructure

Tablet microstructure is created by the interactions among raw materials and manufacturing process. It directly affects the properties of the final dosage form. A fundamental understanding of the structure is a pivotal step toward rational formulation design, as it bridges our knowledge about the manufacturing process and tablet properties. In this chapter we present a microCT data acquisition method coupled with a digital workflow for tablet porosity characterization. The method would be applied toward the characterization of caffeine-lactose directly compressed tablets and compound-A roller compacted tablets, providing insight into material interactions during the manufacturing process. MicroCT imaging of tablet microstructure enables 3-D characterization with direct visualization, bringing us one step closer to Quality by Design of pharmaceutical solid dosage formulations.

4.1 Applications of MicroCT in Pharmaceutical Sciences

X-ray micro computed tomography (microCT) is a technique capable of non-destructively resolving three-dimensional internal structures. X-ray transmission profiles of the target are collected from multiple angles and subsequently reconstructed into two-dimensional cross-section images, which can be stacked into a three-dimensional representation of the target (Figure 4-1). When compared with typical CT scanners in hospitals, microCT machines provide much higher resolutions at micrometer level. Since its introduction in 1982 (1), microCT has been widely used in fields like material and biomedical sciences (2, 3).

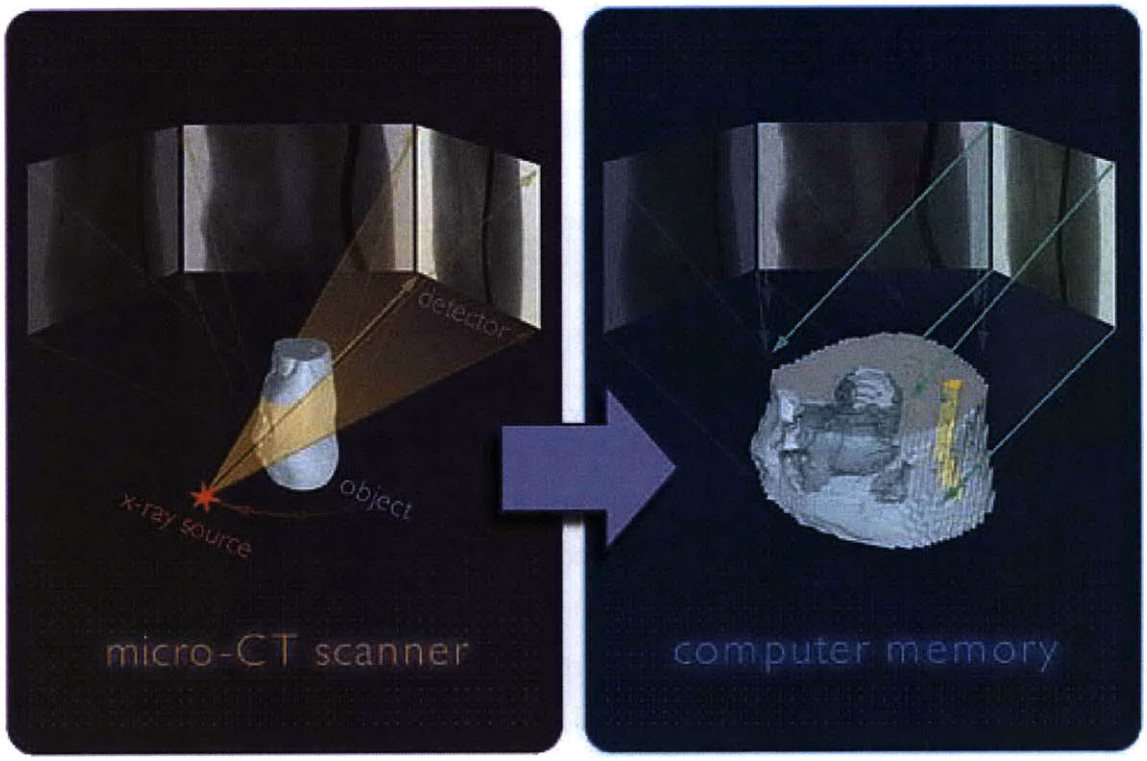

Figure 4-1 Illustration of microCT working mechanism. Source: Skyscan 2007.

The first application of microCT in pharmaceutical science was a study of porosity and morphology of mannitol-lactose-microcrystalline cellulose-based granules (4). Tomographic images showed that the pore network of individual granules comprises mainly of relatively large cavities connected by narrow pore necks. It was indicated that mercury porosimetry recorded pore neck size distribution, while microCT measured true size distribution of pores larger than 4 μm, the resolution limit of the instrument used. The authors concluded that microCT was less precise than mercury porosimetry in total porosity measurement but provided additional morphological information.

MicroCT has helped understand density distribution in pharmaceutical tablets. Sinka et al. demonstrated with microCT study that in microcrystalline cellulose (MCC) tablets, the shape of the tablet could affect density distribution (5). Busignies et al. used microCT to illustrate a higher density in the peripheral region of a cylindrical tablet. They then argued that it is important to distinguish between the mechanical properties representative of the total tablet volume, e.g. tablet hardness, and the mechanical properties representative of the tablet surface, e.g., indentation strength (6). In a more

recent study, microCT was utilized to map the density distribution of NaCl tablets, which exhibited good agreement with results from computer simulations (7).

MicroCT was used to study compaction and mixing process (8). Microcrystalline cellulose particles were labeled via lead impregnation, resulting in higher contrast in microCT scans. Co-processing of unlabeled and labeled powder allowed investigation of blending and compaction behaviors. For V-shaped blending, it was found out that large particles and layer-filling configuration of powders led to better mixing than smaller particles and column-filling configuration. In tablet compaction, significant particle rearrangement at initial stage of compaction was demonstrated. MicroCT images also revealed tablet structural differences from production with different tablet presses, which were in turn linked to varying breakage patterns (7).

In proof-of-concept microCT studies of granule packing (9, 10), Fu et al. demonstrated a good agreement of microCT measurement of particle shape and size with results from scanning electron microscopy (SEM). The measurement data was confirmed by prediction with discrete element method (DEM). MicroCT was also utilized in characterization of tablet fracture (11), demonstrating the role of die wall friction in capping of multi-layer tablets.

MicroCT is often used in combination with other techniques to obtain multi-dimensional information. One field for such application is drug release and dissolution (12, 13). A combination of magnetic resonance imaging and microCT was used to visualize the development of the internal microstructure within compressed tablets during dissolution in water (12). The tablets were made from a combination of insoluble particles (Eudragit®, a polymer) and soluble particles (diltiazem hydrochloride).

In spite of the increasing examples of microCT study in pharmaceutical science, there is currently no published investigation of pharmaceutical solid dosage forms in a quantitative manner. In the next section we introduce a microCT method enabling 3-D

characterization of pharmaceutical tablet microstructure. In Chapter 6 we will further develop the quantitative analysis of microCT data.

4.2 Development of MicroCT Imaging Method

4.2.1 Setup of MicroCT Scanning Configuration

A Skyscan™ 1172 microCT machine (Skyscan N.V., Belgium) was used for tablet imaging in this study. The size of the sensor for detection of X-ray signal is fixed at 4000 pixels X 2096 pixels, which means that in order to achieve higher resolution (smaller μm/pixel), we have to limit the overall size of the sample. At a maximum resolution of 0.7 μm/pixel, the largest sample that could be scanned is a cylinder of about 1.5mm in diameter. A central piece of tablet of this size is cut with a microtome blade, secured by half inserted into a plastic tube, and immobilized on a sample station with plasticine (Figure 4-2). The sample station was center-aligned so that the sample is always within view during the scan.

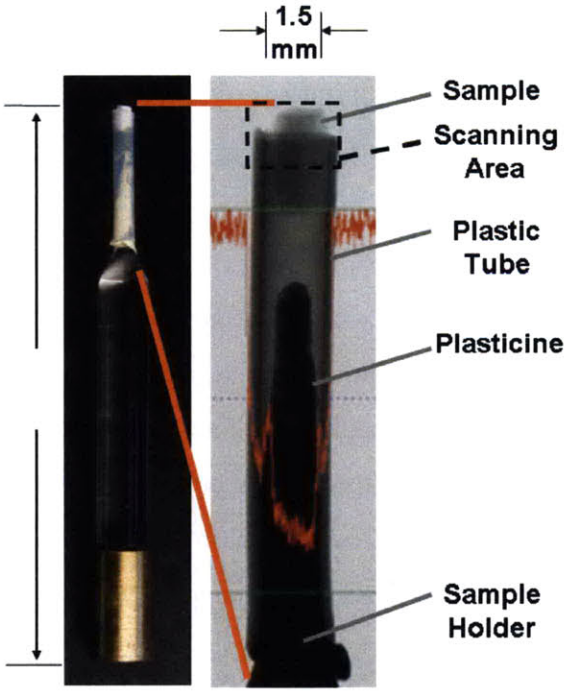

Figure 4-2 Illustration of sample station setup.

Table 4-1 Scanning parameters for tablet fragments.

Scanning Parameters	
Beam Voltage	40 kV
Beam Current	250 μA
Sample Total Rotation	180 °
Rotation Step	0.3 °
Exposure Time	1180 ms
Frame Average	4
Random Movement Correction	10
Pixel Linear Dimension	1.4 μm
Camera Make and Model	Hamamatsu 10mp CCD
Scanning Resolution	2000 x 1048 (native: 4000 x 2096)
Filter	No Filter
Flat Field	Gathered prior to first scan each day
Median Filter	On

Scanning was done with the configuration as shown in Table 4-1. The actual scanning resolution used was 1.4 μm at medium resolution, effectively grouping the signal strength within 4 adjacent sensor dots into one. This was chosen because at the highest natural resolution, the reconstructed cross sections exhibited floating grain artifacts in the pore spaces. These artifacts do not go away even after resizing the high resolution scans into medium resolution ones. On the other side, scans of the same sample directly done with medium resolution and then reconstructured do not have this problem (Figure 4-3).

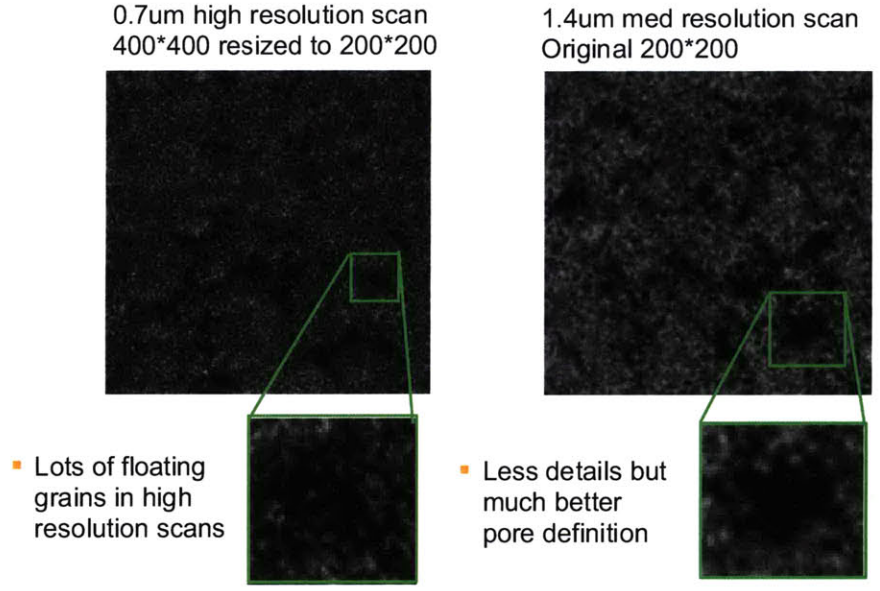

Figure 4-3 High resolution scans exhibit artifact that is absent in medium resolution scans.

4.2.2 Digital Workflow for Data Manipulation

After scanning, the raw data exist as a series of 2-D projection images that reveals little information about 3-D structure of the object. In order to arrive at a 3-D representation of the tablet microstructure with pores and materials separated, a series of digital post-processing steps are necessary (Figure 4-4).

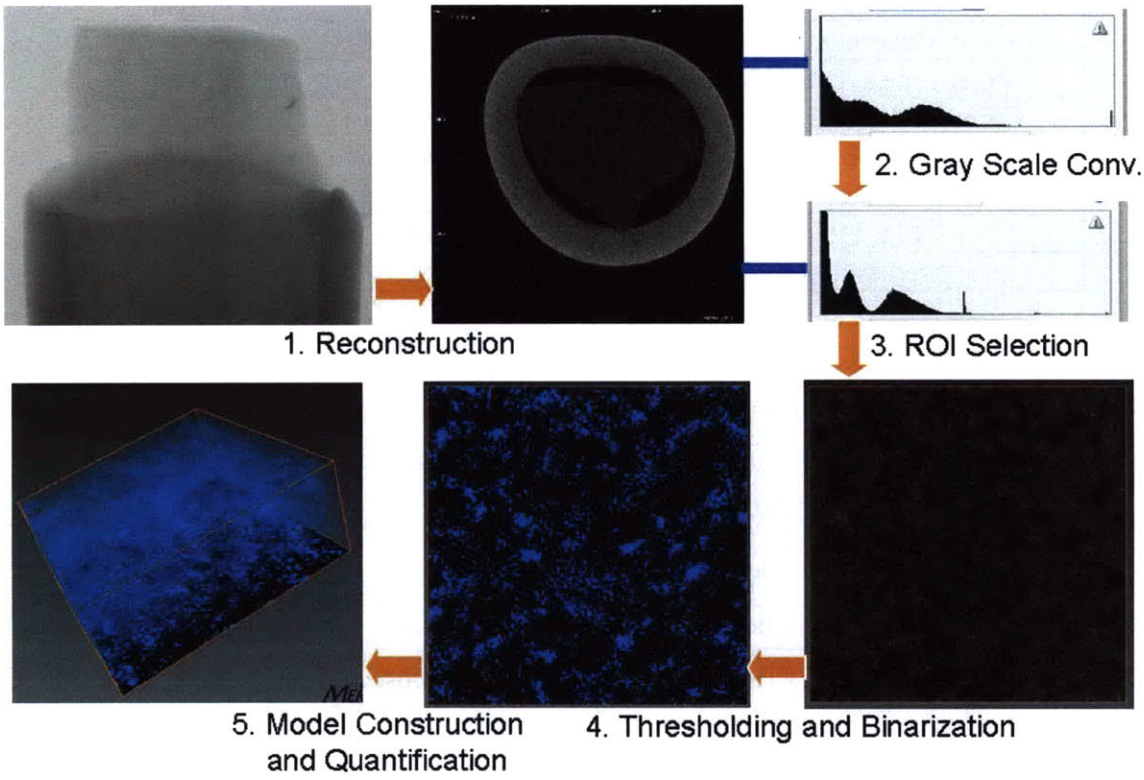

Figure 4-4 Digital post-processing workflow for tablet microCT data. Conv.: Conversion; ROI: Region of Interest.

First, the whole set of projection images go through a thermo-correction process, which corrects for the drift of X-ray signal over the course of the scan. Then, 2-D cross sections of the sample are reconstructed from the projection images using NRecon® software from Skyscan, which uses a Fourier transform-based Feldkamp reconstruction algorithm (14). The misalignment compensation value is fine-tuned so that the edge of a sample is sharp and free of meteor tail artifact. Ring artifact reduction value is set at 10, which reduces the ring-shaped circular artifacts generated in reconstruction. The ring artifact is due to shift of output from a subset of signal detectors that collect signal from the same spots for all the projection images (15). Beam hardening refers to the preferential attenuation of

X-ray signals of lower energy, causing the peripheral of an object to appear brighter in microCT scans (15). Since our sample is very small, beam hardening has not been a problem. Imaging of whole tablet could require special attention to beam hardening.

The 2-D cross section images are then converted into gray-scale images with a Photoshop CS3® script. The initial Bitmap (.BMP) images occupy an indexed colorspace, which does not yield high enough contrast for separating the signal peaks. Conversion to gray-scale JPEG format solves this problem. For tablet structure analysis involving digital imaging, a critical step is to determine the interface between two phases: solid and air-filled pores. Since the images are presented in gray scale with a level between 0 and 255, a threshold value of the materials and pores must be determined, followed by binarization of the two divided sections. In the microCT study of pharmaceutical granules, no information is explicitly given about how this value is determined and whether it differs among various scans (4). The study employing a morphological sieve (16) used an iterative threshold selection method developed by Ridler et. al. in 1978 (17). This method reaches at a threshold midway between the mean luminosity values of the two divided sections. However, this might not represent the best segmentation in the case of tablet microstructure measurement. The luminosity distribution of the pores and materials differ significantly in shape and magnitude, which might introduce bias with the algorithm. In this study, we realized that the converted JPEG image yields clear dividing points for the peaks of pores and materials, and thus represents the most practical way of determining the thresholds. The peaks of material, air, and plastic tube can be distinguished in the histogram of the cross section images (Figure 4-5). A threshold between material and air is determined to be the crossing point of the two peaks. Depending on the stability of the X-ray generator for different scans, this threshold may or may not apply to all the dataset collected with the same scanning configuration. Histogram analysis for individual scans is the best way to arrive at optimal threshold for that specific data set.

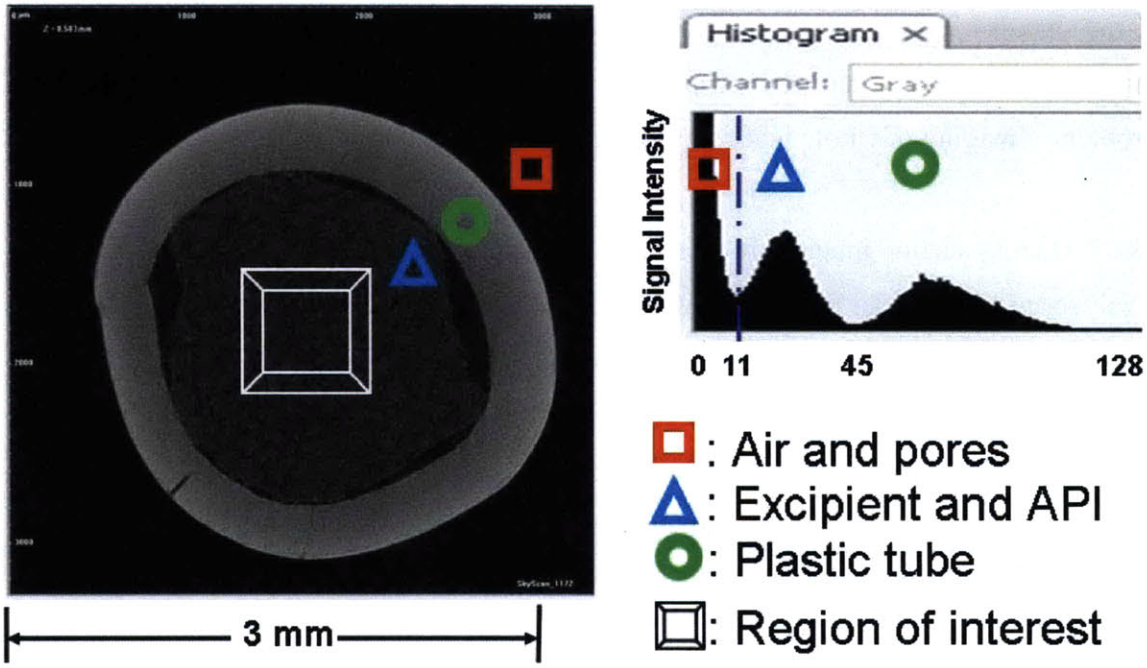

Figure 4-5 Illustration of cross section histogram and the selection of threshold/ROI.

Data visualization and analysis software, Avizo 6® of Visualization Sciences Group, is adopted for further processing of the microCT data. In Avizo software, the Pool contains icons representing data objects and modules currently in use as well as lines connecting icons indicating dependencies between objects and modules. Icon colors are used to indicate different types of objects. Data objects are shown in green and are the only objects which can be saved to disk using *File/Save*. Computational modules are shown in red, visualization modules are in yellow, and visualization modules of *slicing* type are in orange. Such modules may be used to clip the graphical output of any other module. Lastly, the light green items are colormaps that are used for visual presentation. Connections between data objects and processing modules, shown as blue lines, represent the flow of data. For display modules, these connections show the data used to generate the display. You may connect or disconnect objects by picking and dragging a blue line between object icons.

A stack of reconstructured cross section images are loaded into the software in luminance mode, with voxel size specified as the actual resolution of the images. A series of manipulations are then performed on the loaded data as shown in Figure 4-6. Orthoslice

module is connected to display cross section images, while bounding box is used to define the physical boundary of the object. Binarization is conducted with I_threshold module at the threshold value determined as discussed above. The result is a set of thresholded images, presented with pores in blue and other materials in black. The pore clusters could be visualized via surfacegen module, providing an opportunity for direct examination of the porosity structure. At this point, total porosity can be calculated as the percentage of blue voxels in total voxels with the volume3d module.

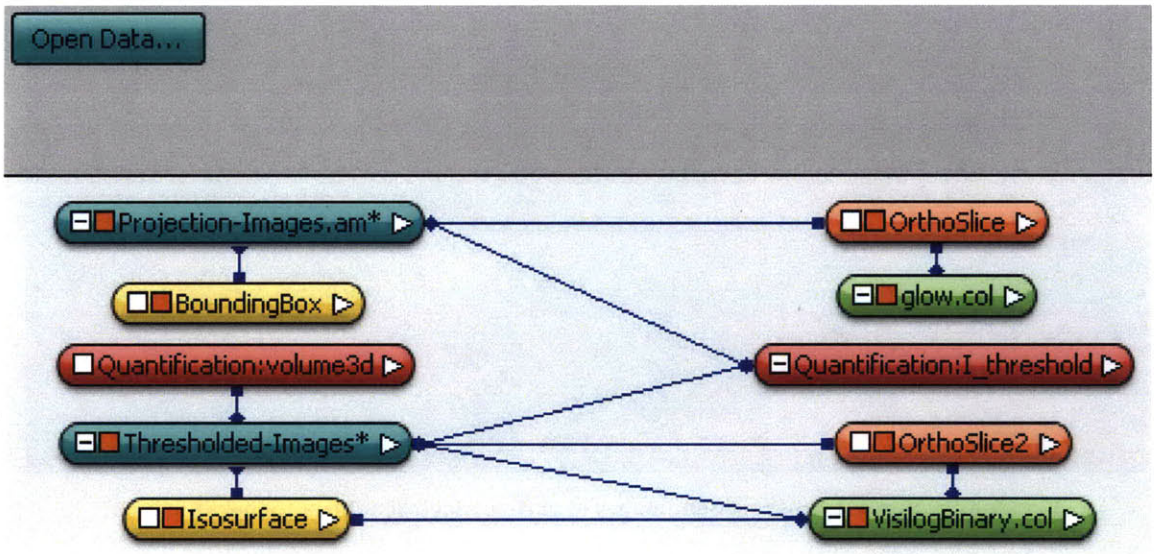

Figure 4-6 Avizo workflow for basic microCT data manipulation.

4.3 MicroCT Imaging Studies of Caffeine-Lactose Tablets

The caffeine-lactose tablets as described in Chapter 2 were first studied with the microCT toolbox. The tablets were made from the same amount of initial materials but were compacted into different final thickness. The highest compaction force was applied to 2.3mm tablets, while the lowest was applied to 3.2mm ones. Scanning and reconstruction were conducted as described above. A set of cross sections of the tablets are shown in Figure 4-7. As discussed in Chapter 2, spray-dried lactose mainly undergoes fragmentation during compaction process. The microCT images illustrate the various degrees of fragmentation and the resulted microstructure. The hard tablets show a much more homogeneous appearance, probably due to extensive breakdown of the powder granules during compression process. The pore sizes are small and relatively uniform. As the tablets become softer, there are significantly more large pores. The

brighter aggregates are powder granules that have not fragmented during the compaction process.

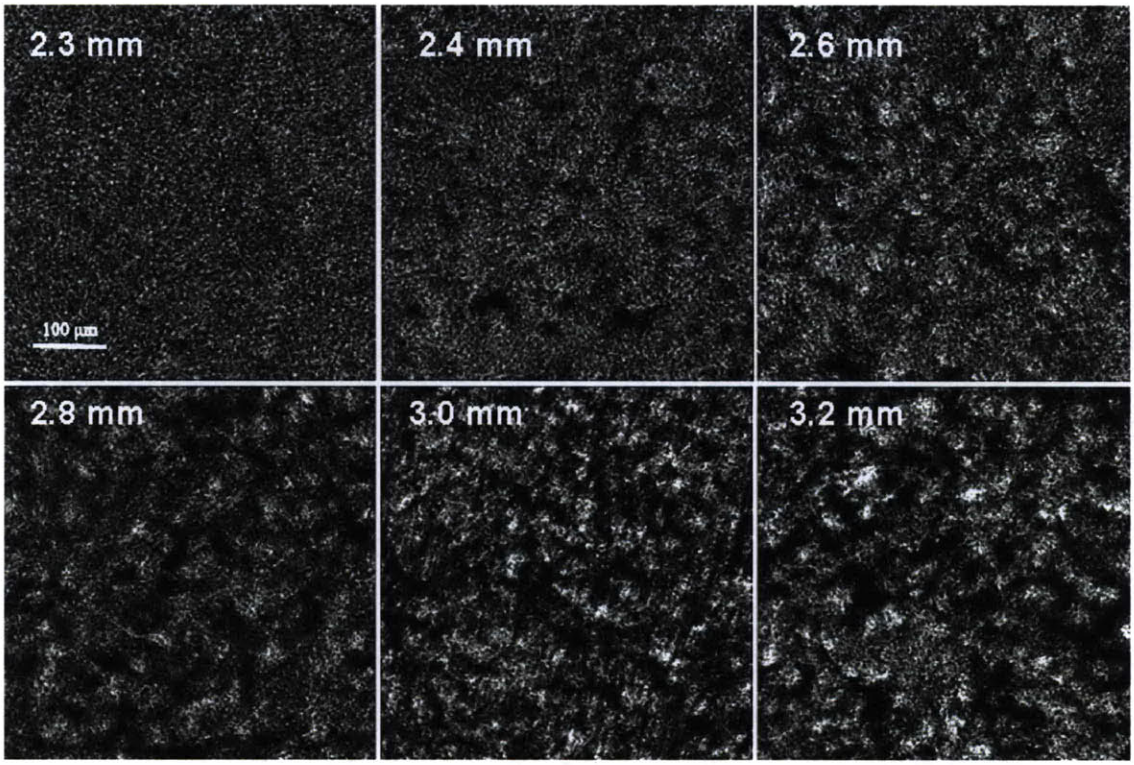

Figure 4-7 MicroCT cross section images of caffeine-lactose tablets. 500umX500um.

Next, the total porosity of the microCT 3-D models were determined and compared with those obtained via two other techniques (Figure 4-8). Helium pycnometry was adopted to measure the absolute density of the powder mixture used for tablet production. With the knowledge of tablet's physical dimension and weight, it is now possible to calculate a theoretical porosity value for each tablet:

$$P = \left(\frac{\pi r^2 H \rho_T - W}{\pi r^2 H \rho_T}\right)$$

Where ρ_T is the material true density, H is tablet thickness, W is tablet weight, r is tablet radius. A polynomial fitting curve across the theoretical porosity values represents the theoretical porosity curve. Both MicroCT and mercury porosimetry measurements have good agreement with theoretical values in hard and medium-strength tablets, but microCT is more accurate in measuring soft tablets. It is possible that in mercury porosimetry tests, the walls of soft tablet might not withstand the pressure of initial

mercury filling and collapse before measurement starts, resulting in significantly lower porosity recorded.

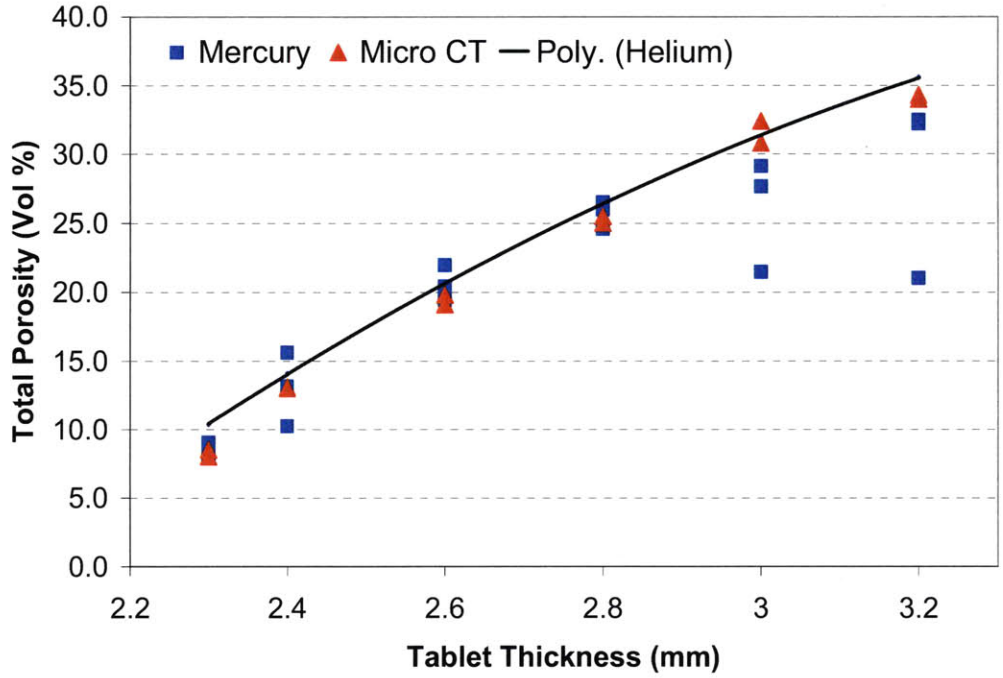

Figure 4-8 Comparison of microCT porosity data with those obtained via helium pycnometry and mercury porosimetry.

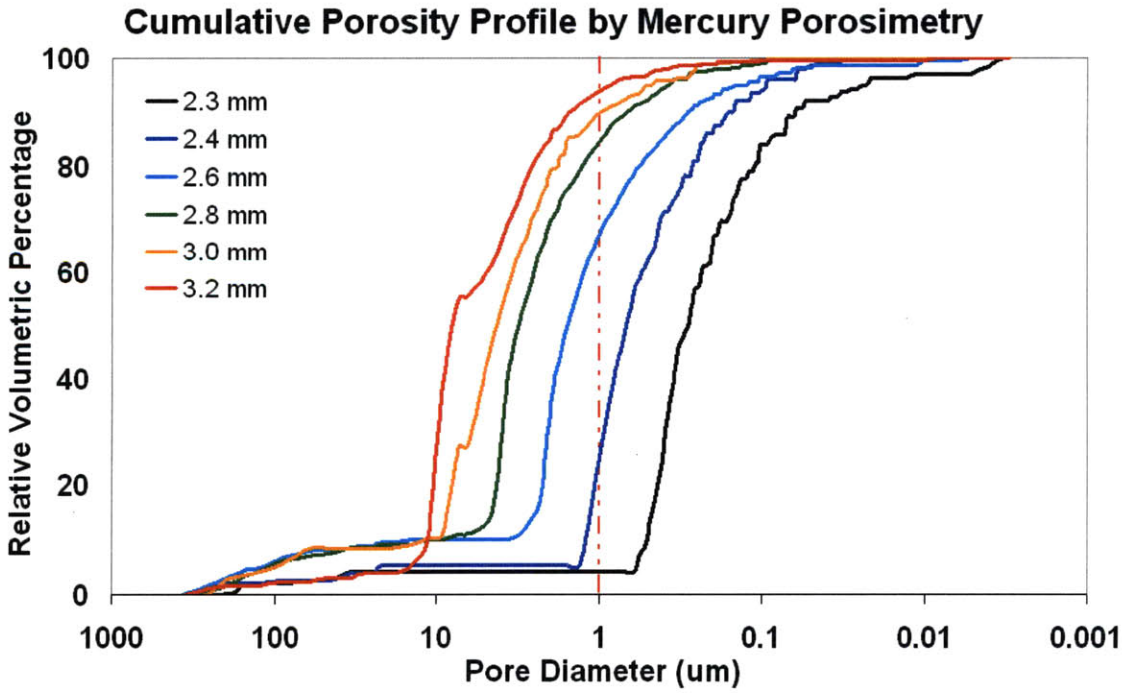

Figure 4-9 Representative porosity profiles of caffeine-lactose tablets by mercury porosimetry.

Figure 4-9 displays a series of representative porosity profiles obtained with mercury porosimetry. The mercury porosimetry profiles show that there are two groups of pore sizes in all tablets, with one group in the range of 10-500 μm in diameter and another in the range of 0.01-10 μm. The diameters of the smaller pores, the majority of the population, increase as tablet goes softer. The relative volumetric percentage of large pores in hard tablets (2.3mm and 2.4mm) is ~5%, which jumps to 10% in medium-strength to soft tablets (2.6mm, 2.8mm and 3.0mm). In the softest tablet (3.2mm), contrary to expectation, this percentage drops to 5%. This further indicates that some of the largest pores in the soft tablets could have been taken up during the initial mercury filling stage, leading to inaccurate measurement. On the other hand, microCT cross section images seem to indicate that large pores occupy a higher volumetric percentage than what is recorded by mercury porosimetry.

The resolution used in the microCT measurement is 1.39 μm/pixel. Taking partial-volume effect into consideration, 1 μm is probably the smallest pore diameter that can be detected with microCT measurement. According to the porosity profile by mercury porosimetry, the majority of pores in hardest tablet (2.3mm) would be under 1 μm in diameter. If this were true, the porosity measured with microCT would be 95% lower than the results of mercury porosimetry. However, the reconstructed microCT images of the 2.3mm tablets clearly show a significant group of pores larger than 1 μm in diameter (Figure 4-10). Since the two methods yield very similar results in total porosity, they are possibly measuring the same pore volumes but giving different readings of pore diameter.

The discrepancy in pore size measurement can be explained by the theoretical bases of the two methods. Mercury porosimetry was developed on the principles of capillary hydrostatics, which state that for a cylindrically shaped pore, the pressure needed to push mercury into the pore is inversely related with the diameter of the pore (18). In pharmaceutical tablets, however, the pores take irregular shapes and might be interconnected with each other via smaller channels. As a result, both methods would

measure the volume of the pores, but mercury porosimetry reports the equivalent diameter of the channels instead of the pores, as illustrated in Figure 4-11.

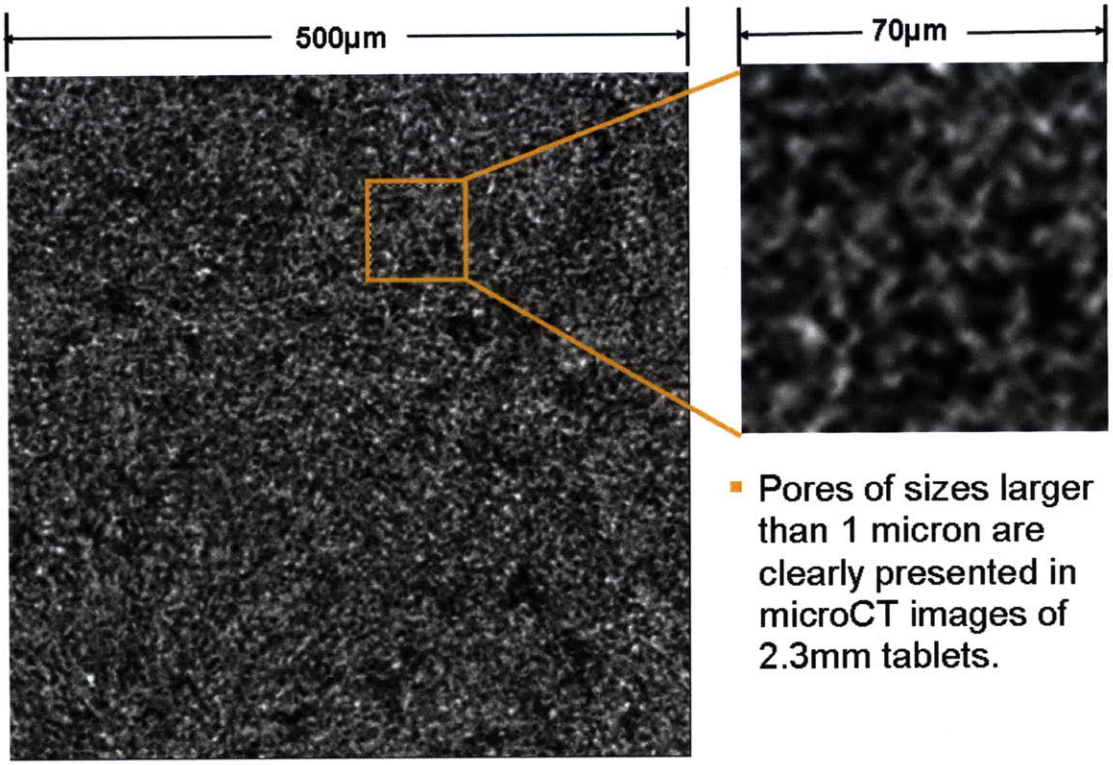

Figure 4-10 MicroCT cross section images show abundant amount of pores larger than 1 um in diameter.

If a string of pores are interconnected, the diameter reading for the pore spaces will be reported as the smallest pore neck encountered during the mercury intrusion process. This systematic bias is absent in microCT measurement, in which the 3-D dimension of the actual pores is directly visualized and quantified. MicroCT measurement coupled with digital post-processing holds the promise of precise description of tablet microstructure, which is not possible with current standard methods. The combined data suggests that the hard lactose tablets have pores of > 1µm diameter connected with channels of 0.1-1µm in diameter. Method for detailed characterization of porosity profiles will be discussed in Chapter 6.

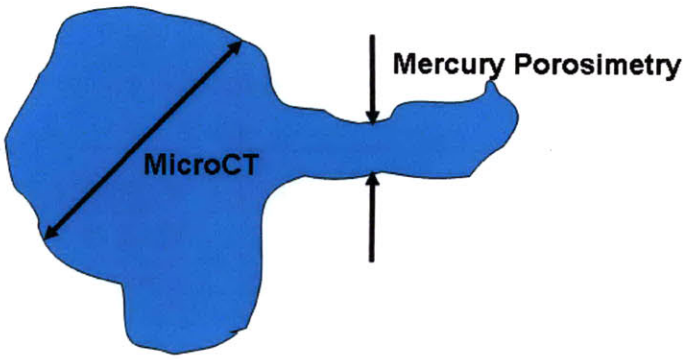

Figure 4-11 Illustration of pore diameter measurement in a typical pore structure of lactose tablets.

Next, the relationship between total porosity and tablet properties are evaluated. An exponential relationship is observed when tablet tensile strength is plotted against microCT derived porosity (Figure 4-12). This exponential relationship was first observed in sintered metals(19), and is then realized to be applicable to a range of pharmaceutical powders (20, 21).

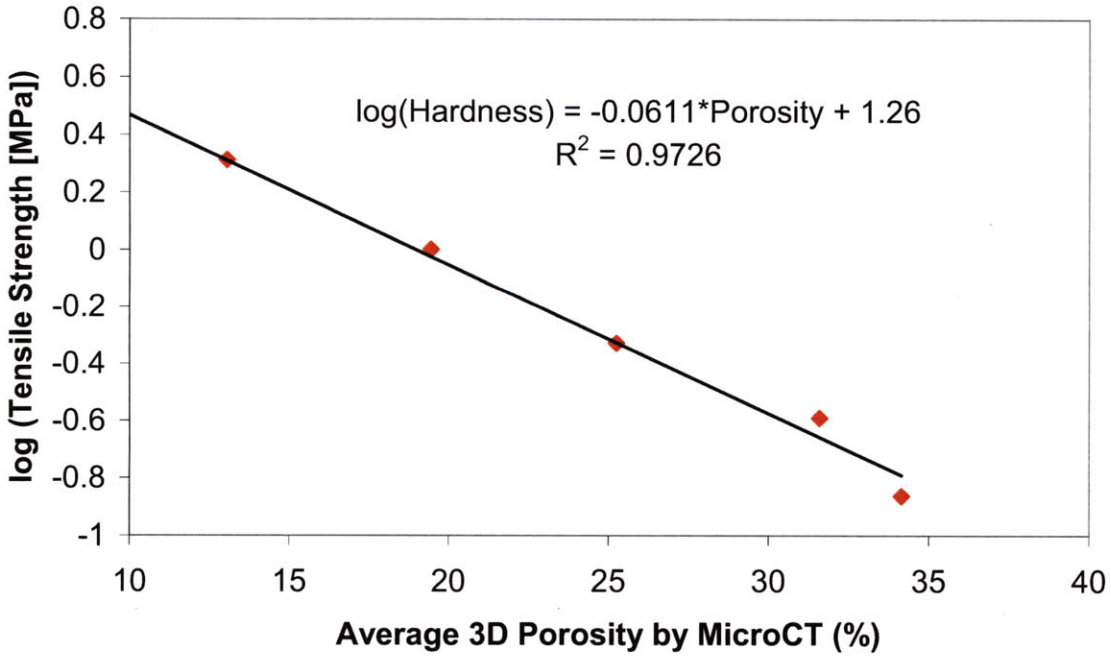

Figure 4-12 Exponential relationship between tablet tensile strength and microCT porosity.

The relationship between tensile strength and porosity is termed compactibility, the ability of a material to produce a tablet with sufficient strength under certain degree of

densification. Another two terms that used frequently in characterizing tabletting properties are tabletability and compressibility. Tabletability is the ability of the powder to be transformed into a tablet of specified strength under the effect of compression pressure, while compressibility is the ability of a material to reduce in volume as a result of applied pressure (20). The three properties assess relationships among volume reduction, strength, and external pressure of the tablets (Figure 4-13). Since the tablet press used in the study is not instrumented, compression pressure could not be recorded in this case. This study demonstrated the capability of microCT analysis in evaluating important tabletting properties of pharmaceutical powders.

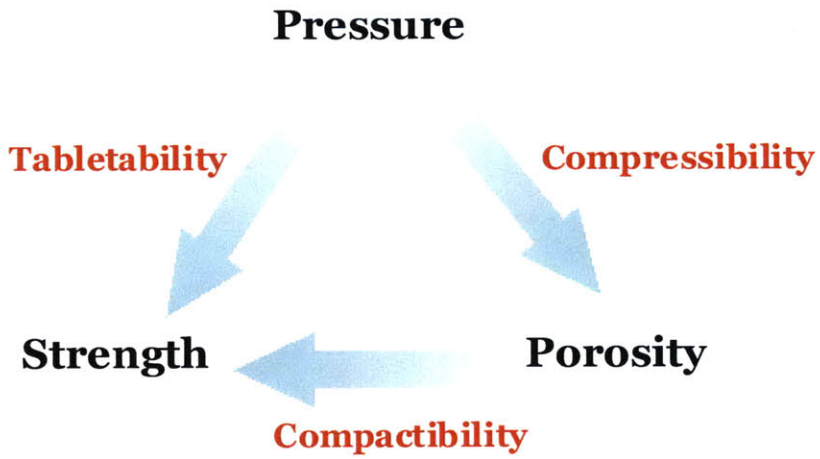

Figure 4-13 Relationship among compression pressure, tablet strength, and porosity.

4.4 MicroCT Imaging Studies of Compound-A Tablets

After experimentation with the caffeine-lactose tablets, a more extensive formulation system would be explored. A natural extension in this study is to bridge the caffeine-lactose direct compression system and the compound-A roller compaction system. Compound-A roller compaction formulations are expanded to also include 10% and 30% drug load, where lactose becomes the dominant material in the formulation. The formulations are listed in Table 4-2 and the manufacturing process is the same as that for the previous compound-A roller compaction formulations. Lubrication levels are kept the same so that the impact of the additional excipients remains similar.

Table 4-2 Composition of M10/M30/M50/M70 formulations.

MIT (M10/M30/M50/M70)	wt%
Compound A	10/30/50/70
Spray-dried Lactose DCL14 (DMV)	85/65/45/25
Colloidale silicon anhydrous (Aerosil 200)	1
Magnesium stearate (Faci)	4

All the formulations performed well during the roller compaction and tablet compaction stages. Tablets with target hardness of 100N/75N/50N/25N are produced for each of the formulations. For microCT analysis, whole tablets were placed inside of a plastic tube and scanned at 3μm resolution with 2.3s scanning time, while tablet fragments were scanned at 1.4μm resolution with 1.18s scanning time.

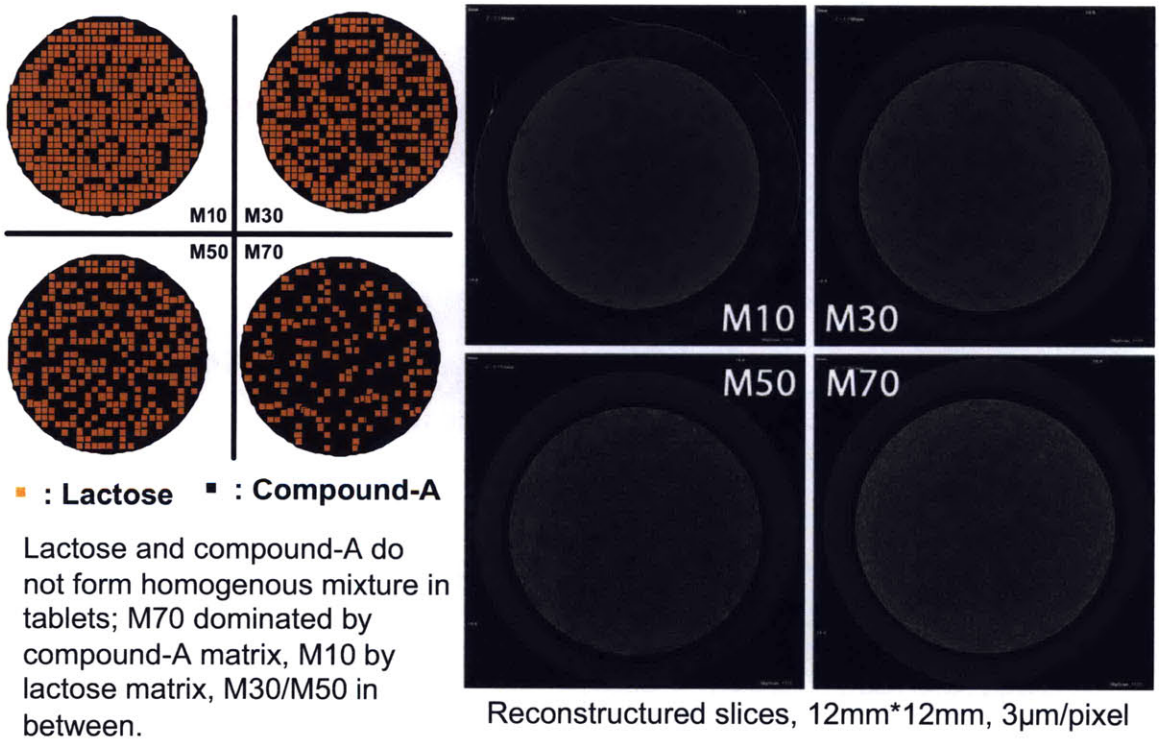

Figure 4-14 Cross sections and illustration of whole-tablet microCT scans for compound-A tablets.

A set of reconstructed microCT cross-section images are displayed in Figure 4-14. Because of the much higher density of lactose, it manifests itself as the brighter areas. The darker areas are compound-A. From the cross sections it is immediately apparent that lactose and compound-A do not form homogenous mixture. The distribution pattern

is illustrated with the figures on the left, where yellow dots represent lactose and black dots represent compound-A. In M10, lactose forms the dominant structure, with sparing compound-A regions spotted randomly throughout the tablet. In M70, compound-A forms the supporting structure. The scenarios for M30/M50 are mid-way between those for M10 and M70.

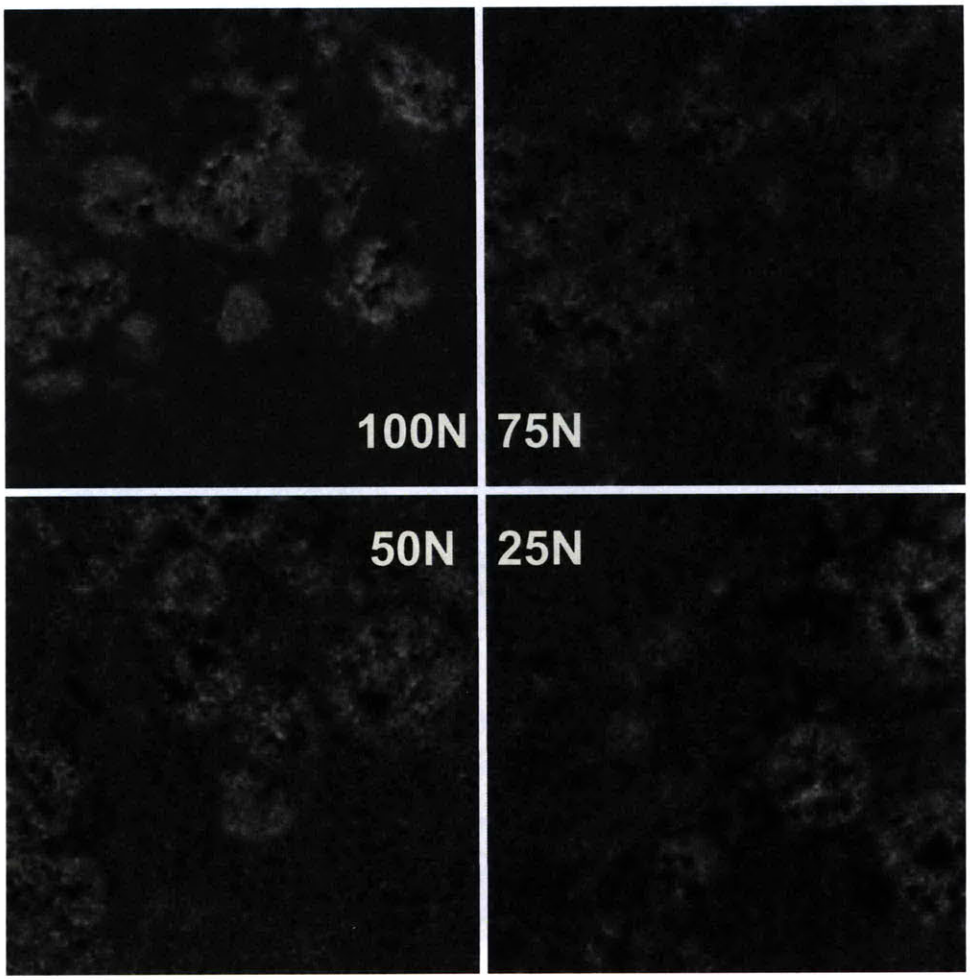

Figure 4-15 Cross section microCT images of M70 compound-A tablets. 500umX500um.

A closer look at the reconstructed microCT images for tablet fragments reveals more striking features of the microstructure. The lactose granules are largely intact within the M70 tablets, surviving the roller compaction, milling, and tablet compression stages. Even the intra-granular pores of the lactose particles have been well preserved, albeit squeezed to smaller sizes in harder tablets. It seems that compound-A goes through plastic densification during the manufacturing process, providing a cushion for the lactose granules.

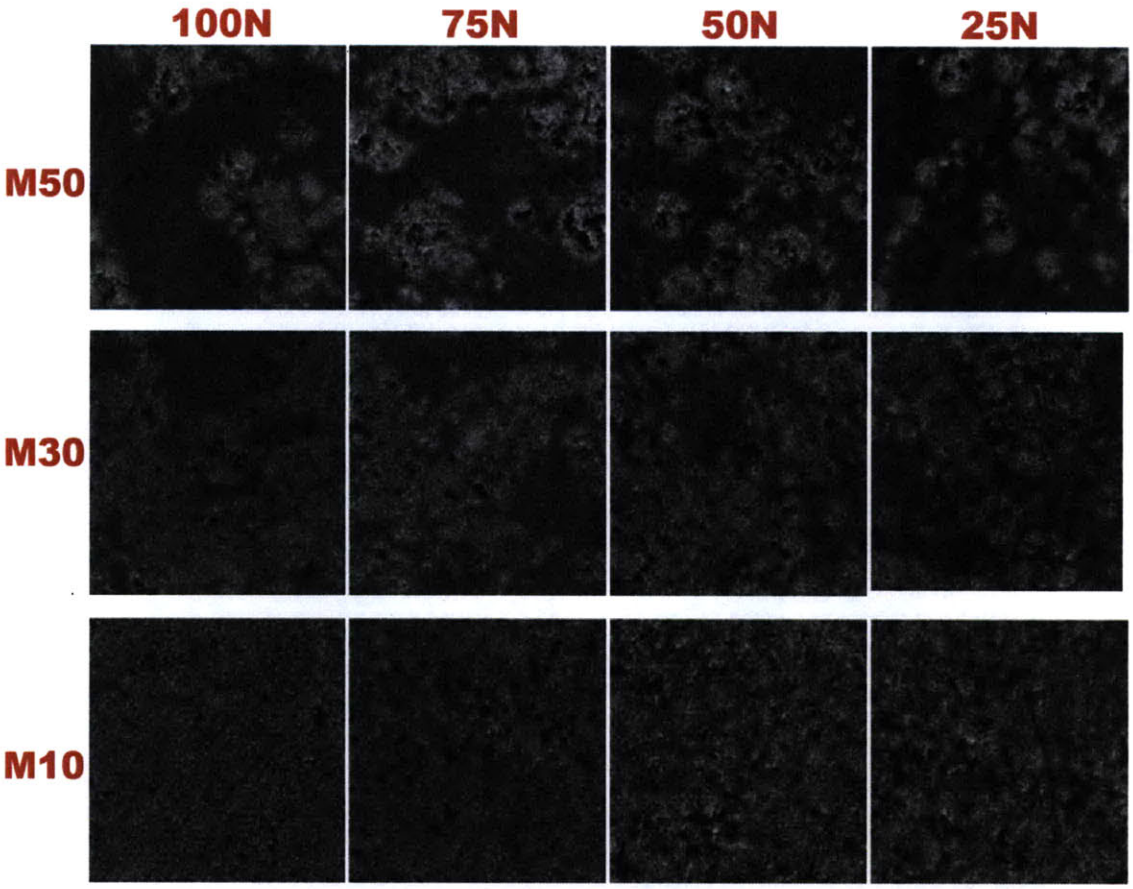

Figure 4-16 Cross section MicroCT images of M10/M30/M50 compound-A tablets. 500umX500um.

The cross-section images of the other formulations are demonstrated in Figure 4-16. The M50 microstructure looks very similar to that of M70, but with a larger number of lactose granules embedded. In M30 tablets, the lactose granules start to go through deformation, losing the original spherical shapes and forming dense clusters. For M10 tablets, lactose assumes dominant role and undergoes extensive fragmentation, forming structures very similar to those of 10% caffeine-lactose tablets.

It is clear that the transition of material composition first imposes incremental changes but eventually induced dramatic alteration of tablet microstructure. In order to evaluate the impact on mechanical properties of the tablets, compaction response curves, where tablet strength is plotted against tablet bulk density, are prepared for the compound-A formulations (Figure 4-17).

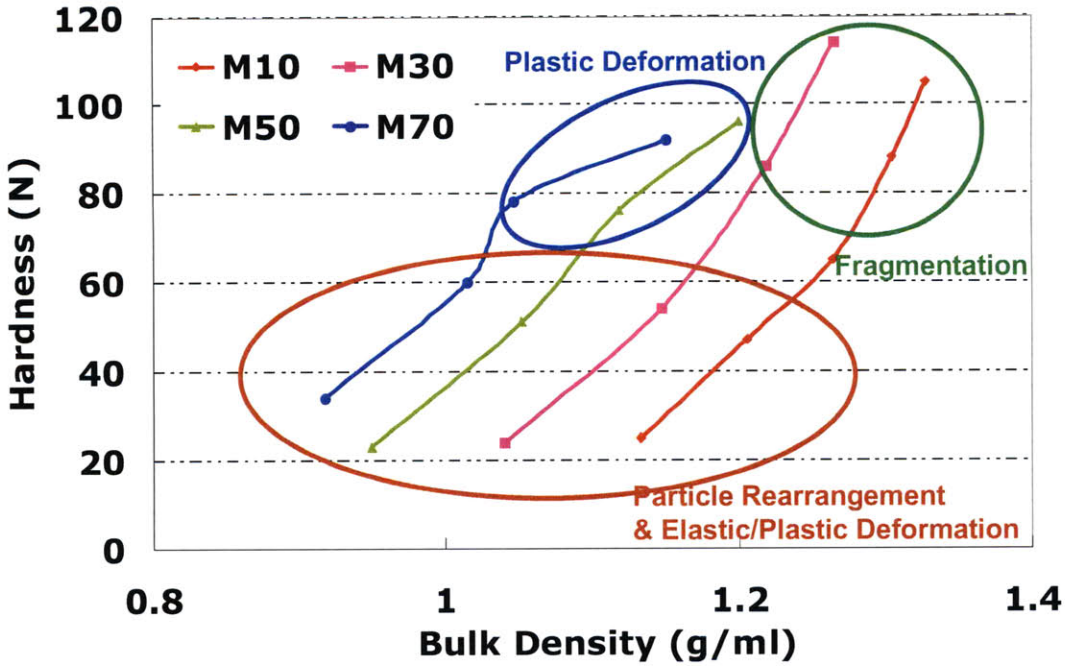

Figure 4-17 Compaction response curves for M10/M30/M50/M70 compound-A tablets.

The initial compaction stage reaching a hardness of 50N assumes the same slope for different compound-A loadings, suggesting similar strength gains during the particle rearrangement and initial deformation process. For M50/M70, it takes much more density gain than that for M10/M30 to reach the same strength level. The results indicate that lactose fragmentation develops stronger solid bonding than compound-A plastic deformation, potentially via the formation of solid bridges with mechanical interlocking.

Based on the microCT and mechanical strength data, the following compaction mechanisms could be summarized (Figure 4-18). For compound-A dominated compaction process, compound-A provides a cushion for lactose granules and preserves their shapes, while compound-A itself first fills up the large voids and then undergoes plastic densification, eventually forming a densely packed solid form. In lactose dominated compaction process, without the cushion layer of compound-A, lactose undergoes extensive fragmentation to form the tablet matrix, squeezing compound-A into small segments.

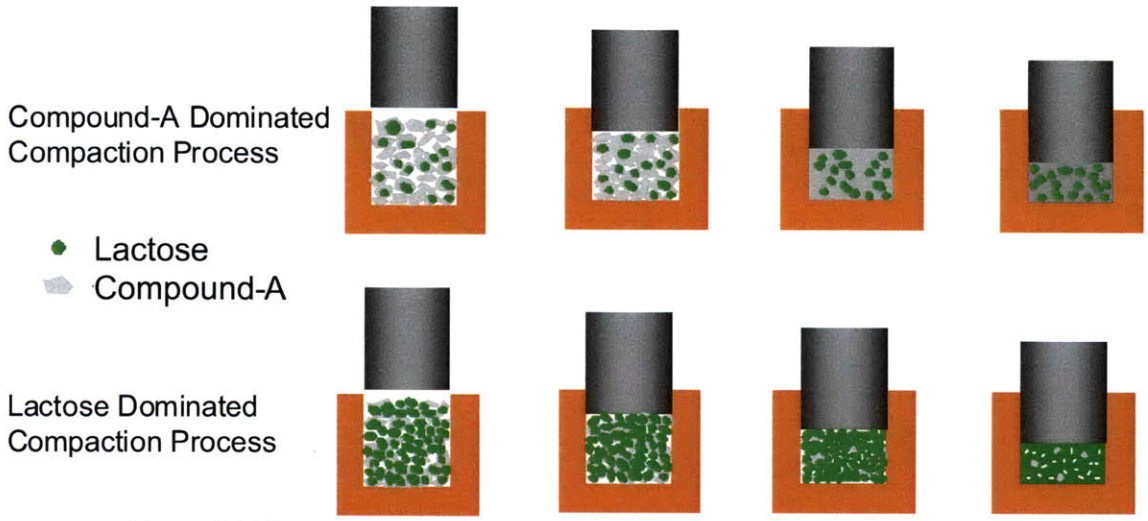

Figure 4-18 Proposed tablet compaction mechanisms for compound-A tablets.

MicroCT measurement of total porosity for M70 tablets are shown in Figure 4-19. Except for the data of 100N tablets, all the other microCT data points are lower than expected. This is counter-intuitive as microCT is supposed to be more accurate for softer tablets.

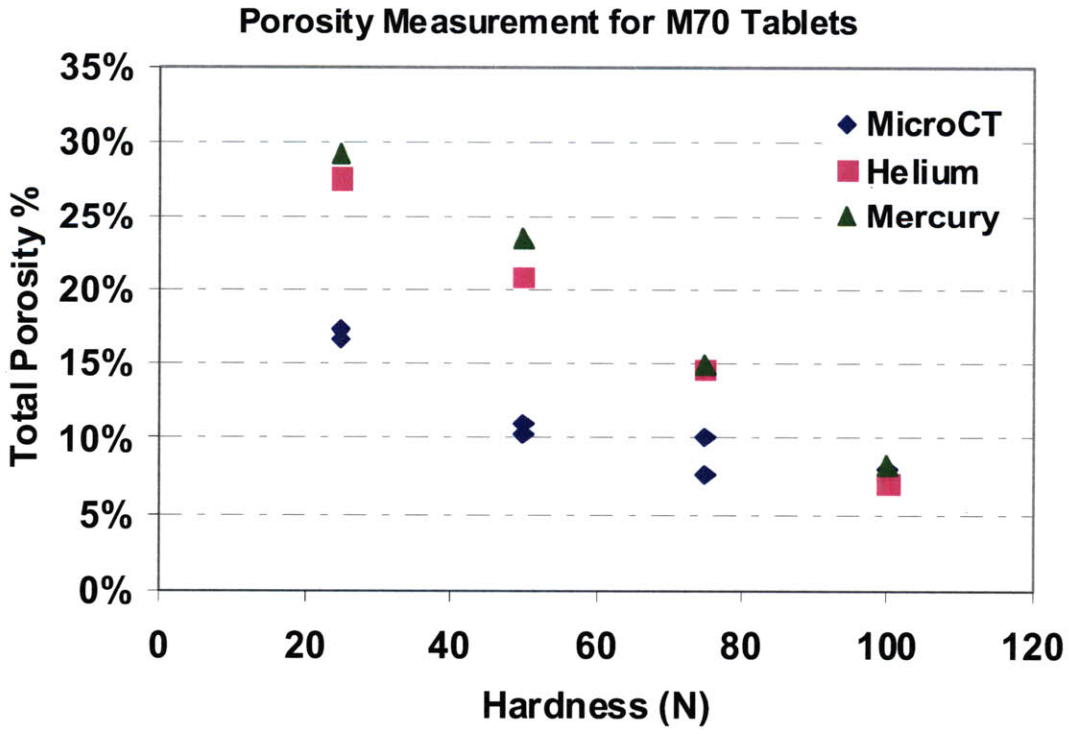

Figure 4-19 Total porosity measurements of M70 tablets.

The microCT porosity profile of 100N M70 tablet (Figure 4-20) provides important information to explain the data. According to microCT, most of the pores are single voxel (equivalent diameter = 1.72 μm) or 2-3 voxels in size. There are some larger pores representing pore space within the embedded lactose granules. With the focused ion beam scanning electron microscopy (FIB-SEM) study described in Chapter 7, we would identify a typical pore diameter of 0.2 μm – 0.4 μm for 100N M70 tablets. Therefore, a large number of microCT single voxel pores are incorrect identifications probably due to partial volume effect. They will add to total pore volume quickly as a single-voxel pore is equal to 60-100 pores in volume at the average pore size given by FIB-SEM. This resulted in the coincidentally "correct" total porosity values by microCT for 100N M70 tablets. With a softer M70 tablet, the compound-A matrix relaxes and the pores become larger in size. However, before the pore sizes catch up with microCT resolution, microCT identified pore volume would not grow as fast as actual pore volume would. This led to the lower total porosity values by microCT for softer M70 tablets. The data suggests that microCT resolution must be smaller than the typical pore size in order to obtain adequate microstructural characterization.

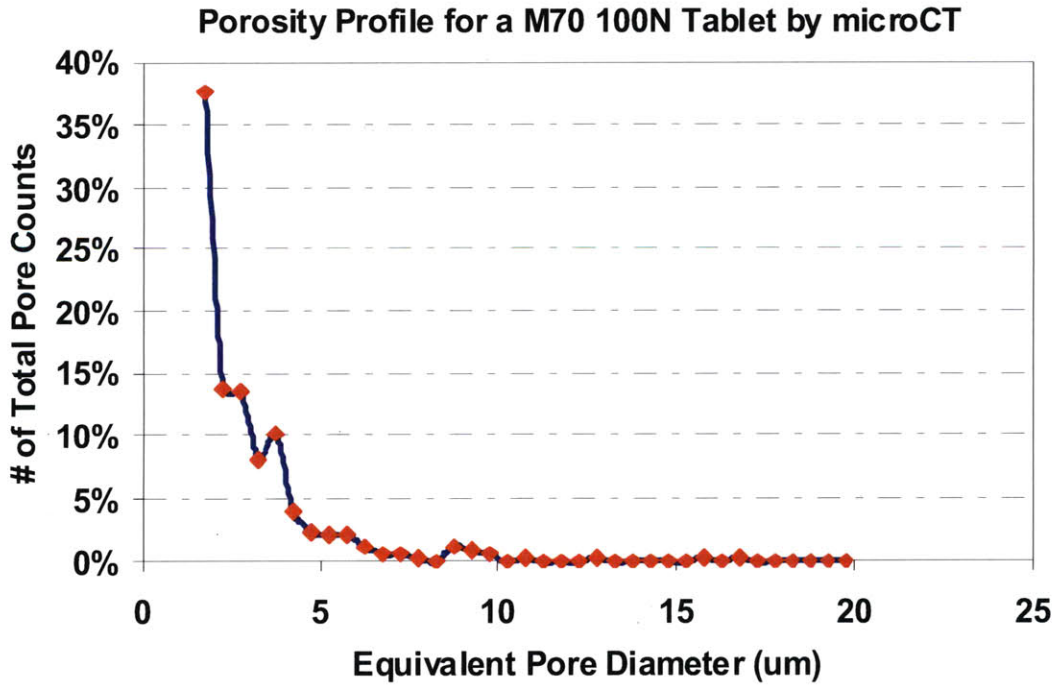

Figure 4-20 Porosity profile of 100N M70 tablet as measured by microCT.

4.5 Summary

In this chapter we have described the establishment of a microCT data acquisition method for pharmaceutical tablets and the development of a digital post-processing workflow. The internal pore space of tablets could be separated from the other materials and visualized in a 3-D model, facilitating the characterization of the internal structure. The total porosity could be calculated based on the model.

In microCT study of 10% caffeine-lactose direct compression tablets, various degrees of lactose granule fragmentation were observed in tablets of different strength. The total porosity measurement of microCT is in excellent agreement with theoretical values predicted from true density measurements. When compared with mercury porosimetry, microCT is more reliable for soft tablets, while the measurements for hard tablets are slightly lower than predicted due to the inability to capture pores smaller than resolution power. The orders of magnitude of pore sizes as measured by the two techniques are different. This could be explained by the discrepancy in theoretical bases of the two methods. Mercury porosimetry measures the diameter of the pore necks while microCT allows direct characterization of the pores. The combined data suggests that the hard lactose tablets measured have pores of $> 1\mu m$ diameter connected with channels of 0.1-$1\mu m$ in diameter.

The microCT study of the M-series compound-A roller compaction formulations illustrate that transition of material composition first imposes incremental changes but eventually induces dramatic alteration of tablet microstructure. In M70 tablets, compound-A forms the supporting structure while acting as a cushion for lactose granules, preserving the latter throughout the manufacturing process. In M10 tablets, lactose forms the majority of the tablet matrix and undergoes fragmentation similar to that in 10% caffeine-lactose tablets. M30/M50 formulations are in-between of the two extreme scenarios. The compaction response curves of the formulations further point out that the fragmentation of lactose represents a more effective binding power than the densification of compound-A in creating a tablet of higher strength. Scenarios for tablet compaction were proposed based on the information revealed by microCT measurements. MicroCT

resolution was not sufficient for quantitative study of M70 tablet microstructure, indicating a technical barrier to be addressed by technology advancement.

4.6 Chapter Bibliography

1. J.D. Elliott, SD. X-ray microtomography. Journal of Microscopy:211-213 (1982).
2. S.R. Stock. Recent advances in X-ray microtomography applied to materials. International Materials Reviews. 53:129-181 (2008).
3. S.R. Stock. X-ray microtomography of materials. International Materials Reviews. 44:141-164 (1999).
4. L. Farber, G. Tardos, and J.N. Michaels. Use of X-ray tomography to study the porosity and morphology of granules. Powder Technology. 132:57-63 (2003).
5. I.C. Sinka, S.F. Burch, J.H. Tweed, and J.C. Cunningham. Measurement of density variations in tablets using X-ray computed tomography. Int J Pharm. 271:215-224 (2004).
6. V. Busignies, B. Leclerc, P. Porion, P. Evesque, G. Couarraze, and P. Tchoreloff. Quantitative measurements of localized density variations in cylindrical tablets using X-ray microtomography. Eur J Pharm Biopharm. 64:38-50 (2006).
7. T. Sovany, P. Kasa, K. Vakli, and K. Pintye-Hodi. X-ray computed microtomography for determination of relationships between structure and breaking of scored tablets. X-Ray Spectrometry. 38:505-509 (2009).
8. C.Y. Yangand X.Y. Fu. Development and validation of a material-labeling method for powder process characterization using X-ray computed tomography. Powder Technology. 146:10-19 (2004).
9. X.W. Fu, J.A. Elliott, A.C. Bentham, B.C. Hancock, and R.E. Cameron. Application of X-ray microtomography and image processing to the investigation of a compacted granular system. Particle & Particle Systems Characterization. 23:229-236 (2006).
10. X.W. Fu, M. Dutt, A.C. Bentham, B.C. Hancock, R.E. Cameron, and J.A. Elliott. Investigation of particle packing in model pharmaceutical powders using X-ray microtomography and discrete element method. Powder Technology. 167:134-140 (2006).
11. S.J. Inman, B.J. Briscoe, and K.G. Pitt. Topographic characterization of cellulose bilayered tablets interfaces. Chemical Engineering Research & Design. 85:1005-1012 (2007).
12. E. Karakosta, P.M. Jenneson, R.P. Sear, and P.J. McDonald. Observations of coarsening of air voids in a polymer-highly-soluble crystalline matrix during dissolution. Phys Rev E Stat Nonlin Soft Matter Phys. 74:011504 (2006).
13. G. Chauve, F. Raverielle, and R.H. Marchessault. Comparative imaging of a slow-release starch exciplent tablet: Evidence of membrane formation. Carbohydrate Polymers. 70:61-67 (2007).
14. L.A. Feldkamp, L.C. Davis, and J.W. Kress. Practical Cone-Beam Algorithm. Journal of the Optical Society of America a-Optics Image Science and Vision. 1:612-619 (1984).
15. G.R. Davisand J.C. Elliott. Artefacts in X-ray microtomography of materials. Materials Science and Technology. 22:1011-1018 (2006).
16. Y.S. Wu, L.J. van Vliet, H.W. Frijlink, and K.V. Maarschalk. Pore size distribution in tablets measured with a morphological sieve. International Journal of Pharmaceutics. 342:176-183 (2007).

17. T.W. Ridlerand S. Calvard. Picture Thresholding Using an Iterative Selection Method. Ieee T Syst Man Cyb. 8:630-632 (1978).
18. E.W. Washburn. The dynamics of capillary flow. The Physical Review. 17:273-283 (1921).
19. E. Ryshkewitch. Compresssion strength of porous sintered alumina and zirconia. Journal of American Ceramics Society. 36:65-68 (1953).
20. E. Joiris, P. Di Martino, C. Berneron, A.M. Guyot-Hermann, and J.C. Guyot. Compression behavior of orthorhombic paracetamol. Pharm Res. 15:1122-1130 (1998).
21. C.Q. Sunand D.J.W. Grant. Influence of crystal structure on the tableting properties of sulfamerazine polymorphs. Pharm Res. 18:274-280 (2001).

Chapter 5 Dissolution Mechanism Study with Novel Tablet Holder

Dissolution is a central test that is widely utilized by the pharmaceutical industry in multiple aspects. In Chapter 2, a detailed dissolution study of lactose-caffeine tablets with the standard paddle dissolution method was described. An empirical relationship between tablet mechanical strength, storage condition, and dissolution speed was developed. However, the test did not give further information about the mechanism of dissolution. The complex hydrodynamics situation and changing dosage form morphology in standard dissolution methods make it difficult to describe the process with analytical models, preventing our understanding of the rate-limiting steps of dissolution. In this chapter, a novel tablet holder designed for probing dissolution mechanism of USP #2 paddle method is presented. Its applications in dissolution mechanism study of tablets made from direct compression as well as roller compaction are described. Combined with standard paddle dissolution, the tablet holder is shown to help identify the intrinsic drivers of dissolution process, bringing us one step closer to rational formulation design.

5.1 The Models of Pharmaceutical Dissolution Tests

Dissolution in general is defined as "the process by which a solid substance enters the solvent phase to yield a solution" (1). Study of dissolution was initiated by physical chemists at the end of the 19th century. The dissolution rate of a solid substance was described by the Noyes-Whitney equation (2) shown below,

$$\frac{dC}{dt} = k(C_s - C_t)$$

where the proportionality constant k is addressed as the "apparent dissolution rate constant", C_s is the saturated concentration, C_t is the bulk concentration of the dissolved drug at time t. The driving force for dissolution is the concentration gradient between the saturated concentration and bulk concentration. This physical model became the basis for thinking about solid-liquid mass transfer and has been widely used.

A few years later, Erich Brunner further developed dissolution theory in collaboration with Nernst based on diffusion layer theory and Fick's second law (3). In this Brunner-Nernst equation, the dissolution rate constant is expressed as:

$$k = \frac{A \cdot D}{\delta_{HL} \cdot V}$$

where D is the effective diffusion coefficient of the drug molecule, A is the surface area available for dissolution, δ_{HL} is the thickness of the diffusion layer, and V is the media volume employed in the test.

Higuchi analyzed the dissolution kinetics from an ointment assuming homogenous distribution of drug and sink condition in the medium (4). He arrived at the following expression of dissolution rate:

$$\frac{q(t)}{q(\infty)} = K\sqrt{t}$$

This was further developed by Peppas into a power-law equation for generalized description of dissolution from polymeric dosage forms (5):

$$\frac{q(t)}{q(\infty)} = K_1 t^n$$

Where K_1 is a constant reflecting the structural and geometric characteristics of the delivery system expressed in time^n units and n is a release exponent the value of which is related to the underlying mechanism(s) of drug release (6). Both equations are only applicable to the first 60% of the dissolution for a tablet, the period of which a tablet typically still holds its shape.

These models are based on the assumption that diffusion through a stagnant film layer is the rate limiting step. An alternative model is called the interfacial barrier model, where the interfacial solid-liquid mass transfer is the rate limiting step due to a relatively high activation energy barrier (7). This model has not seen full development and does not have an explicit mathematical description. Another model worth mentioning maps dissolution data to a Weibull equation, a cumulative function of a continuous probability distribution. The relationship was first discovered by Langenbucher (8) and then

confirmed by other studies utilizing Monte Carlo simulations (9, 10). The cumulative fraction of dissolved material is expressed as:

$$x = 1 - \exp\left[\frac{-(t-T)^b}{a}\right]$$

Where t is time, T is lag time, a is a scale constant and b is a shape constant. For a thorough review of the physical / mathematical models developed for pharmaceutical dissolution tests, please refer to Dokoumetzidis and Macheras (11).

The models described above have two common points. They all consider dissolution as a single process that can be described with one set of equations, and none of them considered the impact of tablet microstructure, which could be very important for dissolution speed as we will demonstrate in this Chapter.

5.2 Design of Tablet Holder for Mechanism Study of Paddle Dissolution

Paddle dissolution (USP #2) method has remained the most popular method in dissolution testing during the last a few decades. However, the simple setup of the paddle dissolution method is accompanied by a complex hydrodynamics condition. From CFD simulation (12) and experimental results, it is observed that right under the paddle there is a region with highly unpredictable swirling flows (Figure 5-1). This region, nicknamed the "dead zone", is often the region that tablet sits in during most of the dissolution period. The flow speed at 1cm from the bottom center could be three times as high as that at the bottom center, so the positioning of the tablet could potentially have a big impact on the dissolution results (13). A tablet can also collapse into a pile of debris, further complicating the understanding of the dissolution mechanism and impede *in vitro-in vivo* correlation (IVIVC) studies.

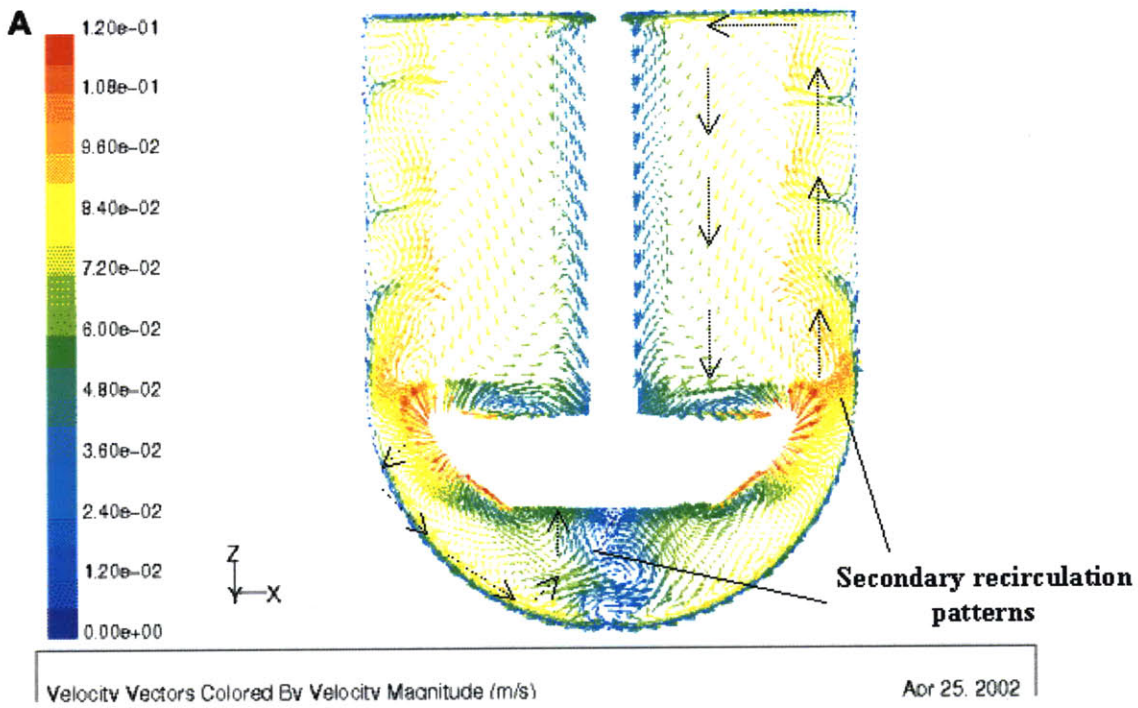

Figure 5-1 Computational fluid dynamics simulation of paddle dissolution test, 50 RPM, adapted from McCarthy, et al., 2003

5.2.1 Previous Efforts

The major problems outlined above are unpredictable hydrodynamics condition and constantly changing tablet morphology. In order to better understand the dissolution process, multiple studies have targeted these two problems. Wu, et al. designed a cylinder-shaped tablet holder (Figure 5-2) to be placed at the bottom center of dissolution vessels (14). The holder was shown to help differentiate dissolution profiles of Theophylline and Naproxen tablets subjected to paddle dissolution with various paddle designs, but no detailed analysis was conducted on the new hydrodynamics conditions. Elevated platform with distinctive edges could result in turbulent flow pattern close by and thus further complicate the dissolution process.

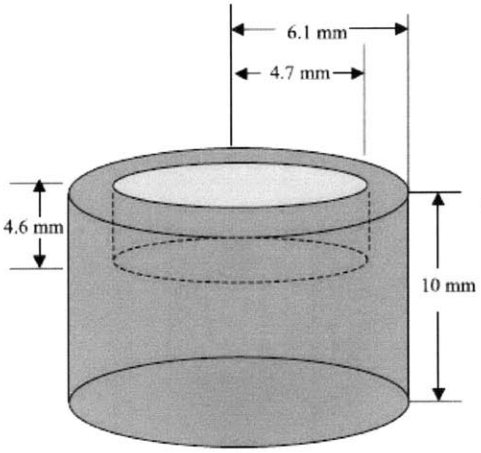

Figure 5-2 Tablet holder designed to fix dissolution surface. Adapted from Wu, et al., 2004

Peltonen et al. designed a channel flow method to both define exposure area and generate a consistent laminar flow hydrodynamics condition (15, 16). The tablet is placed inside a holder, with only one surface exposed to a laminar flow controlled via a peristaltic pump (Figure 5-3).

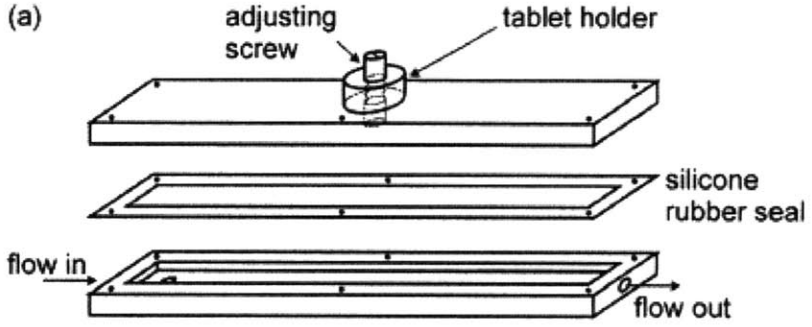

Figure 5-3 Channel flow method for understanding dissolution. Adapted from Peltonen, et al., 2003

The author concluded that the channel flow cell allows a smooth initial dissolution, and the mass transfer process can be modeled. However, at a later stage the dissolution data can fluctuate quite significantly. It also needs the establishment of an integrated system, including coupled UV system, pump, and a thermo-stating bath.

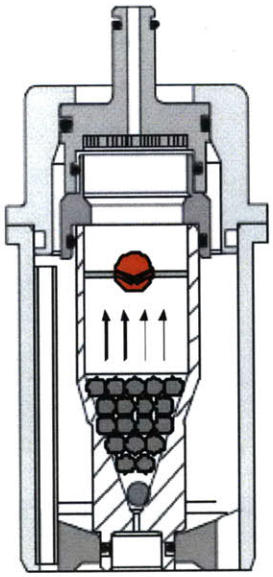

Figure 5-4 Illustration of flow-cell apparatus in packed/laminar flow mode. Red object is tablet. Modified from SOTAX Corp., Horsham, PA, USA

Within USP compendial dissolution methods, flow-cell dissolution (USP #4) is the most amenable method for studying dissolution mechanism. Flow cell dissolution has relatively mild agitation and mathematically definable medium flow patterns, where a tablet is placed on a supporter and subjected to a laminar flow in packed bed scenario (Figure 5-4). Flow-through cell dissolution is often configured as an open system, in which the medium flows through without being recycled. This generates a perfect "sink" condition for poorly soluble drugs, where concentration in the medium is close to zero. Flow-through cell dissolution has not gained massive popularity in the last a few decades. Instead, paddle method and basket method with proper agitation rate (50-100 RPM for paddle, 50-150 RPM for basket) have been suggested by FDA to be the most suitable for routine dissolution testing (17) and bioavailability / bioequivalence studies (18).

The flow-through cell apparatus is not an ideal tool to mimic and understand the dissolution mechanism in paddle apparatus. The flow speed in this USP #4 test is typically at least an order of magnitude slower than that in paddle test (19) and thus can not accurately reflect the actual mass transportation process in paddle test; Instead of a steady flow, the flow in USP #4 test has a sinusoidal profile with a pulsation of 120

pulses per minute; the tablet is also subjected to a continuously changing morphology and collapses at a certain stage of the dissolution.

5.2.2 Design of the Novel Tablet Holder

The lack of appropriate tools for probing dissolution mechanism is impeding Quality by Design (QbD) in formulation development. Without a good understanding of the intrinsic drivers of dissolution process, it is difficult to fine-tune formulation design to specifically promote these drivers. In this study, we present a novel tablet holder to be used with paddle dissolution that is (1) simple to use, (2) directly comparable to the standard paddle method, (3) capable of simplifying the hydrodynamics condition so that the dissolution process can be described with physical/mathematical models, and (4) capable of suppressing disintegration induced by liquid penetration or tablet swelling to a large degree.

In order to understand the paddle dissolution test, it is logical to start from examining the hydrodynamics situation within the vessel. Renolds number is a dimensionless number that gives a relative ratio of inertial forces to viscous forces. It can be used to characterize different flow regimes, e.g., laminar flow vs. turbulent flow. Laminar flow occurs at low Renolds number and features smooth and consistant flow patterns, while turbulent flow occurs at high Renold number and tends to generate random flow instabilities, such as eddies and vortices. This is important in dissolution as the flow pattern could dramatically affect mass transfer mechanism, speed, and variability. In a cylindrical vessel stirred by a center-rotating paddle, as is the case of paddle dissolution test, the Renold number can be expressed as:

$$\mathrm{Re} = \frac{\rho N D^2}{\mu}$$

Where,

ρ is the density of the medium, 0.99370 g/ml for water at 37°C;

μ is the viscosity of the medium, 0.006915 g/(cm*sec) for water at 37°C;

N is the rotational speed (rotations per second), 0.83/sec for 50 RPM

D, characteristic dimension of the apparatus, is the diameter of the paddle, 7.5cm.

The Renold number in the paddle apparatus is around 5000, below the 10000 level required to develop a turbulent flow regime (20). The flow is turbulent behind the path of the paddle tips, while there is a relatively steady region of laminar flow near the wall between the paddle and the upper surface of the medium.

After multiple iterations, a tablet holder, built to be a simple accessory to study dissolution mechanism, was designed to utilize this relatively steady flow regime with minimal disturbance and consistent tablet exposure area. The holder is made from DuPont™ Delrin® acetal resin, a material that is abrasion and solvent resistant. The holder surface in contact with medium is comprised of two arcs interconnected at an inflection point, where the curvature changes sign (Figure 5-5). Such a design ensures a smooth flow pattern along the holder surface with minimized development of eddy flow. In the setup, a constant tablet surface area is exposed to a relatively steady flow, facilitating the establishment of mathematic models for the dissolution process. This could in turn allow quantitative exploration of the role of microstructure in dissolution.

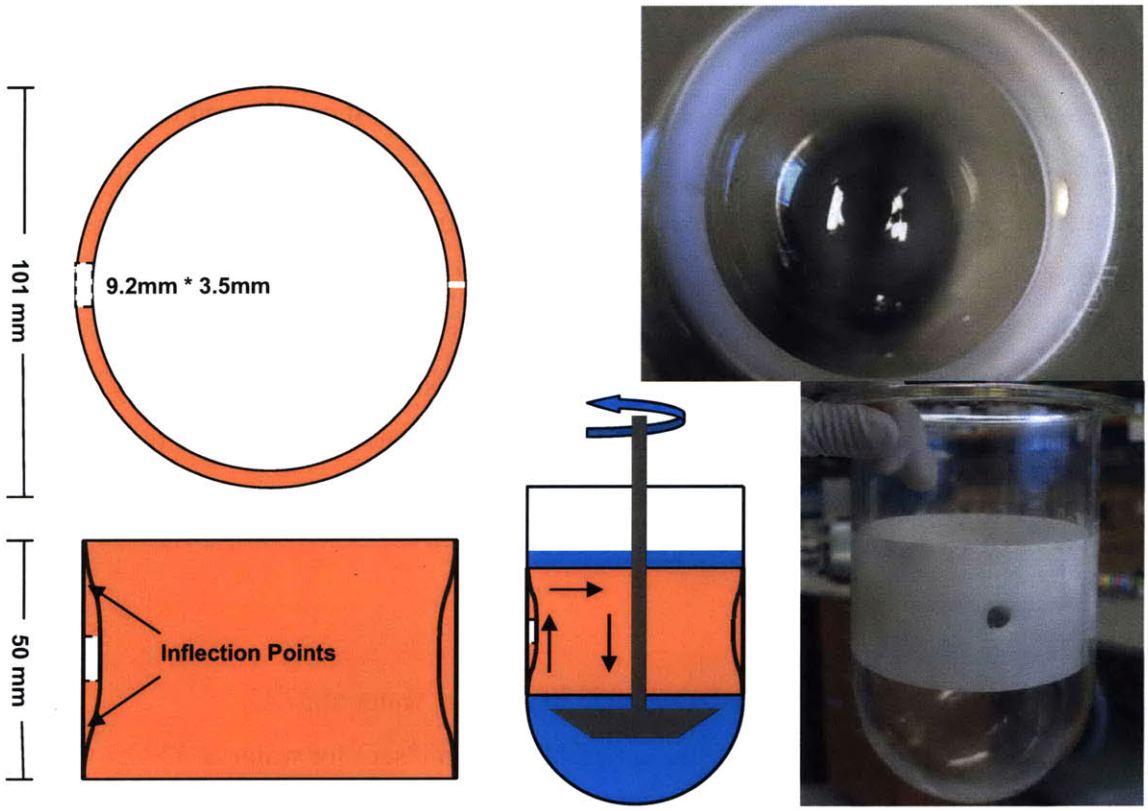

Figure 5-5 Design of the tablet holder for usage in combination with paddle test.

For many formulations, the process of dissolution includes surface dissolution and tablet disintegration. In the case of surface dissolution, solid material first dissolves in the liquid and then is transported away; in tablet disintegration, solid material first detaches from the bulk solid and then dissolves. For dissolution with a tablet holder, tablet disintegration due to medium penetration and tablet swelling can often be suppressed, with only surface dissolution left to be characterized. The tablet physical structure exposed to the medium could be derived fully or partially from the microCT measurement/analysis. The use of this tablet holder in combination with standard paddle test would not only help understand the dissolution mechanism but also facilitate mathematical modeling of the dissolution process, with tablet microstructure incorporated.

5.2.3 Physical/Mathematical Model of Holder Dissolution

A simplified two-step surface dissolution model for holder dissolution is illustrated in Figure 5-6. The first step is dissolving of the solid into the liquid phase, for which the available area is the nominal exposed surface area $A=\pi r^2$ and additional pore surface area A_p. The second step is convective diffusion of the dissolved material from the surface into the bulk flow, for which the available area is the nominal surface area. A linear flow velocity profile is assumed within the boundary layer, which allows an analytical solution to the problem while achieving similar accuracy as the actual parabolic flow scenario (21). The flow near the tablet surface is assumed to be a parallel laminar flow (x-axis), while the diffusion process is assumed to be perpendicular to the tablet surface (z-axis).

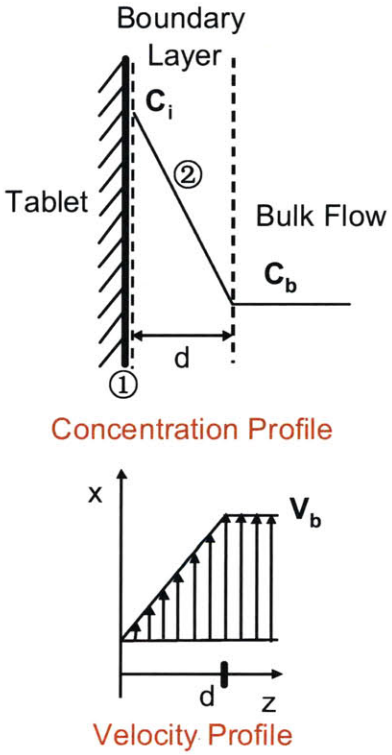

Figure 5-6 Simplified physical model of tablet holder dissolution.

The rate of dissolution can be expressed as:

$$R = k_d A_{tot}(C_s - C_i)$$

Where,

$$A_{tot} = A + A_p$$

As for convective diffusion, we have,

$$D\frac{\partial^2 C}{\partial z^2} = V_x \frac{\partial C}{\partial x}$$

where the left term corresponds to the diffusion speed, the right term to the convective transport speed. We can also write a few boundary conditions,

$C = C_i$ $\qquad 0 < x < 2r$

$C = C_b$ $\qquad z \to \infty$

$C = 0$ $\qquad x = 0$

Combining which we can solve (Eq-3) and integrate over the surface of tablet, arriving at the rate of convective diffusion,

$$R = 0.687 A D^{2/3}(\frac{V_b}{\delta r})^{1/3}(C_i - C_b)$$

Where D is the diffusivity, V_b is the bulk flow speed, δ is the boundary layer thickness, r is the radius of the tablet. The rate-limiting step determines the dissolution mechanism of the tablet, which in turn determines the impact of tablet microstructure in holder dissolution (Figure 5-7). In surface-dissolving-limited holder dissolution, porosity profile contributes to the dissolution speed by providing additional surface area, while in a convective-diffusion-limited holder dissolution, porosity profile has little to no impact on dissolution speed.

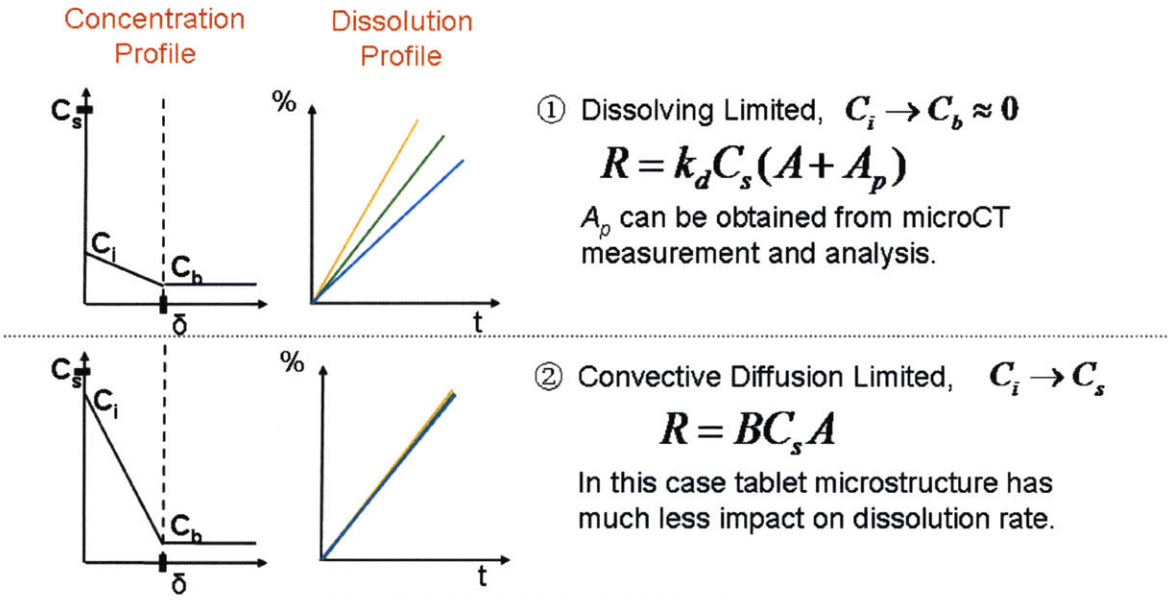

Figure 5-7 Dissolution model as controlled by rate-limiting steps.

5.2.4 Testing of the Novel Tablet Holder

Paddle dissolution with tablet holder (holder dissolution) is fine-tuned with 10% caffeine - lactose tablets. Initial testing in a prototype tablet holder demonstrated linear dissolution of the retained tablet through 90% completion. In a standard paddle dissolution testing, a three-stage dissolution process was observed, with initial linear dissolution (0-10 min) followed by collapse-induced rapid dissolution (10-13 min) and then a final stage leveling off (14-20min) (Figure 5-8). It appears that the holder test successfully achieved more consistent dissolution speed by controlling the hydrodynamics near the tablet surface and exposure area of the tablet enclosed.

However, when the holders are manufactured and tested in larger numbers, significant inconsistency in dissolution profile was observed (Figure 5-9). During dissolution, bubbles could be seen leaking out of tablet sidewalls from behind the tablet. Total collapse of tablet happens at various time points of the dissolution process. It was concluded that a hydrodynamic pressure induced by paddle agitation is pushing air bubbles trapped behind the holder to squeeze through the interface between tablet

sidewall and holder, weakening the tablet structure as well as changing hydrodynamics surrounding the tablets.

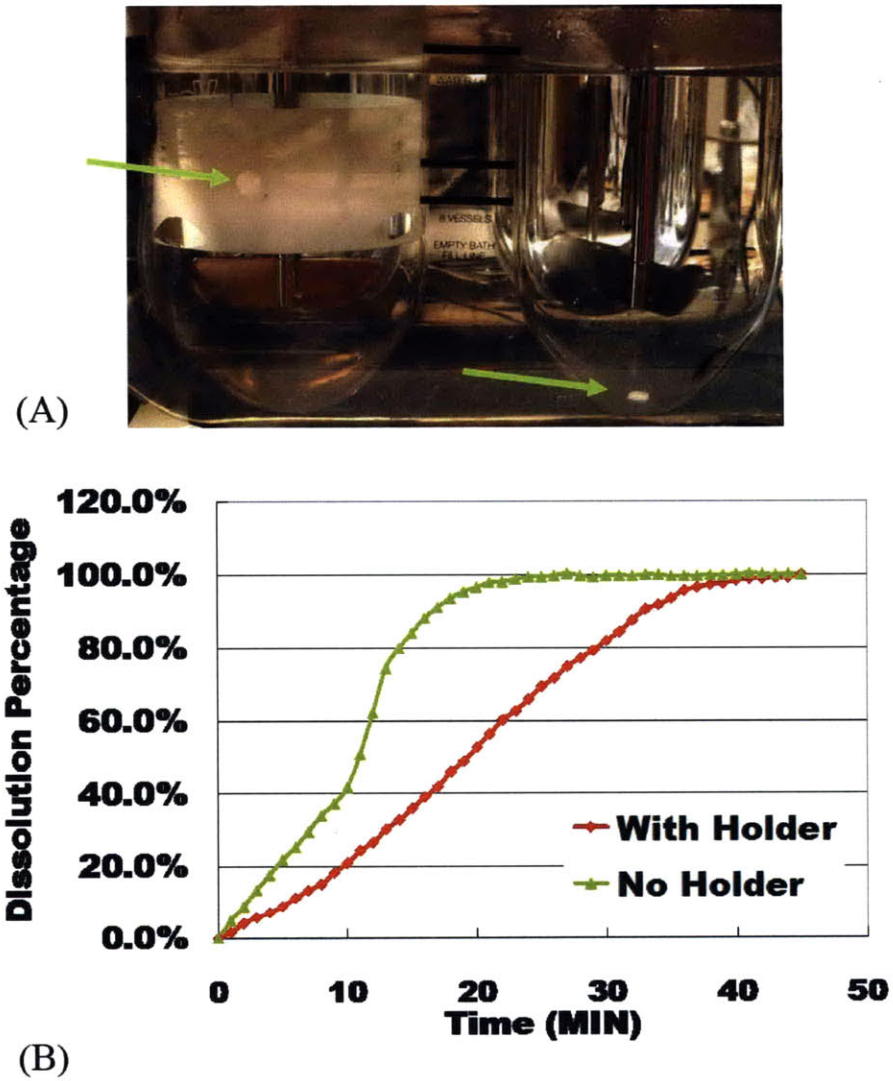

Figure 5-8 Paddle dissolution with and without tablet holder. (A) Experimental setup; (B) Dissolution profile comparison for 48N 10% Caffeine-90% Lactose tablets.

Waxing of Holder Sidewall/ Parafilm Wrapping of Tablet for Leakage Prevention

In order to generate a tight seal between the tablet and the holder wall, multiple methods have been attempted, with wax sealing and partial parafilm^{TM} (Pechiney Plastic Packaging, Menasha, WI) wrapping being the most efficient ones. For wax sealing, bees wax (Sigma-Aldrich), Carnauba wax (Sigma-Aldrich), or a combination of the two are melted on a hot plate at 100°C and applied to tablet hole sidewall with a cotton Q-tip.

The tablet is quickly pushed into the hole from the inner side of the holder. Multiple trials identified bees wax as the best candidate amongst those tried, providing adequate softness and cooling speed. Only the side wall and partial back of the tablet are waxed, so the impact on dissolution of the tablet's exposed front side is minimal to none.

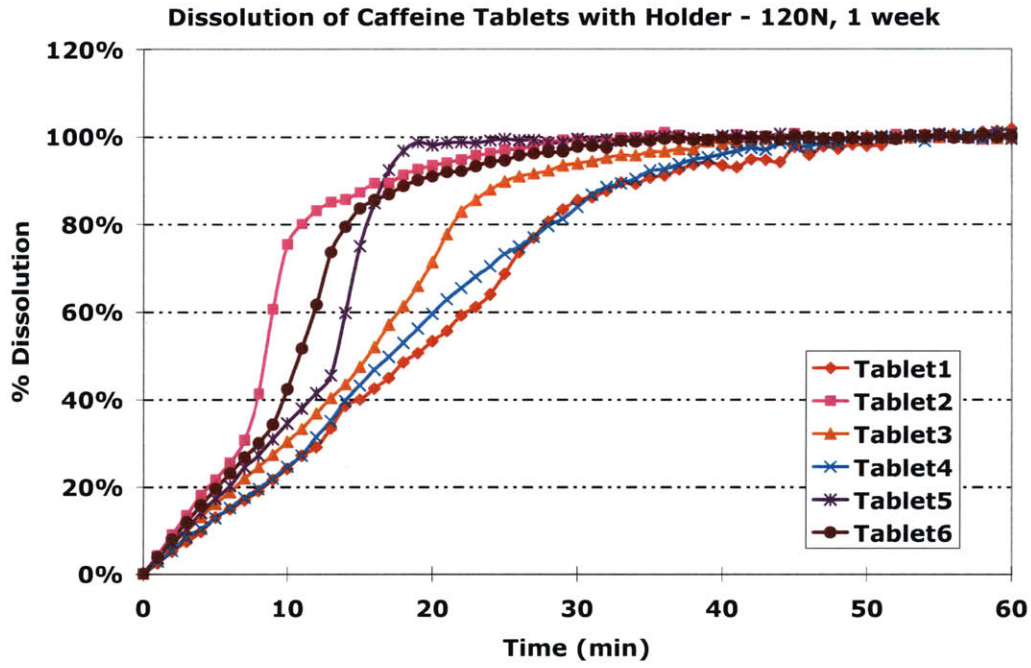

Figure 5-9 Inconsistent dissolution results with original tablet holder.

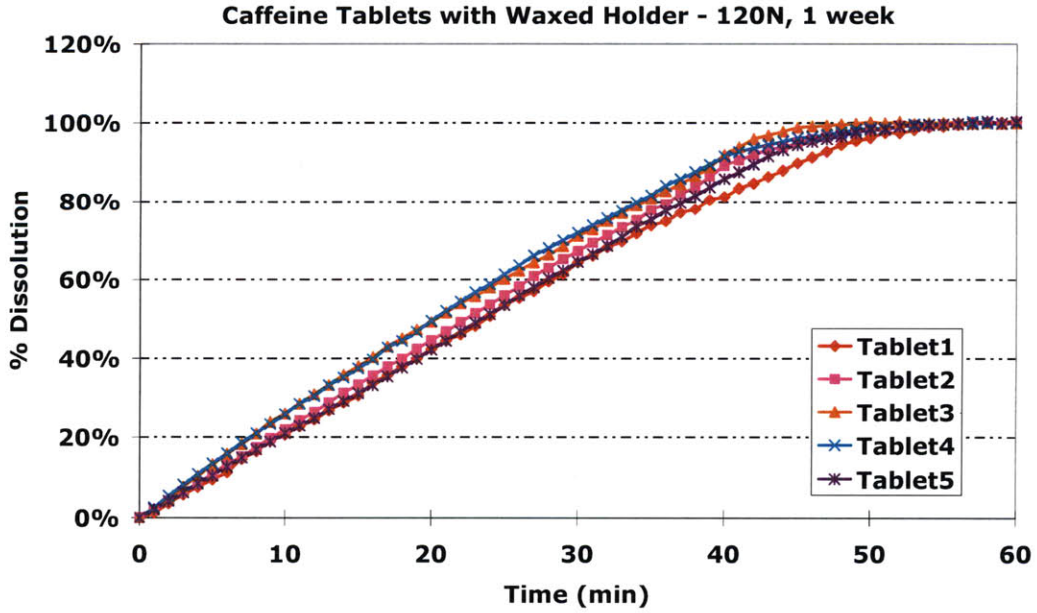

Figure 5-10 Dramatically enhanced consistency in holder dissolution with waxing.

Holder dissolution of the same caffeine tablets with wax sealing yields much more consistent dissolution profiles with an average standard deviation of <5%, as shown in Figure 5-10. No bubble leakage is observed. Dissolution is consistent and steady through majority of the process. The tablet flat surface gradually retreated as dissolution goes on, demonstrating a surface erosion dissolution process.

Parafilm™ wrapping is another effective method in preventing sidewall leakage. In this case, tablet's curved sidewall is carefully wrapped with a parafilm™ strip, leaving only the flat surfaces exposed. The tablet is then inserted into the tablet hole of the holder for dissolution testing. In the holder dissolution of 50% compound-A tablets, parafilm™ wrapped tablets demonstrated consistent and reproducible dissolution patterns with an average standard deviation of 1.6% (Figure 5-11). When compared with holder sidewall waxing, parafilm™ wrapping of tablet is a lot more tedious and error-prone. In subsequent tests where waxing technique was optimized, standard deviation was controlled to be within 2%. As a result, most of the holder tests conducted in this study were done with the use of a wax seal.

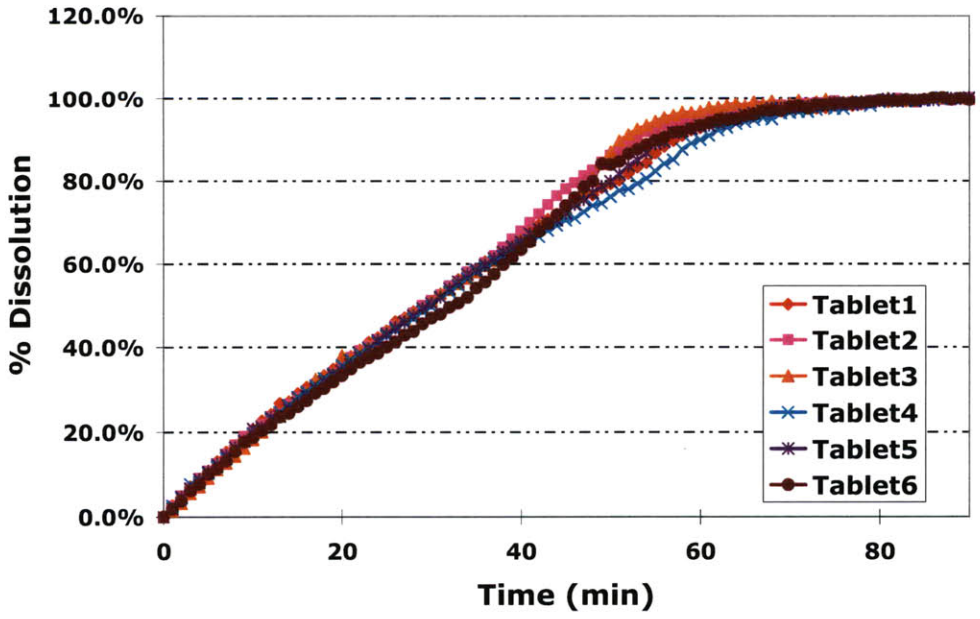

Figure 5-11 Consistent dissolution profiles in M50 holder test with parafilm wrapping.

Location of Holder in Dissolution Vessel

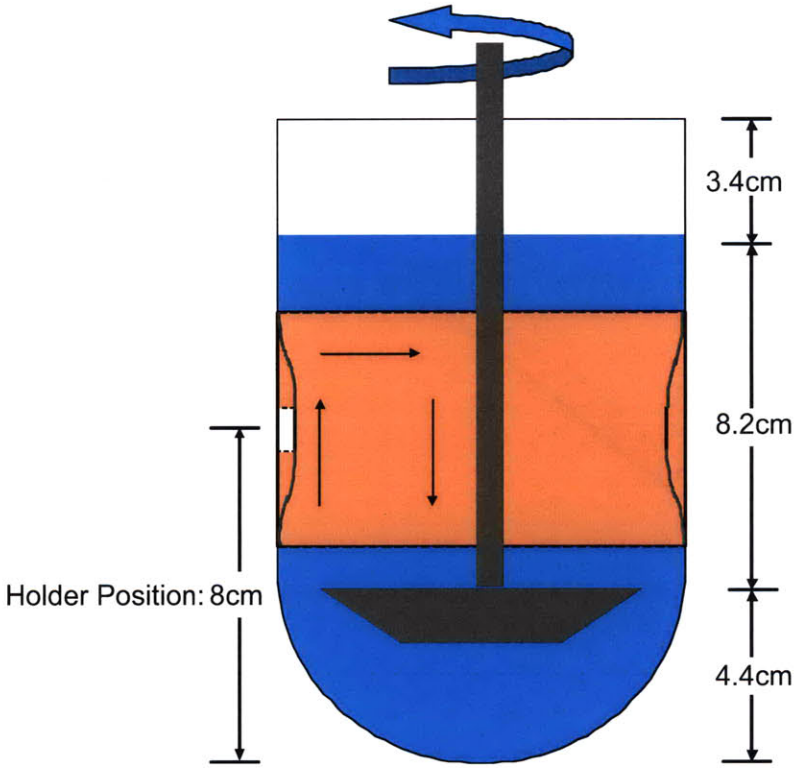

Figure 5-12 Illustration of tablet holder position with 900ml medium in dissolution vessel.

As can be seen in Figure 1-9, only certain regions along the dissolution vessel sidewall have a steady flow pattern. Therefore, the positioning of the tablet holder is very important to achieve consistent hydrodynamics condition at the exposed surface of the tablet. A position too close to the rotating paddle would be impacted by the turbulent flow adjacent to the paddle, while a position too close to the dissolution medium upper surface will be subjected to a surface effect of the flow.

Figure 5-12 illustrates the position of the holder in a 1-liter dissolution vessel filled with 900ml medium. The total height of the vessel is roughly 16 cm. Holder positions with tablet center at 7, 8, and 10 cm away from the vessel bottom were tested with 10% caffeine-lactose tablets (100N strength, N=6) (Figure 5-13). The results showed that dissolution at holder position of 8cm has the smallest average standard deviation of 1.11%. At holder position of 7cm, average standard deviation is slightly higher at 1.23% but still very satisfactory. At holder position of 10cm, average standard deviation of

dissolution profiles is considerably higher at 1.64%. Overall speaking, 8cm from the vessel bottom is the optimal position for tablet center and is used in the subsequent tests.

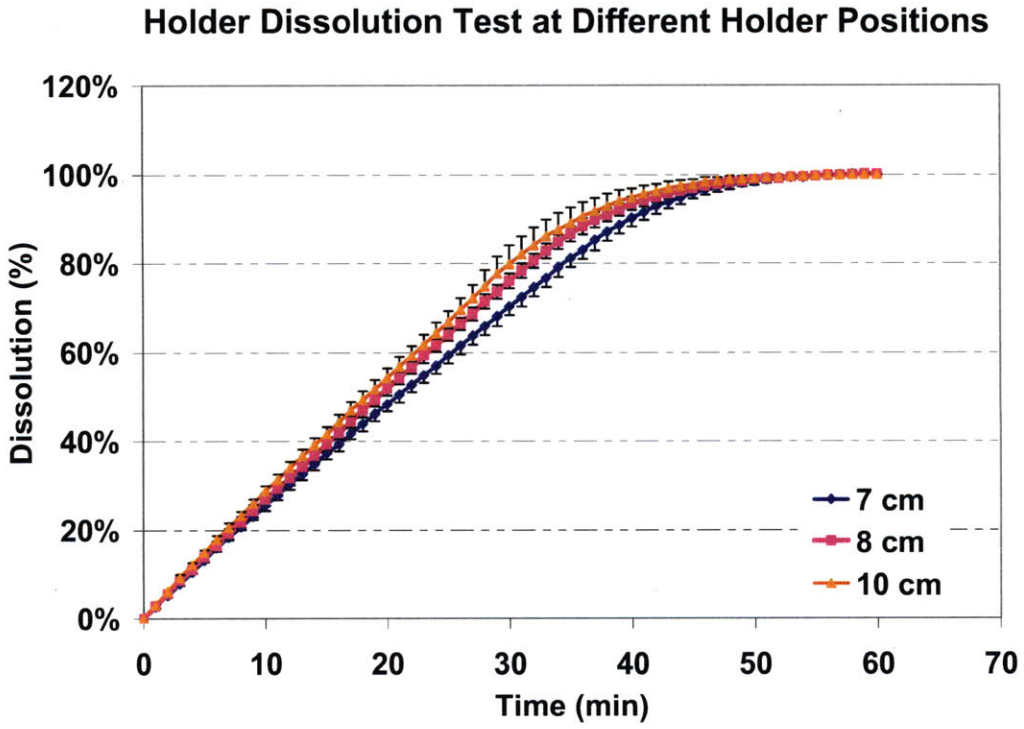

Figure 5-13 Holder dissolution test at different holder position with 100N caffeine tablets. N=6.

5.3 Holder Dissolution Study of Caffeine-Lactose Tablets

Holder dissolution was first utilized in understanding the dissolution mechanism of caffeine-lactose tablets, starting with a typical dissolution setting of 900ml water, 37°C water bath temperature, and 50 RPM paddle rotation speed. The 200mg tablets were made from 10% caffeine (Sigma-Aldrich), 89.5% spray-dried lactose SuperTab® 11SD (DMV-Fonterra), and 0.5% magnesium stearate (Sigma-Aldrich). Tablets of six hardness levels were tested, ranging from the softest 9N tablets to the hardest 120N ones.

At 50 RPM, most tablets share the same dissolution profile in holder test, with only the softest tablets exhibiting faster dissolution due to disintegration (Figure 5-15 A). MicroCT analysis shows that tablets with various hardness levels have distinctive internal microstructure, with softer tablets possessing a higher number of larger pores (Figure 5-14). Combined with the theoretical model for holder dissolution described in section 5.2.3, it is hypothesized that holder dissolution speed of caffeine-lactose tablets at 50 RPM was limited by convective-diffusion.

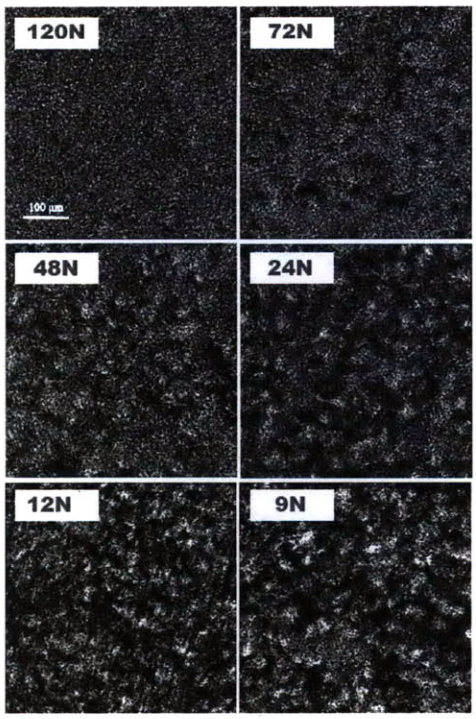

Figure 5-14 MicroCT reconstructured cross section images of caffeine-lactose tablets. 500umX500um.

In order to test the impact of hydrodynamics on dissolution profiles, paddle rotation speed was increased to 100RPM (Figure 5-15 B). There is a general shift of dissolution profiles toward left, indicating a higher dissolution speed under the more intensive agitation condition. However, the profiles of tablets with different strength still do not differentiate from each other, demonstrating convective-diffusion-limited dissolution at 100 RPM.

Although the dissolution medium was degassed right before dissolution tests (degassing procedure described in section 2.3), there is still a risk of pre-existing air bubbles within tablet microstructure to deter liquid penetration into the pores. In subsequent experiments, 0.2% (w/v) sodium dodecyl sulfate (SDS, Sigma-Aldrich) was added as a surfactant to dissolution medium, which should reduce the surface tension at the solid-liquid interface and facilitate the wetting process (22). The addition of surfactant did not help isolate the dissolution profiles, further confirming the convective-diffusion-limited scenario for dissolution of lactose-caffeine tablets (Figure 5-15 C).

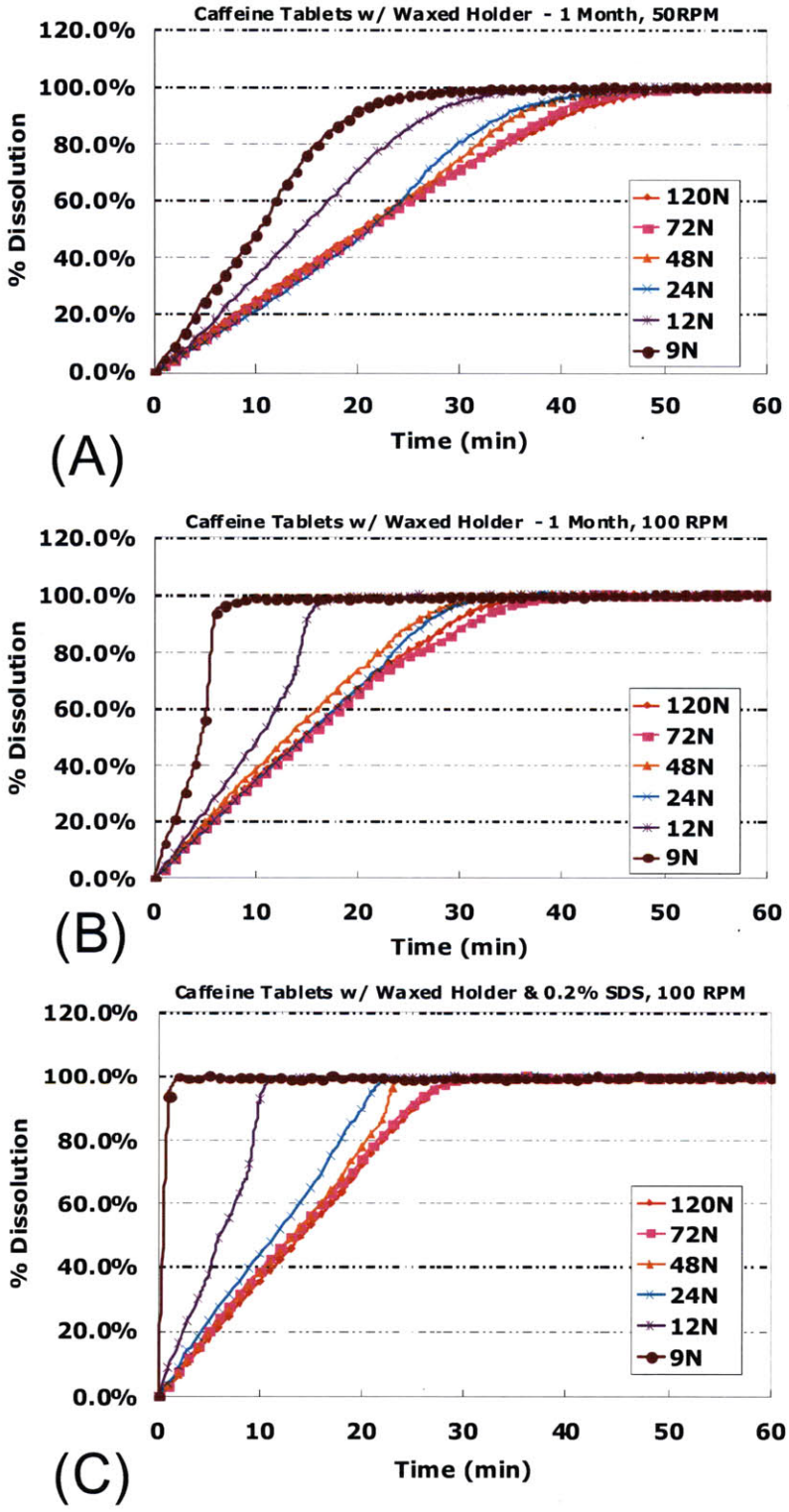

Figure 5-15 Holder dissolution test results of caffeine-lactose tablets. N=6.

A more quantitative analysis of the dissolution speeds further confirms the hypothesis about dissolution mechanism. From the theoretical model for convective-diffusion-limited dissolution, we have,

$$R = 0.687 A D^{2/3} (\frac{V_b}{\delta r})^{1/3} (C_i - C_b)$$

According to Blasius solution to a unidirectional flow parallel to the tablet surface, the boundary layer thickness is proportional to the inverted square root of bulk flow speed (23). Integrating the relationship back to the dissolution rate expression above, we find that the dissolution rate is proportional to the square root of the bulk flow speed. Assuming that the bulk flow speed at 100RPM is twice the flow speed at 50RPM, we reach at the conclusion that dissolution speed at 100RPM should be 1.44 times the speed at 50RPM, which is true for tablets from hardness levels of 120N to 12N (Figure 5-16). In this case we are defining dissolution speed as the average % of dissolution progress per minute for the first 60% of the whole process. The softest 9N tablets had higher dissolution speed at 100 RPM due to a larger impact of mechanical stress applied on the tablet. The addition of surfactant accelerated the dissolution process of softer tablets, possibly by enhancing the wetting process and thus expediting disintegration.

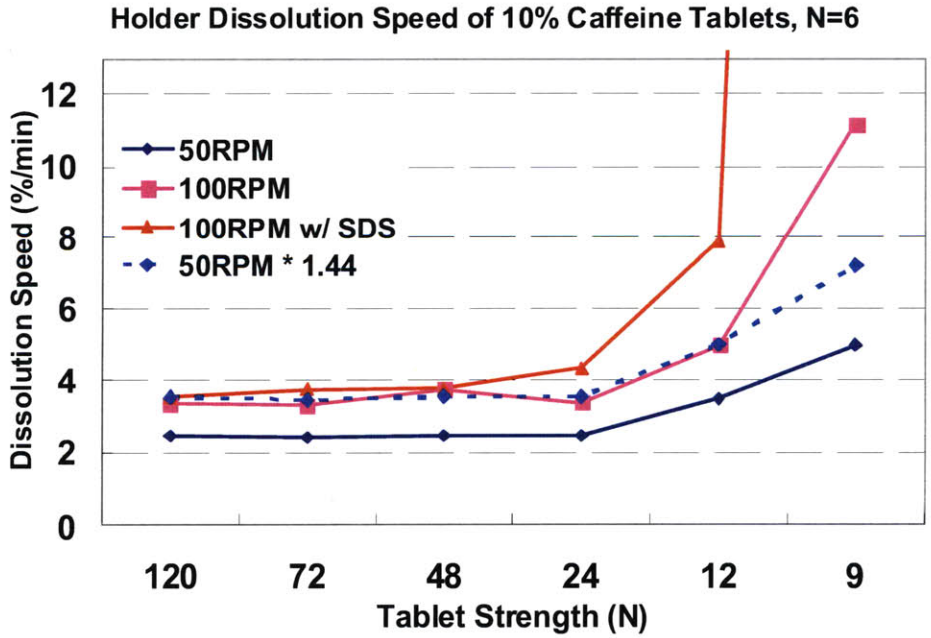

Figure 5-16 Comparison of caffeine-lactose holder dissolution speeds at various settings.

Based on the experiments and analyses shown above, we can conclude that 10% caffeine-lactose tablets go through convective-diffusion-limited dissolution in holder dissolution test. As demonstrated in Chapter 2, caffeine-lactose tablets of different strengths show distinctive dissolution profiles in standard paddle dissolution test. Based on the design of the holder and observation of the dissolution processes, it is hypothesized that disintegration induced by medium penetration leads to the differential dissolution speeds in standard paddle test. In Chapter 6, numerical simulations with microCT-acquired tablet microstructure would help confirm this hypothesis.

5.4 Holder Dissolution Study of Compound-A Roller-Compacted Tablets

In holder dissolution study of compound-A roller-compacted tablets, one additional dimension, the loading percentage of compound-A in the formulation, is considered and evaluated. Standard paddle dissolution and holder dissolution were performed for 200mg M-series formulation roller-compacted tablets M10/M30/M50/M70, as described in Chapter 4. The tests were conducted with 900ml 0.01N HCl solution as dissolution medium, a 37°C water bath and 50RPM paddle rotation speed.

The findings are presented in Figure 5-17 and Figure 5-18. The M10 tablet dissolution profiles resemble those of 10% caffeine tablets, with similar profiles in holder dissolution but very different profiles in standard paddle dissolution. It confirms the convective-diffusion-limited dissolution for lactose dominant tablets. In M30 tablets, holder dissolution profiles show a small sign of divergence, while paddle dissolution profiles converge slightly. As demonstrated in Chapter 4, the dominant structure in M30 is still lactose, but the presence of more compound-A could partially deter medium access to some of the pore space, resulting in smaller dissolution speed differences (brought by disintegration). In M50 and M70 tablets, holder dissolution profiles continue to diverge, indicating a surface-dissolving-limited scenario for tablets with compound-A dominant structure. The paddle dissolution profiles for M50 and M70 are similar, with 100N tablets dissolving considerably slower than the others.

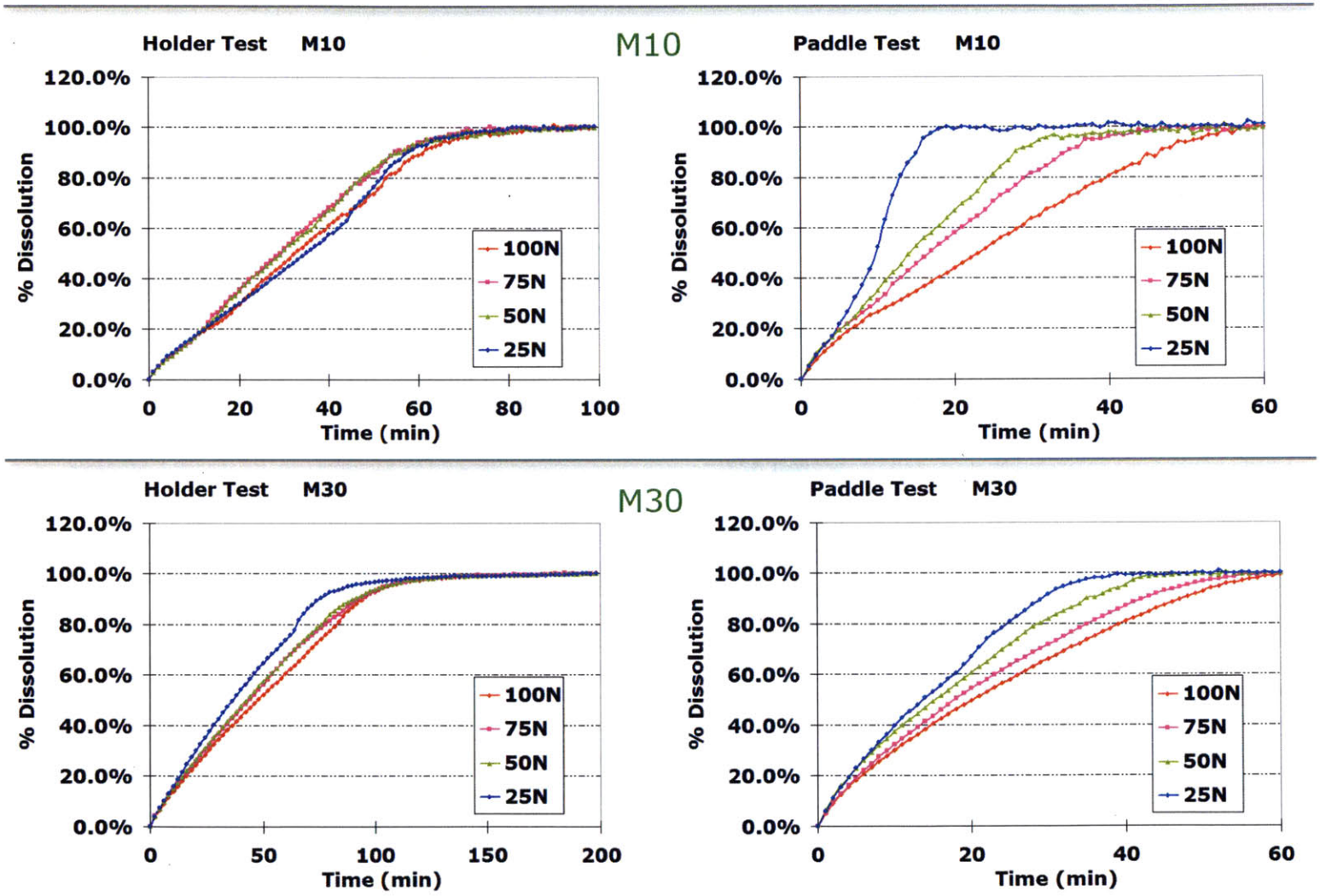

Figure 5-17 Holder and paddle dissolution results of M10/M30 compound-A tablets. 900ml 0.01N HCl, 50RPM. N=12.

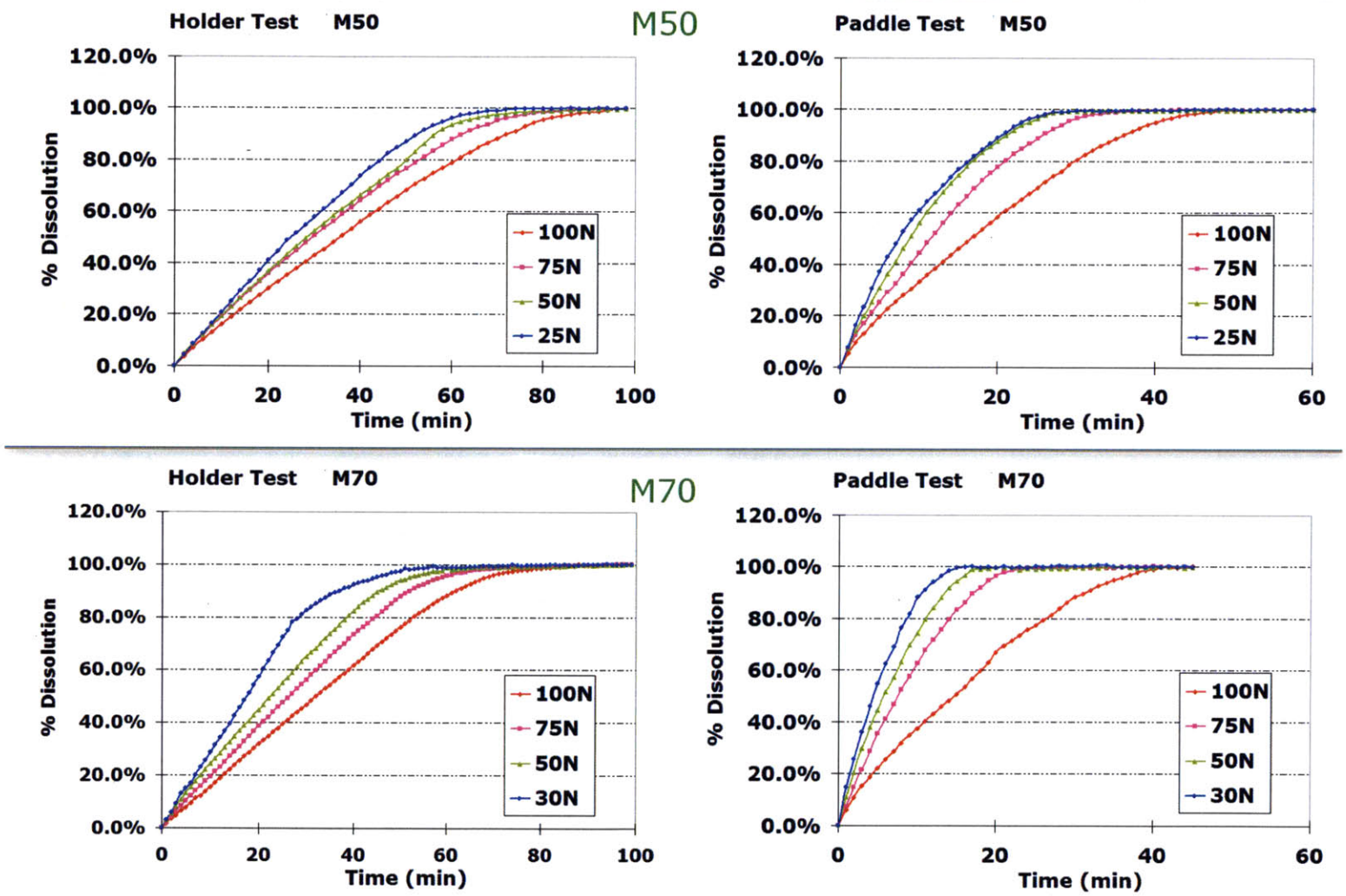

Figure 5-18 Holder and paddle dissolution results of M50/M70 compound-A tablets. 900ml 0.01N HCl, 50RPM. N=12

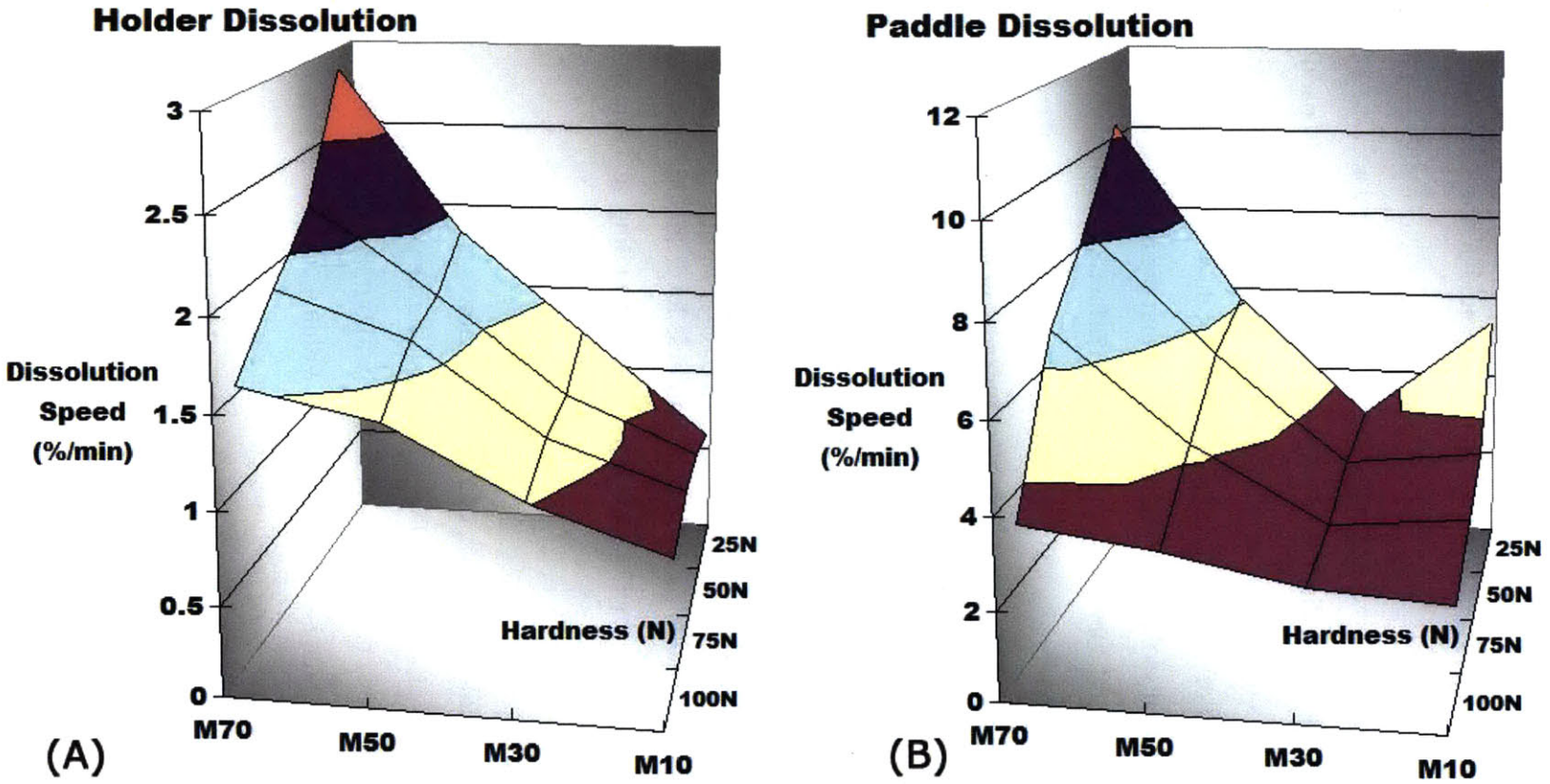

Figure 5-19 Dissolution surface map of compound-A tablets in holder dissolution (A) and paddle dissolution (B) tests.

In this study, we define a dissolution surface map as dissolution speed plotted against tablet composition and tablet strength. The dissolution surface maps for paddle test and holder test of compound-A tablets give us a thorough overview of the dissolution characteristics (Figure 5-19). In general, the more compound-A, the faster the dissolution is. However, M10 dissolution is faster than M30 in paddle test. A logical explanation from the microCT data is that the compound-A in M30 deters liquid access to the pore network of the lactose, delaying disintegration from happening. The M10 paddle dissolution speed curve is upward, compared with the flat curve in holder dissolution, indicating that the impact of medium-penetration-induced disintegration is an important driver in standard paddle dissolution. We can also see that the more compound-A, the steeper the dissolution speed curve, again indicating a surface-dissolving-limited scenario for compound-A dominant tablets. Useful learnings can be drawn from the data. For lactose dominant formulation, the most important measure to enhance dissolution rate is to promote disintegration. When used in combination with other excipients that undergo plastic densification, lactose pore network interconnectivity could be reduced, resulting in less disintegration and slower dissolution. For compound-A dominant formulation, maximizing the surface area available for dissolution is crucial to achieving faster dissolution speed. At high compound-A loadings, a compromise between hardness and dissolution rate needs to be made. An adequate hardness level should be the lowest to allow enough strength for the tablet to sustain packaging, handling, and transportation induced stress.

As mentioned above, paddle dissolution of 100N M70 tablets is considerably slower than that for M70 tablets of other strengths. During the dissolution process, it was observed that 100N tablets tended to sink at the vessel bottom without changing position significantly, 75N tablets swung around the bottom within a circle of ~4 cm in diameter, 50N/25N tablets first floated in the medium, but then sank and swung around the bottom. The hypothesis is that 100N tablet dissolution is much slower because it mainly happens from the curved side wall and the upper flat surface, in which case we define the dissolution process to be in sink scenario (we are not using "sink condition" as it has

different meaning in dissolution). We also define the dissolution of floating or swinging tablets to be in floating scenario, where dissolution happens from all the surfaces. Since dissolution only happens from one flat tablet surface in the holder test, we can first calculate the effective dissolution rate per unit surface area and then derive the equivalent dissolution rate in sink or floating scenarios (Figure 5-20). The converted dissolution rates can then be compared with the standard paddle dissolution rates. For the same dissolution scenario, this is effectively comparing dissolution speeds under two sets of hydrodynamics condition.

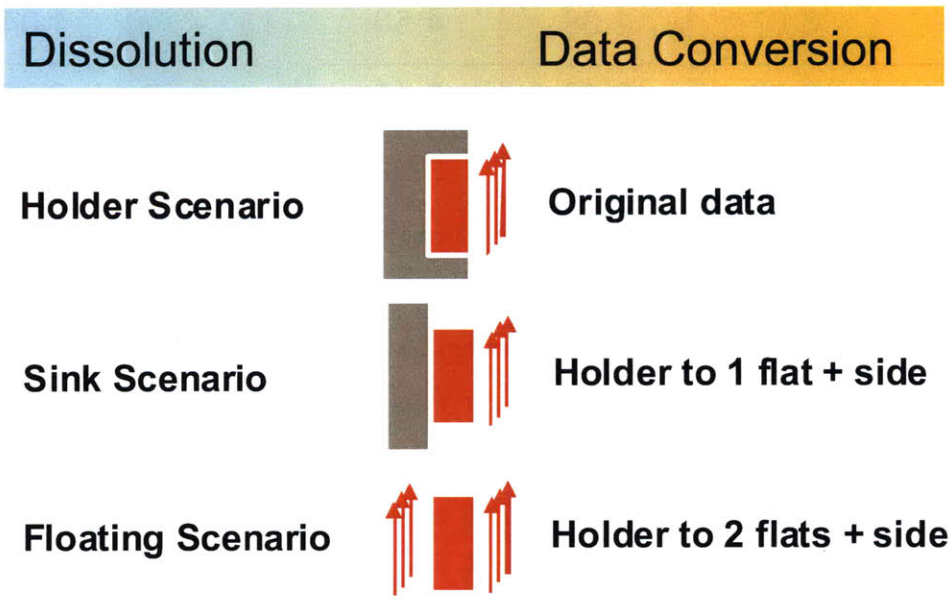

Figure 5-20 Illustration of different dissolution scenarios and correspondent data conversion methods.

As shown in Table 5-1, dissolution speed of 100N tablet in holder-converted sink scenario (green) agrees very well with that in standard paddle test condition (yellow), while dissolution speeds of tablets with other hardness in holder-converted floating scenario (green) agree well with those in standard paddle test condition (yellow). This observation confirms our hypothesis about the dissolution scenarios. It also further illuminates the surface-dissolving-limited nature of compound-A dominant tablets in the current dissolution settings, as the dissolution speeds per unit surface area under different hydrodynamics conditions are the same. Tablet density was hypothesized to be the primary driver for different dissolution scenarios. The bulk density of M70 100N tablets, 1.15 g/ml, is 15% higher than the 1g/ml density of the dissolution medium, while the bulk

density of 75N tablets, 1.04 g/ml and 4% higher than that of medium, was not sufficient to withstand the agitation of a dissolution paddle rotating at 50 RPM.

Table 5-1 Comparison between dissolution speeds of standard paddle test and converted holder test.

M70 Tablets Target Hardness	Standard Test Speed (%/min)	Holder Speed (%/min)	Holder to 1 flat + side (%/min)	Holder to 2 flats + side (%/min)	Density (g/ml)
100N	3.33	1.54	3.47	5.01	1.15
75N	6.67	1.88	4.50	6.37	1.04
50N	8.22	2.18	5.45	7.63	0.99
30N	10.34	2.86	7.36	10.22	0.92

In order to test the hypothesis about density in a broader setting, a value between the bulk density of 100N and 75N M70 tablets, 1.10g/ml at 10% higher than dissolution medium density, is adopted as a threshold for determining dissolution scenarios. Any tablet with bulk density below this value is assumed to be in floating scenario, and any tablet above this is assumed to be in sink scenario. All the compound-A tablets with different drug loadings can be classified into the two categories based on the threshold (Figure 5-21).

In order to compare equivalent dissolution speeds under two different hydrodynamics conditions, i.e., in the tablet holder and at the vessel bottom, holder dissolution speeds for all the tablets are converted to speeds of correspondent dissolution scenarios. A comparison between the standard paddle dissolution speeds and the converted holder dissolution speeds is done by subtracting the latter from the former and plotting the differential dissolution surface map (Figure 5-22). For M50/M70, the differential speeds are mostly near the zero point, indicating that both tablets are surface-dissolving-limited in the tests. For M10, the differential speeds are higher than zero and goes up with decreasing strength, indicating the impact of disintegration via medium penetration. For M30, even though lactose is assuming a relatively large volumetric portion of the tablet, the presence of significant amount of compound-A is deterring pore access and preventing massive disintegration.

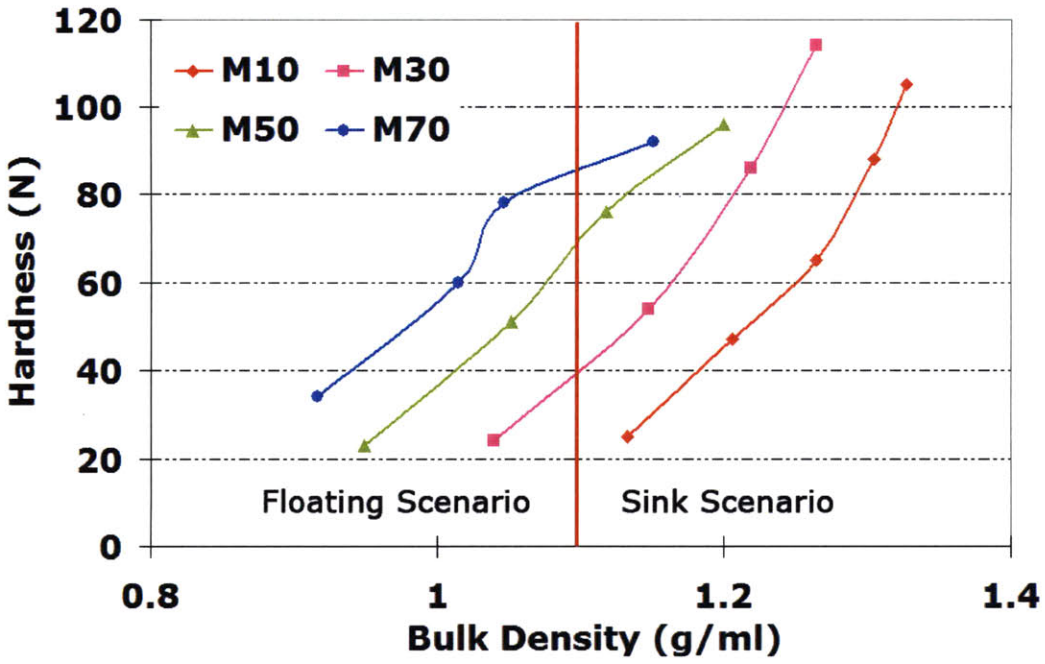

Figure 5-21 Thresholding of compound-A tablets into sink or floating dissolution scenarios.

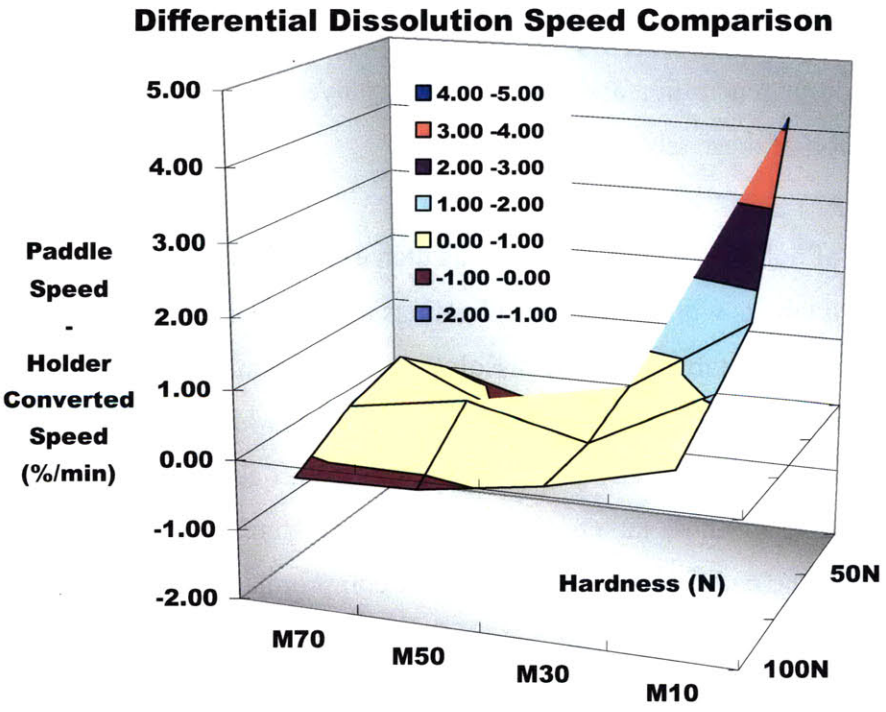

Figure 5-22 Differential dissolution speed surface map of paddle test and converted holder test.

5.5 Summary

A novel tablet holder was designed as a piece of simple accessory for paddle dissolution test in aiding dissolution mechanism investigation. After a series of alterations in holder design and testing method, the holder helped establish a consistent dissolution scenario within the paddle dissolution settings, where disintegration due to medium penetration and tablet swelling is suppressed. The surface dissolution process with the holder was described with a physical/mathematical model. Two surface dissolution mechanisms, surface-dissolving-limited dissolution and convective-diffusion-limited dissolution, were identified and characterized.

In holder dissolution study of 10% caffeine-lactose tablets, it was demonstrated that convective diffusion is the rate limiting step in the typical dissolution settings tested. The tablets exhibited similar dissolution profiles, except for the softest tablets with significant disintegration. In contrast, caffeine-lactose tablets of different strengths exhibited distinctive dissolution profiles in regular paddle tests, indicating that disintegration induced by medium penetration and tablet swelling played important roles in expediting paddle dissolution of these tablets.

The dimension of holder dissolution study was then expanded to include compound-A roller compacted tablets with various drug loadings and mechanical strengths. Unlike that for caffeine-lactose tablets, paddle dissolution for compound-A dominant tablets (M50/M70) is limited by the surface dissolving process, to which the available surface area at solid-liquid interface is key to a faster dissolution process. The dissolution speed per unit surface area for those tablets is the same under different hydrodynamics conditions within the paddle dissolution setup. A compromise between hardness and dissolution rate must be made for compound-A dominant tablets. An adequate hardness level should be the lowest to allow enough strength for the tablet to sustain packaging, handling, and transportation induced stress.

It was also discovered that dissolution could happen in sink scenario or floating scenario, with a threshold of tablet bulk density at 110% of dissolution medium density. This is easily overlooked during formulation development and could lead to inconsistent dissolution profiles should tablet density be set near the threshold and shift from batch to batch. The differential dissolution speed surface map is a powerful tool in understanding the critical role of disintegration for lactose dominant tablets (M10). In addition, it demonstrates that the porosity network connectivity is probably essential to disintegration induced by medium penetration, as M30 paddle dissolution is slower than that of M10 potentially due to the blockage of pore network access by the significant presence of compound-A.

Through the case studies described in this chapter, we have demonstrated that the novel tablet holder is a great addition to the toolbox of pharmaceutical scientists. When used appropriately, it could help dissect dissolution mechanism of pharmaceutical tablets, yielding critical information for guidance of rational formulation development.

5.6 Chapter Bibliography

1. U. Banakar. Introduction, Historical Highlights, and the Need for Dissolution Testing. Pharmaceutical Dissolution Testing:1-18 (1991).
2. A.W. Noyes, WR. The rate of solution of solid substances in their own solutions. Journal of American Chemical Society. 19:930-934 (1897).
3. E. Brunner. Reaktionsgeschwindigkeit in heterogenen Systemen. Z Phys Chem. 47:56-102 (1904).
4. T. Higuchi. Rate of release of medicaments from ointment bases containing drugs in suspension. Journal of Pharmaceutical Sciences. 50:874-875 (1961).
5. N.A. Peppas. Analysis of Fickian and Non-Fickian Drug Release from Polymers. Pharm Acta Helv. 60:110-111 (1985).
6. P.L.P. Ritger, N.A.,. A simple equation for description of solute release II. Fickian and anomalous release from swellable devices. J Controlled Release. 5:37-42 (1987).
7. M. Wilderman. Uber die Geschwindigkeit molekularer und chemis- cher Reaktionen in heterogenen Systemen. Erster Teil Z Phys Chem. 66:455-495 (1909).
8. Langenbu.F. Linearization of Dissolution Rate Curves by Weibull Distribution. Journal of Pharmacy and Pharmacology. 24:979-& (1972).
9. K. Kosmidis, P. Argyrakis, and P. Macheras. Fractal kinetics in drug release from finite fractal matrices. J Chem Phys. 119:6373-6377 (2003).
10. K. Kosmidis, P. Argyrakis, and P. Macheras. A reappraisal of drug release laws using Monte Carlo simulations: The prevalence of the Weibull function. Pharmaceutical Research. 20:988-995 (2003).
11. A. Dokoumetzidisand P. Macheras. A century of dissolution research: From Noyes and Whitney to the Biopharmaceutics Classification System. International Journal of Pharmaceutics. 321:1-11 (2006).
12. L.G. McCarthy, C. Kosiol, A.M. Healy, G. Bradley, J.C. Sexton, and O.I. Corrigan. Simulating the hydrodynamic conditions in the United States Pharmacopeia paddle dissolution apparatus. AAPS PharmSciTech. 4:E22 (2003).
13. D.M. D'Arcy, O.I. Corrigan, and A.M. Healy. Hydrodynamic simulation (computational fluid dynamics) of asymmetrically positioned tablets in the paddle dissolution apparatus: impact on dissolution rate and variability. Journal of Pharmacy and Pharmacology. 57:1243-1250 (2005).
14. Y. Wu, D.O. Kildsig, and E.S. Ghaly. Effect of hydrodynamic environment on tablets dissolution rate. Pharmaceutical Development and Technology. 9:25-37 (2004).
15. L. Peltonen, P. Liljeroth, T. Heikkila, K. Kontturi, and J. Hirvonen. Dissolution testing of acetylsalicylic acid by a channel flow method - correlation to USP basket and intrinsic dissolution methods. European Journal of Pharmaceutical Sciences. 19:395-401 (2003).
16. L. Peltonen, P. Liljeroth, T. Heikkila, K. Kontturi, and J. Hirvonen. A novel channel flow method in determination of solubility properties and dissolution profiles of theophylline tablets. Journal of Drug Delivery Science and Technology. 14:389-394 (2004).

17. F.a.D. Administration. Guidance for industry: Dissolution testing of immediate release solid oral dosage forms, 1997.
18. FDA. Guidance for Industry: Bioavailability and bioequivalence studies for orally administered drug products—General Considerations. (2003).
19. D.M. D'Arcy, B. Liu, G. Bradley, A.M. Healy, and O.I. Corrigan. Hydrodynamic and Species Transfer Simulations in the USP 4 Dissolution Apparatus: Considerations for Dissolution in a Low Velocity Pulsing Flow. Pharmaceutical Research. 27:246-258 (2010).
20. R.K. Sinnott. Coulson & Richardson's Chemical Engineering. Vol. 6: Chemical Engineering Design, Butterworth-Heinemann, p. 473.
21. S. Neervannan, J.D. Reinert, V.J. Stella, and M.Z. Southard. A Numerical Convective-Diffusion Model for Dissolution of Neutral Compounds under Laminar-Flow Conditions. International Journal of Pharmaceutics. 96:167-174 (1993).
22. W. Sun, C.K. Larive, and M.Z. Southard. A mechanistic study of danazol dissolution in ionic surfactant solutions. Journal of Pharmaceutical Sciences. 92:424-435 (2003).
23. H. Blasius. Grenzschichten in Flussigkeiten mit kleiner Reibung. Z Math Phys. 56:1-37 (1908).

Chapter 6 Microstructure Characterization and Numerical Simulation of Liquid Intrusion

In Chapter 4 we have introduced a microCT scanning method and procedures for general characterization of tablet microstructure. In this chapter, we describe detailed examination of microstructural features for a caffeine-lactose tablet. Based on the results, numerical simulation was adopted to understand liquid penetration into tablet microstructure. Permeability for microstructure could be derived from the simulation results, which greatly enhances our understanding of the dissolution process.

6.1 Characterization of Throats and Pores in a Tablet Porosity Network

Tablet microstructure contains abundant information about the way a tablet is formed and how that would affect tablet properties. The difficult part is extracting and organizing the information so that it could be used as guidance for rational formulation / process design and operations management. In this session we describe a detailed procedure to reproduce tablet internal structure with representative structural modules, unveiling the characteristics for reference of further quantitative analysis. For detailed steps and codes, please refer to Appendix B.

The sample studied is a 100 μm cubic of 96N 10% caffeine-lactose tablet microstructure. The original microCT scan was done at 1.4 μm/pixel. A 4X upsampling procedure is conducted to smooth the internal structure and gain a certain level of additional resolution (Figure 6-1). This is done by inserting 3 extra voxels between each pair of neighboring voxels, with the gray scale values set at equal distance. In the next step, pore spaces are separated from the materials through the same binarization procedure as described in Chapter 4. After obtaining the pore space, a procedure called skeletonization is carried out by eroding the pore structure until only a single-pixel-wide backbone line is left for each pore. This creates a network demonstrating the connectivity patterns of the pore structure (Figure 6-2). The pores in this lactose dominant tablet are highly inter-connected according to the pattern shown.

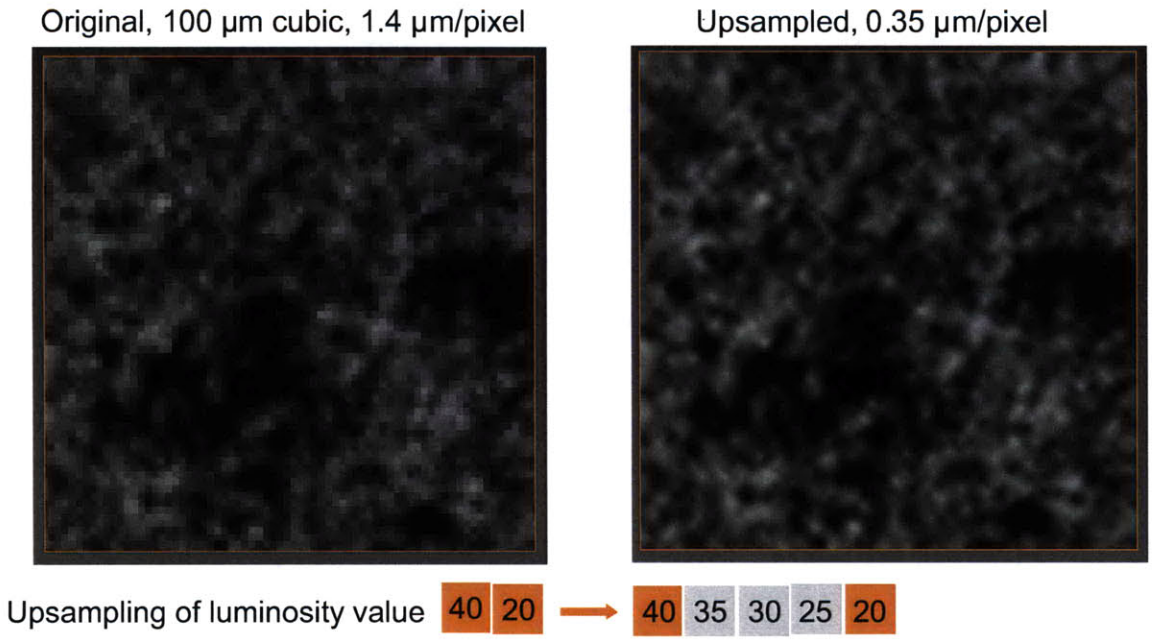

Figure 6-1 Upsampling by 4X smooths out internal pore structure.

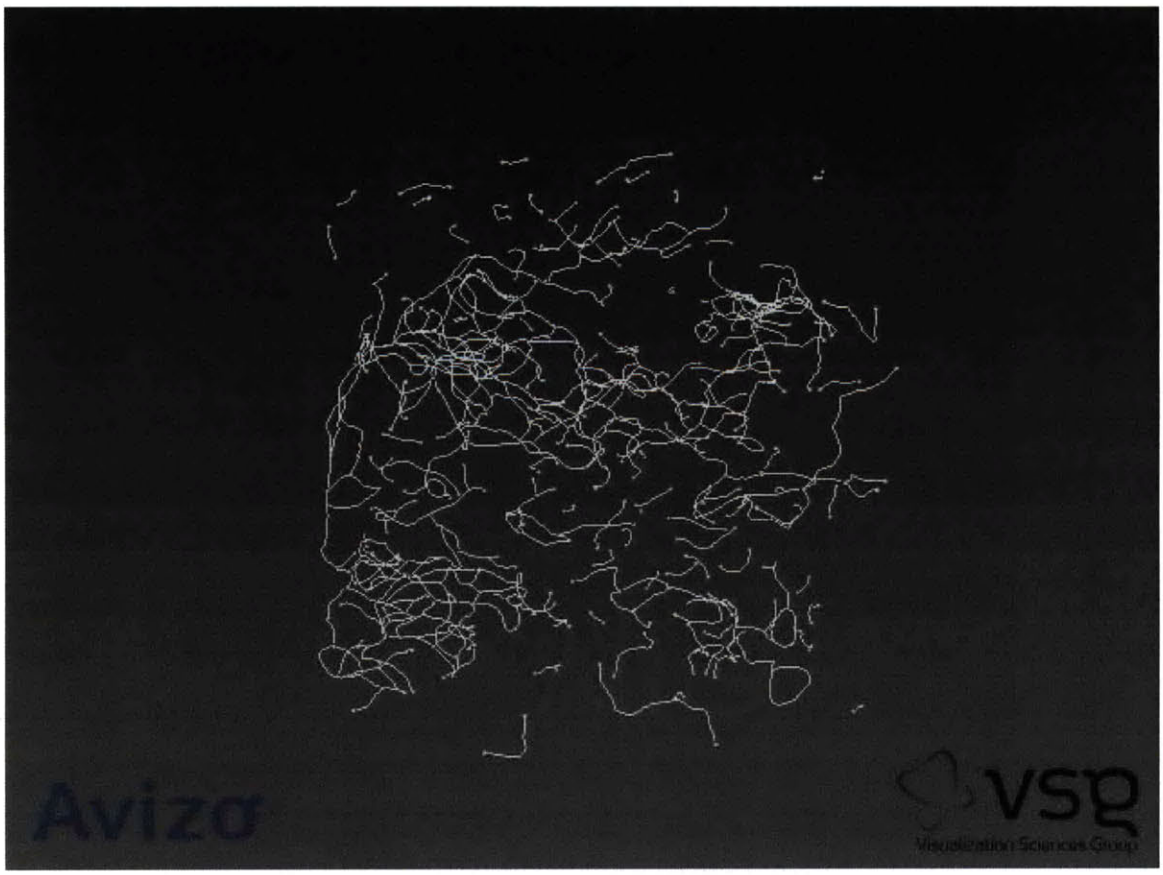

Figure 6-2 Skeletonization reveals the backbone structure and connectivity patterns of the pore space.

A distance map is then computed for the pore space, with the value assigned to a voxel equal to its minimum distance from an edge of the pore space (Figure 6-3). This procedure combined with skeletonization allows the extraction of thickness information for the pore network, as the backbone voxels on the distance map have the highest distance values relative to neighboring voxels. Ball-shape clusters with diameters proportional to the distance value can be built on the backbones, forming a 3-D representation of the internal microstructure (Figure 6-4).

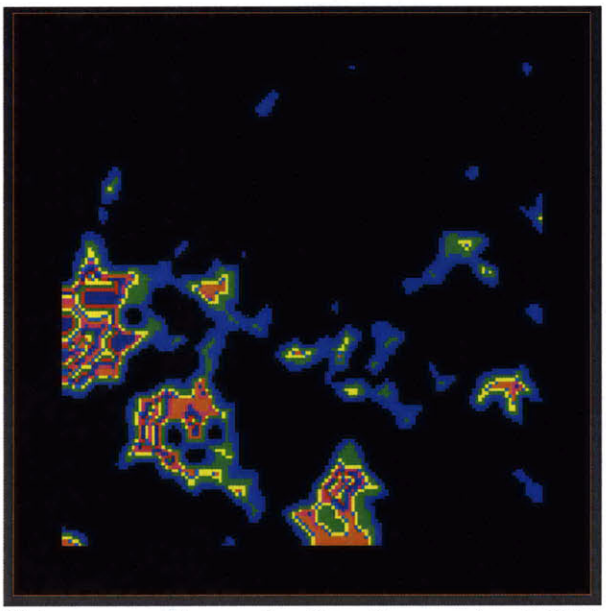

Figure 6-3 Distance map allows extraction of pore network thickness information.

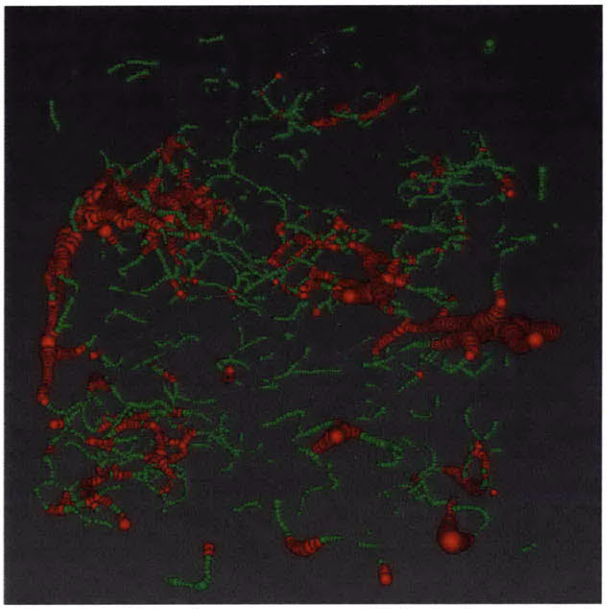

Figure 6-4 Representation of tablet microstructure with ball-shaped clusters. Green: throats; red: pores; sample size: 50 μm cubic.

In reality, it is impossible to reach at absolute definitions of throats and pores. As a result, assumptions have to be made to enable separation of throats and pores. In this case, we assumed that throat volume is 20% of the total pore space volume and arrived at a threshold of 3 μm. The clusters shown in red are the pores while the clusters shown in green are the throats (Figure 6-5). Most of the throats are linear in shape and relatively uniform in diameter, while the pores could exist in clusters, with multiple branches reaching out. The pore space features extremely high inter-connectivity and pore shapes that are difficult to characterize with morphological parameters.

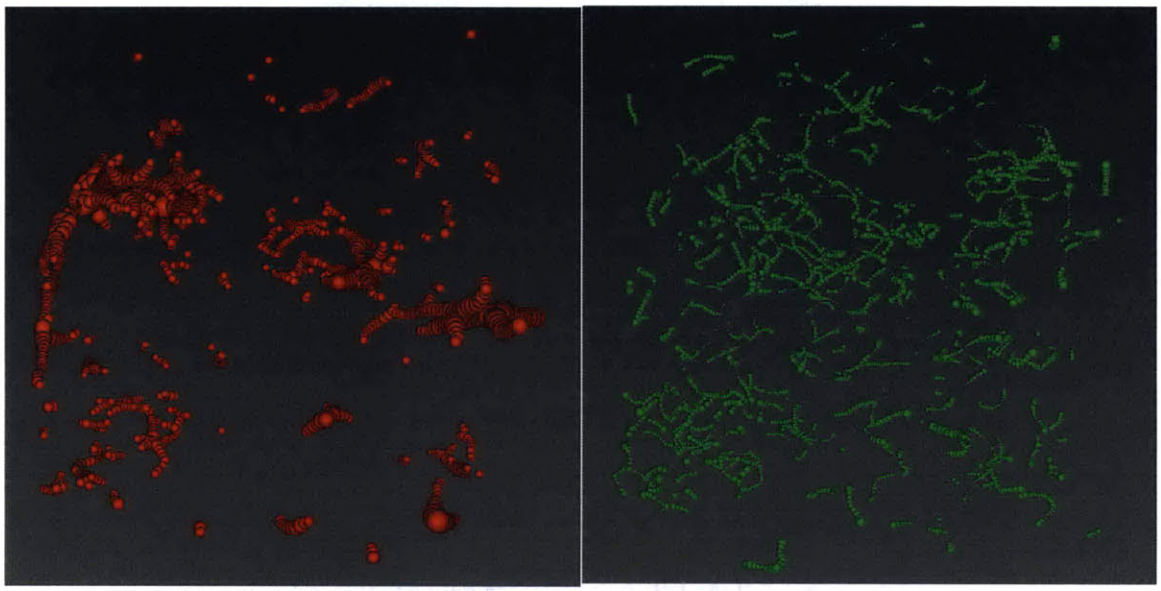

Figure 6-5 Separation of throats and pores reveals structural features.

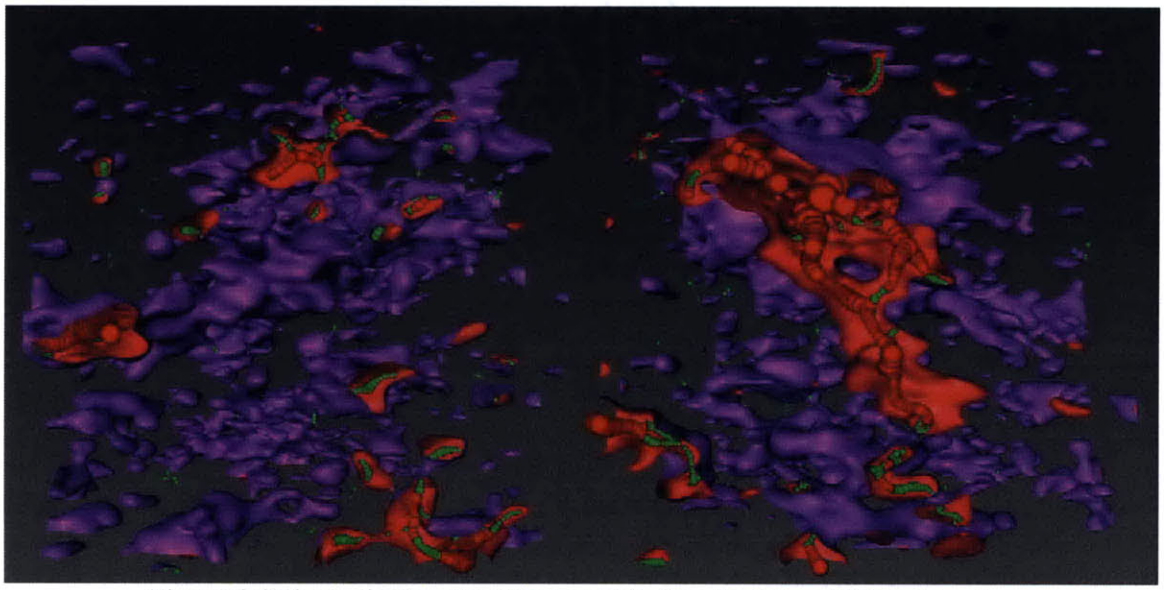

Figure 6-6 Views of microstructural organization from two different angles.

A surface view can be generated for the pore space and overlapped with the internal structure, which allows direct examination of the arrangement of throats and pores. It also reveals a generally flattened pore shape. As tablet compaction was done from the top, this data suggests a perpendicular relationship between compaction direction and pore orientation.

6.2 Numerical Simulation of Liquid Intrusion into Tablet

With microCT-captured tablet microstructure, there are in general two ways to utilize it for quantitative analysis. First, a microstructure can be converted into a binarized 3-D dataset representing the allocation of pores and materials, which is then used in numerical simulations to understand tablet properties. Potential applications include the study of dissolution process, e.g. penetration of dissolution medium into tablet internal structure, and the study of tablet hardness, e.g. propagation of force within the material matrix. Second, characteristics of the microstructure can be defined, quantitatively described, and incorporated into theoretical / empirical models to understand and predict tablet properties.

The microstructure of caffeine-lactose tablet reveals a pore shape with multiple branches and interconnections, making proper definition of pore morphology parameters a difficult task. On the other side, numerical simulation of liquid penetration and calculation of permeability, an intrinsic material property, becomes an attractive option to understand dissolution.

6.2.1 Methodology of Liquid Penetration Simulation

Numerical simulation of liquid penetration found its earliest applications in geosciences, where it was used to explore transport properties of fluid-saturated rocks (1). A number of studies have been conducted to solve linear-Stokes or Navier-Stokes equations of fluid flow in rock microstructures (2-6). In this study, we present for the first time an

application of the methodology in understanding tablet microstructure permeability and dissolution properties.

Navier-Stokes equation has been widely used in describing fluid flow based on the assumption that it is always a continuum (7). For a slow incompressible laminar flow, the equation has a linear format:

$$\eta \nabla^2 \vec{V}(\vec{r}) = \vec{\nabla} p(\vec{r})$$
$$\vec{\nabla} \bullet \vec{V}(\vec{r}) = 0$$

Where $\vec{V}$ and p are local velocity vector and pressure field at position $\vec{r}$. The first equation describes that the flow is driven by pressure gradient and is related with the viscosity of the fluid; the second equation refers to the incompressible nature of the flow.

For the purpose of simulation on tablet microCT structure, we modified a Stokes solver developed by National Institute of Standards and Technology (NIST) based on finite difference scheme (8). The solver was developed in conjunction with the artificial compressibility relaxation algorithm (9) and was originally applied to understand permeability and microstructure of cement (5). For details of the modification and execution steps, please refer to Appendix A.

In brief, microCT gray-scale structure is first binarized via thresholding, with materials taking value 1 and pores taking value 0. The binarized structure is then converted with a set of C language code into a marker-and-cell mesh, where pressures are defined at the nodes (center of each voxel) and fluid velocity components are defined at the midpoint of the bonds connecting nearest neighbor nodes (Figure 6-7). The simulation is set up as shown in Figure 6-8. Two boundary conditions are utilized in the simulation. A pressure gradient is applied on two sides of the sample, providing a driving force for liquid flow. A zero velocity is further assumed at solid-pore interfaces. All the pores are assumed to be filled up with liquid, and the flow speeds at four planes of the sample are calculated. When the four speeds converge, steady state is considered to be reached.

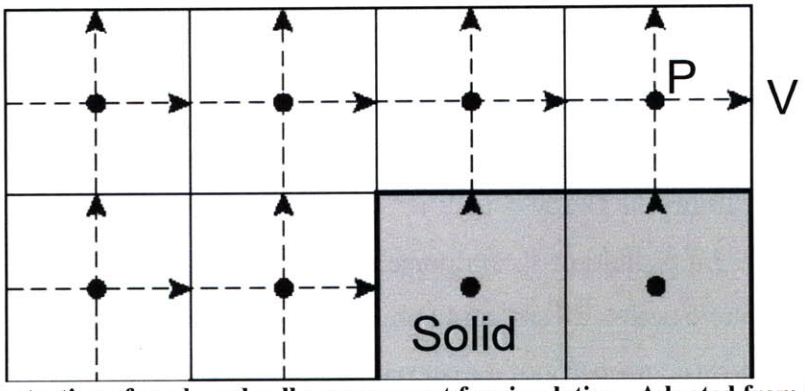

Figure 6-7 Illustration of mesh-and-cell arrangement for simulation. Adapted from Bentz et al. 2007.

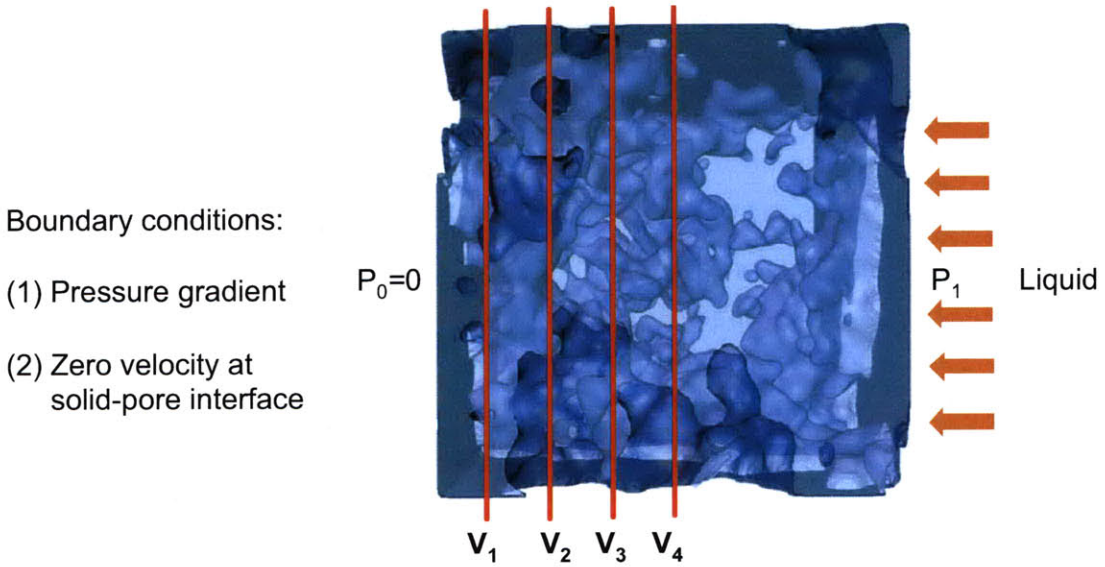

Figure 6-8 Illustration of simulation setup.

According to Darcy's law that describes fluid flow through a porous material (10), we have,

$$u = -\frac{k}{\eta}\frac{\Delta P}{L}$$

Where u is the average liquid velocity in the direction of pressure gradient, k is the permeability of the materials, η is the viscosity of the liquid, ΔP is the pressure gradient, and L is the length of the material in the direction of pressure gradient. A specific way to write the equation in the context of this simulation is,

$$k = \frac{u}{\mathrm{Re}} \bullet (PixelResolution)^2$$

Where Re is the Renolds number specified for the flow in the simulation (default 0.01). The pixel resolution in the microCT sample tested is 1.39 X 10^{-6} m/pixel.

The default unit for permeability is m^2. More often than not, Darcy or miliDarcy is used as the unit for permeability. 1 Darcy = 10^{-12} m^2, 1 miliDarcy = 10^{-15} m^2. One Darcy is equal to the flow of 1 ml of fluid of 1 centipoise viscosity in 1 second under a pressure gradient of 1 atmosphere across a 1cm^2 and 1 cm long section of porous material. Permeability is an intrinsic property of a material and does not change with regard to the liquid flowing through or the pressure gradient applied. A material with a permeability of less than 0.5 miliDarcy is typically considered impervious.

6.2.2 Permeability and Dissolution Speed

The permeability of caffeine-lactose tablets and M70 tablets at various hardness levels were computed with the process described above. The samples used were 500 μm binarized cubics. The permeability values are summarized in Figure 6-9.

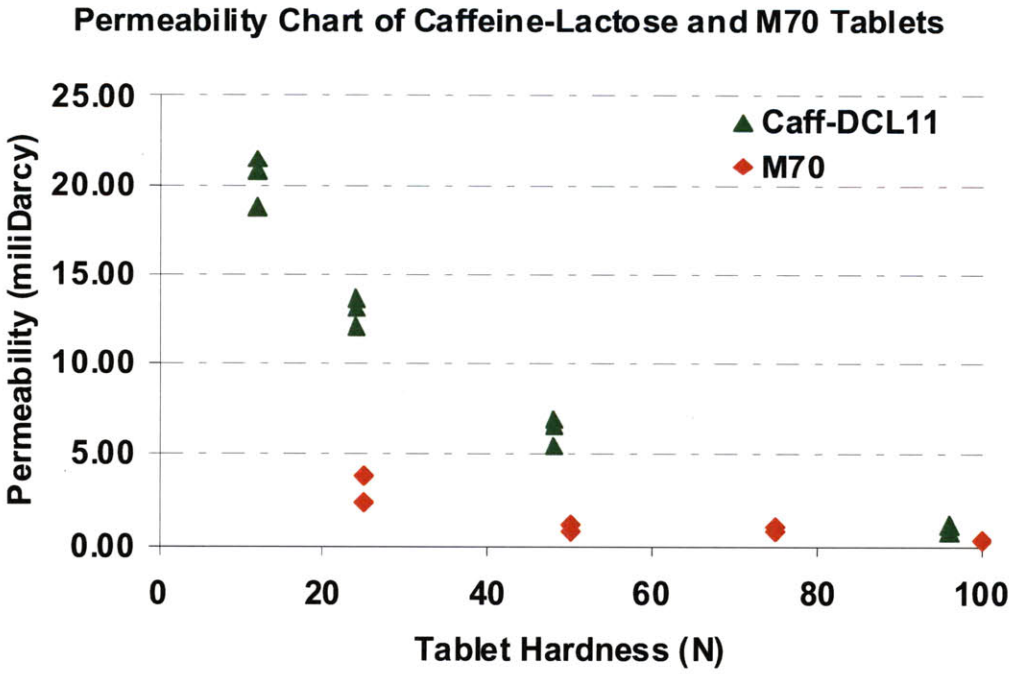

Figure 6-9 Permeability results for caffeine-lactose tablets and M70 tablets.

It is worth noting that the permeability of caffeine-lactose tablets increases dramatically with reducing hardness, while that of M70 tablets remain below 1 miliDarcy except for the softest 25N tablet. At similar hardness levels, the permeability of caffeine-lactose tablets is much higher than that of M70 tablets. When permeability value is plotted against microCT-determined porosity of the structure used in simulation, a clear linear relationship is observed for lactose-caffeine tablets (Figure 6-10). The porosity value corresponding to zero permeability is the percolation threshold for lactose-caffeine tablets, in this case 7.9%. For M70 tablets, the data points are not sufficient to draw a conclusion about linearity. However, it is clear that at the same porosity level, permeability for caffeine tablets is higher than that of M70 tablets. The permeability of caffeine tablets also increases a lot faster than that of M70 tablets with higher porosity. All the data point to a much higher pore interconnectivity of caffeine-lactose tablets than M70 tablets.

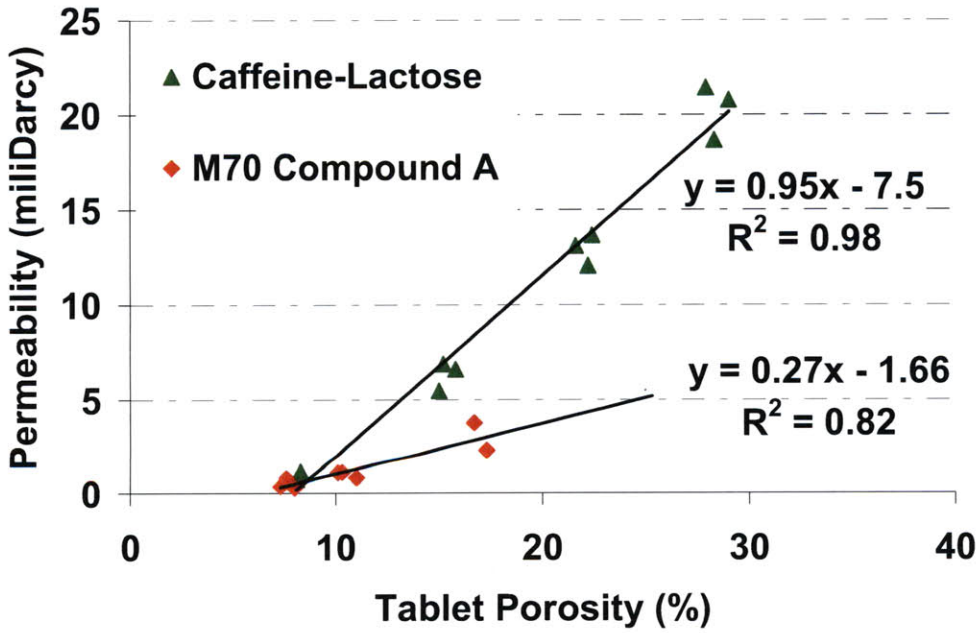

Figure 6-10 Relationship between permeability and porosity.

In the dissolution study of M-series tablets described in Chapter 5, we have derived the portion of paddle dissolution speed as contributed by disintegration (Figure 6-11). Only the lactose dominant M10 tablets exhibited significant portions of dissolution speed as contributed by disintegration. We made the assumption that the disintegration activity is induced by the high interconnectivity of the porosity network in lactose dominant tablets.

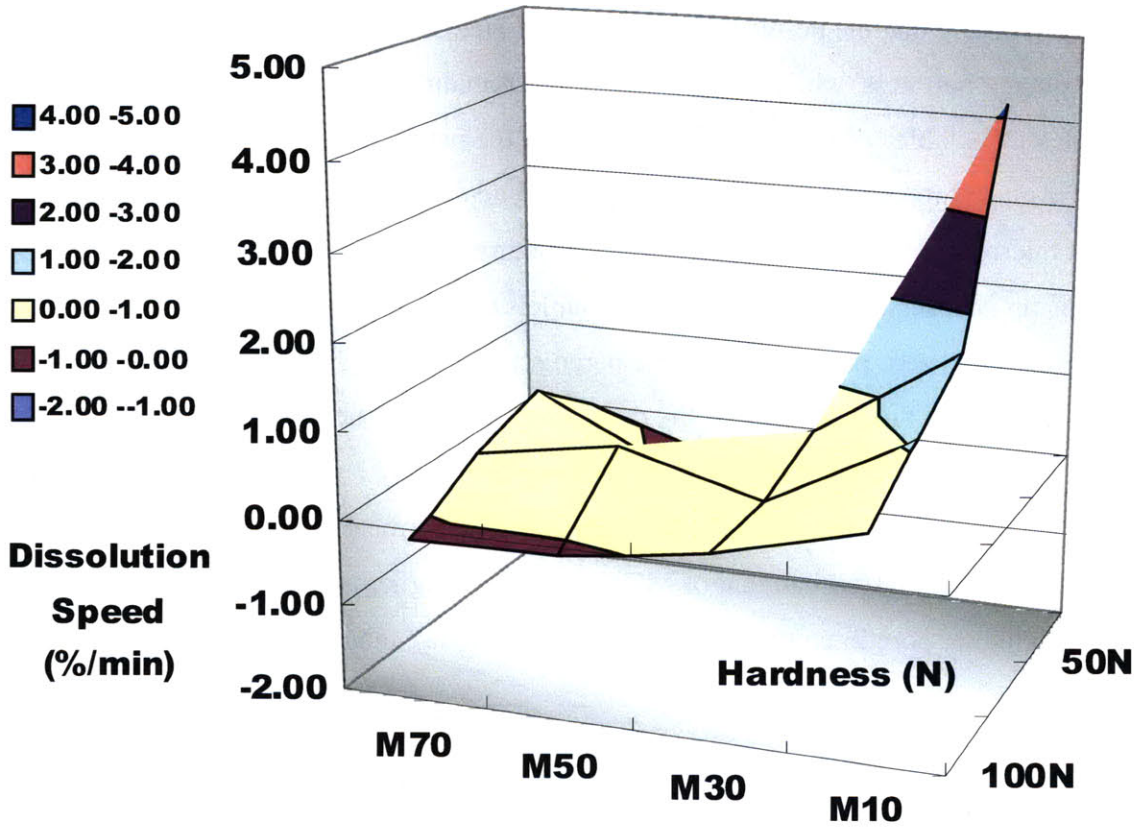

Figure 6-11 Portions of paddle dissolution speed as driven by disintegration for M-series tablets.

According to our assumptions, the paddle dissolution speed of caffeine-lactose tablets should be divided into two portions, disintegration speed and surface dissolution speed. The disintegration portion is related with permeability and material physical properties. When the paddle dissolution speed for caffeine-lactose tablets is plotted against the square of permeability, a linear relationship is observed within the normal 9mm tablet hardness range of 24N – 96N (Figure 6-12). The 12N data point was not adopted for two reasons. Firstly, for a tablet as soft as 12N, the mechanical stress induced by local hydrodynamics would contribute significantly to the dissolution speed. This effect is neither common for a tablet with normal strength nor considered in our model. From the data the mechanical stress is seemingly contributing to one-third of the overall dissolution speed. Secondly, the variation of both dissolution speed and permeability measurement in 12N tablets is very high, rendering the data point unreliable.

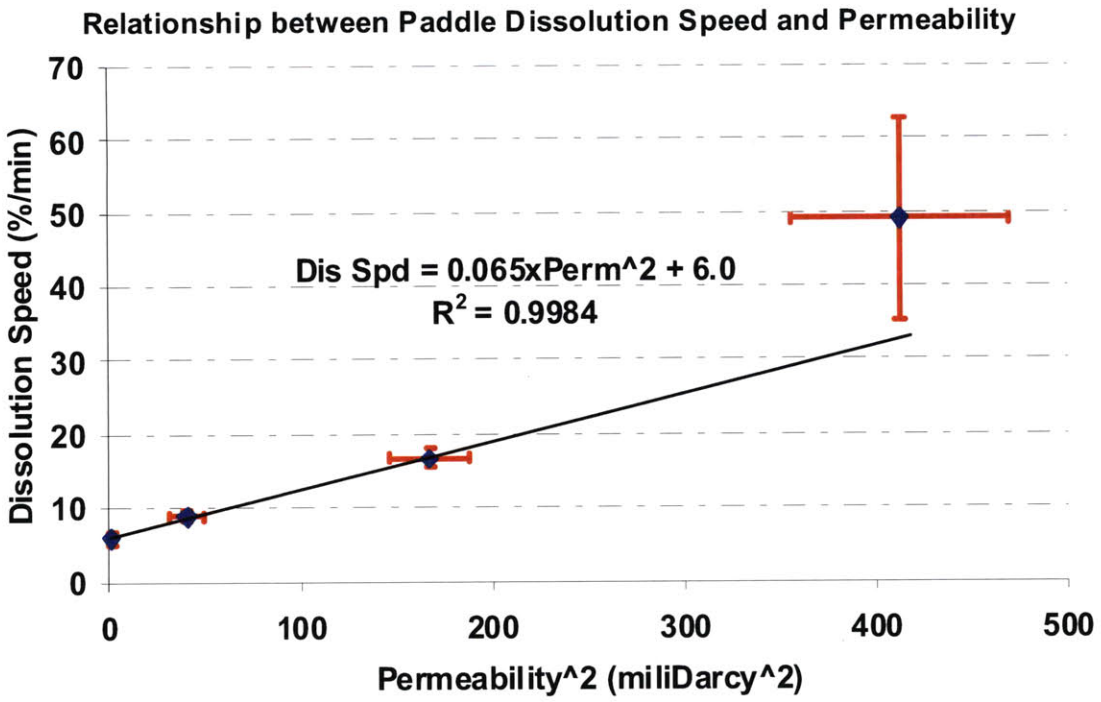

Figure 6-12 Relationship between paddle dissolution speed and permeability.

The equation can be generalized into the following form,

DissSpd = DF*Perm^2+SDS

Where DF = Disintegration Factor for the Excipient

SDS = Surface Dissolution Speed

In this case, DF (lactose) = 0.065, SDS (lactose, 50RPM paddle) = 6.0. The surface dissolution speed as converted from holder dissolution test is 5.8, very close to the value obtained in the formula. Depending on the dissolution scenario determined in holder dissolution test, SDS could be limited by different factors. For a convective-diffusion-limited scenario, SDS would be controlled by hydrodynamics condition. When the hydrodynamics condition remains the same as in the current test, SDS becomes a constant. For a surface-dissolving-limited scenario, SDS would be proportional to the tablet microstructure surface area available for dissolution.

It is worth noting that although the formula was found to be applicable to caffeine-lactose tablets, the validity for general application will need to be determined by studying more formulation systems. Nevertheless, it provides a novel framework for quantitatively dissecting the dissolution mechanism and understanding the drivers, paving the way for rational formulation design.

6.2.2 Comparison with Permeability by Mercury Porosimetry

In order to evaluate the accuracy of permeability calculation via microCT numerical simulation, we measured the permeability of tablets from the same batches using mercury porosimetry.

For caffeine-lactose tablets, mercury porosimetry derived permeability is lower than simulation derived permeability except for the softest 12N tablet (Figure 6-13). We believe that mercury porosimetry systematically underestimates the permeability levels for caffeine-lactose tablets, as at the levels indicated for 48N and 96N tablets there should be no disintegration happening. In actual paddle dissolution process, disintegration was observed for tablets of both strengths, especially the 48N ones. The underestimation in permeability by mercury porosimetry could be related to the underestimation of pore diameter, which is used in the calculation of permeability.

For M70 tablets, the advantage of permeability calculation via numerical simulation becomes obvious. The values obtained are not only consistent in trend (with higher permeability for softer tablets), but also agree well with experimental observation. The permeability values obtained by mercury porosimetry are not convincing, with erroneous readings for 25N and 50N tablets. Mercury porosimetry was inadequate to characterize permeability for M70 tablets, whose pore space is much less interconnected than that for caffeine-lactose tablets.

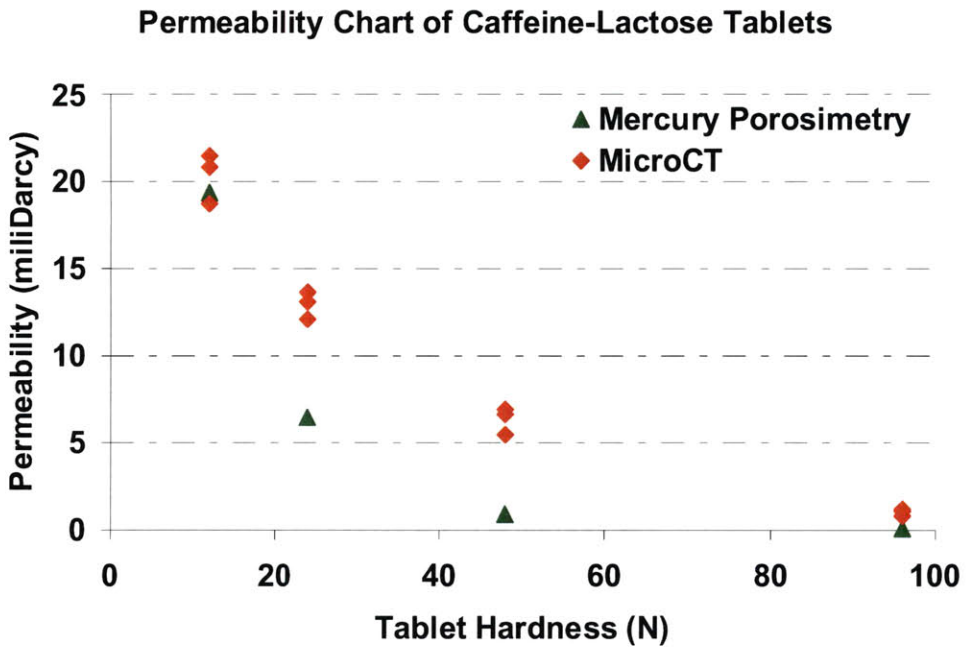

Figure 6-13 Comparison of caffeine-lactose tablet permeability by Hg porosimetry and microCT.

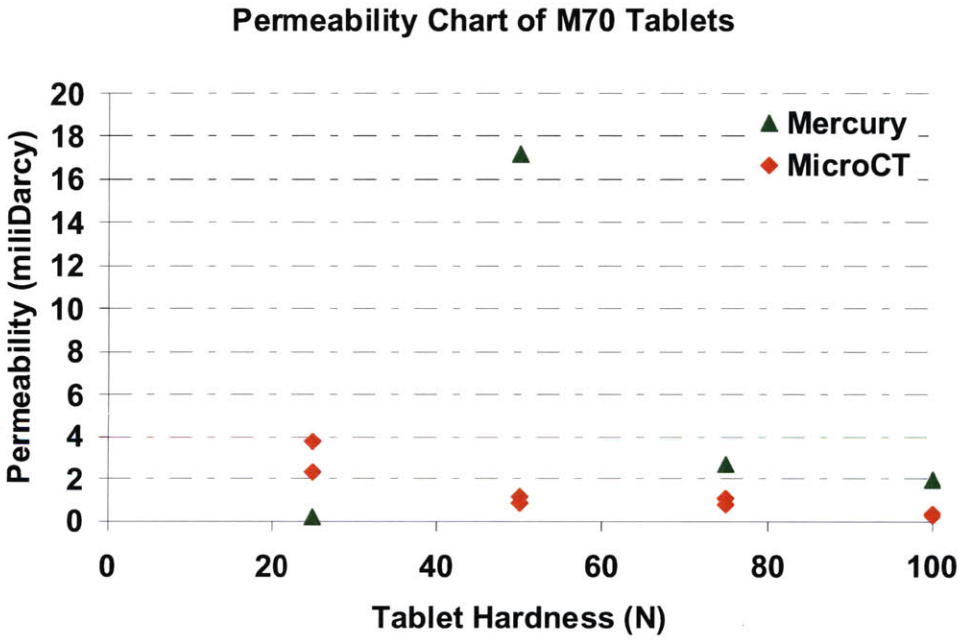

Figure 6-14 Comparison of M70 tablet permeability by Hg porosimetry amd microCT.

We believe that the root cause for inaccuracy in mercury permeability measurement lies in its calculation method. The calculation of permeability in the Autopore IV 9200 mercury porosimeter system used in this study requires identification of an inflection point on the curve of cumulative intrusion volume vs. pore diameter (11) (Figure 6-15). The precise selection of the point is critical to a fair estimation of permeability, but this is often difficult for two reasons. First, the infection point sits in an area that intrusion volume changes most rapidly, making the identification relatively inaccurate; second, in the scenarios where multiple S shapes appear in the curve, it might become impossible to select the inflection point.

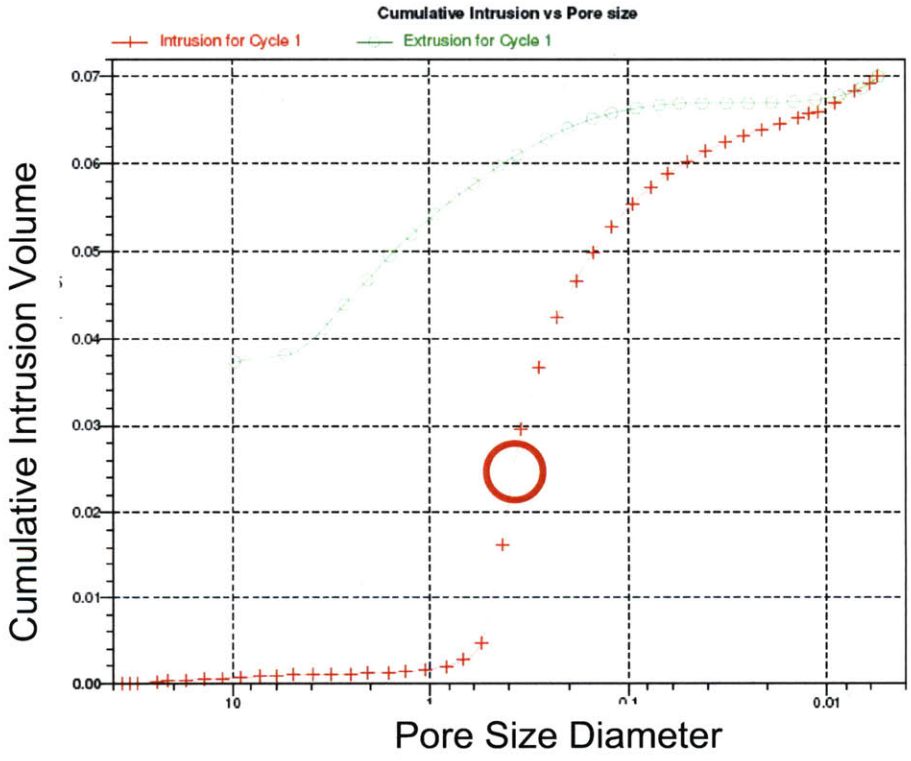

Figure 6-15 Difficulty in determing inflection point for permeability study in mercury porosimetry.

When compared with mercury porosimetry, numerical simulation based on microCT structure was proved to be more reliable and accurate in determining the permeability of pharmaceutical tablets.

6.3 Summary

In this chapter we first introduced a series of imaging analysis techniques transforming the original pore space into a 3-D model illustrating the interconnection and relative size of the pores and throats. This model helps understand the arrangement patterns of the pore space and thus guide the next steps of quantitative analysis. Caffeine-lactose tablets were discovered to have a pore network that is highly interconnected. The throats are mainly linear in shape and relatively uniform in diameter. However, the pores could exist in aggregation with multiple branches reaching out.

Next, numerical simulation of liquid intrusion was adopted to understand the relationship between tablet microstructure and dissolution process. The results demonstrated that permeability of caffeine-lactose tablets increases quickly with decreasing tablet hardness, while the permeability of M70 tablets remains at impervious levels for tablets between 50N and 100N. For tablets at the same hardness and porosity level, the permeability for caffeine-lactose tablets is much higher than that for M70 tablets. When permeability value is plotted against microCT-determined porosity of the structure used in simulation, a clear linear relationship is observed for lactose-caffeine tablets, indicating that permeability can be estimated just based on the total porosity of the tablets.

With the calculation of permeability levels, the dissolution speed for caffeine-lactose tablets was separated into two portions representing the contributions from disintegration and surface dissolution, respectively. The disintegration speed is proportional to a disintegration factor and the square of permeability values. The surface dissolution speed is dependant upon the dissolution mechanism identified in holder dissolution test. In a convective-diffusion-limited scenario, it is controlled by the hydrodynamic conditions around the tablet; in a surface-dissolving-limited scenario, it is controlled by the tablet surface area in contact with dissolution medium.

Tablet permeability calculation via microCT-based numerical simulation was demonstrated to be a superior choice when compared with that via mercury porosimetry.

An intrinsic defect in calculation method by mercury porosimetry makes it an unreliable technique for determination of tablet permeability.

Permeability derived from microstructural numerical simulation was established as a new parameter for describing tablet dissolution properties. It provides novel insights into the dissolution process and a mechanistic linkage between two common parameters: tablet porosity and dissolution speed.

6.4 Chapter Bibliography

1. I. Chatzisand F.A.L. Dullien. Application of the Percolation Theory for the Simulation of Penetration into Porous-Media of a Non-Wetting Fluid and the Prediction of the Relative Permeability Curve. Revue De L Institut Francais Du Petrole. 37:183-205 (1982).
2. C.H. Arns, Bauget, F., Ghous, A., Sakellariou, A., Senden, T.J., Sheppard, A.P., Sok, R.M., Pinczewski,W.V., Kelly, J.C. and Knackstedt, M.A. Digital Core Laboratory: Petrophysical Analysis from 3D Imaging of Reservoir Core Fragments. Petrophysics. 46:260-277 (2005).
3. A. Kameda. Permeability evolution in sandstone: digital rock approach, Vol. Ph.D., Stanford University, 2004.
4. Y.M. KEEHM, T; NUR,A. Computational rock physics at the pore scale: transport properties and diagnosis in realistic pore geometries. The Leading Edge:180-183 (2001).
5. N. Martysand E.J. Garboczi. Length Scales Relating the Fluid Permeability and Electrical-Conductivity in Random 2-Dimensional Model Porous-Media. Physical Review B. 46:6080-6090 (1992).
6. L.M. Schwartz, N. Martys, D.P. Bentz, E.J. Garboczi, and S. Torquato. Cross-Property Relations and Permeability Estimation in Model Porous-Media. Physical Review E. 48:4584-4591 (1993).
7. G.K. Batchelor. An Introduction to Fluid Dynamics, Cambridge University Press, 1967.
8. D.P. Bentzand N.S. Marty. A Stokes Permeability Solver for Three-Dimensional Porous Media, NIST, 2007.
9. N.S. Martys, S. Torquato, and D.P. Bentz. Universal Scaling of Fluid Permeability for Sphere Packings. Physical Review E. 50:403-408 (1994).
10. H. Darcy. Les Fontaines Publiques de la Ville de Dijon. (1856).
11. P.A. Webb. An Introduction To The Physical Characterization of Materials by Mercury Intrusion Porosimetry with Emphasis On Reduction And Presentation of Experimental Data, Micromeritics Instrument Corp., Norcross, Georgia, 2001.

Chapter 7 Preliminary and Future Work

The development of the microCT_dissolution-holder toolbox in this study provides a systematic approach for microstructural characterization of pharmaceutical tablets. Equally importantly, it paves the way for further utilization of the techniques in different aspects of pharmaceutical manufacturing, e.g. tablet coating quality examination. The resolution limitation revealed also inspires exploration of another novel technology, the focused ion beam scanning electron microscopy (FIB-SEM). Abundant opportunities exist for future work in tablet microstructure and dissolution mechanism. The direction and speed of technological innovation in this space are critical factors in the adaptation of the toolbox in the industry.

7.1 MicroCT Investigation of Tablet Coating

Coating is often an important step in tablet manufacturing process, as it can be used to improve appearance/flavor or strengthen the tablet to endure handling and transportation. Coating could also be utilized to alter the pharmacological properties of the tablets. The dissolution time of coated tablets is typically longer than that of uncoated tablets. Enteric coatings can be applied to tablets so that they can resist the strong acid of stomach fluid and dissolve in less-acidic intestines (1). Several coating materials could provide a moisture barrier for the tablets coated, rendering essential protection for ingredients that are highly sensitive to moisture (2).

Because of coating's critical functionalities, tablet coating quality has been studied extensively. Visual inspection is a most basic and straightforward method, but a better understanding requires going below the surface layer. Two technologies currently under development for coating characterization are near-infrared (NIR) spectroscopy (3-5) and terahertz pulsed imaging (TPI) (6-8). Both technologies depend on the correlation of collected sample spectrum with tablet physical structure to derive information about the coatings. Only a general thickness might be calculated, with no detailed information

about local coating structure. Nevertheless, both technologies can be operated on a real-time basis, so they are well suited for online monitoring of coating process (3, 9).

MicroCT represents a novel technology that might achieve 3-D location-dependant characterization of tablet coatings. In this preliminary study, a placebo tablet coated with Opadry® AMB is scanned with Skyscan 1172® microCT instrument at a resolution of 3 μm/pixel and a scanning time of 2340ms. A reconstructured cross section of the tablet is shown in Figure 7-1, where coating layer is manifesting itself as a white circle around the tablet. A thresholding procedure was then performed to separate the coating layer from the bulk material, resulting in the extraction of a 3-d coating shell (Figure 7-2).

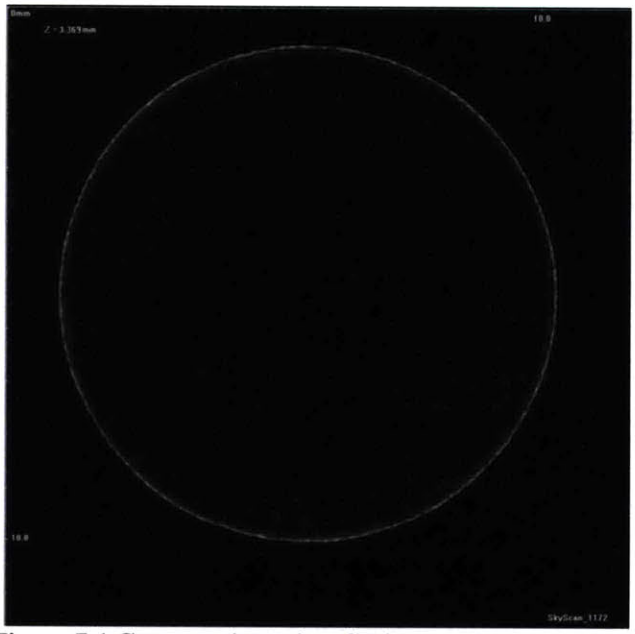

Figure 7-1 Cross section microCT image of coated tablet.

The thickness of the coating can be extracted by calculating a distance map of the coating and obtaining the distance values on the skeleton layer. A new 3-D model comprised of thickness information can be built, allowing direct visualization and examination of coating patterns (Figure 7-3). Thinner and uneven coating is observed on the embossed side of the tablet, especially at the locations of the numbers. On the side wall there are strips of thin coating, most probably formed due to the local physical structure. On the other flat side there is a circular ring of thin coating, potentially formed due to tablet contact during the coating process.

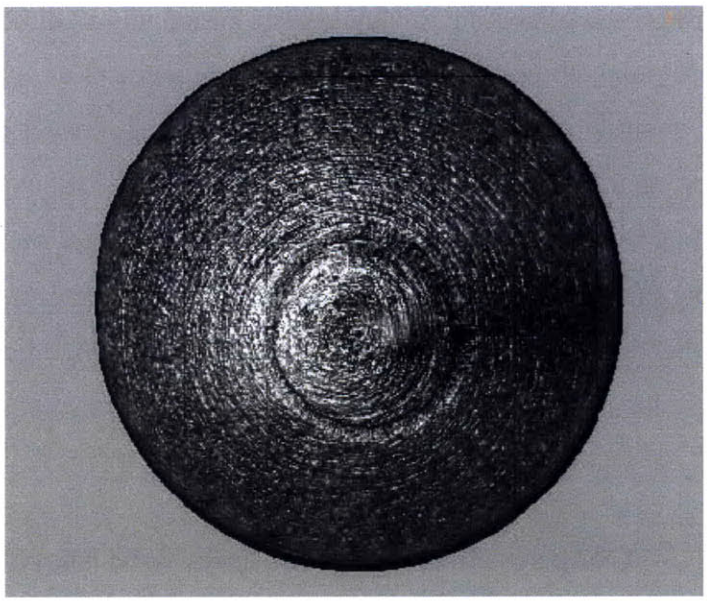

Figure 7-2 MicroCT 3-D model of tablet coating.

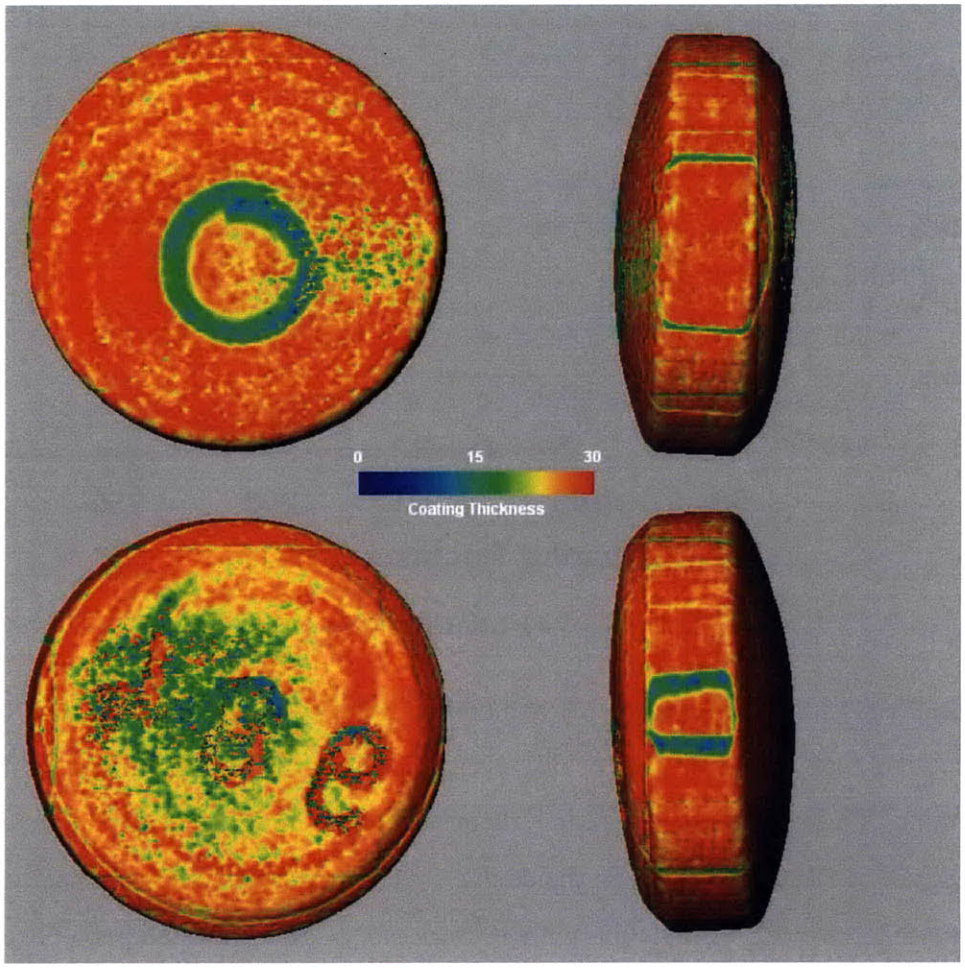

Figure 7-3 Coating thickness distribution on different tablet surfaces. 1 unit = 3 um.

The visualized presentation of coating thickness distribution allows direct examination of coating patterns, providing abundant information for improvement of coating techniques. On the other hand, quantitative analysis of the coating thickness creates a new dimension in quality measures. In the histogram of coating thickness, it was shown that a representative coating thickness for the tablet is 82 μm, with most of the tablet surface spots having coating thickness between 50 μm and 100 μm (Figure 7-4). However, it is also worth noting that about 15% of the surface spots have a coating thickness lower than 50 μm. This represents the region that improvements in coating technique need to be geared toward.

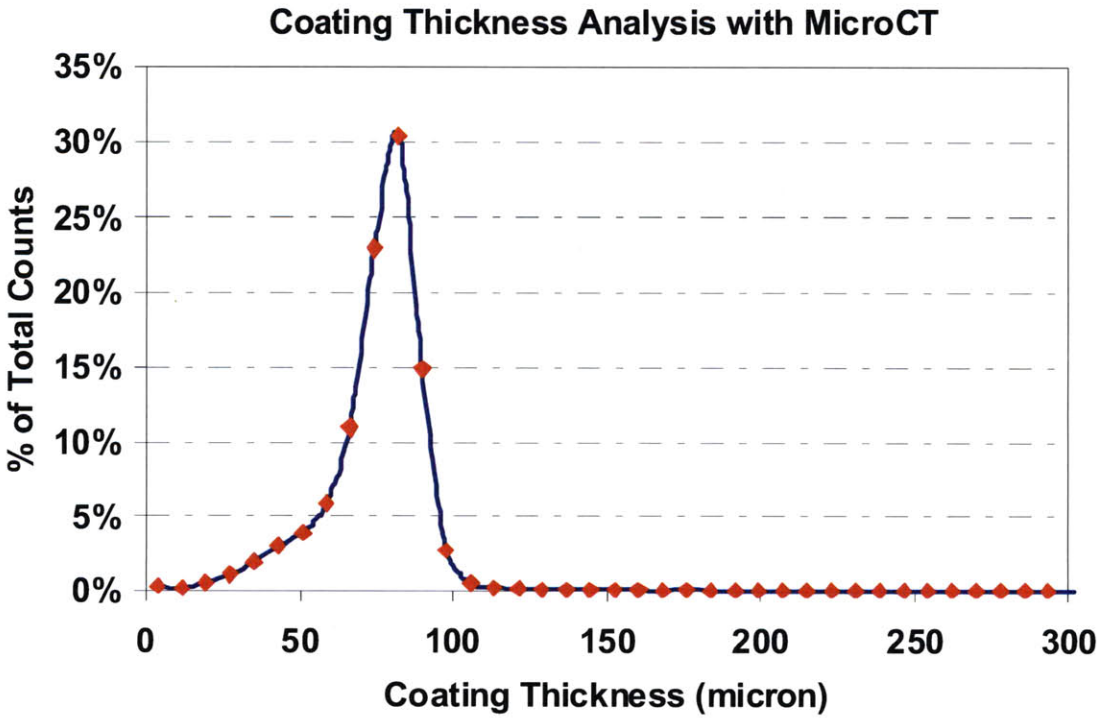

Figure 7-4 Quantitative analysis of tablet coating thickness.

This preliminary study of tablet coating demonstrates the power of microCT as a tool for pharmaceutical manufacturing R&D. However, it also reveals certain current limitations. The scanning of a sample takes 2.5 hours, reconstructing a sample takes 16 hours on a 4-processor desktop computer, while the analysis with Avizo® 6.2 software had to be conducted on a powerful workstation with 8GB memory. These limitations will certainly be addressed with the rapid technology development in the near future.

7.2 FIB-SEM Investigation of Tablet Microstructure

MicroCT has been demonstrated to be a powerful tool in characterizing pharmaceutical tablets. In comparison with the current standard method mercury porosimetry, the most significant drawback of microCT is the relatively low resolution. When studying 100N M70 compound-A tablets, insufficient microCT resolution was observed. In order to address the resolution limitation of microCT, alternative technologies were evaluated. Focused ion beam scanning electron microscopy (FIB-SEM) emerged as a great candidate for 3-D microstructure characterization with super high resolution.

Scanning electron microscopy (SEM) is a method of producing images of a surface by scanning a finely focused electron beam over the sample and mapping the electron interactions produced. With a resolution as high as 5-20 nm, SEM is a 2-D technology and only characterizes material surfaces. Recently, a novel platform combining the traditional resolution power of SEM with a sample manipulation capability of focused ion beam (FIB) brings the promise of 3-D SEM characterization of material structures.

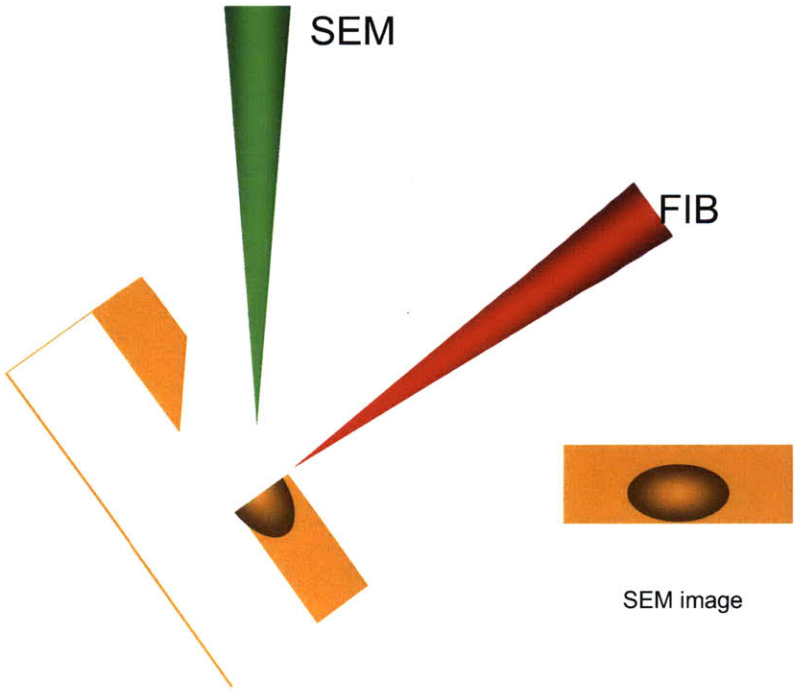

Figure 7-5 Illustration of FIB-SEM working mechanism.

In a FIB-SEM scanning experiment, a focused ion beam is used to cut off a thin slice of the object, with a SEM scan done after each cut (Figure 7-5). The thinnest slice that could be cut is ~10 nm with current technology, representing a 10 nm resolution power in all the three dimensions when combined with SEM. The series of SEM scans can then be aligned and constructed into a 3-D model of the sample internal structure.

In this preliminary study, a fragment of a 100N M70 compound-A tablet was scanned with a piece of Zeiss FIB-SEM instrument. A SEM image with scanning parameters is shown in Figure 7-6. The SEM scanning was done with 41 nm resolution, the FIB cutting was done at 50 nm intervals. A low electron current was selected so that electrostatic charge on material surface is minimized. The image demonstrates that the pores in 100N M70 tablet are mostly smaller than 1 μm in diameter and are much less inter-connected than the pores in 96N caffeine-lactose tablets.

Figure 7-6 FIB-SEM image of M70 tablet cross section with experimental parameters.

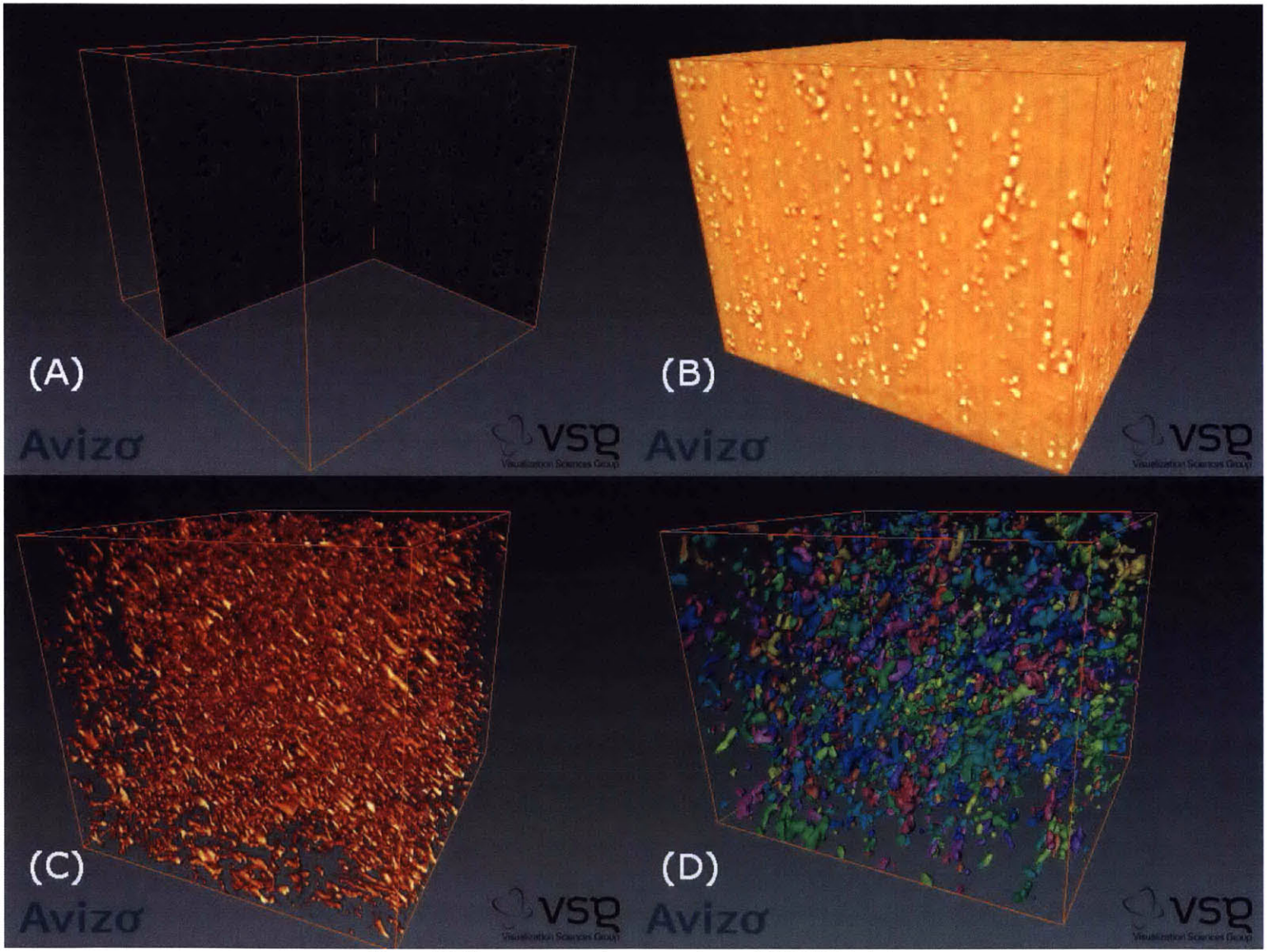

Figure 7-7 Image processing procedure of FIB-SEM data.

In order to extract 3-D structural information from the FIB-SEM data set, a series of image processing was conducted in Avizo® 6.2 software. First, a Noise Reduction Minimum Filter was applied to remove noise signals embedded in the scans (Figure 7-7 A); A gray-scale microstructure model is obtained (Figure 7-7 B). Next, pore space segmentation of the dataset was conducted with a combination of Thresholding and Magic Wand selection (Figure 7-7 C). Island Removal was applied to remove the single voxel noises from the selection. Finally, Smoothing was applied to the pore spaces and pores were labeled as individuals (Figure 7-7 D). At this stage, quantitative characterization can be conducted on the pores.

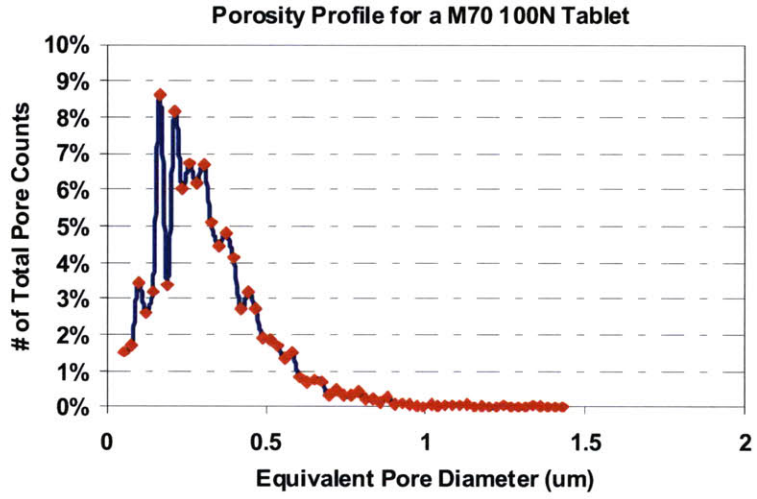

Figure 7-8 Incremental pore size distribution of FIB-SEM data for 100N M70 tablet.

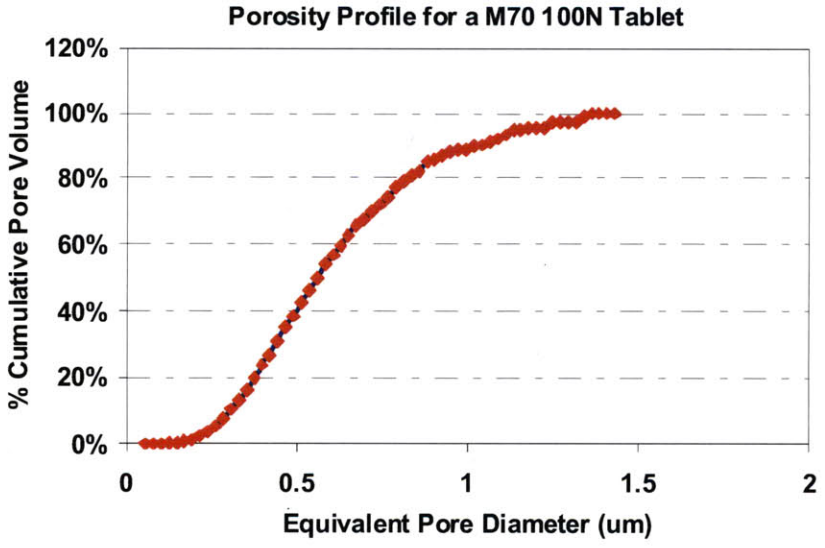

Figure 7-9 Cululative pore volume distribution of FIB-SEM data for 100N M70 tablet.

It was shown that most of the pores in 100N M70 tablets are around 0.3 μm in diameter, compared with mercury porosimetry's 0.016 μm. The multiple peaks are due to arbitrary allocation of histogram bins rather than actual discontinuity in pore size. According to FIB-SEM, 90% of the total pore volume belongs to pores with a diameter between 0.2 μm and 1 μm. This is one to two orders-of-magnitude larger than mercury porosimetry's estimation of 0.006-0.2 μm for 90% pore volume of 100N M70 tablets. The total porosity measured by FIB-SEM is 5.6%, a lower value than the theoretical porosity of 7.0%. Two reasons might explain the discrepancy. First, the sample studied was very small and did not contain any lactose granules at much higher porosity; second, it is possible that there are a group of pores smaller than 40μm in size that were not captured by FIB-SEM.

The application of FIB-SEM in this preliminary study complimented microCT with data at high resolution, providing more detailed quantitative information about tablet microstructure. The more accurate FIB-SEM structure is used for permeability simulation. Resulted permeability is 0.25 miliDarcy, compared with 0.29 and 0.35 miliDarcy from microCT structure. It demonstrates that a lack of interconnectivity of the pore space in both dataset contributed to very low permeability values. The FIB-SEM permeability is slightly lower probably due to the absence of lactose structure in the sample tested.

FIB-SEM is a promising technology for potential applications in understanding pharmaceutical materials. It provides ultra high resolution in 3-D characterization of microstructure, enabling a head-to-head comparison with mercury porosimetry. However, being a 2-D technology in its core, a series of drawbacks were also revealed during the preliminary trial.

A lot of pharmaceutical ingredients are prone to electrostatic charge buildup. In a regular SEM experiment, a thin coating like 5nm platinum can be applied to the surface of the sample to eliminate the electrostatic problem. In real-time FIB cutting, coating is impossible. As a result, data could be easily impacted by the electrostatic charge buildup.

FIB cutting is destructive and has a potential to skew the material structure. Since the slice is milled away, there is no record of the transition structure, causing occasional discontinuity in consecutive SEM images. Being a 2-D technique, it is also not suitable to study highly porous materials due to the complications introduced by the shadow of the pores.

With careful experimental design and data processing, FIB-SEM could bring valuable microstructure information at ultra-high resolution. Further study is suggested to better explore its utilization in the pharmaceutical industry.

7.3 Future Work in Tablet Microstructure Investigation

The tablet microstructure characterization described in this thesis lays a solid foundation for further exploration. Thorough investigation of tablet microstructure and its relationship with the materials, manufacturing process, and tablet properties could provide significant guidance for pharmaceutical manufacturing. This would enable more efficient formulation and process design, better operational control, and more stringent quality assurance.

- New excipients could be studied with the toolbox developed in this study. Although spray-dried lactose is a very common excipient for pharmaceutical tablets, it is not representative of all the common excipients. Other ingredients, e.g. microcrystalline cellulose (MCC), polyethylene glycol (PEG), and the inorganic calcium phosphate dibasic, might exhibit completely different material behaviors and form distinctive microstructure in tablet manufacturing process.

- New aspects of a tablet might be investigated with microCT. The analysis of coating quality is a good example. Heterogeneity of tablet microstructure can be assessed by examining fragments cut from different locations of a tablet. Chemical mapping is possible when the contrast between the API and the excipients in microCT scan is high enough.

- Dynamic microCT study could be carried out to understand the evolution of microstructure during manufacturing or analytical testing processes. Whole tablet scan coupled with step-wise compaction of the same tablet could reveal particle reorganization and deformation patterns during tablet compaction. Analyzing freeze-dried tablet matrix before and after dissolution could help understand microstructural changes induced by liquid penetration.

- MicroCT study of novel dosage forms could provide in-depth information about the products and associated manufacturing processes. Innovative drug products, like extruded and molded tablets or thin-film compacted tablets, are produced via manufacturing processes completely different from traditional ones. The capability to characterize 3-D microstructure of these novel products would provide much better understanding of the material transformation processes and their impact on tablet qualities.

- More advanced quantitative analysis can be developed for tablet microstructures. Pore shape and orientation can be characterized by calculating the momentum vector of the individual pores. Throat diameter can be extracted from a distance map, while the throat length can be obtained by measuring the throat skeleton length. Pore interconnectivity can be determined by counting the number of throats connected to a pore. These parameters could potentially be built into realistic physical / mathematical models describing tablet properties like dissolution profiles, leading to better understanding and control of tablet manufacturing. On the numerical simulation side, liquid penetration study from different side of a sample should be conducted to investigate anisotropic properties of permeability. Force propagation within a tablet microstructure matrix can be simulated, which could yield constructive information about obtaining proper tablet strength via microstructural designs.

- Further exploration of FIB-SEM in pharmaceutical applications should be continued, as the ultra high resolution and superb phase contrast of FIB-SEM might prove to be valuable addition to the 3-D characterization capability of microCT.

7.4 Future Work in Dissolution Mechanism Investigation

The exploration of tablet dissolution mechanism in this study leads to the dissection of dissolution into surface dissolution and disintegration. Within surface dissolution, two extreme scenarios were identified, i.e. surface-dissolving-limited dissolution and convective-diffusion-limited dissolution. An equation for calculating dissolution speed is suggested. However, only two formulation systems were studied due to time limitation. More work is needed to confirm and further polish the theory.

- More formulation systems need to be tested with the tablet holder for evaluation of dissolution mechanism, e.g. immediate release formulations featuring other common excipients. Dissolution medium mimicking *in vivo* conditions, such as fast and fed status, should be utilized to understand the potential dissolution mechanisms *in vivo*. The impact of disintegrants on dissolution mechanism can be evaluated as well.

- Extended-release formulations featuring insoluble excipient matrix could be tested with the tablet holder, creating a uni-directional material transport process with little tablet swelling. This combined with microCT study could help understand the diffusion process happening within the tablet matrix and guide extended-release formulation design.

- Representative formulations need to be identified for each category of dissolution mechanisms suggested in this study. Dissolution theory proposed can be further refined based on these additional studies. Incorporation of microstructural

analysis and dissolution mechanism theory should be attempted to reach at a sophisticated theoretical system describing dissolution activity on a microstructural level. This would enable ultimate Quality by Design in pharmaceutical tablet manufacturing.

7.5 Outlook of the Technologies

This study explored the utilization of several novel technologies/designs in understanding tablet microstructure and pharmacological properties. Meanwhile, it also reveals the shortcomings in what is currently available. Some of the issues might be resolved as technology advances in the next 5-10 years.

The technology of microCT has been developed rapidly within the last decade. Current generation of desktop microCT scanners enjoy a highest resolution of 1-10 μm / pixel. When a special synchrotron x-ray source is connected from a few facilities, resolution can reach sub 60 nm level, enabling whole cells microstructure imaging (10-12). The advancement in desktop microCT technology has yielded a new class of CT scanners called nanoCT, referring to a maximum resolution at nm level. The Skyscan® 2011 nano-CT has a maximum resolution of 150 nm, while Xradia® nano-XCT 100 is capable of producing a maximum resolution of 50 nm. The continuing improvement in scanning resolution will enable affordable bench-top units with adequate resolution for the majority of pharmaceutical materials utilized in the industry.

Another direction of improvement has been geared toward speed, which involves both scanning speed and post processing speed. Currently, a scanning session for a tablet fragment at 1.4 μm / pixel resolution with Skyscan® 1172 scanner takes about 1-1.5 hrs, the reconstruction of the 3-D structure at 360X360X1024 size takes 0.5 hr on a 4-processor 32-bit workstation with 4GB memory. With the new high-throughput Skyscan® 1178 scanner, comparable scanning and reconstruction would take a total of less than 5 minutes. Although the 1178 scanner is designed for small animal live imaging and thus has a rather low resolution of 80 μm / pixel, a higher resolution scanner with similar speed can be expected in the near future.

Innovative approaches are under development for better scanning capability. Dr. Ge Wang of Virginia Tech is leading an effort to design the next generation nano-CT combining interior tomography capability. This would allow examination of local portions of a sample object without cutting the portions off, realizing non-destructive location-dependent high-resolution characterization of pharmaceutical dosage forms.

In currently available commercial software products, the capability of 3-D imaging analysis has been mainly developed for applications in fields such as geosciences, material sciences, and biomechanical sciences. Avizo® from Visualization Sciences Group has the most powerful quantitative package and is the software used in this study. It combines impressive visualization capability with quantitative analysis and is developer friendly. The downside of Avizo® is that it provides so many functionalities and options that the user interface becomes relatively difficult to manipulate. Voxblast® 3D from Vaytek Inc is less powerful and is mainly geared toward biochemical and biomaterial applications. Another major 3D imaging visualization and analysis software is VGStudio® Max from Volume Graphics GmbH, which is used extensively in industrial designs but less so in scientific research.

A promising option is to develop customized application modules for pharmaceutical dosage form microstructure characterization based on the platform of Avizo®. After identification of key parameters and design of workflows to characterize them, application packages featuring simple and interactive graphical user interface (GUI) can be tailor-made for microstructure analysis in pharmaceutical R&D and manufacturing settings. This could enable the full integration of microstructure control into current practices, the details of which are discussed in Chapter 8.

A wide-spread usage of the tablet holder designed in this study would require a viable commercial production plan. The biggest issue incurred when the holders were manufactured to a standard size was the variation in dissolution vessel dimensions. The Varian® 1-liter dissolution vessels had varying internal diameters, causing significant fit

problem for the holders. In a commercial scale production, there are two ways to overcome the difficulty. One is to incorporate an elastic session at the connection line of the holder, allowing a certain degree of variation in vessel size; the other is to build new dissolution vessels with tablet holder incorporated in the design. In both approaches, exchangeable tablet holder modules fitting tablets of different size and shape can be designed.

The successful integration of the microCT-dissolution_holder toolbox in the pharmaceutical manufacturing industry could provide a wide range of benefits, as will be detailed in the next chapter. The technology advance in the foreseeable future would certainly accelerate the adaptation process, leading us to an era of microstructure analysis in pharmaceutical dosage form characterization.

7.6 Selection of Technologies for Microstructural Analysis

In this study, multiple technologies for microstructural acquisition have been discussed, including microCT, nanoCT, and FIB-SEM (Table 7-1). Selection of adequate technology is an important step in microstructural analysis. The discussion within this session is based on the assumption that all the three pieces of instrument are readily available.

Table 7-1 Comparison of technologies for microstructural analysis.

Technology	Resolution	Sample Size @ Max Resolution	Note
microCT	0.7-10 μm	1.5-20 mm	Insufficient for densificated structure
nanoCT	50-150 nm	0.07-0.2 mm	Might not be representative
FIB-SEM	5-20 nm	5-20 μm	Might not be representative Inadequate for highly porous material

In oil industry, companies adopt a step-wise methodology with rock microstructure analysis (personal communication with Dr. Shawn Zhang of Visualization Sciences Group). They start with CT scans at resolutions of cm level, and then move toward microCT, nanoCT, and maybe finally FIB-SEM. At each step, the significance of the

additional microstructure information provided at higher resolution is evaluated. The process is stopped when a higher resolution is not adding significant value.

This methodology is equally applicable to pharmaceutical tablets, with the exception that we start with microCT. A two-tier microCT/nanoCT analysis is recommended, with FIB-SEM adopted only if truly necessary. The technology with which the final data acquisition and analysis will be performed is dependant on two factors. First, resolution should be sufficient to characterize the microstructure studied; second, when the resolution requirement is met, the sample size should be large enough to be representative of the tablet microstructure. Eventually, data might come from multiple levels, with qualitative learning obtained at a lower resolution level and quantitative characterization done at a higher resolution level.

7.7 Chapter Bibiography

1. F. Liu, R. Lizio, C. Meier, H.U. Petereit, P. Blakey, and A.W. Basit. A novel concept in enteric coating: A double-coating system providing rapid drug release in the proximal small intestine. Journal of Controlled Release. 133:119-124 (2009).
2. E. Mwesigwa, G. Buckton, and A.W. Basit. The hygroscopicity of moisture barrier film coatings. Drug Development and Industrial Pharmacy. 31:959-968 (2005).
3. J.J. Moes, M.M. Ruijken, E. Gout, H.W. Frijlink, and M.I. Ugwoke. Application of process analytical technology in tablet process development using NIR spectroscopy: Blend uniformity, content uniformity and coating thickness measurements. International Journal of Pharmaceutics. 357:108-118 (2008).
4. J. Muselik, K. Krejcova, M. Rabiskova, A. Bartosikova, M. Drackova, and L. Vorlova. Determination of the Thickness of Tablet Coating by Near-Infrared Spectroscopy. Chemicke Listy. 104:41-45 (2010).
5. M. Romer, J. Heinamaki, C. Strachan, N. Sandler, and J. Yliruusi. Prediction of Tablet Film-coating Thickness Using a Rotating Plate Coating System and NIR Spectroscopy. Aaps Pharmscitech. 9:1047-1053 (2008).
6. A.J. Fitzgerald, B.E. Cole, and P.F. Taday. Nondestructive analysis of tablet coating thicknesses usign terahertz pulsed imaging. Journal of Pharmaceutical Sciences. 94:177-183 (2005).
7. L. Ho, F. Muller, M. Romer, K.C. Gordon, J. Heinamaki, P. Kleinebudde, M. Pepper, T. Rades, Y.C. Shen, C.J. Strachan, P.F. Taday, and J.A. Zeitler. Analysis of tablet film coating quality using terahertz pulsed imaging. Journal of Pharmacy and Pharmacology. 59:A20-A21 (2007).
8. L. Ho, R. Muller, K.C. Gordon, P. Kleinebudde, M. Pepper, T. Rades, Y.C. Shen, P.F. Taday, and J.A. Zeitler. Terahertz pulsed imaging as an analytical tool for sustained-release tablet film coating. European Journal of Pharmaceutics and Biopharmaceutics. 71:117-123 (2009).
9. L. Ho, R. Mueller, K.C. Gordon, P. Kleinebudde, M. Pepper, T. Rades, Y.C. Shen, P.F. Taday, and J.A. Zeitler. Terahertz-pulsed imaging as an analytical technique for tablet film coating: monitoring the unit operation and process scale-up. Journal of Pharmacy and Pharmacology. 60:A8-A9 (2008).
10. C.A. Larabelland M.A. Le Gros. X-ray tomography generates 3-D reconstructions of the yeast, Saccharomyces cerevisiae, at 60-nm resolution. Molecular Biology of the Cell. 15:957-962 (2004).
11. M.A. Le Gros, G. McDermott, and C.A. Larabell. X-ray tomography of whole cells. Current Opinion in Structural Biology. 15:593-600 (2005).
12. D.Y. Parkinson, G. McDermott, L.D. Etkin, M.A. Le Gros, and C.A. Larabell. Quantitative 3-D imaging of eukaryotic cells using soft X-ray tomography. Journal of Structural Biology. 162:380-386 (2008).

Chapter 8 Applications and Benefits of the MicroCT-Dissolution_Holder Toolbox

The development of the microCT-dissolution_holder toolbox provides a piece of magnifying glass to track the material changes during a manufacturing process. It allows detailed examination of the interactions among materials, the microstructure, and the resulting tablet properties. This new capability enables pharmaceutical scientists to obtain significant insight into the pharmaceutical manufacturing process, potentially leading to more efficient formulation and process designs. The toolbox can also be introduced into the quality control and troubleshooting of commercial scale production, providing additional dimensions of quality assurance and better informed diagnosis procedures. In this chapter we discuss in details the applications and benefits of the microCT-dissolution_holder toolbox in the pharmaceutical industry.

8.1 Applications and Benefits in Research & Development

Scientists working on research & development (R&D) of pharmaceutical manufacturing are often the early adopters of novel tools in the industry. They are eager to utilize new technologies to further their scientific understandings and are thus the best candidates to fully integrate the microCT-dissolution_holder toolbox with the current R&D procedures.

8.1.1 Development of Excipient Microstructure Library

Excipients are inactive substances that are used as carriers for active ingredients in medications. In a pharmaceutical tablet, excipients include fillers/binders, disintegrant, lubricant, glidants, preservatives, coating materials, etc. As drug discovery advances, the active ingredients are becoming increasingly potent, especially for medications in therapeutic areas like cancer. Often a tablet would contain <10% wt of active ingredient(s), with all the rest made up in excipients. Among the excipients, fillers/binders typically make up a majority of the volume. The implication of such an

arrangement is that one or two fillers/binders could form the supporting matrix of a tablet and have a dominant influence on its properties.

Fillers are materials used to fill up the volume of a tablet so that it becomes convenient to manufacture and to be consumed by customers. Binders are materials used to hold the ingredients together and form a tablet with required mechanical strength. About a dozen of excipients often take a dual role of filler/binder, e.g., lactose, microcrystalline cellulose, mannitol, polyvinylpyrrolidone (PVP), and polyethylene glycol (PEG). For each material, there are typically several popular grades / trade names that are widely used in formulations of pharmaceutical tablets.

Since the selection is very limited, it is viable to conduct detailed microstructure and dissolution mechanism analysis for the individual excipients. A potential procedure is shown in Figure 8-1. First, formulation scientists need to identify the few common fillers/binders that are used most widely in formulations of their products. Next, an experimental design space needs to be established around the typical manufacturing procedures used for correspondent materials. Impacts of different operational parameters on microstructure and dissolution mechanism could be examined via careful experimental design, e.g., maximum compaction force in tablet compaction or amount of liquid binder in wet granulation. If necessary, a model API like caffeine could be added to the formulation to better understand material interactions.

Various aspects of tablet microstructure could be examined. Qualitatively, the homogeneity of the materials and the deformation mechanism (fragmentation or densification) could be revealed. Detailed quantitative study of pore structure could be carried out, including but not limited to the pore size and shape, pore/throat relationship, interconnectivity and permeability. Holder dissolution study of the tablets would help identify the rate-limiting steps and intrinsic drivers of the dissolution process. Investigation of the relationship between microstructure features and dissolution process would provide information about the characteristics of the material that could be utilized in rational formulation design. For example, we learned that the fragmentation of spray-

dried lactose leads to a tablet microstructure with high connectivity and permeability, which in turn facilitates the disintegration of the tablet and promotes high dissolution speed. Therefore, lactose is a great candidate for formulation with high potency immediate release drug formulations.

Figure 8-1 Procedure for building excipient microstructural library (EML).

8.1.2 Rational Formulation / Manufacturing Process Design

With guidance from the excipient microstructure library (EML), a rational formulation design process could be pursued (Figure 8-2). It starts with the identification of the dosages of the API(s) and desired tablet properties (immediate release or extended release, target hardness level, etc.). This stage is typically done concurrently with early clinical development, where a matrix of tablet quality could be deduced from the clinical investigation and scientific understanding of the drug action mechanism. Then the EML can be screened for best matches in property profiles. Here the microstructural characteristics would be taken into consideration, e.g. whether the co-processing of an API with lactose would reduce the permeability of the tablet and thus hinder tablet disintegration. Physicochemical compatibility study would further narrow down the excipient list.

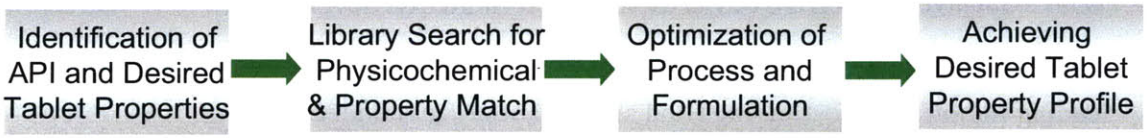

Figure 8-2 Example procedure for rational formulation design.

By this stage, the major excipient(s) and the general microstructure features are known, the tablet performance can be anticipated, and the venue to optimize the formulation should be clear. The optimization of the process and the formulation should be done to facilitate the manufacturing process while maximizing positive (minimizing negative) impact on microstructural features important for superb tablet performance.

The addition of microstructure and dissolution mechanism information leads to clear design strategies of formulations with certain major excipients (**Table 8-1**). Dissolution speed for formulations with significant disintegration can be tuned via microstructure permeability design. Dissolution speed for formulations with dissolving-limited surface dissolution can be tuned via microstructure surface area design.

Table 8-1 Tunable formulations.

	Disintegration	Surface Dissolution	
Rate-limiting Step?	Medium Penetration	Surface Dissolving	Convective Diffusion
Fine tune?	Yes	Yes	No
If yes, via what design?	Microstructure Permeability	Microstructure Surface Area	

Two key features enabled by the toolbox make the new formulation development a rational process. First, the big picture becomes clear once the selection of the main excipient(s) is made, as we have sophisticated understanding of the final tablet microstructure and the resulted property profiles. Second, with the knowledge of structural drivers for tablet properties, microstructural analysis can be used as guidance to fine tune the formulation and manufacturing process. Fewer experiments would be necessary in order to arrive at a satisfactory final dosage form.

With extensive application of the toolbox in formulation development, formulations with less ingredients and manufacturing steps might be designed in a shorter period of time, leading to potential cost savings and significant process understanding.

It is important to emphasize that although the microstructure and dissolution mechanism analysis would bring valuable insights into formulation development, they are not meant to replace the criteria or parameters that are used in current development process, e.g. particle size distribution and powder flowability. The proposed excipient microstructural library should be fully integrated with the current physicochemical library, providing

multi-dimensional information for rational decision making in pharmaceutical formulation development.

8.1.3 Development of New Dosage Forms / Manufacturing Processes

In pharmaceutical industry, innovation in new dosage forms has been an important strategy to attract consumers, conduct product life-cycle management, or achieve novel properties. Examples include Mucinex® bi-layer tablets featuring different release mechanisms in the layers, Claritin® RediTab orally disintegrating tablets and liquid gels, etc. Another motivation for dosage form innovation comes from the need to reinvent the pharmaceutical manufacturing processes with more efficient or sophisticated unit operations. Examples include extrusion coupled with injection molding and thin-film compaction. The former dramatically reduces the downstream manufacturing procedure into two unit operations, while the latter allows novel mixing techniques for API and excipients such as electro-spraying.

The standard evaluation methods, e.g. paddle dissolution and hardness tests, can only provide superficial comparison between the new dosage forms and traditional tablets. The microCT_dissolution-holder toolbox would enable much deeper understanding of the new manufacturing processes and the dosage forms resulted. In a preliminary microCT scanning of a tablet of 90% API 10% PEG 8000 produced by melt extrusion, it was demonstrated that air bubbles trapped or formed during the extrusion process would lead to cavities in final tablets, potentially reducing their mechanical strength (Figure 8-3 C). This bubbling phenomenon was absent in another batch of production. It was also demonstrated that a tablet with 50% API 50% PEG (Figure 8-3 A) had the same homogeneous microstructure as that of a tablet with 100% pure API (Figure 8-3 B). Similar techniques could be applied to tablets compressed from thin-film to understand the microstructural patterns and their impact on tablet properties.

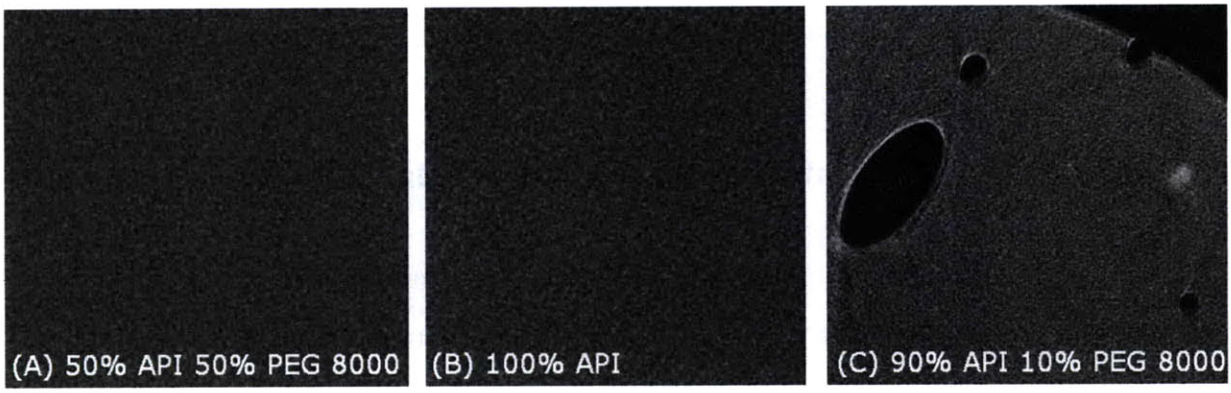

Figure 8-3 Preliminary microCT scans of melt-extruded tablets.

8.2 Applications and Benefits in Manufacturing

The toolbox developed in this study can also find useful applications in commercial scale pharmaceutical manufacturing, as the microstructure of a tablet provides abundant information about what happens in a manufacturing process. The capability of quantitative and qualitative description of microstructure renders us new dimensions in understanding and controlling the manufacturing processes.

8.2.1 Establishment of New Quality Assurance Criteria

Due to the desired clinical efficacy and potential toxicity of the pharmaceutical products, quality assurance (QA) has always been a critical component of the manufacturing process. Most of the currently available QA methods directly test the properties of final dosage forms, e.g. mechanical strength and *in vitro* bioavailability. The tests give relatively superficial presentation of the tablet properties. Tablets could potentially have similar dissolution profiles but drastically different microstructure and *in vivo* behaviors. MicroCT characterization enables tracing the properties backward to the internal structure of the tablets, potentially allowing a more fundamental control of tablet quality.

Depending on the key microstructural characteristics identified during formulation development, adequate parameters can be adopted as new quality assurance criteria for

tablet manufacturing, e.g. homogeneity, total porosity, average pore size, surface area, permeability and interconnectivity. Sample tablets from each batch can be scanned with microCT and characterized with quantitative analysis, ensuring batch-to-batch consistency on a microstructural level.

8.2.2 Application as a Investigation Toolkit

The microCT_dissolution-holder toolbox helps bridge our knowledge of the raw materials and the tablets by revealing the interactions among materials during the manufacturing process. The 3-D quantitative characterization and visualization of the microstructure provide unsurpassed information for guidance of manufacturing process. Meanwhile, it also represents a powerful tool for troubleshooting of manufacturing problems, which could stem from the materials, the manufacturing process, or a combination of both.

The examination of tablet coating quality, as described in Chapter 7, is an excellent example of troubleshooting capability by microCT characterization. The 3-D revelation of coating thickness distribution on a tablet surface directly exhibited the potential coating defect patterns on correspondent regions of a tablet, providing invaluable guidance for improvement of the coating process.

In a troubleshooting scenario where tablet quality is off the mark, a detailed examination of the tablet microstructure could potentially lead to a quick diagnosis of the problem, minimizing the loss of production power. If the problem is dissolution related, holder dissolution can be used to dissect the different segments of dissolution and understand where the changes happened.

8.2.3 Examination Tool for SUPAC

In pharmaceutical manufacturing and development, one of the most difficult tasks is to scale up or alter the manufacturing process while producing identical products. In scale-up or post-approval changes (SUPAC), the same tablet property profile needs to be

achieved and demonstrated to regulatory agents. Operational parameters in the new process are explored until a satisfactory profile is achieved. However, since the profile contains multiple properties, e.g. mechanical and pharmacological properties, it is difficult to design an optimization strategy.

The establishment of direct relationship between tablet microstructure and tablet properties provides an alternative option, in which the goal of optimization is to achieve the same tablet microstructure as before, while the examination of the tablet properties would only be used as a verification step. In such a setup, optimization is easier to coordinate as only one target object is involved. More importantly, an identical microstructure replicates a tablet at a fundamental level, ensuring comparable performance both *in vitro* and *in vivo*.

8.3 Summary

In this chapter we have discussed in details the potential applications of the microCT_dissolution-holder toolbox in pharmaceutical industry. It was demonstrated that the toolbox could prove to be valuable addition in both R&D and production settings (Figure 8-4).

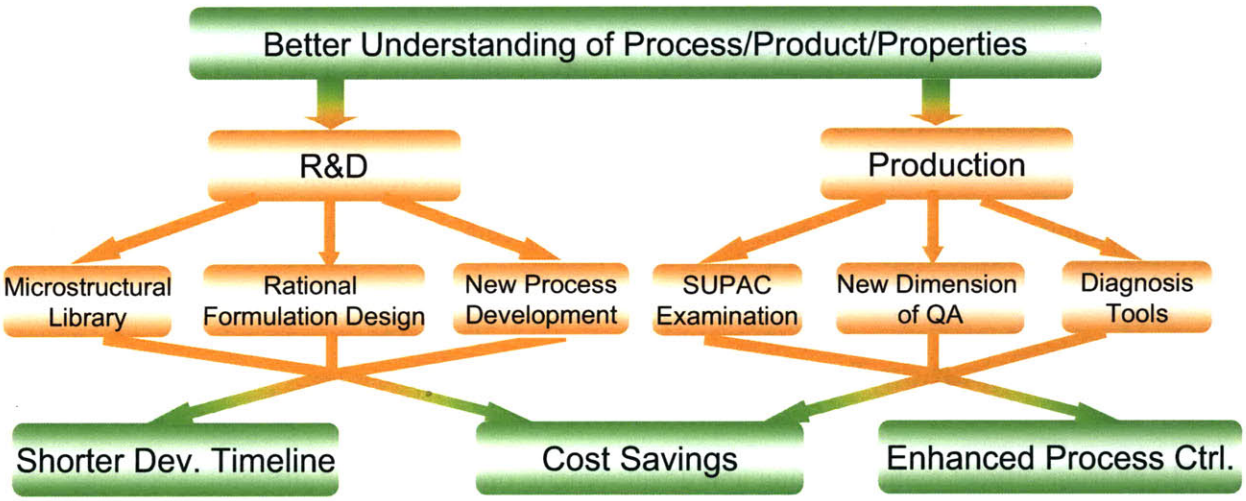

Figure 8-4 Applications and benefits of the microCT_dissolution-holder toolbox.

In R&D, an excipient microstructure library (EML) can be built for the common excipients used, providing guidance for rational formulation and process design. In actual design, optimization of the formulation and process could be done to facilitate the manufacturing process while maximizing positive (minimizing negative) impact on microstructural features important for superb tablet performance. The toolbox can also be utilized in understanding innovative manufacturing processes and products, providing in-depth characterization for promising new product/process designs.

The addition of microstructural and dissolution mechanism information allows fine tuning of formulations containing certain major excipients. Dissolution speed for formulations with significant disintegration can be fine-tuned via microstructure permeability design. Dissolution speed for formulations with dissolving-limited surface dissolution can be fine-tuned via microstructure surface area design.

With extensive application of the toolbox in formulation R&D, simpler formulations with less complex manufacturing processes might be designed in a shorter period of time, leading to potential cost savings and significant process understanding.

The capability of quantitative and qualitative description of the microstructure renders us new dimensions in understanding and controlling the manufacturing processes. MicroCT characterization enables tracing tablet properties backward to the internal structure of the tablets, potentially allowing a more fundamental control of tablet quality.

Depending on the key microstructural characteristics identified during formulation development, adequate parameters can be adopted as new quality assurance criteria for tablet manufacturing. In a troubleshooting scenario where tablet quality is off the mark, a detailed examination of the tablet microstructure could potentially lead to a quick diagnosis of the problem, maximizing the saving of production powers. If the problem is dissolution related, holder dissolution can be used to dissect the different segments of dissolution and understand where the changes happened. In a SUPAC situation,

optimization of new process can be geared toward reproducing the original tablet microstructure, ensuring comparable performance both *in vitro* and *in vivo*.

A wide-spread adoption and further development of the microCT_dissolution-holder toolbox in the pharmaceutical industry holds the promise of delivering shorter development time, better process control, as well as significant cost savings.

Chapter 9 Conclusion and Impact

In the current design and operational activities for secondary pharmaceutical manufacturing, a knowledge gap exists concerning material transformation and the subsequent impact on tablet properties. This gap presents a barrier to rational formulation / process design, where the selection of materials and manufacturing process is based on scientific understanding of the physicochemical transformation and the resulting tablet properties. In this study, it was hypothesized that the understanding of tablet microstructure is pivotal in bridging our knowledge about the materials, the manufacturing process, and the tablet properties.

A series of studies were carried out to characterize tablet microstructure and its relationship with the different aspects of pharmaceutical manufacturing, leading to a workflow as shown in Figure 9-1. The microstructure of a tablet is acquired via micro/nanoCT or FIB-SEM. Qualitative analysis of the microstructure leads to understanding of material interactions during manufacturing process, e.g. compaction mechanism. It also leads to identification of microstructural features, e.g., interconnectivity, which could be further characterized in quantitative analysis, e.g. permeability analysis via numerical simulation. The dissolution mechanism of a tablet could be studied via a combination of holder and paddle dissolution tests. When combined with results of quantitative microstructure analysis, this could lead to establishment of dissolution models providing mechanistic and quantitative description of the dissolution process. The understanding of material interactions, microstructural features, and dissolution models can then be used in designing the tablet by optimizing its microstructure, starting another round of characterization (if necessary).

The study opens up an approach in building an integrated formulation design and characterization system incorporating microstructural analysis. In this chapter we summarize the conclusions and impact generated.

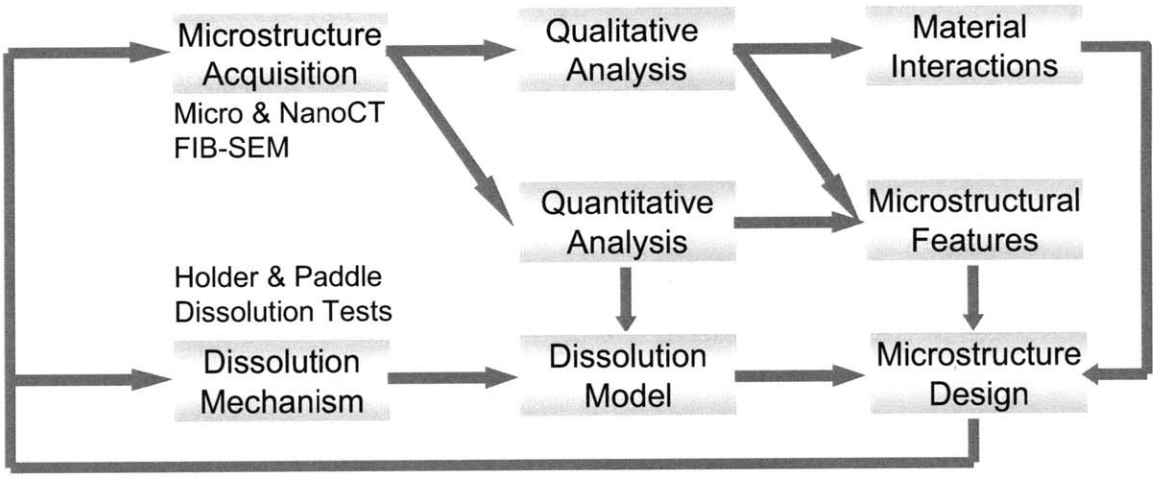

Figure 9-1 Workflow for tablet microstructure characterization and design.

9.1 Conclusion

Firstly, microCT imaging and analysis were shown to provide novel information of tablet microstructure, bridging our knowledge about the different components of pharmaceutical manufacturing and enabling a thorough understanding of the process.

- Qualitative microCT analysis could untangle the material interactions during manufacturing process, leading to clear pictures of unit operation mechanism. It could also describe the microstructure with representative structural modules, which helps understand arrangement patterns of the porosity network and provides guidance for quantitative analysis.

- Quantitative microCT analysis via numerical simulation of liquid intrusion is a reliable method for calculating the permeability of pharmaceutical tablets. It establishes permeability as a new parameter in quantitative description of tablet dissolution properties. Mercury porosimetry calculation of permeability is error-prone due to an intrinsic defect in the methodology adopted. At the same tablet hardness/porosity level, lactose dominant tablets have much higher permeability values than compound-A dominant tablets.

- Quantitative microCT analysis of tablet coating enables visualized inspection of location-dependent tablet coating quality, providing specific guidance for improvements in coating procedures.

- Resolution and speed are two major limitations for wide-spread adoption of microstructure analysis utilizing microCT. The resolution issue is being solved with the development nanoCT or alternative technologies like FIB-SEM. The speed issue is being addressed via the development of hardware and software.

Secondly, the design and application of tablet holder for paddle dissolution brings a convenient tool for probing dissolution mechanism, enabling the classification of dissolution mechanisms and identification of correspondent formulation design strategies.

- Paddle dissolution with tablet holder establishes a dissolution scenario with consistent hydrodynamics and exposed tablet surface area. In addition, disintegration due to medium penetration and tablet swelling is suppressed. This leads to a surface dissolution process that can be described with a physical / mathematical model.

- Two dissolution scenarios are identified for the surface dissolution process in holder test: surface-dissolving-limited scenario and convective-diffusion-limited scenario. In a typical paddle dissolution setup, lactose dominant tablets belong to the former while compound-A dominant tablets belong to the latter.

- Combining holder dissolution and paddle dissolution tests reveals an important contribution of disintegration to the paddle dissolution speed of lactose dominant tablets. It also helps identify a tablet density threshold between sink scenario and floating scenario in paddle dissolution test. The density threshold is 110% of the dissolution medium density in paddle dissolution test with 50 RPM agitation speed.

Thirdly, when the permeability simulation results are integrated with dissolution investigation, we identified a new way to dissect paddle dissolution speed of lactose dominant tablets into disintegration speed and surface dissolution speed. The disintegration speed is proportional to a disintegration factor and the square of permeability values. The surface dissolution speed is dependant upon the dissolution mechanism identified in holder dissolution test. In a convective-diffusion-limited scenario, it is controlled by the hydrodynamic conditions around the tablet; in a surface-dissolving-limited scenario, it is controlled by the tablet surface area in contact with dissolution medium.

In this study we also developed a compound-A roller compaction formulation from scratch. The development started with fundamental understanding of material properties and was adjusted according to specific problems discovered through the process. When compared with a benchmark formulation, the M-series formulation features fewer manufacturing steps and ingredients, is continuous-manufacturing friendly, and exhibits superior dissolution properties.

Lastly, in the investigation of hardness and dissolution of caffeine-lactose tablets, we demonstrated that moisture in storage environment could have a clear impact on these tablet properties. High moisture level tends to increase the tablet hardness and slow down the dissolution process. The extent of the impact is related with tablet microstructure. High porosity and interconnectivity would facilitate the intrusion of moisture and thus results in a larger impact on the tablet properties.

9.2 Impact

The study presents a fully integrated tablet characterization system that clearly reveals material interactions during the manufacturing process, the tablet microstructure formed, and the tablet properties resulted. Establishment of an excipient microstructural library (EML) and the rational formulation / process development procedures incorporating

EML could dramatically increase the efficiency of the development process, potentially leading to simpler formulations with less manufacturing steps and better tablet properties. The characterization system could also be used in manufacture settings, establishing new quality assurance dimensions and helping investigate manufacturing problems or changes.

The characterization of tablet microstructure and the numerical simulation represent a novel approach in quantitative investigation and application of tablet microstructure. It provides a practical example in how microstructure could be utilized to derive critical information for understanding tablet properties. The numerical simulation introduces a new parameter, tablet permeability, as an indicator of tablet dissolution properties. This leads to the proposal of a mathematical approach to separate the contributions to general dissolution from disintegration and surface dissolution, enhancing our understanding of the dissolution process and facilitating Quality by Design.

The design and application of the tablet holder in paddle dissolution help classify formulations into categories of different dissolution mechanisms. With distinctive drivers of dissolution process identified for each mechanism, tunable formulations can be developed with specific microstructure design strategy.

This work provides a strategy for building an integrated formulation design and characterization system incorporating microstructural analysis. It opens up an approach in which microstructure becomes a critical target for design and optimization.

Appendix A Procedures for Numerical Simulation

The numerical simulation is conducted via a modified set of C and Fortran computer programs originally developed by NIST for geosciences research. The original codes could be downloaded at ftp://ftp.nist.gov/pub/bfrl/bentz/permsolver.

I. Preparation of Simulation Environment

The codes are designed to be run on Linux or UNIX platforms. In order to create a Linux-like platform on a Windows-based system with proper compilers, the following procedure is recommended.

1. Download Cygwin software installer from www.cygwin.com. Cygwin creates a Linux-like environment in Windows.

2. Install Cygwin. When asked to select packages, expand Devel subcategory and choose the following items: gcc-core, gcc-g77, gdb. Proceed with installation as instructed.

II. Modification of Codes

The codes need to be modified in order to run successfully in the Cygwin environment with microCT-derived microstructure. Please refer to NISTIR7416.pdf for more detailed information.

1. In the following files, replace **jishft** and **jiand** commands with **ishft** and **iand**: **readp.f, readvx.f, readvy.f, readvz.f**. For the files to be displayed correctly, a code text editer might be needed.

2. The file **Inpuf256** contains a list of input parameters. The ones need to be changed are pl and pr, which are the pressures applied at the left and right side of the microstructure, respectively. Typically a pressure drop of one unit per voxel is used. For example, for a 300X300X300 microstructure, pl would be 301 and pr would be 1.

3. The file **bcfeed256** contains the common variable list and sets the dimensions of the system and the number of expected porosity (pressure) nodes. The default dimension is 300X300X300. The correspondent statement is **parameter (ix=304,iy=304,iz=304).** The values of ix, iy, and iz are 4 greater than 300 to allow for a two-voxel rim surrounding the microstructure for the implementation of the periodic boundary conditions. The statement should be changed to reflect the dimension of your microstructure to be tested. Another important parameter to change in this file is the expected maximum number of

porosity nodes, which is a one-dimensional array used to store the information. The current statements are like:
common/tabs1/lvxi(7500000),lvyi(7500000),lvzi(7500000)
indicating an expected maximum porosity on the order of 7,500,000/300/300/300 = 27.8 %. If the system porosity is greater than this, all arrays dimensioned at 7,500,000 should be increased accordingly. When the **bcfeed256** file is modified, the **perm3d3.f** program has to be recompiled for these changes to be implemented into the executable version (**perm3d3**).

III. Compilation of Codes

The two sets of codes need to be compiled into executable files within the Cygwin environment using the compilers that we installed earlier on.

1. Open a Cygwin window, use CD command to change directory to the folder /permsolver.

2. Use the following command to compile the pre-processor C code:
   cc microperm.c –o microperm –lm

3. Use the following command to compile the permeability solver Fortran code:
   f77 perm3d3.f –o perm3d3 –lm

4. Step 2 and 3 should lead to two new executable files in the same folder.

IV. Preparation of Microstructure Data

The microCT data needs to be converted into a binary data set with material shown as 1 and pores shown as 0, in order for it to be recognized by the programs.

1. Load a set of consecutive microCT 2-D reconstructured images in Avizo 6 software in Luminosity mode.

2. Crop the images into a cubic with the size specified in the programs.

3. Apply thresholding to the data. Pores should be assigned value 0 instead of 1 in this case. For example, if in the previous procedure a threshold window of 0-11 is used, in this case we should use 12-255.

4. Save data in 3-D raw data format.

V. Generating Data Structure for Simulation

The pre-processor **microperm** is used to convert the 3-D microCT raw data into a structure that could be recognized by the permeability solver.

1. Copy the 3-D raw data file to the folder of /permsolver and rename it to **image3d**.

2. Start a Cygwin window and CD to the folder, start the pre-processor by typing **./microperm**

3. When asked, put in a random number and press Enter.

4. Choose option 13 to read in the microstructure data, then choose 9, 10, 11, and 12 to generate the data structure files needed for simulation.

5. Choose 15 to exit the program.

VI. Simulation of Liquid Intrusion and Calculation of Permeability

The permeability solver is finally used to simulate the process of liquid intrusion and calculate the permeability of the materials.

1. Use the following command to start the simulation
   ./perm3d3 >perm3d3.out &

2. When the simulation is finished, two files are generated: **perm256** for velocity and **press256** for pressure. They record the correspondent values at four different depths of the microstructure. Average the four values in perm256 to obtain the average velocity of the fluid.

3. Permeability (m2) = LiquidVelocity/RenoldsNumber*Resolution^2, where RenoldsNum is preset as 0.1 in **Inpuf256** file, Resolution is the scanning resolution of microCT. A better unit of permeability is Darcy or miliDarcy. One Darcy is equal to the flow of 1 ml of fluid of 1 centipoise viscosity in 1 second under a pressure gradient of 1 atmosphere across a 1cm^2 and 1 cm long section of porous material. 1 miliDarcy = 0.001 Darcy =1X10^{-15} m^2

4. The data files generated during the simulation should now be removed from the original file folder and stored separately.

Appendix B Procedures for 3-D Pore Structure Representation

The detailed workflow for 3-D pore structure representation is listed below, with codes attached. The workflow is the result of collaboration with Marsh Mike and Shawn Zhang from Visualization Sciences Group. Marsh Mike provided significant technical support on programming, while Shawn offered constructive suggestions in workflow design.

Workflow step-by-step:

1. Load data.
2. Crop data. (CropEditor)
3. Upsample data by 4x (Resample module)
4. Threshold data on interval [0,a] (Quantification-Threshold)
5. Autoskeleton with Distance Map
6. SpatialGraphToLineSet Generate lineset
7. linesetToCluster.hx Generate cluster
8. ThroatFraction.scro Determination of Pore or Throat
9. SurfaceGen Generate surface
10. DemoMaker Create Animation

Steps 2-5 are handled by distanceHistogram.scro
Step 7 is handled by linesetToCluster.hx
Step 8 is handled ThroatFraction.scro

Detailed file names within the codes might need to be adjusted according to the naming in actual processing. The codes are listed below.

distanceHistogram.scro

```
#Amira-Script-Object V3.0


$this proc createUI {} {

        $this newPortIntTextN xCrop 2
        $this newPortIntTextN yCrop 2
        $this newPortIntTextN zCrop 2

        $this newPortIntTextN resampleFactor 1
        $this resampleFactor setValue 4

        $this newPortIntSlider lowerBound
        $this newPortIntSlider upperBound
        $this upperBound setMinMax 0 11
        $this upperBound setValue 11
}

##########################################################################
####
$this proc connectDataUpdateUI {newData} {
        set dims [$newData getDims]
        $this xCrop setValue 1 [expr [lindex $dims 0] - 1]
        $this yCrop setValue 1 [expr [lindex $dims 1] - 1]
        $this zCrop setValue 1 [expr [lindex $dims 2] - 1]

        set min  [lindex [$newData getRange]  0]
        set max  [lindex [$newData getRange]  1]
        $this lowerBound setMinMax $min $max
        $this lowerBound setValue $min
        $this upperBound setMinMax $min $max
        $this upperBound setValue 11
}


##########################################################################
####
$this proc constructor {} {
        $this createUI
        $this newPortDoIt action
}
```

```
##########################################################################
####
$this proc apply {} {

        #Crop the input data
        $this setVar cropEditor [create HxImageCrop]
        [$this getVar cropEditor] attach [$this data source]
        [$this getVar cropEditor] setMinX [$this xCrop getValue 0]
        [$this getVar cropEditor] setMaxX [$this xCrop getValue 1]
        [$this getVar cropEditor] setMinY [$this yCrop getValue 0]
        [$this getVar cropEditor] setMaxY [$this yCrop getValue 1]
        [$this getVar cropEditor] setMinZ [$this zCrop getValue 0]
        [$this getVar cropEditor] setMaxZ [$this zCrop getValue 1]
        [$this getVar cropEditor] doIt

        #Resample the cropped data
        $this setVar resample [create HxResample]
        [$this getVar resample] data connect [$this data source]
        [$this getVar resample] mode setValue 0
        set dims [[$this data source] getDims]
        [$this getVar resample] resolution setValue 0 [expr [lindex $dims 0] * [$this
resampleFactor getValue]]
        [$this getVar resample] resolution setValue 1 [expr [lindex $dims 1] * [$this
resampleFactor getValue]]
        [$this getVar resample] resolution setValue 2 [expr [lindex $dims 2] * [$this
resampleFactor getValue]]
        [$this getVar resample] action setValue 0
        [$this getVar resample] fire
        $this setVar resampled [[$this getVar resample] getResult]
        remove [$this getVar resample]

        #Threshold the resampled data
        set thresholded [create HxAnnaScalarField3 [$this data source].bin]
        remove $thresholded
        $this setVar quant [create HxVisilog]
        [$this getVar quant] exeCommand "cmd=threshold input=[$this getVar
resampled] param={[$this lowerBound getValue],[$this upperBound getValue]}
output=$thresholded"
        $this setVar thresholded $thresholded

        #Skeltonize the thresholded data
        $this setVar autoSkeleton [create HxExtAutoSkeleton]
        [$this getVar autoSkeleton] data connect $thresholded
        [$this getVar autoSkeleton] Options setValue 0 1
        [$this getVar autoSkeleton] Options setValue 1 0
        [$this getVar autoSkeleton] ExposeObjects setValue 0 1
```

```
[$this getVar autoSkeleton] Threshold setValue 0.4
[$this getVar autoSkeleton] doIt setValue 0
[$this getVar autoSkeleton] fire
[$this getVar autoSkeleton] Threshold setValue 0.4
[$this getVar autoSkeleton] doIt setValue 0
[$this getVar autoSkeleton] fire
#remove [$this getVar autoSkeleton]


#Display histogram
$this setVar histogram [create HxHistogram]
foreach object [all] {
        if { [string match *DistField $object] } {
                $this setVar distMap $object
        }
        if { [string match *SptGraph $object] } {
                $this setVar graph $object
        }
}
[$this getVar histogram] data connect [$this getVar distMap]
[$this getVar histogram] action hit
[$this getVar histogram] fire
[$this getVar histogram] data disconnect

#Cast pores binary map as labelfield
$this setVar cf [create HxCastField]
[$this getVar cf] data connect [$this getVar thresholded]
[$this getVar cf] outputType setValue 6
[$this getVar cf] action hit
[$this getVar cf] fire
set porosityLabelfield [[$this getVar cf] getResult]
remove [$this getVar thresholded]
remove [$this getVar cf]

#Use Material Statistics to make spreadsheet
set matStat [create HxTissueStatistics]
$matStat data connect $porosityLabelfield
$matStat doIt hit
$matStat fire
set sheet [$matStat getResult]
remove $matStat
remove $porosityLabelfield

#Compute and display Porosity
set matrix [$sheet getValue 2 0]
set pores  [$sheet getValue 2 1]
```

```
        set porosity [expr $pores / ( $pores + $matrix) ]
        $this newPortInfo porosityInfo
        $this porosityInfo setLabel Porosity
        $this porosityInfo setValue $porosity
        remove $sheet

        remove [$this getVar resampled]
        remove [$this getVar graph]
        remove [$this getVar quant]
        [$this getVar distMap] setLabel distanceMap
        [$this getVar histogram] setLabel Histogram.[$this data source]

        remove *DistField
        remove *SptGraph

}

##########################################################################
$this proc destructor {} {
        #remove [$this getVar histogram]
        remove [$this getVar distMap]
}


##########################################################################
$this proc compute {} {

        set data [$this data source]
        if {$data == ""} {
                return
        }

        #if { [$this isFirstCall] } {
                #return
        #}

        #update for new Data
        if { [$this data isNew] } {
                $this connectDataUpdateUI [$this data source]
        }

        if { [$this action wasHit] } {
                $this apply
        }
}
```

LineSetToCluster.hx

```
# Avizo Script

proc makeCluster { LineSet distanceMap } {
        #initialize PointProbe
        set probe [create HxPointProbe]
        $probe data connect $distanceMap
        $probe lineOptions setValue 0 1
        $probe lineOptions setValue 1 1

        #initialize Cluster
        set cluster [create HxCluster]
        $cluster setNumDataColumns 1
        $cluster setDataColumnName 0 "Distance"

        #Add LineSet points to cluster
        set numPoints [$LineSet getNumPoints]
        for { set pointIndex 0} {$pointIndex < $numPoints} {set pointIndex [expr
$pointIndex+1]} {
                set position [LineSet getPoint $pointIndex]
                set x [format %f [lindex $position 0]]
                set y [format %f [lindex $position 1]]
                set z [format %f [lindex $position 2]]
                $probe controlpoint setValue $x $y $z
                $probe fire
                set distance [$probe currentValue]

                $cluster addPoint $x $y $z
                #$cluster setId $pointIndex $pointIndex
                $cluster setDataValue 0 $pointIndex $distance
        }
        remove $probe
        return $cluster
}

#makeCluster LineSet image1.DistField
makeCluster LineSet image1.DistField
```

Throatfraction.scro

```
#Amira-Script-Object

$this proc constructor {} {
        $this script show
        $this newPortConnection cluster HxCluster
        $this newPortFloatSlider pointDisplaySize
        $this pointDisplaySize setMinMax 0 .5
        $this pointDisplaySize setValue 0.1
        $this newPortFloatSlider distanceThreshold
        $this distanceThreshold setMinMax 1 50
        $this newPortFloatSlider k
        $this k setMinMax 0 100
        $this k setValue 1
        $this newPortInfo throatVolume
        $this newPortInfo poreVolume
        $this newPortInfo throatFraction
}

$this proc computeVolume { k } {
        set throatVolume 0
        set poreVolume 0

        set numPoints [[$this cluster source] getNumPoints]
        for { set index 0 } { [expr $index < $numPoints] } { set index [expr $index + 1] }
{
                set distance [[$this cluster source] getDataValue 0 $index]
                set additionalVolume [expr $distance * $distance * $distance * $k]

                if { [expr $distance < [$this distanceThreshold getValue] ] } {
                        set throatVolume [expr $throatVolume + $additionalVolume]
                } else {
                        set poreVolume [expr $poreVolume + $additionalVolume]
                }
        }
        $this throatVolume setValue $throatVolume
        $this poreVolume setValue $poreVolume

        $this throatFraction setValue [expr $throatVolume / ($throatVolume +
$poreVolume)]


}
```

```
$this proc destructor {} {
        remove [$this getVar throatView]
        remove [$this getVar poreView]
}

$this proc compute {} {
        if {[$this cluster isNew]} {
                if {[$this cluster source] != "" } {
                        $this newCluster
                }
        }
        if {[$this distanceThreshold isNew]|| [$this k isNew] } {
                echo updatingDistanceThreshold
                set threshold [$this distanceThreshold getValue]

                [$this getVar throatView] filter setValue "(D<$threshold)"
                [$this getVar throatView] fire

                [$this getVar poreView] filter setValue "(D>=$threshold)"
                [$this getVar poreView] fire

                $this computeVolume [ expr [$this k getValue] * [$this k getValue]]
        }

        if {[$this pointDisplaySize isNew]} {
                [$this getVar throatView] sphereScale setValue [$this pointDisplaySize
getValue]
                [$this getVar throatView] fire

                [$this getVar poreView] sphereScale setValue [$this pointDisplaySize
getValue]
                [$this getVar poreView] fire
        }
}

$this proc newCluster {} {
        echo attaching newCluster
        $this setVar throatView [create HxClusterView]
        [$this getVar throatView] data connect [$this cluster source]
        [$this getVar throatView] options setValue 0 1
        [$this getVar throatView] options setValue 1 1
        [$this getVar throatView] options setValue 4 1
        [$this getVar throatView] sphereScale setValue 0.10
        [$this getVar throatView] colormap setDefaultColor 0 0 1
        [$this getVar throatView] filter setValue "(D<5)"
        [$this getVar throatView] fire
```

```
    $this setVar poreView [create HxClusterView]
    [$this getVar poreView] data connect [$this cluster source]
    [$this getVar poreView] options setValue 0 1
    [$this getVar poreView] options setValue 1 1
    [$this getVar poreView] options setValue 4 1
    [$this getVar poreView] sphereScale setValue 0.10
    [$this getVar poreView] filter setValue "(D>=6)"
    [$this getVar poreView] fire
}
```